STP 1086

Corrosion in Natural Waters

Calvin H. Baloun, editor

ASTM
1916 Race Street
Philadelphia, PA 19103

Library of Congress Cataloging-in-Publication Data

Corrosion in natural waters/Calvin H. Baloun, editor.
(STP ; 1086)
Papers presented at the Symposium on Corrosion in Natural Waters, held in Atlanta, Georgia, 8 Nov. 1988, sponsored by ASTM Committee G01 on the Corrosion of Metals.
"ASTM publication code number (PCN) 04-010860-27"-T.p. verso.
Includes bibliographical references and index.
ISBN 0-8031-1383-8
1. Corrosion and anti-corrosives-Congresses. I. Baloun, Calvin H., 1928- . II. American Society for Testing and Materials. Committee G-1 on Corrosion of Metals. III. Symposium on Corrosion in Natural Waters (1988:Atlanta, Ga.) IV. Series: ASTM special technical publication: 1086.
TA462.C6554 1990
620.1/1223-dc20 90-665
CIP

Peer Review Policy

Each paper published in this volume was evaluated by three peer reviewers. The authors addressed all of the reviewers' comments to the satisfaction of both the technical editor(s) and the ASTM Committee on Publications.

The quality of the papers in this publication reflects not only the obvious efforts of the authors and the technical editor(s), but also the work of these peer reviewers. The ASTM Committee on Publications acknowledges with appreciation their dedication and contribution of time and effort on behalf of ASTM.

Printed in Ann Arbor, MI
August 1990

Foreword

The symposium on Corrosion in Natural Waters was held in Atlanta, Georgia, 8 Nov. 1988. The symposium was sponsored by ASTM Committee GOI on the Corrosion of Metals. Calvin H. Baloun, Ohio University, presided as symposium chairman and is editor of this publication. W. W. Kirk, LaQue Center for Corrosion Technology Inc., presided as symposium cochairman.

Contents

Overview

The origin of the symposium on Corrosion in Natural Waters occurred with the need for a vehicle to present the three-year interim results of the World-Wide Variability of Seawaters study.

Over the past decade or more many papers have been presented concerning degradation of metallic materials in natural or nearly natural waters. Symposia have been sponsored by groups involved in Off Shore Technology, Pipelines, Petroleum and Natural Gas, Waterworks Associations, Nuclear Waste Storage, and other specialized interest areas. Unfortunately, some worthwhile research tends to slip through the cracks between these areas and not be presented.

This symposium has offered a receptacle for a varied collection of research presentations in a timely fashion and should thus be of value to the corrosion community.

Well deserved thanks go to W. W. Kirk as cochairman of this symposium and one of the presenters, to the other authors and presenters, and to the reviewers who devoted much time and effort to these thankless tasks.

Calvin H. Baloun

Stocker Center 180, Chemical Engineering,
Ohio University, Athens, OH 45701;
symposium chairman and editor.

W. W. Kirk[1] *and S. J. Pikul*[1]

Seawater Corrosivity Around the World: Results from Three Years of Testing

REFERENCE: Kirk, W. W. and Pikul, S. J., "Seawater Corrosivity Around the World: Results from Three Years of Testing," *Corrosion in Natural Waters, ASTM STP 1086,* C. H. Baloun, Ed., American Society for Testing and Materials, Philadelphia, 1990, pp. 2-36.

ABSTRACT: A world-wide test program was undertaken by Task Group G 1.09.02.03 to assess the relative corrosivity of seawater at 14 test sites. Aluminum alloy A95086, copper-nickel alloy C70600, and carbon steel alloy KO150l specimens were prepared at one location, shipped to the various sites, and returned to the original site for final evaluations. Results obtained through three years of testing indicate that average corrosion behavior was generally within limits of previously published results. Individual site characteristics have been identified, however, that can have a profound effect on test results. Even when the ASTM standard test method was prescribed, variations affecting corrosion results became evident. In reality there is no natural seawater environment, as identified to date, in which to test materials. The final five year results are yet to be collected, but the cooperation of all program participants has contributed much toward accomplishment of the objectives. Still, more frequent and broader monitoring of seawater variables at the exposure sites would assist in interpreting corrosion results.

KEY WORDS: seawater, world-wide, aluminum, copper-nickel, steel, localized corrosion, fretting, velocity, biofouling

Within ASTM Subcommittee G 1.09 on Corrosion in Natural Waters, a task group (G 1.09.02.03) was appointed in 1980 to organize a world-wide series of seawater corrosion evaluations. The objective of the task group was to apply existing standards for conducting corrosion tests in natural waters to compare the relative corrosivities of natural coastal sites around the world. This was to be accomplished via the exposure of aluminum alloy A95086, copper-nickel alloy C70600, and KO 150 I steel specimens at the 14 test sites listed in Table 1 and shown on a world map (Fig. 1). A five-year exposure program was initiated with duplicate removals scheduled for 0.5, 1, 3, and 5 year durations. The LaQue Center for Corrosion Technology, Inc. agreed to handle the initiation of the program as well as the final evaluations. This report covers results through three years of testing.

Experimental Procedure

Test Method

The test program was conducted according to the guidelines provided in ASTM Recommended Practice for Conducting Surface Seawater Exposure Tests on Metals and Alloys (G 52). One exception occurred at the Hawaii site where test panels were exposed horizontally

---

[1] President and senior technical supervisor, LaQue Center for Corrosion Technology, Inc., Post Office Box 656, Wrightsville Beach, NC 28480.

TABLE 1—*Test sites for world seawater corrosivity evaluations.*

Site	Contact
Ocean City, New Jersey Bar Graph Code: NJ	G. A. Gehring, Jr. Ocean City Research Corporation
Wrightsville Beach, North Carolina Bar Graph Code: NC	S. J. Pikul LaQue Center for Corrosion Technology, Inc.
Key West, Florida Bar Graph Code: FL	M. H. Peterson U.S. Naval Research Laboratory
Freeport, Texas Bar Graph Code: TX	C. Arnold The Dow Chemical Company
Port Hueneme, California Bar Graph Code: CA	J. F. Jenkins U.S. Naval Civil Engineering Laboratory
Talara, Peru Bar Graph Code: PE	K. D. Efird Occidental Oil and Gas Company
KeAhole, Kona, Hawaii Bar Graph Code: HI	J. Larsen-Basse/T. Daniel University of Hawaii at Manoa
Australia, North Barnard Islands Bar Graph Code: AU	J. J. Batten Materials Research Laboratories
Sakata Harbor, Japan Bar Graph Code: JA	S. Sato Sumitomo Light Metal Industries, Inc.
Genoa, Italy Bar Graph Code: IT	E. Mor Instituto per la Corrosione Marina dei Metalli-del C.N.R.
Sjcelland, Denmark Bar Graph Code: DE	H. Arup Korrosionscentralen, ATV
Studsvik, Sweden Bar Code: ST	S. Henrikson/E. Mattsson Swedish Corrosion Institute
Bohus-Malmon, Sweden Bar Code: BM	S. Henrikson/E. Mattsson Swedish Corrosion Institute
Isle of Wight, England Bar Code: EN	P. E. Francis National Physical Laboratory

rather than vertically, affixed to a nonmetallic pipe resting on the seabed. Environmental characteristics provided by the participants at all sites are summarized in Table 2. Initial exposure times and average seawater temperatures for each test period are given in Table 3.

Test Materials

The materials used in the tests are listed in Table 4 with their compositions. Specimens (6 by 100 by 300 mm) of each material were supplied as-sheared to size and were notch coded for identification (Fig. 2). Table 5 outlines the cleaning procedures used for each material. Following cleaning, specimens were weighed to the nearest 0.1 g.

Test Racks

Specimens were mounted on metallic test racks using nylon bolts and washers for electrical isolation (Fig. 3). The bolts were tightened to a torque of 1.7 nm. Eight specimens of each material were affixed to three individual racks for exposure at each site. The A95086 aluminum specimens were mounted on a 1.3-m-long aluminum alloy test rack. Two Ni-Cu

TABLE 2—*Worldwide seawater exposure site characteristics.*

Site	Rack Location	Range of Environmental Constituents[a]			
		Dissolved Oxygen, ppm	Salinity, ppt	Temperature, °C	pH
Ocean City, NJ	from raft .3 m below surface	5.2 to 11.7	31 to 34	1 to 29	7.5 to 8.2
Wrightsville Beach, NC Banks Channel	from wharf in channel	5.0 to 9.6	31.8 to 37.6	7 to 30	7.9 to 8.2
Key West, FL Fleming Key	under pier	4 to 8	33 to 39	16 to 31	8.0 to 8.2
Freeport, TX	intake flume	1.5 to 6.0	11.7 to 19.4[b]	15 to 27	7.5 to 8.6
Port Hueneme, CA Port Hueneme Harbor	from bulkhead	3.6 to 5.3	33	14 to 21	7.9 to 8.1
Talara, Peru	from pier 180 m from shore	5 to 6	19.8[b]	18 to 22	8.2
Keahole, Koma, Hawaii	45 m from shore on pipe	6 to 14	34.6 to 35	24 to 28	8 to 8.3
Australia North Barnard Islands	from raft	5.1 to 6.5	31.7 to 37.2	23 to 30	8 to 8.5
Japan Sakata Harbor	off docking pier	7.1 to 13	16.8 to 18.3[b]	2 to 28	8.4
Italy Genoa Harbor	from raft	4.5 to 6.0	35	11 to 25	8.1
Denmark Kyndby Isefjord	from raft in Fjord	NA[c]	18 to 28	0 to 18	7.5 to 8.0
Sweden					
Studsvik (Baltic Sea)	from wooden bulkhead	6 to 10	7.8 to 8.1	2 to 20	7.4 to 7.6
Bohus-Malmon (North Sea)	from raft	6 to 10	21 to 28	2 to 20	8.0 to 8.2
England Langstone Harbour	from raft	88 to 118[d]	34 to 34.6	5 to 22	7.8 to 8.4

[a] compiled from information provided by participants.
[b] Chlorinity, g/L.
[c] NA = not available.
[d] % saturation.

FIG. 1—*Approximate location of exposure sites.*

TABLE 3—*Summary of average seawater temperatures at test sites.*

Test Site	Initial Exposure Date	Average Seawater Temperatures, °C 0.5 year Exposure	1.0 year Exposure	3.0 year Exposure
Ocean City, NJ	July 1983	15[a]	15.2	14.7
Wrightsville, Beach, NC	May 1983	25.2	19.5	20.1
Key West, FL	May 1983	28	22[a]	22[a]
Freeport, TX	Oct. 1983	16[a]	22[a]	22[a]
Port Hueneme, CA	May 1983	17.4	16[a]	16[a]
Talara, Peru	March 1984	NA[b]	NA[b]	20
KeAhole, Kona, Hawaii	July 1983	NA[b]	NA[b]	26[a]
Australia	July 1986	...	26[a]	...
Sakata Harbor, Japan	Aug. 1983	5[a]	18[a]	18[a]
Genoa, Italy	Sept. 1983	17.1	17.7	17.7
Sjcelland, Denmark	Oct. 1983	5[a]	9[a]	9[a]
Studsvik, Sweden	Aug. 1983	5[a]	10[a]	10[a]
Bohus-Malmon, Sweden	Aug. 1983	5[a]	10[a]	10[a]
Isle of Wight, England	Aug. 1983	10[a]	14[a]	14[a]

[a] Estimated based on general environmental characteristics provided about test site.
[b] NA = no information available.

TABLE 4—*Test materials chemical analyses.*

Alloy	Composition, weight %		Supplier
A95086	0.14 Si		Kaiser Aluminum and
(H116 temper)	0.33 Fe		Chemical Corporation
	0.030 Cu		(T. J. Summerson)
	0.57 Mn		
	3.89 Mg		
	0.13 Cr		
	BAL Al		
C70600	9.44 Ni		Revere Copper Products, Inc.
(hard)	1.40 Fe		(B. S. Vagnoni)
	0.29 Mn		
	0.008 P		
	0.007 S		
	BAL Cu		
K01501	0.046 C	<0.006 Ti	Armco, Incorporated
(copper-bearing	0.32 Mn	0.008 Al	(H. H. Lawson)
carbon steel)	0.006 P	<0.002 Cb	
	0.009 S	<0.0001 B	
	0.003 Si	<0.002 Zr	
	0.19 Cu	0.004 Co	
	0.019 Ni	<0.006 Pb	
	0.020 Cr	<0.004 Te	
	<0.002 Sn	<0.004 Ce	
	<0.004 V	0.0004 As	
	0.011 Mo		

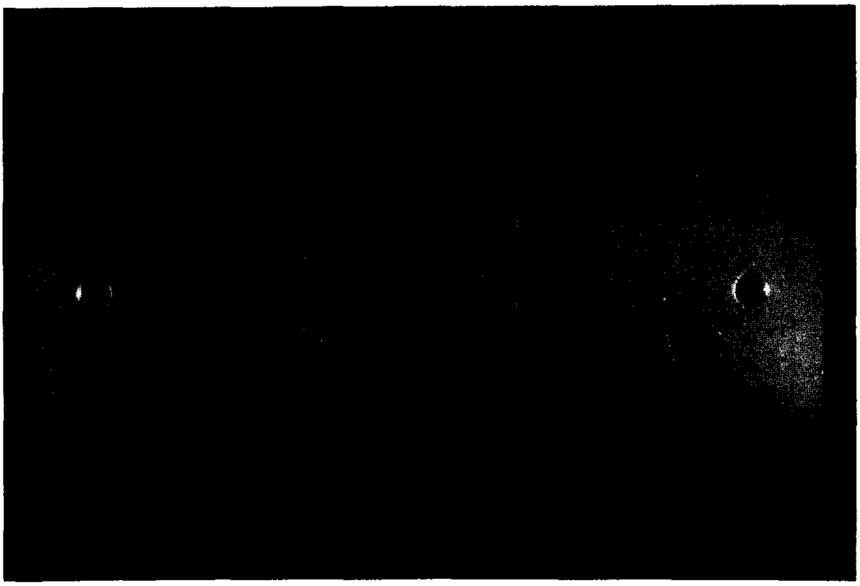

FIG. 2—*Appearance of aluminum alloy A95086 prior to exposure.*

TABLE 5—*Cleaning procedures for test specimens.*[a]

A95086
Acetone degrease
30% HNO_3 pickle (3 min)
Water rinse
Pumice scrub[b]
Water rinse
Alcohol rinse
Dry with towel
Forced hot air dry
Oven dry at 120°C
C70600
Acetone degrease
Water rinse
Pumice scrub (light)[b]
Water rinse
10% H_2SO_4 pickle (3 to 5 min)
Water rinse
Pumice scrub
Water rinse
Alcohol rinse
Dry with towel
Forced hot air dry
Oven dry at 120°C
K01501
Sand blasted
100% HCl pickle (15 to 45 min)
Water rinse
Pumice scrub[b]
Water rinse
Alcohol rinse
Acetone rinse
Dry with towel
Forced hot air dry
Oven dry at 120°C

[a] All specimens were lightly scraped to remove marine biofouling and loose corrosion products. This was followed in each case by pickling, pumice and detergent scrubbing and the remainder of the cleaning procedure. No detectable mass loss was noted on control specimens in any pickling treatment.

[b] Prior to exposure.

alloy 400 test racks (1.3 m long) were used to separately accommodate the C70600 copper-nickel and KO1501 steel specimens.

Eyebolts were affixed to the racks to allow rope support from a fixed structure at each site. The test racks with specimens already mounted were wrapped in plastic with two enclosed cotton bags of desiccant, crated, and shipped to each test site.

Exposures

At each of the 14 test sites, test racks were to be retrieved for removal of two specimens of each alloy after 0.5, 1, 3, and 5 years. Upon removal, specimens were lightly brushed/scraped

FIG. 3—*Assembled test rack prior to exposure.*

to remove excessive biofouling, packaged, and returned to the LaQue Center for evaluation. Photographic documentation of specimens and environmental monitoring were performed at those sites where feasible.

Evaluations

Upon receipt of specimens from each site, the "before-cleaning" appearance was photographically documented. Specimens were then cleaned of corrosion products and any biofouling attachments using the following procedures according to ASTM Standard Practice for Preparing, Cleaning, and Evaluating Corrosion Test Specimens (01-88):

for A95086-ambient temperature, 30% nitric acid (concentrated acid is preferred, but many tests have shown no detectable mass loss on controls within three minutes immersion)
for C70600-ambient temperature, 10% sulfuric acid
for KOI50 I-ambient temperature, 100% hydrochloric acid inhibited with antimony trioxide

Further details of the cleaning procedures are given in Table 5.

Weighing of specimens for mass loss determinations was then performed (± 0.1 g) and measurements of thickness loss or localized attack were obtained using a micrometer (± 0.0 I mm) or depth gage (± 0.0 I mm), respectively. Selected specimens were also photographed after cleaning to illustrate variations observed in the type or extent of corrosion.

Results and Discussion

Corrosion data for each material and exposure time are summarized in Table 6, indicating a rather wide range in both corrosion rates and depths of localized attack. To enable detailed examination and comparisons within and among the 14 test sites, data for each of the 240 specimens removed to date are tabulated in the Appendix, Tables 7 through 20. It should be noted that the original set of specimens sent to Australia were lost in a cyclone and a replacement set was provided. Their late entry into the program, therefore, yields only one-year results at this time.

Aluminum Alloy A95086

Aluminum-magnesium alloys (5000 series) generally have good resistance to both general and localized corrosion in seawater [1]. Some pitting or crevice corrosion, however, can be expected but the extent of such attack in surface seawater will be affected by a number of factors, including oxygen content, temperature, velocity, and crevices such as those areas shielded by the attachment of biofouling organisms or deposits of sand or silt [1,2,3]. Since the corrosion resistance depends upon the maintenance of a passive oxide film, aluminum-magnesium alloys would be expected to be most resistant in seawater that is well aerated, for example near the ocean surface. It is of interest, therefore, to note the variations in corrosion behavior from one site to another.

Mass loss data collected in this program (detailed in the Appendix) reflect the average corrosion rate for alloy A95086 decreased from 11 μm/year after 0.5 year to 7 μm/year after 1 year to 3 μm/year after three years. The corrosion rates compare favorably and are within the range of published data referenced previously. The corrosion rates are calculated from mass loss and, while they are of interest to assess trends of corrosion behavior versus time, one must compare the extent of pitting or crevice corrosion from one test site to another since this is the predominant mode of attack on aluminum alloys when they corrode in seawater. Depth of attack data are summarized in Fig. 4 and show no particular trend toward increasing depth of corrosion with time, as might be expected, except at the California, Japan, and Bohus-Malmon, Sweden sites. The maximum depth of localized attack on a

TABLE 6—*Summary of corrosion data for 14 worldwide seawater test sites.*

Alloy	Exposure Period, year	Corrosion Rate Range, μm/year	Average Thickness Loss Range, mm	Maximum Thickness Loss Range, mm	Maximum Depth of Localized Attack Range, mm
A95086	0.5	3 to 19	...	...	0.01 to 0.32
	1.0	3 to 12	...	...	0.02 to 0.68
	3.0	1 to 12	...	...	0.03 to 0.91
C70600	0.5	6 to 374	...	...	0.03 to 0.46
	1.0[a]	4 to 29	...	...	0.01 to 0.35
	3.0	2 to 24	...	...	0.01 to 2.68
K01501	0.5	82 to 550	0.08 to 0.59	0.16 to 0.95	...
	1.0	86 to 536	0.10 to 1.51	0.22 to 6.07	...
	3.0	62 to 224	0.72 to 2.58	0.92 to 6.07	...

[a] Excludes 1.5 and 2.0 year data from Denmark and California sites, respectively.

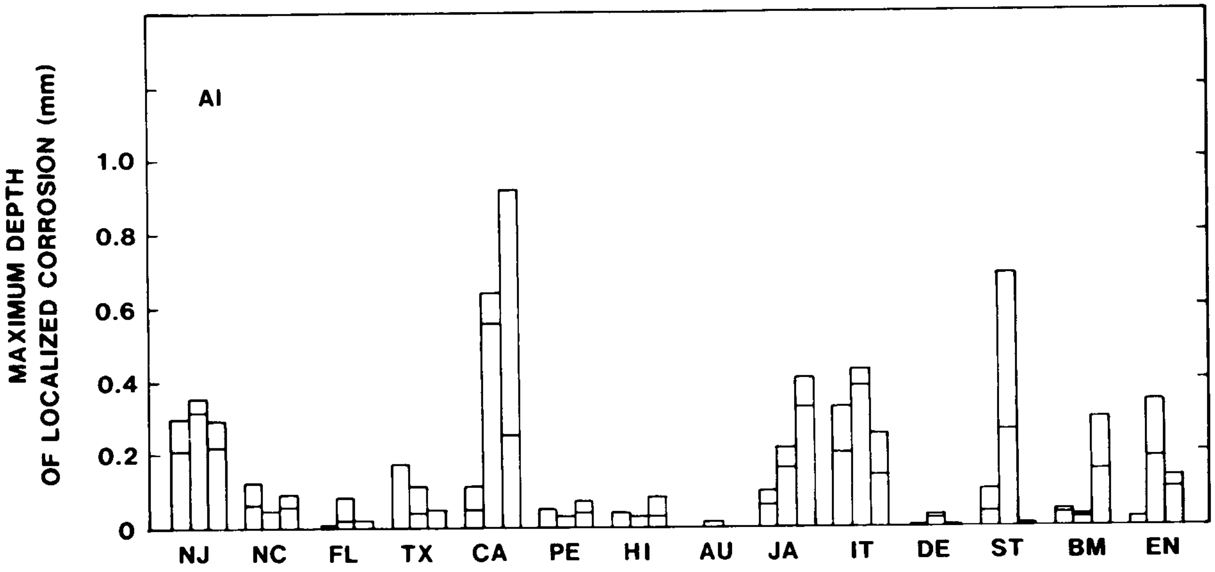

FIG. 4—*Localized corrosion data for A95086 aluminum alloy after 0.5, 1.0, and 3 year exposures* (bars 1–3, left to right) *in seawater at various sites.* (Note that the second bar for the California and Denmark sites represent exposure data for 2 and 1.5 years, respectively, and only 1.0 year results are reported for Australia.)

boldy exposed surface (0.9 mm after 3 years) occurred at Port Hueneme, California, a site where the test racks were subjected to constant wave action. This would normally bring a greater oxygen supply to the specimen surfaces lending to maintenance of the protective oxide film and rapid film repair when it is disrupted, for example by the chloride ion or by impingement. Opposing effects, however, could be also present since marine organism attachment and growth would be also encouraged. The shielding effect of the naturally created crevices, would tend to break down the passive film and lead to sites of crevice corrosion. This is the most likely mechanism leading to pitting of the aluminum alloy and was previously observed and documented by Ailor [1]. This localized corrosion mechanism, in turn, could be adversely affected by anode to cathode area ratios depending on the crevice geometry. Whether similar effects of seawater velocity were present at any other sites is not known, since complete documentation of site characteristics is difficult to obtain. The maximum pit depth reported by Brouillette [3] for alloy A95052 at the same Port Hueneme Harbor location was also 0.9 mm.

The second deepest localized attack (0.7 mm) occurred after one year at Studsvik, Sweden, a brackish water site. Even more noteworthy is the fact that no measurable localized attack was noted on the two Studsvik panels removed after three years. Since some measurable corrosion occurred on all four of the panels removed earlier, this perhaps can be attributed only to a matter of probability.

In regard to seawater temperature, there appears to be some evidence of lesser attack at the warmer sites, for instance North Carolina, Florida, Texas, Peru, Hawaii, and Australia. The very slight attack at the colder Denmark site, however, directly opposes that argument. The extent to which biofouling, silting index or any other environmental factors may affect results is impossible to assess due to insufficient documentation of such characteristics.

Copper-Nickel Alloy C 70600

The 90/10 Cu-Ni alloy C70600 selected for this program is known for its resistance to corrosion in seawater and to biofouling [4-10]. It's corrosion resistance is attributed to the growth of a protective corrosion product film which in the classical sense is "passive." This film growth, although initiated quickly upon exposure to seawater, may take very long times to reach steady state, eventually yielding very low corrosion rates on the order of 3 !lm/year [6]. As in the case of aluminum alloys, many factors within the seawater environment can affect the corrosion behavior of this alloy. It appears obvious from the data summarized in Table 6 that a large site to site variability exists.

Corrosion rate data shown in Fig. 5 demonstrate a general trend toward decreasing corrosion rates as a function of exposure time. Maximum depths of localized corrosion shown in Fig. 6 increased with increased time, though not linearly, at most of the sites. In contrast to the very low corrosion rate mentioned previously, specimens from only half of the test sites show a rate less than 10 !lm/year after three years. Reinhart [11] reported corrosion rates decreasing from 25 to 13 !lm/year for 6 months to two years of expsoure for this alloy at Point Mugu, California, not far from Port Hueneme. It is interesting to observe that the low rate calculated for both panels removed after three years at the North Carolina site equals that reported at the same site in long-term tests concluded eleven years earlier [6].

The highest corrosion rate was noted at Port Hueneme, California, on one panel removed after six months. The validity of the extremely high rate was questioned, but thorough review of the specimen history (original and final weights and dimensions) confirm this observation. Once again the constant wave action at this site appears to be the reason for this severe corrosion. The specimen in question was mounted on the end of the rack receiving the first full impingement from the seawater velocity. The companion specimen also exhibited a high

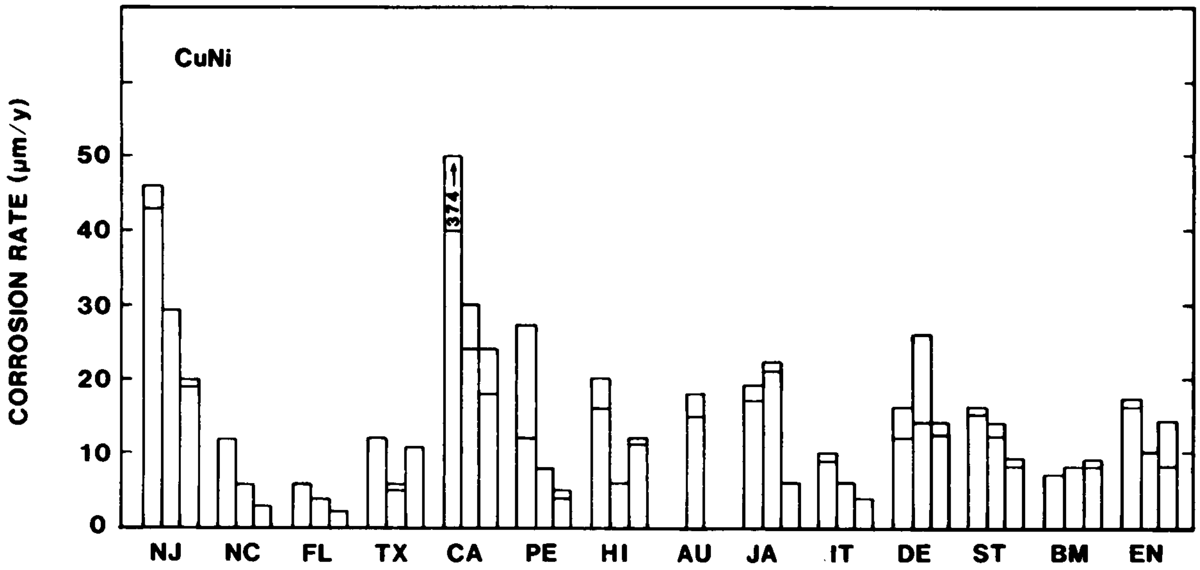

FIG. 5—*Corrosion rate data for copper-nickel alloy C70600 after 0.5, 1.0, and 3 year exposures* (bars 1–3, left to right) *in seawater at various sites.* (Note that the second bar for the California and Denmark sites represent exposure data for 2 and 1.5 years, respectively, and only 1.0 year results are reported for Australia.)

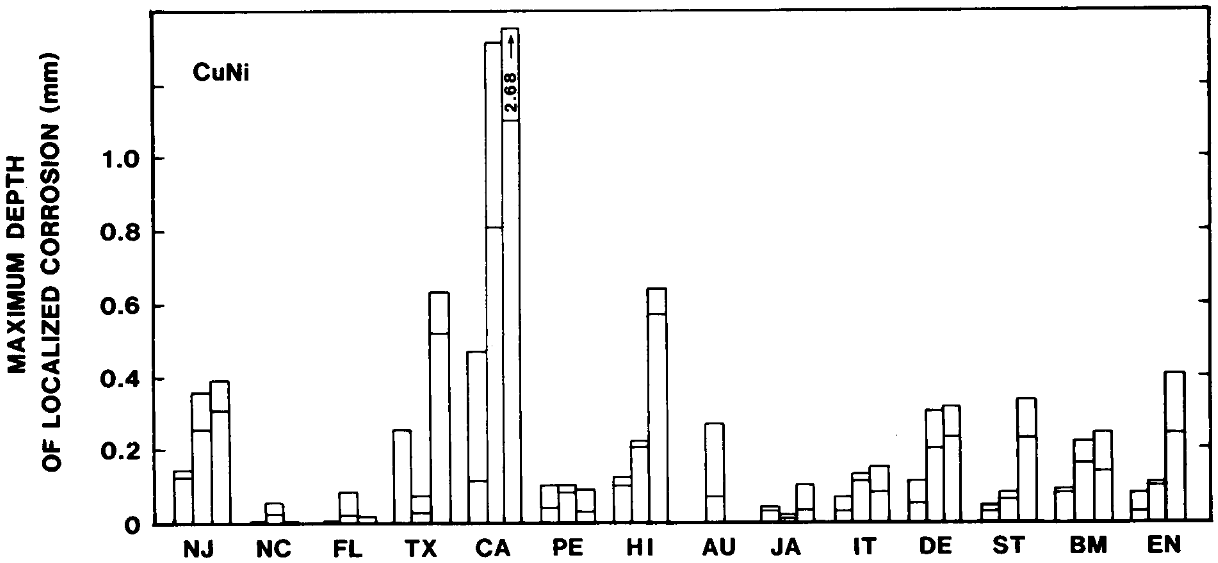

FIG. 6—*Localized corrosion data for copper-nickel alloy C70600 after 0.5, 1.0 and 3 year exposures* (bars 1–3, left to right) *in seawater at various sites.* (Note that the second bar for the California and Denmark sites represent exposure data for 2 and 1.5 years, respectively, and only 1.0 year results are reported for Australia.)

corrosion rate of 40 ILm/year but benefitted from being shielded by the first panel. In each successive removal, the leading edge panel exhibited significantly more corrosion (much of it on the leading edge) than its companion. The end of the rack, of course, shielded all panels except the first from the most severe impingement by wave action.

The deepest localized corrosion, noted in Fig. 6, also occurred at the California site on both panels removed after three years. A maximum depth of 2.68 mm was measured at the mounting washer as shown in Fig. 7 and is attributed to fretting corrosion. This severe localized attack results from a rather complex sequence of events beginning with a metal ion concentration cell type of crevice corrosion adjacent to the crevice former. The constant wave-driven seawater impingement serves to wash away some of the corrosion products such that small unfilmed areas become anodic to the much larger film covered surface. The corrosion process is then driven galvanically and proceeds under the mounting washer until the panel loosens from its previously tight mount. Physical motion then aggravates the situation by also serving to wear away corrosion products and constantly expose new unfilmed alloy surface that is anodic to the surrounding area. The net result, classified as fretting corrosion, literally "drills" through the test panel. The authors have experienced this type of attack on copper-base alloys on previous occasions when test specimens were exposed between ceramic insulators fastened to the test rack. This did not ensure a tight mount at all contact points and often resulted in localized corrosion, mistakenly labeled crevice corrosion. It was only after extensive investigation that the real corrosion mechanism was identified. To minimize this problem, all test specimens in this program were fastened to the racks with plastic bolts, washers, spacers and nuts, rather than using fixed ceramic insulators to slide the specimen into place as is often done.

Corrosion rates at the New Jersey site were also comparatively high. A high silt index usually present at the site appears to be the only environmental factor that can be identified to tie with the corrosion behavior noted. Just how this may affect the corrosion rates and

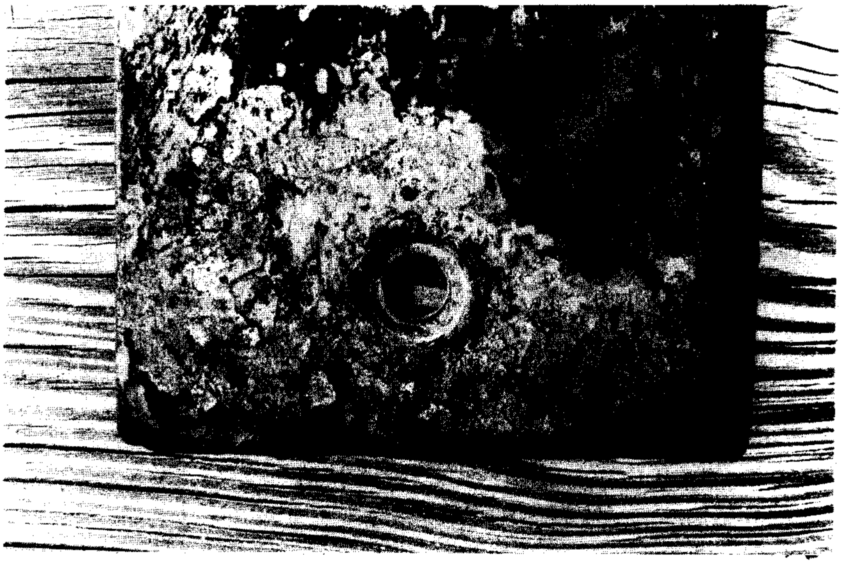

FIG. 7—*Fretting corrosion after 3 years under the mounting washer on alloy C70600 exposed at Port Hueneme, California.*

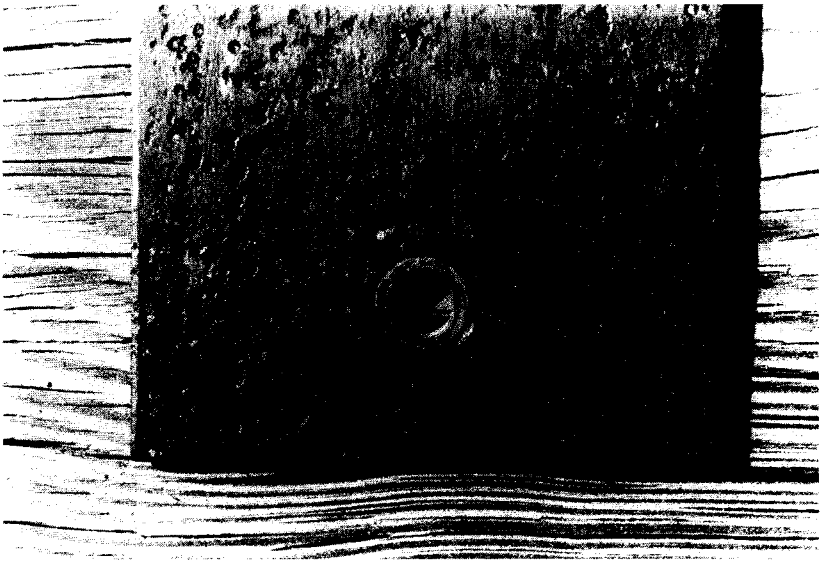

FIG. 8—*Pitting after 3 years on the side oriented toward the surface on alloy C70600 exposed at KeAhole, Kona, Hawaii.*

depth of localized corrosion has not been identified. Silt index information was not provided from other sites, precluding any comparisons based on this factor.

Deep pitting occurred on only one side of the specimens at the Hawaii site as depicted in Fig. 8. This was the top side of these specimens that were exposed horizontally. The bottom of these specimens was not pitted. Deposits, such as sand or silt, may have shielded the surface in small areas causing this pitting mechanism.

It is difficult to assess any effects of seawater temperature since much of the information reported contains averages or estimates. There is an indication, however, that corrosion is generally less at the warmer sites. Alloy C70600 generally displays good resistance to biofouling but some attachment has been noted. Figure 9 shows the test panels at the North Carolina site immediately after the rack was lifted from the water after three years of exposure. Most of the biofouling is attached to the rack or the plastic fasteners and overhangs the test panels. A few isolated instances of attachment and growth, however, can be noted. This appearance can be contrasted with the appearance of the steel panels (Fig. 10) after the same length of time.

It is well known that the corrosion resistance of copper-based alloys is sensitive to the sulfide ion in seawater, usually as hydrogen sulfide (fl$_2$S), when found [11-13]. None of the sites reported the presence of sulfides in the water, but it is also known that even brief presence, for example, from sulfide containing silt when stirred up from bottom anaerobic sediments, can be detrimental to the normally protective corrosion films on alloy C70600.

Carbon Steel KOJ50J

The corrosion of carbon steel in seawater is generally governed by the rate of diffusion of oxygen through the layers ofmst and marine organisms that attach and grow on all exposed surfaces. Corrosion rates in the range of 75 to 200 /Lm/year are found in the literature

FIG. 9—*90/10 CuNi after 3 years at Wrightsville Beach, North Carolina. Most of the biofouling is overlapping from the test rack and nonmetallic fasteners.*

FIG. 10—*Typical biofouling on carbon steel after 3 years' exposure at Wrightsville Beach, North Carolina.*

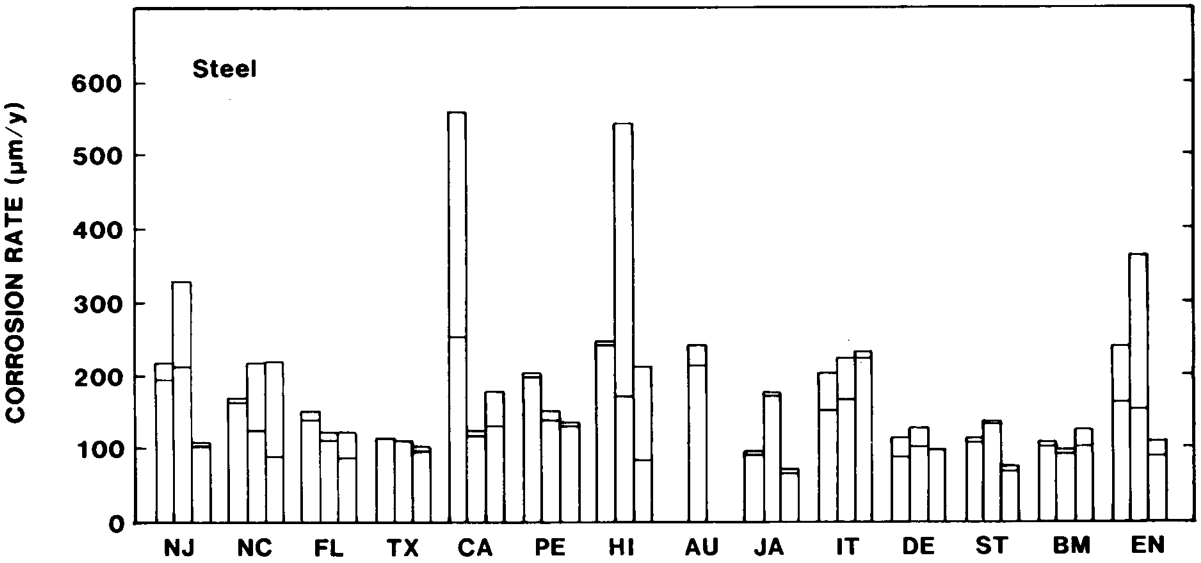

FIG. 11—*Corrosion rate data for K01501 steel after 0.5, 1.0 and 3 year exposures* (bars 1–3, left to right) *in seawater at various sites.* (Note that the second bar for the California and Denmark sites represent exposure data for 2 and 1.5 years, respectively, and only 1.0 year results are reported for Australia.)

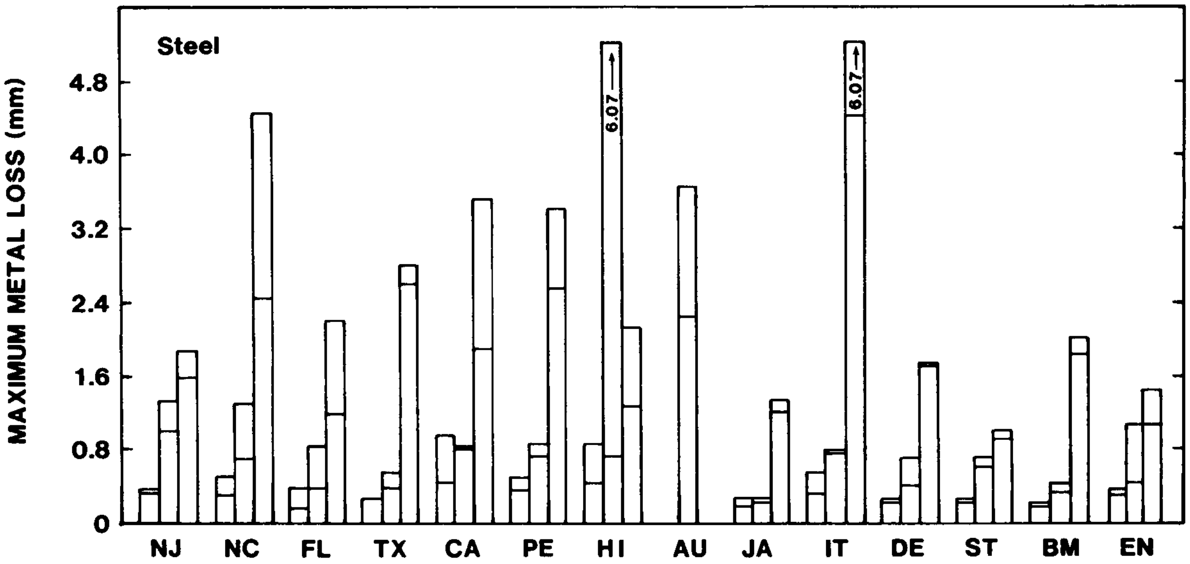

FIG. 12—*Maximum metal loss data for K01501 steel after 0.5, 1.0, and 3 year exposures* (bars 1–3, left to right) *in seawater at various sites.* (Note that the second bar for the California and Denmark sites represent exposure data for 2 and 1.5 years, respectively, and only 1.0 year results are reported for Australia.)

[2.4.5,15,16] for exposure times of at least six months. Although carbon or structural steels corrode over 100% of the surface exposed, the result is not uniform thickness loss. It is labeled as uniform corrosion in most of the results reported herein simply for lack of a better term that adequately describes the form of corrosion.

Average corrosion rates for carbon steel in this program were the same after six months and one year (168 and 172 jlm/year) and decreased to 117 jlm/year after three years, as indicated in Fig. 11. This is the commonly accepted rate throughout the industry for static exposure in relatively quiescent seawater. No clear trend of an increase or decrease in corrosion rate as a function of time at any site is apparent. This observation also compares favorably with documented experience [17].

An increase in the maximum depth of attack with increased exposure time is shown in Fig. 12, and the rate of increase appears constant with time. This is also expected of carbon steel in seawater based upon experience [15.16]. Complete penetration through the 6-mm panel was noted on one panel removed from the Hawaii site after one year (Fig. 13). This panel was exposed horizontally and therefore was subjected to deposits such as sand and silt settling out of the water and on to the top surface. Biofouling is also expected to be profuse, as shown in Fig. 12, at all of the test sites, since no pollution has been reported from any of the participants. Normally expected levels of dissolved oxygen, salinity and pH of both seawater and brackish water, as reported in Table 2, would be expected to support marine life. A previous example of rather severe localized penetration of a steel H-beam piling was described by LaQue [18]. In that case, sea urchins had been noted to have settled on the surface and remained for a long period of time. Their periodic movement was sufficient to brush away corrosion products so that the freshly exposed steel beneath the urchins was continually corroding at the relatively high rate characteristic of the early stages of corrosion of

FIG. 13—*Steel perforated after 1 year of exposure at the Hawaii coastal site. The panel was positioned horizontally.*

steel in seawater. The surrounding surface was at least partially covered and protected with the barrier layers ofbiofouling (hence a feeding ground for the sea urchins). This mechanism (caused by any mobile organism) may have occurred at the Hawaii site, but this has not been proven. Observations of this panel upon receipt at the LaQue Center, however, indicated significant rust remaining in the severely corroded area with significant biofouling having adhered to the surrounding area.

One other perforation of a steel panel occurred after 3 years' exposure at Genoa, Italy, where the test racks were exposed vertically. The companion specimen suffered a maximum thickness loss of 4.4 mm in a rather broad area, as noted in Fig. 14. These specimens also displayed evidence of heavy biofouling over most of the panel surfaces, except for rust displayed in the severely corroded area. This severe localized penetration could have been caused by the same mechanism described previously (associated with continual removal of corrosion products), particularly since LaQue's observation [18] was on a vertical surface.

Although theory predicts that an increase in the corrosion rate of carbon steel may be expected with increased water temperature [2,19], no clear evidence of this is apparent in this program. It may be noted, however, that maximum penetrations greater than 2.5 mm within three years occurred at half of the test sites, most of which are warm water sites. The Florida site is the most obvious exception.

Heavy growths of biofouling are also known to slough off steel surfaces and expose the base steel [5]. If the bare steel is exposed to any velocity of the seawater, before any barrier layer of biofouling forms, acceleration of corrosion can be expected. Copson [20] demonstrated a tripling of the corrosion rate of carbon steel at less than 2 mls velocity. This effect can be minimized if layers of marine organism growth provide an effective barrier to the seawater velocity. The complexity of such reactions or occurrences is affected by a number offactors, for example, dissolved oxygen, water temperature, rate of flow, biological nutrients

FIG. 14—*Corrosion of carbon steel after 3 years at Genoa, Italy.*

that encourage and support attachment and growth, etc. Detailed observations, monitoring, and reporting of environmental variables far beyond those collected here would be required to understand and document results any more than has been accomplished to date.

Observations

I. Average corrosion behavior was generally within limits of previously published data; however, some unexplainable corrosion behavior was observed on the three alloys at certain exposure sites.

2. Even with standardized testing methods, there really is no universal "natural seawater environment" that has been defined. As progress is made in advancing seawater corrosion technology, we must anticipate the unknown unknowns.

3. Frequent monitoring of the effects of individual and combined variables in the environments must be accomplished to better interpret the results of a testing program of this world-wide magnitude. For example:

   (a) The constant wave action at the California site had significant effects on test results.

   (b) The unusual exposure method at the Hawaii site affected results on at least two of the alloys.

   (c) The Key West, Florida, site is not affected by the presence of land as are most of the other sites; hence it is more representative of the open ocean. Yet test results show a comparatively mild corrosivity.

4. Experiments that rank materials may show differences in corrosion severity, but the ranking generally remains the same. Experiments that rank or characterize test sites can be significantly affected by many variables and the rankings may change. For instance the California site in this test program could be ranked the most severe (due to the wave action as described) on the corrosion of at least the three alloys tested, yet the seawater *per se* may be no different in corrosivity from any other site.

5. Perhaps a follow-up program should be planned with careful and in-depth thought given to the variables to be monitored and frequency of monitoring.

6. It has been said that 90% of the success in any testing program is in getting the samples back. If this is a true measure then the task group has been eminently successful toward accomplishing its objectives.

Acknowledgments

This project involved the commitment and support of numerous people beginning with the individual site representatives and the material suppliers listed in Tables I and 4, respectively. Special thanks must be given to the following: C. E. Bancroft, LaQue Center for Corrosion Technology, Inc., D. G. Beason, LaQue Center for Corrosion Technology, Inc., K. B. Horrell, LaQue Center for Corrosion Technology, Inc., A. G. S. Morton, David Taylor Research Center, and T. S. Lee, III, National Association of Corrosion Engineers (and original task group chairman).

References

[1] Ailor, W. H., "Ten-Year Seawater Tests on Aluminum," *Corrosion in Natural Environments. ASTM STP* 558. American Society for Testing and Materials, Philadelphia, 1974, p. 117.

[2] Beavers, J. A., Koch, G. H., and Berry, W. E., "Corrosion of Metals in Marine Environments-A State of the Art Report," MCIC Report 86-50, Metals and Ceramics Information Center, Battelle Memorial Institute, July 1986.

[3] Brouillette, C. V., *Corrosion.* National Association of Corrosion Engineers, Vol. 14, No.8, 1958, p. 352t.
[4] LaQue, F. L., *Marine Corrosion Causes and Prevention.* Wiley, New York, 1975, pp. 143-149.
[5] Efird, K. D., *Materials Performance,* National Association of Corrosion Engineers, Vol. 15, No.4, 1976, p. 16.
[6] Efird, K. D. and Anderson, D. B., *Materials Performance,* National Association of Corrosion Engineers, Vol. 14, No. II, 1975, p. 37.
[7] Bailey, G. L. J., *Journal oftheInstitute of Metals.* Vol. 79, 1951, p. 243.
[8] Kirk, W. W., Lee, T. S., and Lewis, R. 0., "Corrosion and Marine Fouling Characteristics of Copper-Nickel Alloys," *Proceedings.* CDA Conference on Copper Alloys in Marine Environments, Birmingham, England, April 1985.
[9] Steward, W. C. and LaQue, F. L., *Corrosion.* National Association of Corrosion Engineers, Vol. 8, No.8, 1952, p. 259.
[10] Gilbert, P. T., Paper No. 194, presented at NACE Annual Conference, National Association of Corrosion Engineers, Houston, TX, 1981.
[11] Reinhart, F. M., "Corrosion of Copper Alloys in Hydrospace," *Corrosion in National Environments. ASTM STP* 558. American Society for Testing and Materials, Philadelphia, 1974, p. 135.
[12] Gudas, J. P. and Hack, H. P., Paper No. 93, presented at NACE Annual Conference, National Association of Corrosion Engineers, Houston, TX, 1977.
[13] Gudas, J. P., Danek, G. J., and Niederberger, R. B., Paper No. 76, presented at NACE Annual Conference, National Association of Corrosion Engineers, 1976.
[14] Efird, K. D. and Lee, T. S., Paper No. 24, presented at NACE Annual Conference, National Association of Corrosion Engineers, Houston, TX, 1978.
[15] Tuthill, A. H. and Schillmoller, C. M., "Guidelines for Selection of Marine Materials," Marine Technology Society Conference, Washington, DC, June 1965.
[16] Di Gregorio, J. S. and Fraser, J. P., "Corrosion Tests in the Gulf Floor," *Corrosion in Natural Environments. ASTM STP* 558. American Society for Testing and Materials, Philadelphia, 1974, p.185.
[17] "General Seawater Corrosion," Bulletin A-1276, The International Nickel Company, New York, March 1978.
[18] LaQue, F. L., "Corrosion and Fouling," *Proceedings.* Third International Congress on Marine Corrosion and Fouling, Gaithersburg, MD, Oct. 1972.
[19] The Corrosion Handbook. Uhlig, H. H., ed., Electrochemical Society, Wiley, New York, 1948.
[20] Copson, H. R., *Corrosion,* National Association of Corrosion Engineers, Vol. 16, No.2, 1960, p. 861.

APPENDIX

TABLE 7—*Corrosion data for specimens exposed in Ocean City, New Jersey.*

Alloy	Exposure Duration, year	Mass Loss		Corrosion Rate,[a] µm/year	Thickness Loss[b]		Maximum Depth of Localized Attack,[b] mm	Observations[d]
		g	g/m^2		Average,[c] mm	Maximum, mm		
5086 aluminum (A95086)	0.5	0.9	12.7	10			0.30[e]	CC, P
	0.5	0.7	9.9	8	...	...	0.21[e]	CC, P
	1.0	0.9	12.5	5	...	...	0.31	P
	1.0	0.8	11.1	4	...	...	0.35	P
	3.0	1.5	21.3	3	...	...	0.22[e]	CC, P
	3.0	1.4	19.9	2	...	...	0.29	CC, P
90/10 CuNi (C70600)	0.5	14.2	197	46	...	...	0.14	P
	0.5	13.2	183	43	...	...	0.12	P
	1.0	18.6	263	29	...	...	0.35	P
	1.0	18.7	265	29	...	...	0.25	P
	3.0	37.1	515	20	...	...	0.38	UC, P, EA
	3.0	36.2	503	19	...	...	0.30	UC, P, EA
Carbon steel (K01501)	0.5	53.1	745	192	0.25	0.36	...	P
	0.5	58.7	824	213	0.25	0.33	...	P
	1.0	118.4	1655	209	0.54	1.00	...	UC
	1.0	181.5	2553	322	0.63	1.31	...	UC
	3.0	160.9	2260	100	1.11	1.57	...	UC
	3.0	179.8	2525	107	1.12	1.87	...	UC

[a] Assuming uniform corrosion over entire surface.

[b] Dash indicates measurements were less than 0.01 mm.

[c] Based on 14 measurements.

[d] UC = uniform corrosion.
CC = crevice corrosion beneath mounting washers.
NUC = nonuniform general corrosion.
P = bold surface pitting possibly associated with biofouling attachments if present.
BP = broad pits.
EA = edge attack.

[e] The reported depth of attack occurred at the mounting washers.

TABLE 8—*Corrosion data for specimens exposed in Wrightsville Beach, North Carolina.*

Alloy	Exposure Duration, year	Mass Loss		Corrosion Rate,[a] μm/year	Thickness Loss[b]		Maximum Depth of Localized Attack,[b] mm	Observations[d]
		g	g/m²		Average,[c] mm	Maximum, mm		
5052 aluminum (A95086)	0.5	1.2	17.0	13	...	...	0.12	P
	0.5	1.2	17.0	13	...	...	0.06	P
	1.0	1.2	17.0	6	...	...	0.05	P
	1.0	1.1	15.6	6	...	...	0.05	P
	3.0	1.7	24.1	3	...	...	0.09	P, CC
	3.0	1.6	22.7	3	...	...	0.06	P, CC
90/10 CuNi (C70600)	0.5	3.7	51.3	12	...	...	...	UC
	0.5	3.6	50.0	12	...	...	...	UC
	1.0	4.2	58.3	6	...	...	0.05	P
	1.0	4.1	56.9	6	...	...	0.02	P
	3.0	6.4	88.9	3	...	...	...	UC
	3.0	6.4	88.9	3	...	...	...	UC
Carbon steel (K01001)	0.5	44.6	626	161	0.15	0.31	...	UC
	0.5	45.5	639	165	0.22	0.50	...	UC
	1.0	69.6	976	123	0.30	0.68	...	UC
	1.0	118.0	1680	213	0.47	1.28	...	UC
	3.0	146.3	2055	87	1.36	2.44	...	UC, BP
	3.0	360.4	5062	214	2.58	4.44	...	UC, BP

[a] Assuming uniform corrosion over entire surface.

[b] Dash indicates measurements were less than 0.01 mm.

[c] Based on 14 measurements.

[d] UC = uniform corrosion.
NUC = nonuniform general corrosion.
CC = crevice corrosion beneath mounting washers.
P = pitting on bold surface possibly associated with biofouling attachments if present.
BP = broad pits.
EA = edge attack.

TABLE 9—*Corrosion data for specimens exposed in Key West, Florida.*

Alloy	Exposure Duration, year	Mass Loss		Corrosion Rate,[a] μm/year	Thickness Loss[b]		Maximum Depth of Localized Attack,[b] mm	Observations[d]
		g	g/m^2		Average,[c] mm	Maximum, mm		
5051 aluminum (A95086)	0.5	0.6	11.7	6	...	...	...	UC
	0.5	0.8	11.3	8	...	...	...	UC
	1.0	0.6	8.3	3	...	...	0.08	P
	1.0	0.5	6.9	3	...	...	0.02	P
	3.0	0.9	12.8	2	...	...	0.02	P
	3.0	0.8	11.4	1	...	...	0.02	P, CC
90/10 CuNi (C70600)	0.5	2.0	27.7	6	...	...	...	UC
	0.5	1.7	23.6	6	...	...	...	UC
	1.0	2.8	39.6	4	...	...	0.08	P
	1.0	2.7	38.2	4	...	...	0.02	P
	3.0	4.4	61.1	2	...	...	0.01	UC
	3.0	4.5	62.5	2	...	...	0.01	UC
Carbon steel (K01501)	0.5	37.5	527	136	0.10	0.16	...	UC
	0.5	40.2	565	146	0.13	0.36	...	UC
	1.0	60.7	852	107	0.25	0.81	...	UC
	1.0	67.1	941	119	0.24	0.39	...	UC
	3.0	207.8	2919	124	1.31	2.17	...	UC, BP
	3.0	140.2	1969	84	0.75	1.19	...	UC

[a] Assuming uniform corrosion over entire surface.

[b] Dash indicates measurements were less than 0.01 mm.

[c] Based on 14 measurements.

[d] UC = uniform corrosion.
NUC = nonuniform general corrosion.
CC = crevice corrosion beneath mounting washers.
P = pitting on bold surface possibly associated with biofouling attachments if present.
BP = broad pits.
EA = edge attack.

TABLE 10—*Corrosion data for specimens exposed in Freeport, Texas.*

Alloy	Exposure Duration, year	Mass Loss		Corrosion Rate,[a] μm/year	Thickness Loss[2]		Maximum Depth of Localized Attack,[b] mm	Observations[d]
		g	g/m^2		Average,[a] mm	Maximum, mm		
5086 aluminum (A95086)	0.5	1.1	15.3	11	...	...	0.17	P
				(only one panel of each alloy removed at 0.5 year)				
	1.0	1.4	19.4	7	...	...	0.04	P
	1.0	1.4	19.4	7	...	...	0.11	P
	3.0	1.8	25.6	3	...	...	0.05	P, CC
	3.0	1.9	27.0	3	...	...	0.05	P
90/10 CuNi (C70600)	0.5	4.0	56.6	12	...	...	0.25	P
				(only one panel of each alloy removed at 0.5 year)				
	1.0	3.4	48.1	5	...	...	0.02	P, CC
	1.0	3.7	52.4	6	...	...	0.07	P, CC
	3.0	20.7	288	11	...	...	0.62[f]	P, CC[e]
	3.0	20.1	279	11	...	...	0.52[f]	P, CC[e]
Carbon steel (K01501)	0.5	31.1	436	110	0.14	0.27	...	UC
				(only one panel of each alloy removed at 0.5 year)				
	1.0	59.4	833	105	0.21	0.37	...	UC
	1.0	59.5	835	105	0.28	0.53	...	UC
	3.0	151.9	2133	91	1.39	2.58	...	UC, BP
	3.0	165.5	2324	99	1.47	2.77	...	UC, BP

[a] Assuming uniform corrosion over entire surface.

[b] Dash indicates measurements were less than 0.01 mm.

[c] Based on 14 measurements.

[d] UC = uniform corrosion.
NUC = nonuniform general corrosion.
CC = crevice corrosion beneath mounting washers.
P = bold surface pitting possibly associated with biofouling attachments if present.
BP = broad pits.
EA = edge attack.

[e] Corrosion adjacent to mounting washer.

[f] The reported depth of attack occurred at the mounting washer.

TABLE 11—*Corrosion data for specimens exposed in Port Hueneme, California.*

Alloy	Exposure Duration, year	Mass Loss		Corrosion Rate,[a] μm/year	Thickness Loss[b]		Maximum Depth of Localized Attack,[b] mm	Observations[d]
		g	g/m^2		Average,[c] mm	Maximum, mm		
5086 aluminum (A95086)	0.5	1.7	24.1	18	...	...	0.05	P
	0.5	1.8	25.5	19	...	...	0.11	P
	2.0	5.1	70.7	13	...	...	0.55	P, CC
	2.0	3.1	43.0	8	...	...	0.63	P, CC
	2.9	6.8	96.6	12	...	...	0.91	P, CC
	2.9	3.7	52.5	6	...	...	0.25	P, CC
90/10 CuNi (C70600)	0.5	115.5	1604	374	...	...	0.46	P, EA
	0.5	12.5	174	40	...	...	0.11	P
	2.0	38.7	548	30	...	...	1.30	P, CC, EA
	2.0	30.3	429	24	...	...	0.80	P, CC
	2.9	44.3	615	24	...	...	2.68[e]	P, UC, CC, EA
	2.9	32.6	453	18	...	...	1.09[e]	P, UC, CC, EA
Carbon steel (K01501)	0.5	151.7	2131	550	0.59	0.95	...	UC
	0.5	67.7	951	245	0.25	0.44	...	UC
	2.0	127.1	1783	113	0.51	0.80	...	UC
	2.0	136.3	1912	121	0.55	0.83	...	UC
	2.9	205.8	2890	125	1.44	3.5	...	UC, BP
	2.9	284.4	3994	173	1.34	1.88	...	UC

[a] Assuming uniform corrosion over entire surface.
[b] Dash indicates measurements were less than 0.01 mm.
[c] Based on 14 measurements.
[d] UC = uniform corrosion.
NUC = nonuniform general corrosion.
CC = crevice corrosion beneath mounting washers.
P = bold surface pitting possibly associated with biofouling attachments if present.
BP = broad pits.
EA = edge attack.
[e] The reported depth of attack occurred at the mounting washer and is classified as fretting corrosion.

TABLE 12—*Corrosion data for specimens exposed in Talara, Peru.*

Alloy	Exposure Duration, year	Mass Loss		Corrosion Rate,[a] μm/year	Thickness Loss[b]		Maximum Depth of Localized Attack,[b] mm	Observations[d]
		g	g/m^2		Average,[c] mm	Maximum, mm		
5086 aluminum	0.5	1.1	15.3	12	...	...	0.05	P
(A95086)	0.5	1.0	13.9	10	...	...	0.05	P
	1.0	1.1	15.3	6	...	...	0.03	P
	1.0	1.1	15.3	6	...	...	0.03	P
	3.0	1.8	25.6	3	...	...	0.07	P
	3.0	1.8	25.6	3	...	...	0.04	P
90/10 CuNi	0.5	8.7	123	27	...	...	0.10	P
(C70600)	0.5	3.7	52.4	12	...	...	0.04	P
	1.0	5.1	72.2	8	...	...	0.08	P
	1.0	4.9	69.4	8	...	...	0.10	P
	3.0	8.8	122	5	...	...	0.09	UC
	3.0	6.9	95.8	4	...	...	0.03	UC
Carbon steel	0.5	55.4	777	196	0.23	0.48	...	UC
(K01501)	0.5	50.9	714	180	0.21	0.35	...	UC
	1.0	83.1	1166	147	0.39	0.73	...	UC
	1.0	76.3	1070	135	0.34	0.84	...	UC
	3.0	214.7	3015	129	1.66	3.40	...	UC, BP
	3.0	209.5	2942	126	1.81	2.52	...	UC, BP

[a] Assuming uniform corrosion over entire surface.

[b] Dash indicates measurements were less than 0.01 mm.

[c] Based on 14 measurements.

[d] UC = uniform corrosion.
NUC = nonuniform general corrosion.
CC = crevice corrosion beneath mounting washers.
P = bold surface pitting possibly associated with biofouling attachments if present.
BP = broad pits.
EA = edge attack.

TABLE 13—*Corrosion data for specimens exposed in KeAhole, Kona, Hawaii.*

Alloy	Exposure Duration, year	Mass Loss		Corrosion Rate,[a] μm/year	Thickness Loss[b]		Maximum Depth of Localized Attack,[b] mm	Observations[d]
		g	g/m^2		Average,[c] mm	Maximum, mm		
5086 aluminum (A95086)	0.5	1.2	17.0	13	...	...	0.04	P
	0.5	1.3	18.4	14	...	...	...	P
	1.0	1.3	18.0	7	...	...	0.03	P
	1.0	1.3	18.0	7	...	...	0.03	P
	3.2	1.5	21.3	3	...	...	0.03	P
	3.2	1.4	19.9	2	...	...	0.08[f]	P, CC
90/10 CuNi (C70600)	0.5	6.2	86.1	20	...	...	0.12	P
	0.5	5.0	69.4	16	...	...	0.10	P
	1.0	3.7	52.4	6	...	...	0.20	P
	1.0	3.6	51.0	6	...	...	0.22	P
	3.2	21.7	301	11	...	...	0.56	P,[e] UC
	3.2	22.6	314	12	...	...	0.63	P,[e] UC
Carbon steel (K01501)	0.5	66.3	931	240	0.35	0.84	...	P
	0.5	65.1	914	235	0.12	0.44	...	P
	1.0	93.1	1306	165	0.51	0.73	...	P
	1.0	303	4251	536	1.51	6.07[e]	...	P
	3.2	345.7	4855	204	1.71	2.11	...	UC
	3.2	133.7	1879	79	0.83	1.27	...	UC

[a] Assuming uniform corrosion over entire surface.

[b] Dash indicates measurements were less than 0.01 mm.

[c] Based on 14 measurements.

[d] UC = uniform corrosion.
NUC = nonuniform general corrosion.
CC = crevice corrosion beneath mounting washers.
P = bold surface pitting possibly associated with biofouling attachments if present.
BP = broad pits.
EA = edge attack.

[e] Perforated.

[f] The reported depth of attack occurred at the mounting washer.

TABLE 14—*Corrosion data for specimens exposed in Innisfail, Queensland, Australia.*

Alloy	Exposure Duration, year	Mass Loss		Corrosion Rate,[a] μm/year	Thickness Loss[b]		Maximum Depth of Localized Attack,[b] mm	Observations[d]
		g	g/m²		Average,[c] mm	Maximum, mm		
5086 aluminum	1.0	1.4	19.9	8	...	...	0.01	P
(A95086)	1.0	1.9	27.0	10	...	...	0.01	P
90/10 CuNi	1.0	9.3	129	15	...	...	0.07	UC, P
(C70600)	1.0	11.1	154	18	...	...	0.26[f]	UC, NUC, P, CC[e]
Carbon steel	1.0	112.1	1574	207	0.79	3.63	...	UC, BP
(K01501)	1.0	125.9	1768	233	0.97	2.23	...	UC, BP

[a] Assuming uniform corrosion over entire surface.

[b] Dash indicates measurements were less than 0.01 mm.

[c] Based on 14 measurements.

[d] UC = uniform corrosion.
NUC = nonuniform general corrosion.
CC = crevice corrosion beneath mounting washers.
P = pitting on bold surface possibly associated with biofouling attachments if present.
BP = broad pits.
EA = edge attack.

[e] Corrosion adjacent to mounting washer.

[f] The reported depth of attack occurred at the mounting washer.

TABLE 15—*Corrosion data for specimens exposed in Sakata Harbor, Japan.*

Alloy	Exposure Duration, year	Mass Loss g	Mass Loss g/m^2	Corrosion Rate,[a] μm/year	Thickness Loss[b] Average,[c] mm	Thickness Loss[b] Maximum, mm	Maximum Depth of Localized Attack,[b] mm	Observations[d]
5086 aluminum	0.5	1.1	15.3	11	...	...	0.06	P
(A95086)	0.5	0.6	8.3	6	...	...	0.10	P
	1.0	0.9	12.5	9	...	...	0.16	P, CC
	1.0	0.9	12.5	9	...	...	0.21	P, CC
	3.1	1.1	15.6	2	...	...	0.40	P, CC
	3.1	1.0	14.2	2	...	...	0.32	P, CC
90/10 CuNi	0.5	5.3	75.0	17	...	...	0.04	UC
(C70600)	0.5	6.0	85.0	19	...	...	0.03	UC
	1.0	6.7	94.9	21	...	...	0.01	UC
	1.0	5.3	75.0	17	...	...	0.02	UC
	3.1	47.3[e]	...	...	...	...	0.03	UC
	3.1	11.0	153	6	...	...	0.10	UC
Carbon steel	0.5	24.2	340	86	0.10	0.18	...	UC
(K01501)	0.5	25.1	352	89	0.15	0.27	...	UC
	1.0	47.3	663	168	0.10	0.22	...	UC
	1.0	48.1	675	171	0.18	0.27	...	UC, P
	3.1	117.9	1656	68	0.87	1.32	...	UC
	3.1	106.4	1494	62	0.77	1.21	...	UC

[a] Assuming uniform corrosion over entire surface.
[b] Dash indicates measurements were less than 0.01 mm.
[c] Based on 14 measurements.
[d] UC = uniform corrosion.
NUC = nonuniform general corrosion.
CC = crevice corrosion beneath mounting washers.
P = bold surface pitting possibly associated with biofouling attachments if present.
BP = broad pits.
EA = edge attack.

TABLE 16—*Corrosion data for specimens exposed in Genoa, Italy.*

Alloy	Exposure Duration, year	Mass Loss		Corrosion Rate,[a] µm/year	Thickness Loss[2]		Maximum Depth of Localized Attack,[b] mm	Observations[d]
		g	g/m²		Average,[c] mm	Maximum, mm		
5086 aluminum (A95086)	0.5	0.8	11.1	8	...	...	0.20	P
	0.5	0.7	9.7	7	...	...	0.32	P
	1.0	0.9	12.5	4	...	...	0.42	P
	1.0	1.9	26.4	10	...	...	0.38	P
	3.0	1.1	15.6	2	...	...	0.14	P
	3.0	1.2	17.0	2	...	...	0.25[f]	P, CC
90/10 CuNi (C70600)	0.5	3.0	42.5	9	...	...	0.03	P
	0.5	3.1	43.9	10	...	...	0.07	P
	1.0	3.9	55.2	6	...	...	0.13	P
	1.0	3.6	51.0	6	...	...	0.11	P
	3.0	7.0	97.2	4	...	...	0.15	UC
	3.0	7.5	104	4	...	...	0.08	UC
Carbon steel (K01501)	0.5	40.9	574	145	0.27	0.54	...	UC
	0.5	54.9	770	194	0.16	0.32	...	UC
	1.0	89.3	1253	158	0.35	0.79	...	UC
	1.0	120.7	1698	214	0.48	0.75	...	UC
	3.0	361.0	5070	215	2.38	4.42	...	UC, BP
	3.0	376.6	5289	224	2.27	6.07[e]	......	UC, BP

[a] Assuming uniform corrosion over entire surface.

[b] Dash indicates measurements were less than 0.01 mm.

[c] Based on 14 measurements.

[d] UC = uniform corrosion.
NUC = nonuniform general corrosion.
CC = crevice corrosion beneath mounting washers.
P = bold surface pitting possibly associated with biofouling attachments if present.
BP = broad pits.
EA = edge attack.

[e] Perforated.

[f] The reported depth of attack occurred at the mounting washer.

TABLE 16—*Corrosion data for specimens exposed in Genoa, Italy.*

Alloy	Exposure Duration, year	Mass Loss		Corrosion Rate,[a] μm/year	Thickness Loss[2]		Maximum Depth of Localized Attack,[b] mm	Observations[d]
		g	g/m^2		Average,[c] mm	Maximum, mm		
5086 aluminum (A95086)	0.5	0.8	11.1	8	. . .	. . .	0.20	P
	0.5	0.7	9.7	7	. . .	. . .	0.32	P
	1.0	0.9	12.5	4	. . .	. . .	0.42	P
	1.0	1.9	26.4	10	. . .	. . .	0.38	P
	3.0	1.1	15.6	2	. . .	. . .	0.14	P
	3.0	1.2	17.0	2	. . .	. . .	0.25[f]	P, CC
90/10 CuNi (C70600)	0.5	3.0	42.5	9	. . .	. . .	0.03	P
	0.5	3.1	43.9	10	. . .	. . .	0.07	P
	1.0	3.9	55.2	6	. . .	. . .	0.13	P
	1.0	3.6	51.0	6	. . .	. . .	0.11	P
	3.0	7.0	97.2	4	. . .	. . .	0.15	UC
	3.0	7.5	104	4	. . .	. . .	0.08	UC
Carbon steel (K01501)	0.5	40.9	574	145	0.27	0.54	. . .	UC
	0.5	54.9	770	194	0.16	0.32	. . .	UC
	1.0	89.3	1253	158	0.35	0.79	. . .	UC
	1.0	120.7	1698	214	0.48	0.75	. . .	UC
	3.0	361.0	5070	215	2.38	4.42	. . .	UC, BP
	3.0	376.6	5289	224	2.27	6.07[e]	. . .. . .	UC, BP

[a] Assuming uniform corrosion over entire surface.

[b] Dash indicates measurements were less than 0.01 mm.

[c] Based on 14 measurements.

[d] UC = uniform corrosion.
NUC = nonuniform general corrosion.
CC = crevice corrosion beneath mounting washers.
P = bold surface pitting possibly associated with biofouling attachments if present.
BP = broad pits.
EA = edge attack.

[e] Perforated.

[f] The reported depth of attack occurred at the mounting washer.

TABLE 17—*Corrosion data for specimens exposed in Kyndby Isefjord, Sjcelland, Denmark.*

Alloy	Exposure Duration, year	Mass Loss		Corrosion Rate,[a] μm/year	Thickness Loss[b]		Maximum Depth of Localized Attack,[b] mm	Observations[d]
		g	g/m^2		Average,[c] mm	Maximum, mm		
5086 aluminum (A95086)	0.5	1.3	18.0	13	...	...	...	UC
	0.5	0.4	5.5	4	...	...	...	UC
	1.5	1.2	16.6	4	...	...	0.02	P
	1.5	1.3	18.0	5	...	...	0.03	P
	3.1	2.2	31.3	4	...	...	...	UC
	3.1	2.2	31.3	4	...	...	...	UC
90/10 CuNi (C70600)	0.5	5.0	70.8	16	...	...	0.11[f]	P CC[e]
	0.5	3.9	55.2	12	...	...	0.05[f]	P CC[e]
	1.5	12.3	174	14	...	...	0.20	P CC[e]
	1.5	22.0	312	26	...	...	0.30	P CC[e]
	3.1	27.7	385	14	...	...	0.31[f]	UC, NUC, CC[e]
	3.1	24.4	339	13	...	...	0.30	UC, NUC, CC[e]
Carbon steel (K01501)	0.5	23.2	325	82	0.17	0.25	...	UC
	0.5	30.0	421	106	0.14	0.22	...	UC
	1.5	68.6	962	95	0.30	0.41	...	UC
	1.5	92.4	1296	122	0.39	0.70	...	UC
	3.1	157.6	2213	91	0.98	1.69	...	UC, BP
	3.1	155.3	2181	90	1.13	1.72	...	UC, BP

[a] Assuming uniform corrosion over entire surface.
[b] Dash indicates measurements were less than 0.01 mm.
[c] Based on 14 measurements.
[d] UC = uniform corrosion.
NUC = nonuniform general corrosion.
CC = crevice corrosion beneath mounting washers.
P = bold surface pitting possibly associated with biofouling attachments if present.
BP = broad pits.
EA = edge attack.
[e] Corrosion adjacent to mounting washer.
[f] The reported depth of attack occurred at the mounting washer.

TABLE 18—*Corrosion data for specimens exposed in Studsvik, Sweden.*

Alloy	Exposure Duration, year	Mass Loss		Corrosion Rate,[a] μm/year	Thickness Loss[b]		Maximum Depth of Localized Attack,[b] mm	Observations[d]
		g	g/m^2		Average,[c] mm	Maximum, mm		
5086 aluminum (A95086)	0.5	0.3	4.2	3	. . .	. . .	0.04	P
	0.5	1.4	13.9	14	. . .	. . .	0.10	P
	1.0	1.9	26.4	10	. . .	. . .	0.68	P
	1.0	1.2	16.6	6	. . .	. . .	0.26	P
	3.2	1.3	18.5	2	. . .	. . .	. . .	UC
	3.2	1.2	17.0	2	. . .	. . .	. . .	UC
90/10 CuNi (C70600)	0.5	5.0	70.8	16	. . .	. . .	0.05	P
	0.5	4.7	66.6	15	. . .	. . .	0.03	P
	1.0	7.7	109	12	. . .	. . .	0.06	P
	1.0	8.8	125	14	. . .	. . .	0.08	P
	3.2	18.6	258	9	. . .	. . .	0.33	UC, P
	3.2	16.2	225	8	. . .	. . .	0.23	UC, P
Carbon steel (K01501)	0.5	30.6	429	108	0.16	0.25	. . .	UC
	0.5	29.1	408	103	0.15	0.22	. . .	UC
	1.0	72.2	1013	128	0.46	0.60	. . .	UC
	1.0	74.1	1040	131	0.36	0.69	. . .	UC
	3.2	122.8	1725	69	0.72	1.00	. . .	UC
	3.2	111.0	1559	62	0.74	0.92	. . .	UC

[a] Assuming uniform corrosion over entire surface.
[b] Dash indicates measurements were less than 0.01 mm.
[c] Based on 14 measurements.
[d] UC = uniform corrosion.
NUC = nonuniform general corrosion.
CC = crevice corrosion beneath mounting washers.
P = bold surface pitting possibly associated with biofouling attachments if present.
BP = broad pits.
EA = edge attack.

TABLE 19—*Corrosion data for specimens exposed in Bohus-Malmon, Sweden.*

Alloy	Exposure Duration, year	Mass Loss		Corrosion Rate,[a] μm/year	Thickness Loss[b]		Maximum Depth of Localized Attack,[b] mm	Observations[d]
		g	g/m²		Average,[c] mm	Maximum, mm		
5086 aluminum (A95086)	0.5	1.1	15.6	11	...	...	0.03	P
	0.5	1.0	14.1	10	...	...	0.04	P
	1.0	1.6	22.1	8	...	...	0.02	P
	1.0	1.5	20.8	8	...	...	0.03	P
	3.1	2.4	34.1	4	...	...	0.29	P
	3.1	2.5	35.5	4	...	...	0.15	P
90/10 CuNi (C70600)	0.5	2.4	33.3	7	...	...	0.08	P
	0.5	2.2	30.5	7	...	...	0.09	P
	1.0	5.0	70.8	8	...	...	0.22	P, CC[e]
	1.0	5.3	75.0	8	...	...	0.16	P, CC[e]
	3.1	14.8	206	8	...	...	0.24	P
	3.1	17.7	246	9	...	...	0.14	P
Carbon steel (K01501)	0.5	28.3	397	103	0.08	0.18	...	UC
	0.5	26.3	369	95	0.13	0.21	...	UC
	1.0	48.6	682	86	0.24	0.35	...	UC
	1.0	53.2	746	94	0.24	0.43	...	UC
	3.1	171.9	2414	99	1.11	2.00	...	UC, BP
	3.1	205.8	2890	119	1.19	1.83	...	UC

[a] Assuming uniform corrosion over entire surface.

[b] Dash indicates measurements were less than 0.01 mm.

[c] Based on 14 measurements.

[d] UC = uniform corrosion.
NUC = nonuniform general corrosion.
CC = crevice corrosion beneath mounting washers.
P = bold surface pitting possibly associated with biofouling attachments if present.
BP = broad pits.
EA = edge attack.

[e] Corrosion adjacent to mounting washer.

TABLE 20—*Corrosion data for specimens exposed in Isle of Wight, England.*

Alloy	Exposure Duration, year	Mass Loss g	Mass Loss g/m^2	Corrosion Rate,[a] μm/year	Thickness Loss[b] Average,[c] mm	Thickness Loss[b] Maximum, mm	Maximum Depth of Localized Attack,[b] mm	Observations[d]
5086 aluminum (A95086)	0.5	0.9	12.5	9	...	...	0.02	P
	0.5	1.5	20.8	15	...	...	0.02	P
	1.0	2.3	31.9	12	...	...	0.33	P
	1.0	2.1	29.1	11	...	...	0.18	P
	3.1	3.0	42.6	5	...	...	0.10	P
	3.1	3.3	46.9	6	...	...	0.13	P
90/10 CuNi (C70600)	0.5	5.4	76.5	17	...	...	0.03	P
	0.5	5.0	70.8	16	...	...	0.08	P
	1.0	6.3	89.2	10	...	...	0.10	P
	1.0	6.3	89.2	10	...	...	0.11	P
	3.1	15.9	221	8	...	...	0.40[f]	NUC, CC[e]
	3.1	28.2	392	14	...	...	0.24[f]	NUC, CC[e]
Carbon steel (K01501)	0.5	64.0	898	226	0.26	0.36	...	UC
	0.5	44.1	619	156	0.18	0.31	...	UC
	1.0	83.9	1177	148	0.34	0.44	...	UC
	1.0	201.4	2820	355	0.85	1.06	...	UC
	3.1	147.0	2065	84	0.78	1.07	...	UC
	3.1	182.6	2565	104	0.97	1.42	...	UC

[a] Assuming uniform corrosion over entire surface.
[b] Dash indicates measurements were less than 0.01 mm.
[c] Based on 14 measurements.
[d] UC = uniform corrosion.
NUC = nonuniform general corrosion.
CC = crevice corrosion beneath mounting washers.
P = bold surface pitting possibly associated with biofouling attachments if present.
BP = broad pits.
EA = edge attack.
[e] Corrosion adjacent to mounting washer.
[f] The reported depth of attack occurred at the mounting washer.

Robert M. Kain[1]

Crevice Corrosion Resistance of Stainless Steels in Waters Containing Chloride and Sulfate Ions

REFERENCE: Kain, R. M., "Crevice Corrosion Resistance of Stainless Steels in Waters Containing Chloride and Sulfate Ions," *Corrosion in Natural Waters. ASTM STP 1086.* C. H. Baloun, Ed., American Society for Testing and Materials, Philadelphia, 1990, pp. 37-53.

ABSTRACT: Crevice corrosion behavior for a series of austenitic and duplex stainless alloys was determined in a number of simple solutions as well as in diluted natural seawater containing up to 10 g/L CI- and 10 g/L S04 ~. Remote crevice assembly technology using zero resistance ammeters revealed differences in initiation and propagation resistance. Effects of solution ion concentration, alloy composition and the influence of crevice geometry and biological activity are discussed.

While S30400 and S31600 were found to be susceptible in all tests considered, other materials (N08904 and S32550), and especially a 6% molybdenum alloy (S31254), were substantially more resistant. Test results indicate some beneficial effects of sulfate at lower levels of chloride. However, at high chloride levels, high sulfate appears detrimental. At comparable chloride levels crevice corrosion was more severe in diluted natural seawater than in synthetic solutions.

This work is part of an on-going study involving additional alloys and more varied water chemistries. The ultimate goal of this research is the preparation of a *Crevice Corrosion Atlas for Stainless Steel in Waters.*

KEY WORDS: stainless steels, crevice corrosion, diluted natural seawater, chloride/sulfate, remote crevice assembly, initiation resistance, propagation resistance, crevice geometry, biological influence

Background

Because of their corrosion resistance, strength, and fabricability, stainless steels are logical materials for consideration in water related engineering projects. Stainless steels, as a whole, offer considerable resistance to a wide range of corrodants. Each, however, may be limited by the aggressiveness of specific environments. Chlorides are particularly troublesome since they can promote localized corrosion in the form of cracks, pits, and underdeposit or crevice attack for susceptible grades of stainless steel. Under ambient conditions, crevice corrosion is the predominant mode of stainless steel failure in chloride containing waters. Resistance to this form of attack is highly dependent on a number of inter-related metallurgical, geometric, and environmental factors. These factors influence both the initiation and propagation stages of crevice corrosion.

Frequently, questions are raised as to safe limits for chlorides. This is especially relevant to the use of stainless steel in, for example, reverse osmosis (RO) [1] service since mineral

---

[1] Corrosion scientist, LaQue Center for Corrosion Technology, Inc., Post Office Box 656, Wrightsville Beach, NC 28480.

content may vary considerably from one location to another. Furthermore, the RO process itself produces a brine which may be significantly more concentrated in chloride than the bulk water source. For RO technology, corrosion resistance is important not only from the obvious concerns of product contamination and equipment integrity but also for the need to minimize the release of corrosion products which are detrimental to membrane performance.

Conventional grades of stainless steel, as well as many higher alloyed stainless type materials, are known to be susceptible to crevice corrosion in seawater [2]. Type 304 (UNS-S30400) and Type 316 (UNS-S31600) may also exhibit crevice attack in estuarian waters and other natural waters of lower chloride content [3-5]. Tests in simulated Colorado River water and potable water have also identified crevice corrosion for S30400 at chloride contents as low as 100 mg/L (ppm) [6]. However, it was also noted that S30400 was resistant in at least 80 percent of the cases involving chlorides in the range of 100 to 1000 mg/L.

The present study addresses the performance of several alloys in aqueous environments containing bulk chloride levels of I and 10 g/L. Again, since water sources may vary considerably, sulfate content was varied by three orders of magnitude starting at 0.1 g/L. While the objective of this work is to develop general engineering guidelines for material selection, it is recognized that other environmental factors may be encountered in service. These include variations in bulk water, velocity, dissolved oxygen (O_2), pH, the presence of hydrogen sulfide *(HzS),* and the use of chlorine as a pretreatment. Previous studies, for example, have described a marked effect oflowering the bulk environment pH from 6 to 3 for several stainless steels in water containing I and 10 g/L chloride [7]. The present work is part of a larger program intended to establish a *Corrosion Atlas for Stainless Steel in Water.*

Crevice Corrosion

As its name suggests, crevice corrosion is more than an alloy-environment related phenomenon. Crevices provide the opportunity for local oxygen cells to develop which can frequently result in subsequent environmental changes within the shielded area. Depending on crevice geometry, hydrolysis reactions may progress sufficiently to lower the pH and raise the chloride concentration within the crevice to levels which will cause breakdown of the stainless steel's passive film. The concentration of chlorides within the crevice confines can be many times greater than that typically present in the bulk environment. Whether or not there is a safe limit for chlorides, for example, depends upon the metallurgical condition of the materials and severity of crevices which may be present.

Recent studies have described the effect of crevice geometry, bulk environment chloride content and other factors on the resistance of S30400 and S31600 stainless steel. Use of a mathematical model [8], for example, has shown that increasing the tightness of a crevice (smaller gap or space between components) will result in more rapid initiation of crevice corrosion [3]. Likewise, increasing the crevice depth will render a material more susceptible to initiation. For a given set of geometric conditions, the tendency for crevice corrosion will increase with increased chloride concentrations. Apparent differences in alloy behavior from one application to another involving similar environments can be often attributed to slight differences in crevice geometry.

Crevices fall into two categories; those occurring naturally and those created during fabrication and assembly of stainless steel equipment. The former are likely to be encountered as a result of debris and deposits. Marine attachments, such as barnacles, have long been associated with localized corrosion of stainless steels in seawater. In many cases, naturally occurring crevice conditions can be minimized by cleanliness and adherence to optimum operating flow conditions. There has been also a growing awareness that certain biological species can colonize on stainless steel surfaces. Some have the ability to concentrate relatively low levels of bulk chloride and promote localized attack [9]. Man-made crevice conditions may involve metal-to-metal crevices such as those found at condenser tube-tubesheet interfaces and at fastener connections. Less obvious sites may be found at defective welds and other microcrevice sites associated with processing and machining.

Nonmetallic crevice formers are usually identified with sheet and a-ring type gasketing materials on piping systems and seal beads on plate type heat exchangers. Other nonmetallic crevice conditions may arise at temporary connections such as hose and pipe clamp joints. Vinyl tubing and nylon compression fittings, for example, have been identified as potential sites capable of causing crevice corrosion for some stainless materials in natural seawater [ID,I1]. In general, nonmetallic type crevice formers are viewed as being more severe since they are more deformable and, hence, can result in tighter gaps. It is recognized, however, that metal-to-metal crevices have two surfaces from which metal ions can enter the crevice solution to promote hydrolysis. As such, conditions associated with comparable geometries can be more severe for metal-to-metal crevices than for nonmetal to metal [8].

Several recent studies have been aimed at quantifying actual crevice conditions for a variety of laboratory prepared crevice assemblies and service type fabricated conditions [3,6,12,13]. It has been shown that many of these produce extremely tight crevices of the type most likely to cause initiation of corrosion. Minor variations in the degree of tightness or crevice gap can sometimes have greater significance than variations in bulk environment chemistry.

Experimental

Materials

Five commercial grade alloys were selected to represent a range of compositions expected to offer varying degrees of corrosion resistance. Conventional grades of austenitic stainless steel S30400 and the 2% molybdenum containing S31600 served as control materials. The corrosion resistance of these two alloys in a variety of natural waters and numerous laboratory prepared chloride containing environments has been reported elsewhere [2-7]. Also included were two higher alloyed austenitics, alloy N08904 (20Cr-25Ni-4Mo-l.5Cu) and alloy S31254 (20Cr-18Ni-6Mo-0.8Cu), and a duplex stainless steel alloy S32550 (26Cr-6Ni-3Mo-l.8Cu). The latter two have nitrogen additions to stabilize austenite. These three alloys have high corrosion resistance to many chemical environments and have found some application in marine service. Under more adverse conditions, all three alloys may exhibit some degree of susceptibility to localized attack in ambient temperature seawater [2,10]. Laboratory controlled tests in natural seawater showed that the corrosion resistance of alloys S32550 and S31254 could be influenced significantly by surface condition of the material and the degree of crevice assembly tightness [14]. Alloy N08904 generally offers more resistance to initiation and propagation than the conventional grades [14,15]. In some cases, however, comparable behavior with S31600 has been observed [2].

Table 1 gives the heat analyses for the preceding alloys along with their common identification.

Specimens

Remote crevice assemblies (RCA), described in more detail elsewhere [7,15] were utilized in the present study. Briefly, each specimen consisted of two "L" shaped members of different size. The larger "cathode" member had a nominal surface area 37 times that of a smaller

TABLE 1—*Chemical analysis of materials tested in RO type waters.*

Commercial Identification	Unified Numbering	Composition, weight %									
		Cr	Ni	Mo	Cu	C	Si	Mn	S	P	N
AISI Type 304	S30400	18.5	8.3	0.08	0.15	0.061	0.48	1.38	0.014	0.019	0.027
AISI Type 316	S31600	17.1	11.3	2.24	0.16	0.058	0.60	1.65	0.011	0.022	0.022
Alloy 904L	N08904	19.7	27.1	4.59	1.32	0.02	0.36	1.49	0.001	0.022	NR[a]
Ferralium 255™	S32550	26.2	5.6	3.2	1.75	0.02	0.37	0.77	NR	NR	0.190
254SMO	S31254	19.9	18.2	6.11	0.75	0.016	0.49	0.48	0.003	0.023	0.205

[a] NR = not reported.

"anode" or crevice member. Physical separation but electrical connection between anode and cathode members through a zero resistance ammeter enabled current measurements which signaled initiation and quantified subsequent propagation of crevice corrosion. In addition, coupled member potentials were also monitored routinely throughout the test period which lasted 1000 h.

All specimen members were prepared with a wet ground 120 grit silicon carbide (SiC) finish (approximately a No.4 finish). Crevices were formed on the anode (1.5 by 1.5 cm) member by positioning it between two acrylic blocks in the device shown in Fig. I and tightening to an initial torque value of2.8 Nm (25 in ·Ib). A plastic tape insert between the acrylic and metal sample helped to insure a tighter and, hence, more severe crevice [15,16]. Examples of crevice gaps produced in remote crevice assembly configurations are shown in Fig. 2. Conditions such as these are likely to be encountered at gaskets and seals in plant equipment.

Environments

Table 2 identifies the various test environments considered. Seven solutions of varying chloride and sulfate contents were prepared with distilled water and the addition of reagent grade sodium chloride and sodium sulfate. Two additional environments were prepared by dilution of natural seawater with distilled water to chloride levels approximating half strength and lfo strength. In all cases, the pH values were near neutral.

Apparatus and Test Conditions

Two nonmetallic tanks measuring 30 by 30 by 60 cm (length) were utilized for each environment. Both were connected to a common heated reservoir by nonmetallic piping and a magnetic drive pump similar to the apparatus shown in ASTM Guide for Crevice Corrosion Testing of Iron Base and Nickel Base Stainless Alloys in Seawater and Other Chloride-Containing Aqueous Environments (G-78-83). Temperature of the test solutions was controlled at 30 ± 2°C. The solutions were recirculated at a rate of about 300 cm/min per tank producing nominally quiescent conditions. Each test tank contained one of the duplicate crevice assemblies for each of the five alloys.

Cathode and crevice members were positioned end to end about 3 cm apart and rigidly secured to a support resting on the tank rim. All electrical connections were made above the waterline using the stem portion of respective members. While this eliminated potential undesirable crevice sites, the resulting waterline was a problem in some cases.

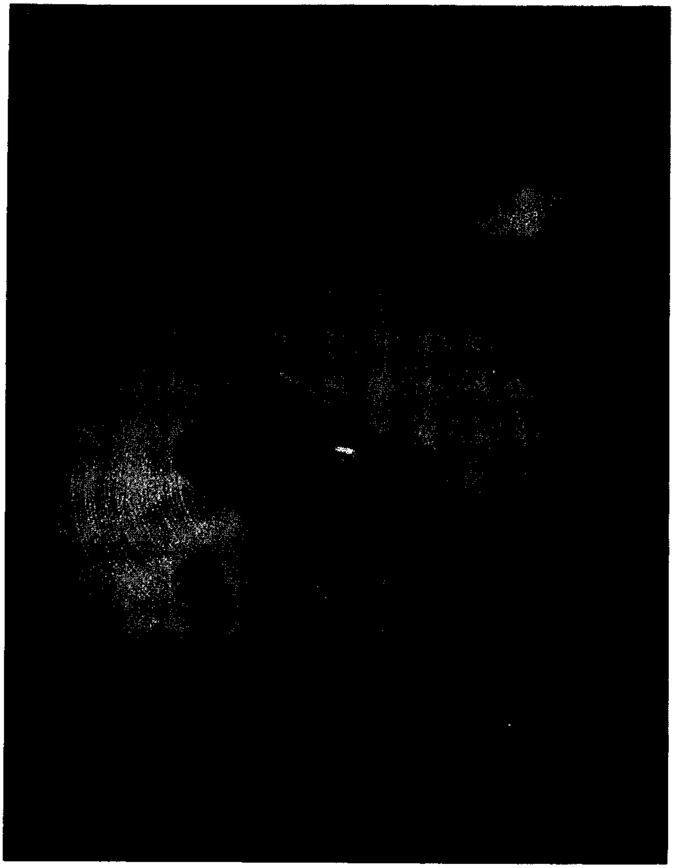

FIG. 1—*Remote crevice assembly "anode" member positioned and secured between acrylic blocks. The severity of the crevice was increased by the presence of a deformable tape insert located between the blocks and the test metals.*

TABLE 2—*Variations in water chemistry considered.*

Environment	Cl^-, g/L	$SO_4^=$, g/L	$Cl^-:SO_4^=$, ratio	$SO_4^=:Cl^-$, ratio	pH	Conductivity, mmhos/cm
Diluted seawater[a]	1	0.1	10:1	0.1:1	7.0	4
	10	1	10:1	0.1:1	8.3	31
Synthetic[b]	1	1	1:1	1:1	7.0	6
	1	10	0.1:1	10:1	7.3	20
	10	0.1	100:1	0.01:1	7.1	28
	10	0.5	20:1	0.05:1	7.1	28
	10	1	10:1	0.1:1	7.2	28
	10	5	2:1	0.5:1	6.9	35
	10	10	1:1	1:1	7.0	44

NOTE—Dissolved oxygen levels ranged from 5.9 to 6.4 mg/L.

[a] Full strength natural seawater diluted with distilled water.

[b] Prepared with distilled water, sodium chloride, and sodium sulfate.

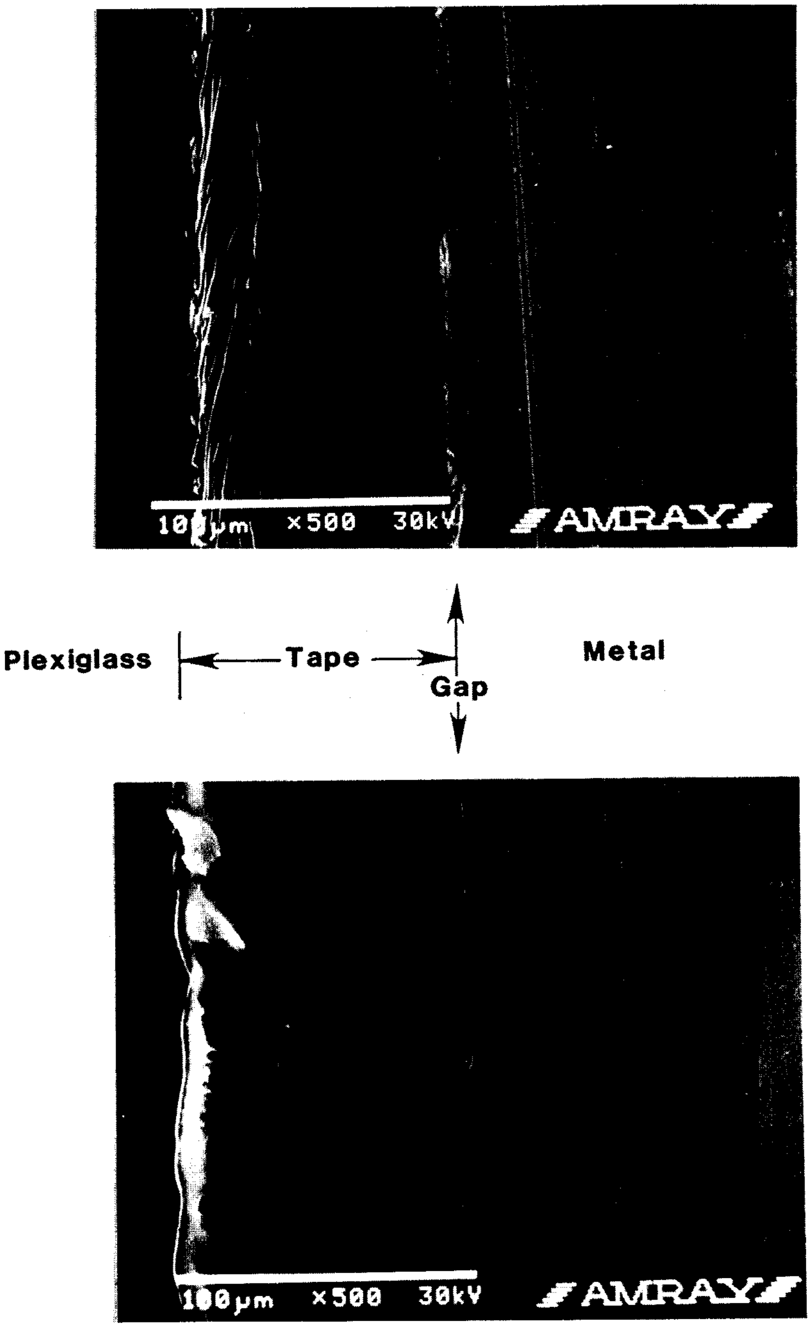

FIG. 2—*Examples of crevice gaps produced in two remote crevice assemblies fitted with deformable tape inserts (120 grit SiC, 2.8 Nm initial torque).*

Results and Discussion

Resistance to Crevice Corrosion Initiation

Figure 3 provides an overview of the corrosion initiation resistance for the five materials. Darkened areas of the chart identify those alloy-environment combinations for which no visible evidence of crevice corrosion was detected. In those cases where some degree of susceptibility was detected, the numbers in parentheses indicate the number of available crevice sites (four maximum) which initiated during the course of the 1000 h exposure. All cases designated [2] reflect initiation at one crevice site for each of the duplicate anode members.

As shown in Fig. 3, the higher molybdenum-nitrogen containing alloy S31254 was resistant to crevice corrosion in all nine environments. This is consistent with predictions noted by Oldfield and Todd [1]. While electrochemical monitoring identified a single, late response (- 35 days) to initiation in the high chloride diluted seawater test, the affected crevice member repassivated without any measurable propagation. Similar occurrences were electrochemically detected for alloy N08904 and alloy S32550 in the I g/L CI~ + I g/L S04~ tests after 15 days. In contrast, S30400 and S31600 stainless steel were found to be susceptible to attack in all nine environments. In most cases, initiation occurred for both of the duplicate specimens. In the I g/L Cl- + 10 g/L S04~ environment, corrosion for both S30400 and S31600 occurred only at the waterline. This occurrence did not necessarily prevent attack at the intended crevice site since both waterline attack and crevice corrosion co-existed on S30400 anode members in two other environments (Fig. 3).

Reporting of this form of attack appears noteworthy since there are numerous applications where stainless steel would only be partially immersed. The precise cause of the waterline attack has not been part of this study. It has also been observed for some alloy/environment combinations in other RCA tests. Some contributing factors suggested include: chloride/mineral concentrations on the anode stem, greater oxygen availability at the water surface,

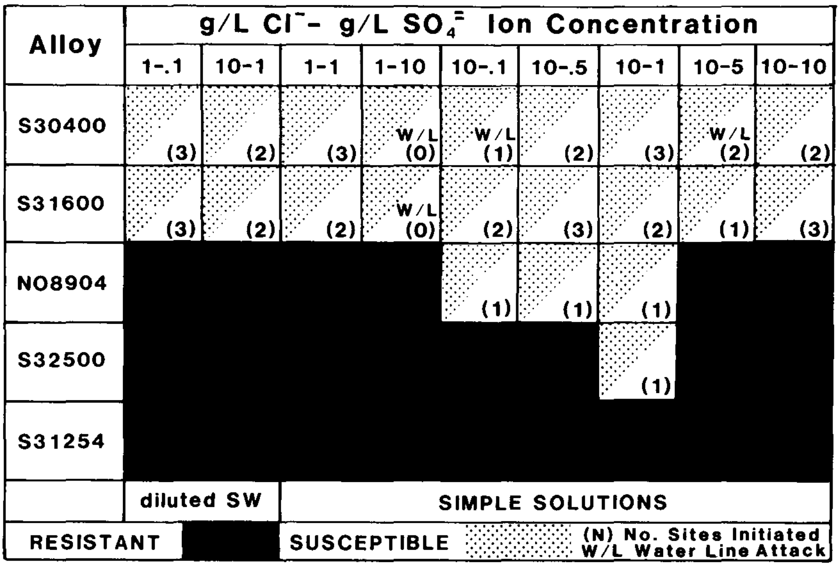

Alloy	g/L Cl^- - g/L $SO_4^=$ Ion Concentration								
	1-.1	10-1	1-1	1-10	10-.1	10-.5	10-1	10-5	10-10
S30400	(3)	(2)	(3)	W/L (0)	W/L (1)	(2)	(3)	W/L (2)	(2)
S31600	(3)	(2)	(2)	W/L (0)	(2)	(3)	(2)	(1)	(3)
NO8904	■	■	■	■	(1)	(1)	(1)	■	■
S32500	■	■	■	■	■	■	(1)	■	■
S31254	■	■	■	■	■	■	■	■	■
	diluted SW		SIMPLE SOLUTIONS						

RESISTANT ■ SUSCEPTIBLE ▨ (N) No. Sites Initiated W/L Water Line Attack

FIG. 3—*Guide to the crevice corrosion resistance exhibited by several stainless alloys in a variety of waters containing chloride and sulfate ions: remote crevice assembly tests.*

and the possible presence of occasionally more susceptible material, for example, exposed sulfide inclusions on the machined edges [7,17].

Although not quite as resistant as alloy S31254, alloy S32550 and alloy N08904 exhibited substantially greater resistance than the conventional grades of stainless steel. In the case of alloy S32550, initiation and sustained propagation was limited to a single crevice site in one of the 10 gjL Cl- environments. Being slightly less resistant to initiation, alloy N08904 was found to be susceptible in three of the 10 gjL chloride containing waters.

All three of these more resistant alloys have exhibited some degree of susceptibility to crevice corrosion in full strength natural seawater *[10,14].* As indicated earlier, the resistance of these materials can be significantly influenced by surface finish and the severity of crevice tightening. In general, material in the as-produced mill finish exhibited greater resistance than surface ground material. In some cases, lowering the crevice assembly torque level prevented initiation.

Time to Initiation-Use of the remote crevice assembly provides a method for detecting the actual time to crevice initiation. This information is valuable in more accurately determining the rate of any subsequent propagation and takes on even greater importance should initiation occur later in the test.

Figure 4, for example, provides the amperometric data collected for the four susceptible alloys in the 10 gjL Cl- + I gjL S04~ solution. The rapid rise in current values is indicative of the onset of attack, that is, breakdown of passivity or crevice initiation. Correspondingly, corrosion potential versus time plots shown in Fig. 5 describe a decrease to more active values upon initiation and during sustained propagation. The absence of measurable anodic current and the stability of the noble potentials confirm the resistance of alloy S31254 in this environment. From Figs. 4 and 5 it can be seen that S30400, as well as S31600, initiated in

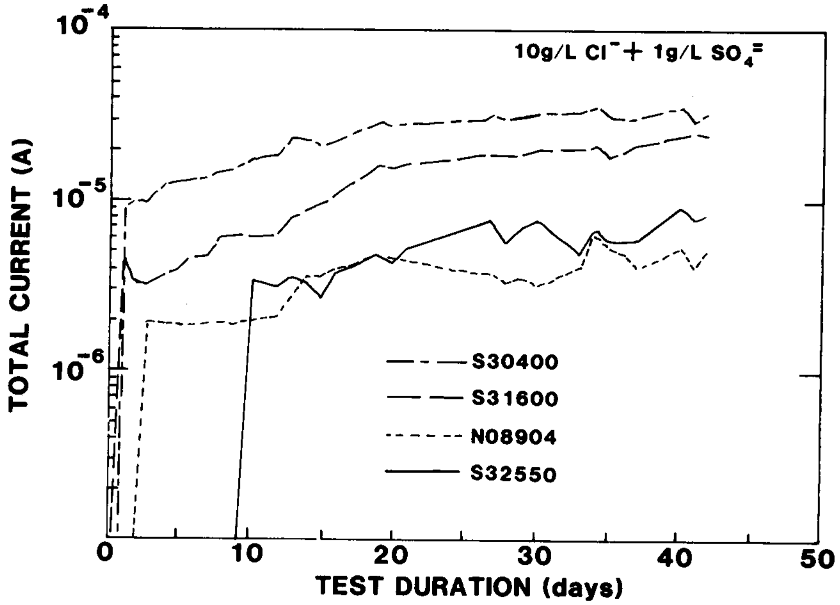

FIG. 4—*Amperometric data showing times to initiation and propagation behavior for susceptible materials in a simple solution containing 10 g/L Cl^- and 1 g/L $SO_4^=$.*

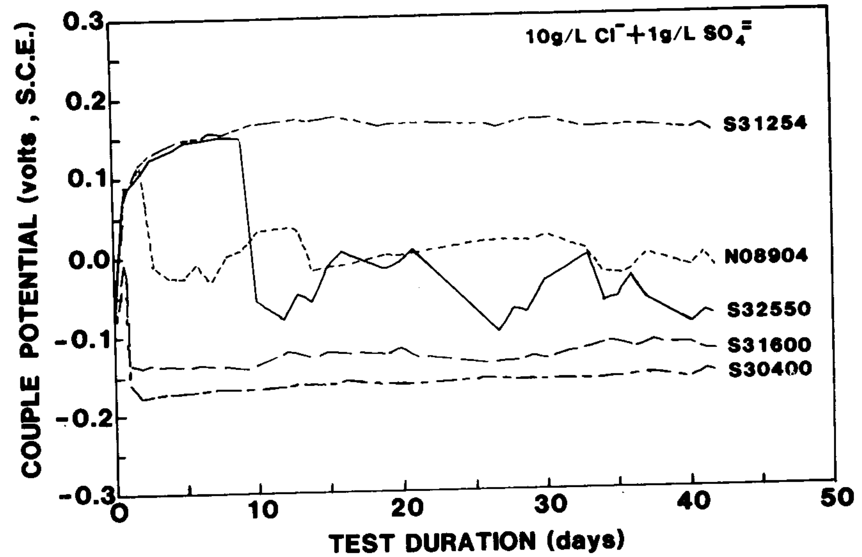

FIG. 5—*Potential-time data for coupled cathode and anode members exposed in simple solution containing 10 g/L* Cl^- + *1 g/L* $SO_4^=$. *Decrease in potential to more active values corresponds to increase in current shown in Fig. 4.*

approximately one day, while alloy N08904 and alloy S32550 initiated within 2 and 9 days, respectively.

Figure 6 shows the appearance of the anode members from the 10 gjL Cl- + 1 gjL S04~ test. With the exception of waterline attack already noted, this appearance is typical of the respective materials which incurred attack in the other environments. As will be discussed later, however, differences in the extent of propagation were noted.

Table 3 summarizes the times to initiation for the various alloy-environment combinations. For the most part, all cases of initiation occurred quite rapidly in these 1000 h (42 day) tests. Somewhat longer times to initiation could be expected at lower chloride levels. This may be reflected by the results in Table 3 for S30400 and S31600 in the simple solutions and to a lesser extent in the diluted seawater environment.

Influence of Environment-Several investigators have identified an inhibiting effect of sulfate on pitting attributable to chlorides. Leckie and Uhlig [18], for example, cited an increase in the critical potential for pitting *(Ec)* to more noble values with increased levels of sodium sulfate at 25°C. For a 0.1 *M* NaCl «3.5 gjL Cl-) solution, no pitting potential was observed at and above 0.15 *M* Na2S04 (< 14.4 gjL SO;). These levels of Cl- and SO; approximate the minimum Cl- (1 gjL) and maximum SO; (10 gjL) identified herein. Considering the 1 gjL Cl- tests (both dilute seawater and other) for S30400 and S31600, some increase in the time to initiation is observed with an increased sulfate level. The presence of sulfate may influence the buildup of chloride in the crevice [1]. This could extend the time to passive film breakdown. Again, corrosion in the 10 gjL SO; test (when it occurred) was limited to waterline attack where higher concentrations of chloride could be also expected. In the 1^0 gj L Cl- tests, however, no beneficial effect of sulfate is apparent for S30400 and S31600 stainless steel. Since both alloy N08904 and alloy S32550 exhibited a very low incidence of initiation overall, the absence of crevice corrosion in the 5 and 10 gjL SO; tests mayor may

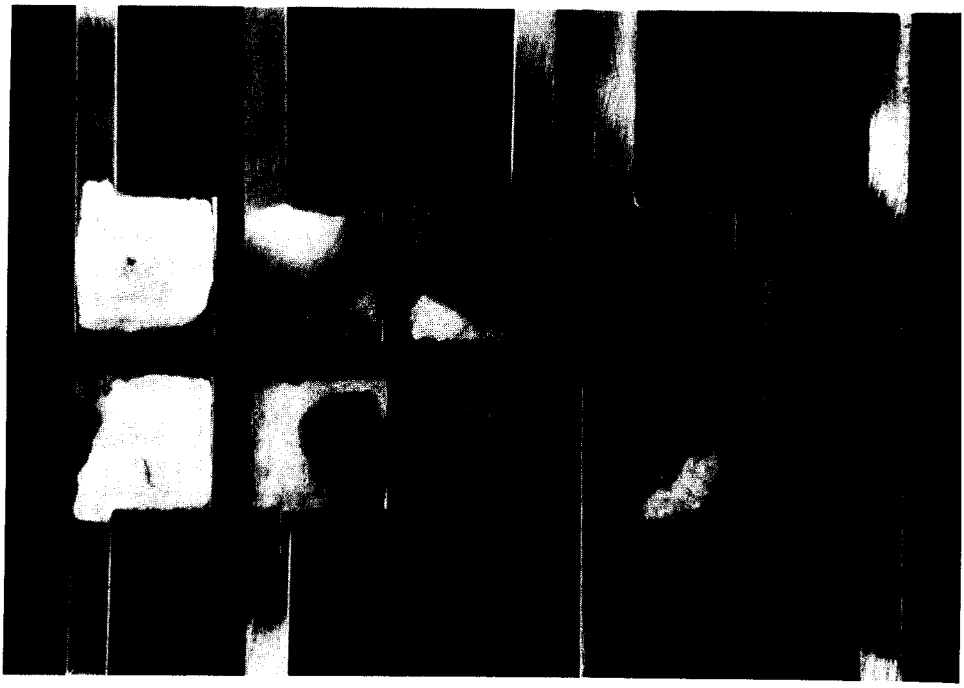

FIG. 6—*Appearance of "anode" members from 10 g/L Cl^- + 1 g/L $SO_4^=$ test showing evidence of crevice corrosion for all materials except alloy S31254.* (Left to right, top and bottom rows): *S30400, S31600, N08904, S32550, and S31254.*

TABLE 3—*Summary of times to initiation of corrosion determined by remote crevice assembly current measurements.*

Environment	Initiation Time (days)				
	S30400	S31600	N08904	S32550	S31254
		DILUTED SEAWATER			
10 g/L C^- + 1 g/L $SO_4^=$	1, 0.5	1, 1	OK, OK	OK, OK	OK[a], OK
1g/L Cl^- + 0.1 g/L $SO_4^=$	0.5, 2	2, 4	OK, OK	OK, OK	OK, OK
		1 g/L CL^- + SULFATE			
1 g/L $SO_4^=$	3, 1	10–13, 10–13	OK, OK	OK[a], OK[a]	OK, OK
10 g/L $SO_4^=$	13*, 10*	. . .[b], OK	OK, OK	OK, OK	OK, OK
		10 g/L CL^- + SULFATE			
0.1 g/L $SO_4^=$	2, 8	2, 7–8	31, OK	OK, OK	OK, OK
0.5 g/L $SO_4^=$	1, 1	2, 2	OK, 2	OK, OK	OK, OK
1 g/L $SO_4^=$	1–2, 2–3	1–2, 1–2	2–3, OK	9, OK	OK, OK
5 g/L $SO_4^=$	1–2, 1	1–2, 1–2	OK, OK	OK, OK	OK, OK
10 g/L $SO_4^=$	1, 2	1–2, 1–2	OK, OK	OK, OK	OK, OK

[a] Specimen repassivated without measurable attack.
[b] Waterline attack.

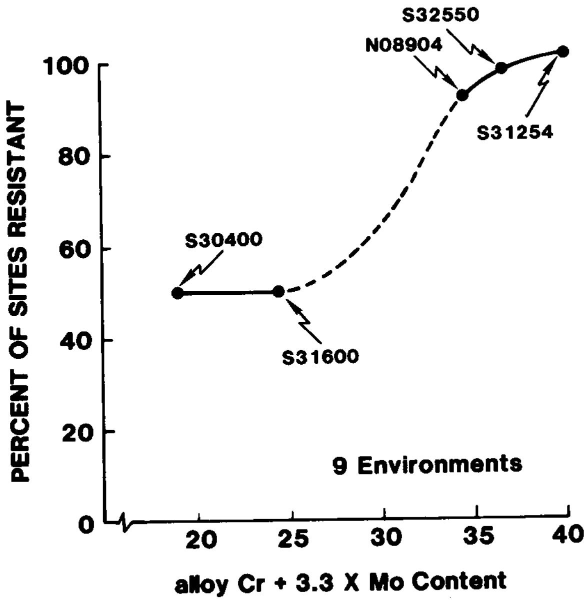

FIG. 7—*Beneficial influence of alloy chromium and molybdenum content on promoting resistance to crevice corrosion initiation in a variety of chloride and sulfate containing waters.*

not be entirely related to a beneficial effect of that anion. As will be discussed later, increased sulfate may actually be detrimental once conditions for initiation have been satisfied.

Alloying Effects-It is expected that alloy composition, particularly chromium and molybdenum levels, playa significant role in offering resistance to passive film breakdown. While S31600 with its 2% molybdenum content is frequently thought to offer a substantial advantage over the molybdenum free grade S30400, this is rarely apparent in crevice corrosion studies at the present and higher levels of bulk chloride.

Figure 7 shows the beneficial effect of higher chromium and molybdenum levels on the overall resistance to crevice initiation. The percent of resistant sites (36 possible in nine environments) is plotted as a function of the relationship %Cr + 3.3 X %Mo. This expression has been cited elsewhere and has been used to identify candidate materials for seawater and chloride containing water service *[19,20].* As can be seen, S30400 and S31600 which have equivalents ofless than 25% were resistant in only about 50 percent of the cases. In contrast, the other three alloys with equivalents of about 35% and greater were resistant in 92 or more percent of the cases. Because crevice corrosion is dependent on a number of inter-related factors, a critical value for %Cr + 3.3 X %Mo cannot be cited to cover all cases. It is safe to expect, however, that materials with greater equivalents will offer greater corrosion resistance over a broader range of geometric and environmental conditions than materials with lesser equivalents.

Crevice Corrosion Propagation Resistance

From Fig. 4, for example, differences in total current are apparent for each material. In this and other environments, S31600 consistently exhibited lower currents than S30400. It is perhaps of interest to note that while alloy S32550 exhibited somewhat greater resistance

TABLE 4—*Summary of remote crevice assembly test propagation results.*

	10 g/L Cl^- at Indicated g/L $SO_4^=$ Level						1 g/L Cl^- at Indicated g/L $SO_4^=$ Level		
	Diluted Seawater	Simple Solutions					Diluted Seawater	Simple Solutions	
UNS Alloy Identification	1	0.1	0.5	1	5	10	0.1	1	10
				AVERAGE MASS LOSS, MG					
S30400	51.7	11.4*	12.2	23.8	20.8[a]	25.4	10.3	8.6	4.2*
S31600	27.0	9.7	7.9	13.5	14.3	11.1	6.9	1.5	Nil*
N08904	Nil	4.4	1.0	3.8	Nil	Nil	Nil	Nil	Nil
S32550	Nil	Nil	Nil	4.5	Nil	Nil	Nil	Nil	Nil
S31254	Nil	Nil	Nil	Nil	Nil	Nil	Nil	Nil	Nil

[a] Crevice or waterline attack or both.

to initiation than alloy N08904, the duplex alloy exhibited somewhat greater anodic currents once initiation occurred.

Table 4 gives average mass loss data for each of the susceptible materials. These gravimetric data are in good agreement with corresponding data calculated from the measured anodic currents (that is, total charge-coulombs). Mass loss provides a general indicator of the severity of crevice attack, encompassing both the area affected and depth of penetration. From Table 4 greater differences can be seen as a function of chloride level than for variations in sulfate. At comparable Cl- and S04~ levels, greater mass loss was encountered in the diluted seawater environment than in the simple laboratory solution.

Alloying Effect-Mass loss results from the five synthetic waters containing 10 g/L Cl- are plotted in Fig. 8 as a function of alloy molybdenum content. Where no symbol is shown, the respective material was resistant. For the austenitic alloys, the beneficial role of molybdenum is clearly evident from the curve drawn through the data from the 10 g/L Cl- + I g/L S04~ test. While it may only be coincidental, this environment approximates the Cl-:S04 ~ ratio occurring in natural seawater. A similar curve can be drawn by plotting the above mass loss versus the previously indicated % Cr + 3.3 X % Mo parameter. In that case, however, the duplex alloy datum point would shift to the right of the austenitic alloy curve. Table 5 compares mass loss for specimens associated with Fig. 4 when the time to initiation is taken into account. The beneficial effect of molybdenum remains evident.

The presence of nickel or the austenitic structure of stainless steels or both have been associated with improved resistance to crevice corrosion propagation [7,21]. Previous RCA tests in waters containing either I or 10 g/L Cl- at pH 6, for example, showed greater resistance for S30400 and S31600 over respective ferritic grades S43000 and S44400.

Environmental Effects-In addition to alloying effects, variations in water chemistry contributed to differences in propagation rates for susceptible alloys, that is, S30400 and S31600. Figure 9, for example, shows amperometric data for S31600 exposed to the two diluted seawater environments at I and 10 g/L Cl- concentrations. While the time to initiation (1 to 2 days) are comparable, the increase in chloride levels promoted an order of magnitude increase in anodic current. These levels, however, are at least one to two orders of magnitude less than those reported for full strength natural seawater [13,15]. Conversely, currents shown in Fig. 9 for S31600 in 10 g/L Cl- diluted seawater are greater than those shown in Fig. 4 for the simple solution at the same Cl- and S04~ levels. This cannot be fully explained by the relatively small difference in solution conductivity shown in Table 2.

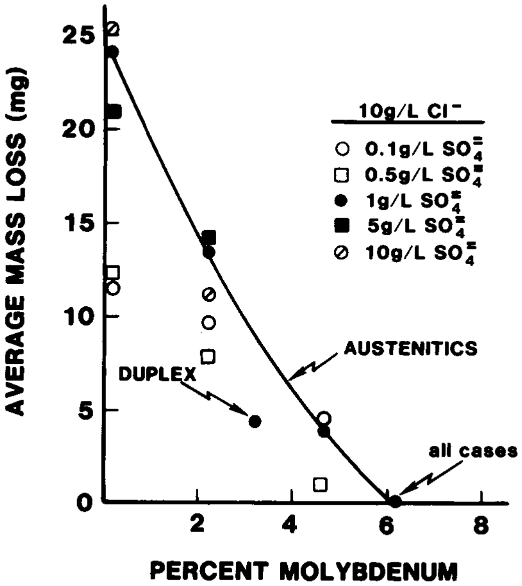

FIG. 8—*Effect of molybdenum content on resistance to crevice corrosion propagation.*

Anion Ratio Effect-The present series of tests considered two levels of chloride and five levels of sulfate ion concentration. In various combinations, these resulted in 0-:S04 ~ ratios ranging from 0.1: I to 100: 1 or conversely, S04~:CI- ratios of 10: I to 0.0 I: 1. Three environments corresponded to 0- :S04 ~ ratios of 10: I and two others produced ratios of I: 1.

As indicated earlier, some beneficial effect of sulfate may be associated with crevice corrosion initiation resistance at lower chloride levels. Propagation data, however, support an opposite effect at higher chloride levels. Figure 10 shows a plot of maximum depth of penetration as a function of sulfate to chloride ratio at a fixed level of chloride (10 g/L). While there is some datum scatter, the overall trend clearly shows an increase in the severity of attack with increased sulfate levels.

Table 6 compares the crevice corrosion propagation resistance for S30400 and S31600 in three waters of similar 0- :S04 ~ ratio (10: 1) but different origin or composition or both. For each parameter considered, S31600 consistently exhibited the greatest resistance. This is in contrast to the similarity in initiation behavior noted previously. As can be seen, crevice corrosion propagation for both alloys was greatest in the seawater diluted to 10 g/L Cl-. This environment also produced the greatest differences in performance between the two alloys.

TABLE 5—*Mass loss based on actual propagation time in 10 g/L Cl^- and 1 g/L $SO_4^=$ environment.*

UNS Alloy	% Mo	mg/day
S30400	Nil	0.60
S31600	2.2	0.34
S32550	3.2	0.14
N08904	4.6	0.10
S31254	6.1	nil

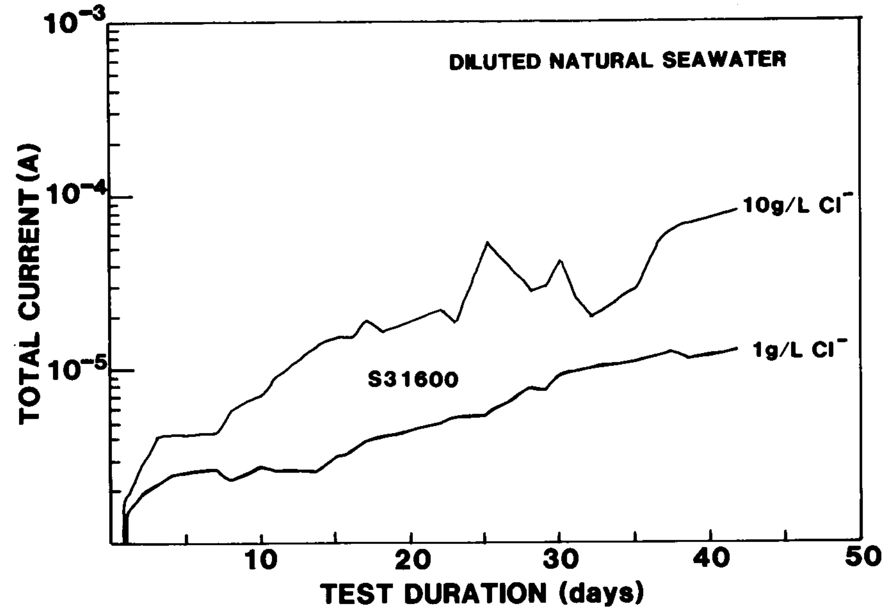

FIG. 9—*Effect of bulk environment chloride on the crevice corrosion propagation resistance of Type 316 stainless steel in diluted natural seawater.*

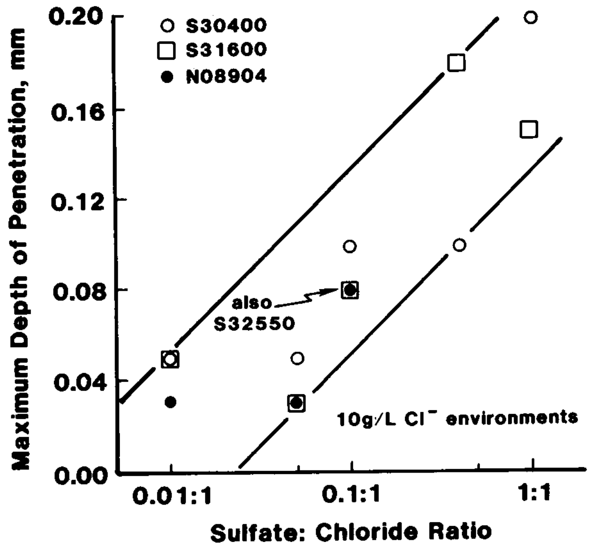

FIG. 10—*Effect of increased sulfate level on the crevice corrosion propagation resistance of several susceptible stainless steels in solutions containing 10 g/L Cl⁻.*

TABLE 6—*Crevice corrosion propagation resistance of S30400 and S31600 stainless steels in waters having comparable $Cl^-:SO_4^=$ ratios.*

		Maximum Depth mm		Total Charge,[a] Coulombs		Average Mass Loss, mg	
Environment	Ratio	S30400	S31600	S30400	S31600	S30400	S31600
		Simple Solution					
10 g/L Cl^- + 1 g/L $SO_4^=$	10:1	0.10	0.08	91	75	24.0	13.5
		Diluted Seawater					
10 g/L Cl^- + 1 g/L $SO_4^=$	10:1	0.23	0.14	250	114	51.7	27.0
1 g/L Cl^- + 0.1 g/L $SO_4^=$	10:1	0.08	0.04	40	29	10.0	7.0
		Simple Solution					
10 g/L Cl^- + 10 g/L $SO_4^=$	1:1	0.20	0.15	97	46	25	11
1 g/L Cl^- + 1 g/L $SO_4^=$	1:1	0.03	0.03	29	7	9	2

[a] Greatest for duplicate RCAs.

Observed differences between the present diluted seawater tests and those in simple solutions at the same Cl- and S04~ levels parallel similar trends established between natural seawater and synthetic seawater tests, further substantiating the unique nature of seawater with its apparent biological influences [13,15,22].

Other dilute seawater tests at the present and other levels of Cl- and S04~ have been reported. Table 7, for example, compares depth of attack results with data from multiple crevice assembly (MCA) tests described elsewhere [3]. While the MCA test was nearly twice as long, no significant increase in depth of penetration was noted. Overall, S31600 was least affected by differences in crevice former and environmental conditions.

Summary and Conclusions

A series of remote crevice assembly tests were conducted for S30400 and S31600 stainless steels, alloy N08904, alloy S32550, and alloy S31254 in a number Cl- + S04~ containing waters. Specimens were exposed for 1000 h in totally synthetic and diluted natural seawater environments containing either 1 or 10 g/L Cl~ and sulfate ranging from 0.1 to 10 g/L.

S30400 and S31600 were found to be susceptible to localized corrosion in all nine environments. The three higher alloyed materials, and particularly the 6% molybdenum containing austenitic alloy S31254 exhibited significantly greater resistance.

TABLE 7—*Maximum depth of penetration, mm.*

	RCA Tests, 1000 h at 30°C		MCA Tests, 2160 h at 35°C	
UNS Alloy	10 g/L Cl^-	1 g/L Cl^-	10 g/L Cl^-	1 g/L Cl^-
S30400	0.23	0.08	0.09	0.13
S31600	0.14	0.04	0.06	0.06

In those cases where the higher alloys exhibited crevice corrosion, substantial improvement in propagation resistance over S30400 and S31600 was realized.

Decreased chloride levels of both the synthetic and diluted seawater environments resulted in some improved performance for the susceptible materials.

Although some benefit of sulfate at lower chloride levels may be realized with regard to crevice initiation behavior, higher sulfate levels appeared to be clearly more detrimental at higher chloride levels.

Depths of penetration and mass loss in diluted seawater tests were about twice those in simple solutions with comparable chloride (10 gjL) and sulfate (I gjL) levels.

The fact that initiation occurred quite rapidly highlights the importance of crevice geometry considerations. This is further supported by evidence which showed that continued exposure through 1000 h or 2 to 3 orders of magnitude in time did not promote additional occurrences of crevice attack.

Other less severe environmental and geometrical conditions would likely extend the usefulness of the materials studied. Conversely, under more adverse conditions an increase in severity of attack may be expected for those already identified susceptible alloys. Likewise, the present resistant alloys may also experience some limiting set of environmental and geometric conditions.

Acknowledgment

Preparation of this report was supported by the Nickel Development Institute (NiDI) and the LaQue Center for Corrosion Technology, Inc. Continuation of this work by Cortest Laboratories, Sheffield, U.K. and the LaQue Center is also supported by NiDI.

References

[1] Oldfield, J. W. and Todd, B., "Reverse Osmosis-Which Stainless Steel to Use?," Nickel Development Institute Technical Series No. 10,003, Reprinted from Middle East Water and Sewage, Vol. I, No.5, Oct. 1986.

[2] Hack, H. P., *Materials Performance*, National Association of Corrosion Engineers, Vol. 22, No.6, June 1983, p. 24.

[3] Kain, R. M., *Corrosion*, National Association of Corrosion Engineers, Vol. 40, No.6, June 1984, p.313.

[4] Kain, R. M., Lee, T. S., and Scully, J. R., *Proceedings*, Ninth International Congress on Marine Corrosion, Toronto, Canada, June 1984.

[5] Flint, G. N., "Resistance of Stainless Steel to Corrosion in Naturally Occurring Waters," Inco Publication A1262, International Nickel Co., New York.

[6] Kain, R. M., Tuthill, A. H., and Hoxie, E. C., *Journal of Materials for Energy Systems*, Vol. 5, No.4, April 1985. p. 205.

[7] Kain, R. M., *Materials Performance*, National Association of Corrosion Engineers, Vol. 23, No. 2, Feb. 1984, p. 24.

[8] Oldfield, J. W. and Sutton, W. H., *British Corrosion Journal*, Vol. 13, 1978, p. 13.

[9] Tatnall, R. E., *Materials Performance*, National Association of Corrosion Engineers, Vol. 20, No. 8, Aug. 1981, p. 41.

[10] Kain, R. M., "Crevice Corrosion and Metal Iron Concentration Cell Corrosion Resistance of Candidate Materials for OTEC Heat Exchangers, Parts I & II," ANL/OTEC-BCM-022, Argonne National Laboratory/U.S. Department of Energy, May 1981.

[11] Kain, R. M., "Crevice Corrosion Resistance of Austenitic Stainless Steels in Ambient and Elevated Temperature Seawater," Paper No. 230, presented at NACE Annual Conference, National Association of Corrosion Engineers, Houston, TX, 1979.

[12] Kain, R. M., "Crevice Corrosion Resistance of Several Iron Base and Nickel Base Cast Alloys ia Seawater," Paper No. 66, presented at NACE Annual Conference, National Association of Corrosion Engineers, Houston, TX, 1982.

[13] "Sea Grant Program on Marine Corrosion-Final Report," Vol. Four-Supporting Data Localized Corrosion, Stainless Alloys, S. C. Dexter and W. H. Hartt, Eds. NOAA, U.S. Department of Commerce, Washington, D.C., May 1985.

[14] Lee, T. S. and Kain, R. M., "Factors Influencing the Crevice Corrosion Behavior of Stainless Steels in Seawater," Paper No. 69, presented at NACE Annual Conference, National Association of Corrosion Engineers, Houston, TX, 1983.

[15] Kain, R. M. and Lee, T. S., "Recent Developments in Test Methods for Investigating Crevice Corrosion," *Laboratory Corrosion Tests and Standards, ASTM STP* 866, American Society for Testing and Materials, Philadelphia, 1985, p. 299.

[16] Oldfield, J. W., "Crevice Corrosion of Stainless Steels-The Importance of Crevice Geometry and Alloy Composition," presented at the 19th Journees de Aciers Speciaux, Saint-Etienne, May 1980.

[17] Lee, T. S., "A Method of Quantifying the Initiation and Propagation Stages of Crevice Corrosion," *Electrochemical Corrosion Testing, ASTM STP* 727, American Society for Testing and Materials, Philadelphia, 1981, p. 43.

[18] Leckie, H. P. and Uhlig, H. H., *Journal of the Electrochemical Society,* Vol. 113, No. 12, Dec. 1966, p. 1262.

[19] Henrikson, S., "Experience of Swedish High Alloy Stainless Steels for Seawater Applications," presented at the Ninth Scandinavian Corrosion Congress, Copenhagen, Denmark, 12-14 Sept. 1983.

[20] Redmerski, L. S. et al., "Crevice Corrosion of Stainless Steel Welds in Chloride Environments," Paper No. 191, presented at NACE Annual Conference, National Association of Corrosion Engineers, Houston, TX, 1982.

[21] Sedriks, A. J., *Corrosion of Stainless Steels,* Chapter 5, Wiley, New York, p. 100.

[22] Lee, T. S., Kain, R. M. and Oldfield, J. W., *Materials Performance,* National Association of Corrosion Engineers, Vol. 23, No.7, July 1984, p. 9.

William H. Hartt[1]

Corrosion Fatigue Testing of Steels as Applicable to Offshore Structures

REFERENCE: Hartt, W. H., "Corrosion Fatigue Testing of Steels as Applicable to Offshore Structures," *Corrosion in Natural Waters, ASTM STP 1086,* C. H. Baloun, Ed., American Society for Testing and Materials, Philadelphia, 1990, pp. 54-69.

ABSTRACT: Fatigue is a potentially important failure mode for offshore structures. Development of realistic data (high-cycle regime of the *S-N* curve or near-threshold region of the crack growth rate-stress intensity range curve) is made difficult by the fact that load excursions are mostly oflow amplitude (high-cycle fatigue) with frequency in the range of 0.05 to 0.5 Hz; and so one or more years of testing may be required to establish a single data point *(S-N* approach) or *dajdN-t1K* curve. In the present paper experimental alternatives for developing both fatigue life and crack growth rate data for offshore applications are presented, with particular emphasis upon test parameters and variables of importance. Special emphasis is placed upon techniques for multiple specimen testing. In addition, a novel approach for characterizing near-threshold fatigue crack growth rates within realistic test periods is proposed and discussed.

KEY WORDS: corrosion fatigue, fatigue testing, crack initiation, crack propagation, steel, welded steel, variable amplitude, polarization

Nomenclature

da/dN	Fatigue crack growth rate
ΔK	Stress-intensity range
ΔK_{TH}	Threshold stress-intensity range
N	Cycles-to-failure
R	Ratio of minimum stress or stress intensity per cycle to maximum
S	Stress range
ρ	Notch root radius

Fatigue has been established as an important failure mode for offshore structures [*1-4*]. In the case of conventional template platforms, normally fabricated from structural steel, fatigue fracture typically initiates at the toe of welded connections, due to the geometrical discontinuity and associated stress concentration [*5*]. For newer, deep water platforms, which often require higher strength steels, welds may be of improved quality or ground (or both), such that subsurface defects (porosity, incomplete fusion, etc.) are important initiation sites. The root of threaded connectors is a potential, alternative location for fatigue crack initiation.

The marine structure fatigue process is complicated by numerous influential variables, as shown by Fig. 1 [*4*]. This represents the various factors influencing fatigue in terms of four general categories: (1) mechanical, (2) material, (3) electrolyte, and (4) electrochemical. How-

---

[1] Professor and director, Center for Marine Materials, Department of Ocean Engineering, Boca Raton, FL 33431.

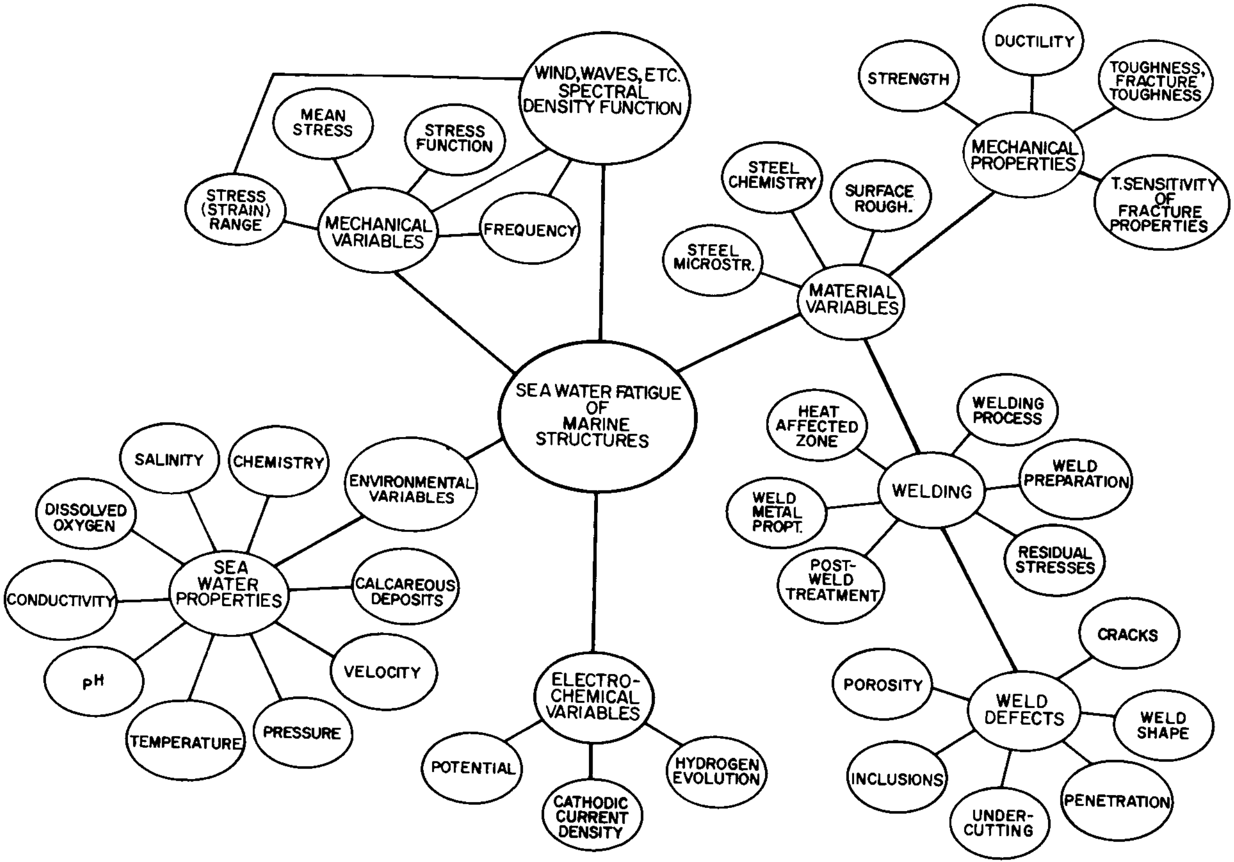

FIG. 1—*Graphical representation of variables influencing seawater corrosion fatigue.*

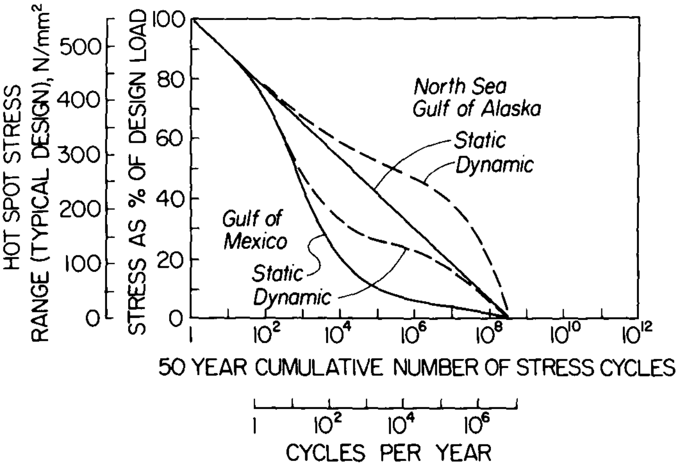

FIG. 2—*Cumulative stress history for offshore structures* [7].

ever, it is important to recognize that the variables in Fig. 1 may be mutually interactive, such that a change in one influences the role of others.

Figure 2 [*3*] projects the cumulative stress cycle history for several generic types of structures and ocean exposure situations. This shows that as many as 10^8 cycles may occur during the design life, and damage assessment reveals that fatigue is most severe in the relatively low stress range regime [*6*]. Thus, it is here (low stress or, alternatively, low stress-intensity ranges) that offshore structure related fatigue research must concentrate. Experimental tasks are complicated, however, by the fact that cyclic stress frequency for both ocean waves and first mode resonance, as may occur for slender and deep water structures, is typically in the range 0.05 to 0.5 Hz [*6*]. Thus, a year or more of test time may be required to obtain one *S-N* datum point in the high cycle regime or a single da/dN-ΔK curve extending to or near the threshold stress intensity range (ΔK_{TH}).

It is recognized that the general fatigue process is comprised, first, of an initiation phase and, secondly, by crack growth to critical size [*7,8*]. Figure 3 [*9*] illustrates that the former occupies a progressively greater fraction of cycles-to-failure as either total life increases or stress concentration factor decreases. Also, weld toe slag inclusions, typically 0.1 to 0.4 mm in size, have been projected to behave as initial cracks [*10*], such that fatigue life of welded connections, tubular joints, for example, is dominated by crack growth. On the other hand, initiation processes should be of increased importance for both ground, dressed or improved profile welds [*11,12*]. This is particularly relevant to relatively new, deep water structural concepts, such as tension leg platforms, where improved fabrication practices and more rigorous quality control are likely compared to conventional structures.

The present paper reviews experimental techniques which have been historically employed at this Laboratory to develop high cycle *S-N* data, as are relevant to present design practices for offshore structures [*13*]. The procedures are based, for the most part, upon the premise that neither stress range enhancement or frequency acceleration are appropriate for increasing rate of testing. In the former case the range over which the *S-N* curve must be extrapolated is greater than if the data extend to the high cycle regime. The effect of frequency is less well defined with some investigators reporting little, if any, influence upon fatigue life [*14,15*] in ranges of interest here, whereas other data [*5,16,17*] suggest this factor to be significant.

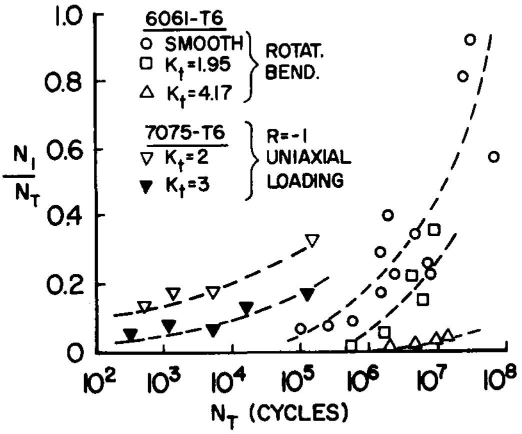

FIG. 3—*Influence of stress concentration and total fatigue life upon the relative role of fatigue crack initiation* [11].

In view of this uncertainty it is prudent to require that fatigue testing in seawater be performed at a frequency relevant to the service application.

Corrosion Fatigue Life Testing

With regard to design criteria for offshore structures there are conflicting opinions regarding whether testing of full-scale tubular connections is required or if the process can be represented by fillet welded plate specimens of comparable thickness but otherwise reduced dimensions. The former approach has been adapted by the European offshore research community with supplemental plate testing, whereas programs in the United States have embodied the latter. In the case of welded plate, competing *S-N* test philosophies involve, on the one hand, a suite of relatively inexpensive single specimen machines [2] and, on the other, a single machine which accommodates multiple specimens. In actuality, the latter approach (single machine, multiple specimen) may involve reduced net capital expenditure and lower overall cost compared to the former.

Figure 4 presents a photograph of the multiple specimen frame which has been employed in this laboratory for the past six years. This system is comprised of two vertically stacked units, each of which is powered by a 245 kN (55 kip) MTS actuator and closed loop, servohydraulic control system. The latter is inclusive of two signal conditioners such that mean and range displacements for each actuator are independently controlled. A single function generator controls the load signal and frequency for both actuators; however, independent control could be realized by addition of a second unit. Either actuator can be independently shut down by closing a hydraulic line valve at the accumulator.

Because specimens are loaded in parallel, as will be illustrated subsequently, it is necessary to operate the actuators in the stroke (displacement) control mode. Historical monitoring of specimens under test by remote strain gages; that is, by gages located away from the anticipated failure origin, has indicated that strain is relatively constant until a crack of macroscopic dimensions forms. Figure 5 reports the strain history for an example specimen and shows that relatively few cycles transpired once compliance increased. Thus, the test results are essentially the same as for a load control procedure. Failure has been defined in programs

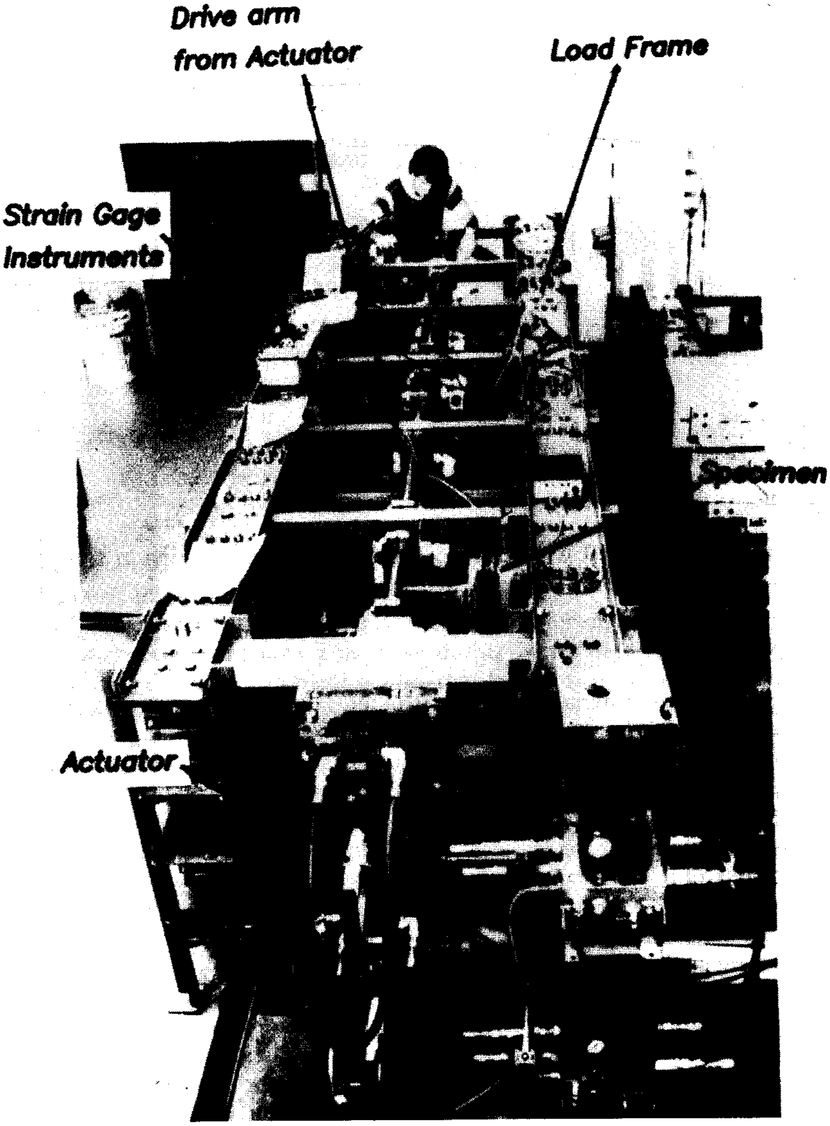

FIG. 4—*Multiple specimen fatigue frame.*

involving this instrumentation as corresponding to a crack depth one half the specimen thickness, at which point strain range is reduced to approximately 70% of the original value. For a few specimens the rate of strain range decrease, for unexplained reasons, has been more moderate than depicted by Fig. 5, in which case the stress control analogy may not be as accurate. Strain readings upon concurrently tested specimens have revealed no interaction between specimens as one or more fails.

Because the operating test frequency has been relatively low (0.3 Hz.) and the testing of a

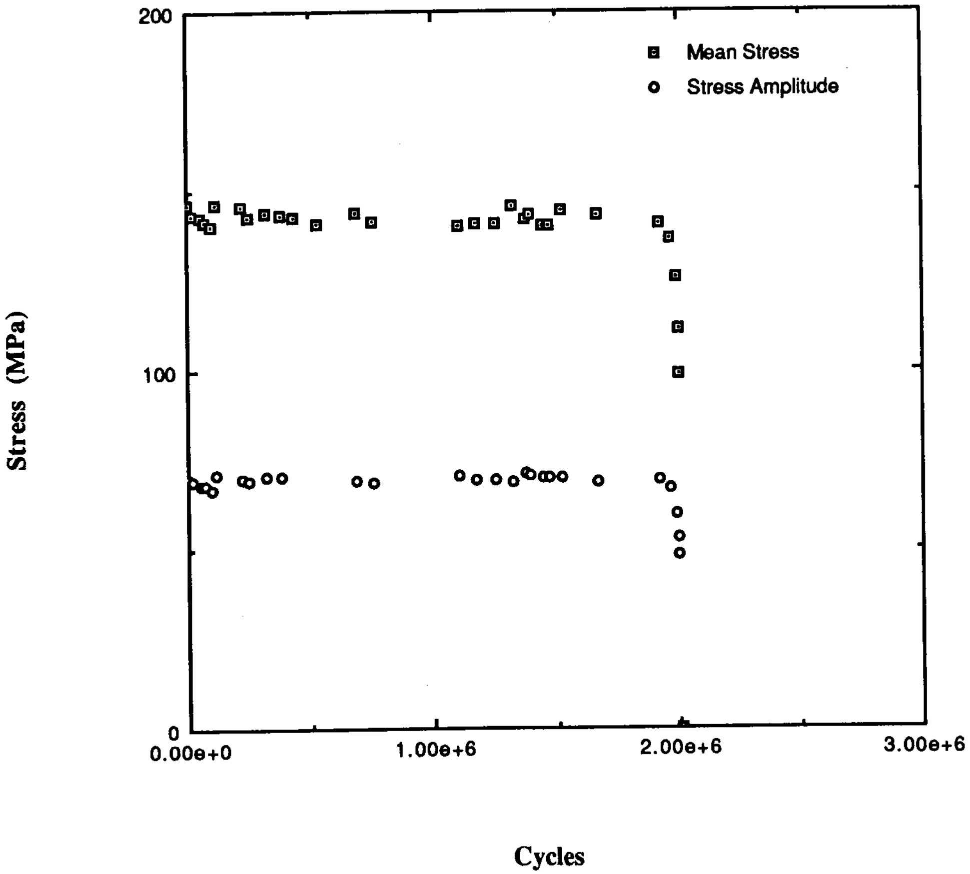

FIG. 5—*Strain history of a typical specimen tested under deflection control.*

high cycle fatigue nature, strain monitoring has been performed manually. This function, of course, could be automated.

Two types of specimens have historically been employed in this test frame. The first is a constant taper, cantilever bend one, which has been discussed in detail elsewhere [4,18]. Figure 6 presents a schematic illustration of this, where for the geometry illustrated here approximately 0.60 m of weld toe is available per specimen for fatigue. While this particular specimen is from 25A-mm plate, other thicknesses as well can be tested. Figure 7 presents a photograph of this specimen type along with the electrolyte bath, as mounted in the test frame. Thus, the broad specimen end is vise clamped and the smaller end bolted through two needle bearings to a pair of 38-mm-diameter high-strength steel rods which connect directly to the actuator. By appropriate positioning of clamping plates in the vise stress in the constant taper region of the specimen can be varied by a factor of about 50% for a given actuator displacement. The frame was designed and built to accommodate 12 specimens per actuator, this number being limited by first physical space according to length of the frame and, second, by the force required per specimen to achieve the desired stress and actuator capacity.

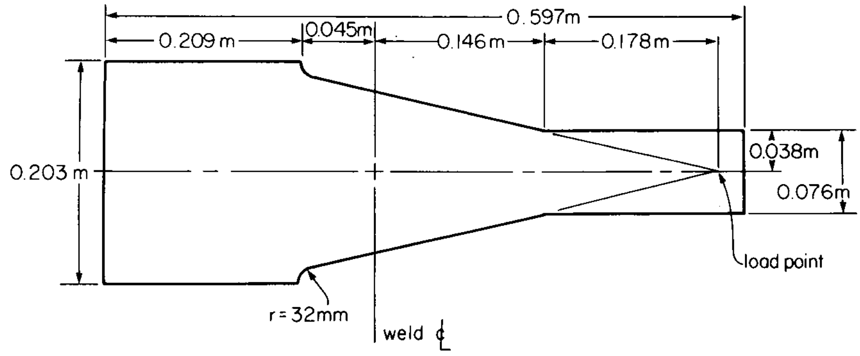

FIG. 6—*Schematic representation of welded constant taper specimen geometry.*

Figure 8 presents data for several 25.4-mm-thick welded linepipe steels (designated *X* and Y) and HY80 (designated *HY)* fatigued in seawater at 0.3 Hz [19] according to the preceding procedure. The data conform to a single band despite variations in material composition and microstructure, as has been observed historically *[20].* Of particular significance here, however, is the relatively steep slope to the *SoN* curve, such that the high-cycle data fall short of the API-X design curve [13] despite the fact that the welds were ground and post-weld heat treated.

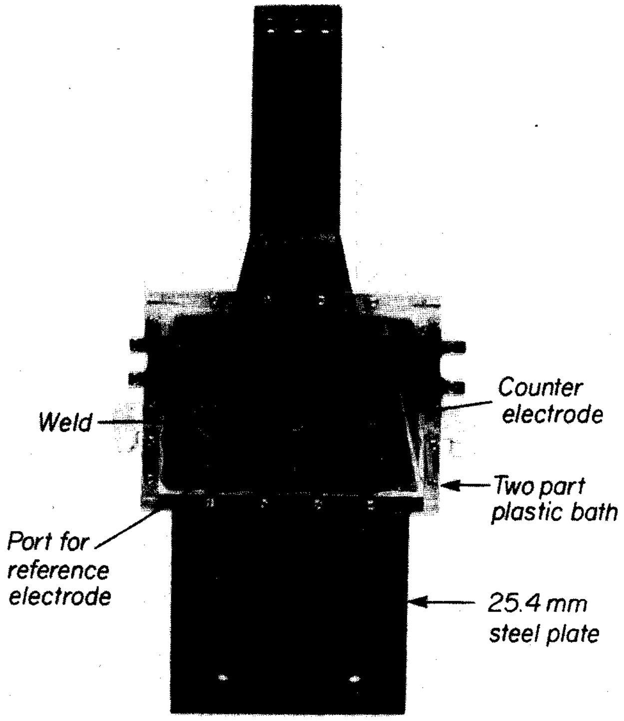

FIG. 7—*Photograph of welded, constant taper specimen and bath.*

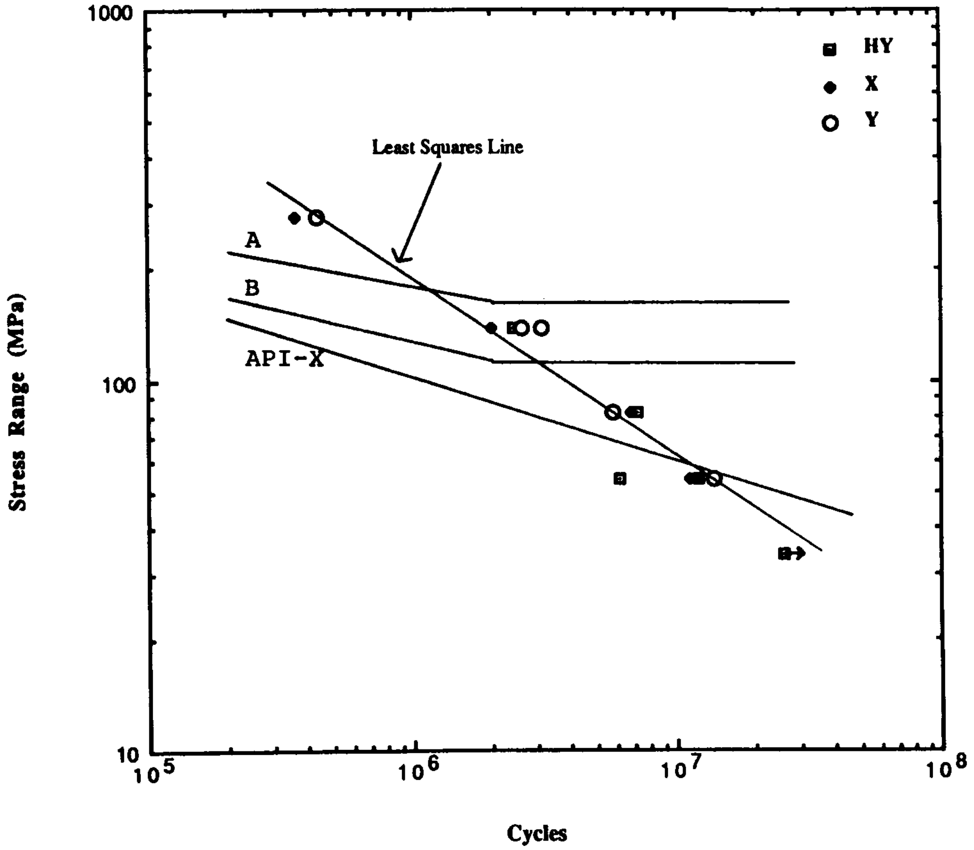

FIG. 8—*Fatigue data for 25.4-mm-thick butt welded, high strength steel tapered beam specimens freely corroding in seawater.*

Modification of fixtures has permitted utilization of a welded stub "tee" type specimen as well. Figure 9 presents a photograph of a 50.8-mm-thick specimen of this type with electrolyte bath, as mounted in the frame. Here loading of the 0.24-m-wide specimen is through the same drive bars as in Fig. 7, except these have been spread to accommodate the greater width of this specimen compared to the cantilever one (Fig. 6). The specimen ends are positioned on half-cylinder bars which, in turn, are bonded to a thick neopreme pad to facilitate transverse specimen motion in response to applied loading in the longitudinal direction. Thus, testing of this specimen type is limited to positive values for R. Because this specimen is larger and requires greater load to achieve a particular stress compared to the cantilever one, fewer tests can be performed at any given time. Figure 10 presents S-N data obtained from 50.8-mm-thick API-2H Grade 42 tee specimens welded according to the AWS Basic [21] criterion (no profile control) and fatigued freely corroding in seawater at 0.3 Hz. Note the reduced cycles to failure for this specimen type compared to the butt welded ones (Fig. 8) and proximity of the data to the appropriate design curve (API-X'). In both cases (Figs. 8 and 10) the high-cycle data (N 105) are considered critical for confident extrapolation into the high-cycle regime.

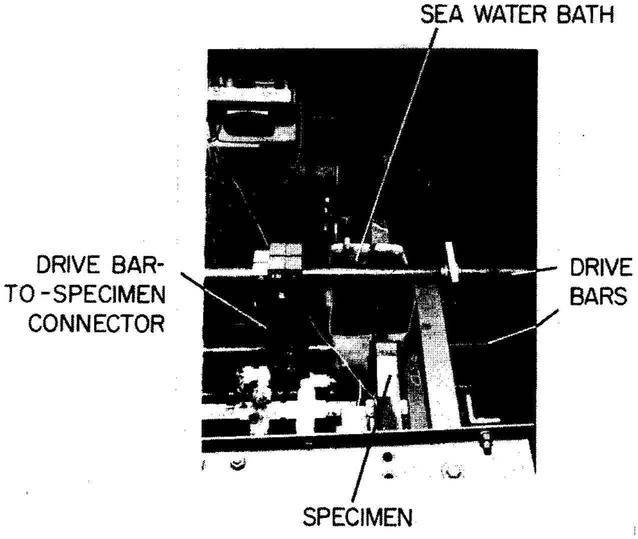

FIG. 9—*Photograph of fillet welded, tee specimen under test.*

Variable Amplitude Testing

The fatigue frame discussed previously has been also employed in variable amplitude programs [22-24] as are particularly relevant to welded connections of offshore structures. This is accomplir'led by inclusion of an appropriate computer and load history program with the controls, according to procedures which are now commonly practiced. Because many of the stress cycles employed in a long-term variable amplitude fatigue program are smaller than for the constant amplitude case, it has proven beneficial to incorporate a second a-c conditioner in series with the first as part of the control system. This reduced the maximum actuator stroke by a factor of ten (200 to 20 mm); but the displacement control was enhanced by a corresponding amount (factor often), thereby insuring accurate correspondence of the actual stroke to the input spectrum for small movements.

Compact Tension Specimen Testing

The utility of the compact tension (CT) specimen for fatigue testing has been documented in the literature, and recommended practices have been developed which pertain to both dimensioning and test procedures [25]. Two alternatives exist depending upon whether a particular study is to focus upon fatigue crack initiation or propagation.

Fatigue Crack Initiation

Previous research [26-28] has indicated the keyhole compact tension specimen to be advantageous with regard to initiation studies. Figure 11 is a schematic representation of this specimen as it has been employed in programs at this laboratory. Thus, initiation occurs at the keyhole base in response to cyclic loading, and the crack subsequently propagates to the keyhole edges and across the specimen faces. Of course, it is not intended that the specimen provide resolution of classical questions regarding demarkation between the initiation and

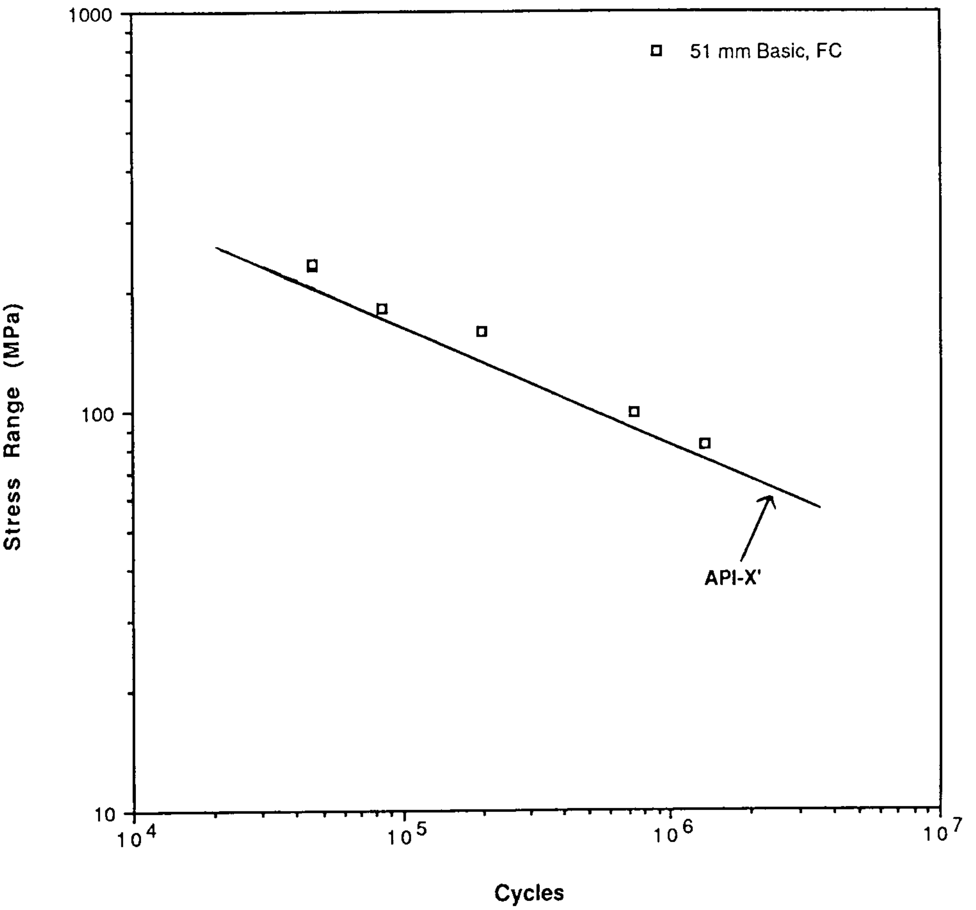

FIG. 10—*Fatigue data for 50.8-mm-thick tee specimens freely corroding in seawater.*

propagation stages. Thus, cycles-to-initiation is defined arbitrarily in terms of a crack achieving a predetermined size. Previous studies have concluded that the specimen is insensitive to keyhole surface finish [27]. Also, cracks, once detected, have been reported to spread relatively fast across the keyhole and specimen sides [28], thus making cycles-to-initiation relatively definition insensitive.

Because the same high-cycle low-frequency criteria discussed previously with regard to offshore structure relevancy of data apply here as well, a fatigue frame for multiple CT specimens has been fabricated, as shown in Fig. 12. This accommodates up to eight specimens in series with the loading provided by a 98 kN (22 kip) actuator. The unit is operated in load control with the interlock set in displacement control to interrupt testing once displacement exceeds a predetermined value slightly greater than the peak value per cycle under normal operation (no cracked specimens). It was found that this shut-down often occurred prior to the crack in a single specimen growing out of the keyhole.

Figure 13 presents freely corroding S-N type data based upon this test procedure, where stress range has been represented in terms of the fracture mechanics parameter $\Delta K(\rho)^{-1/2}$

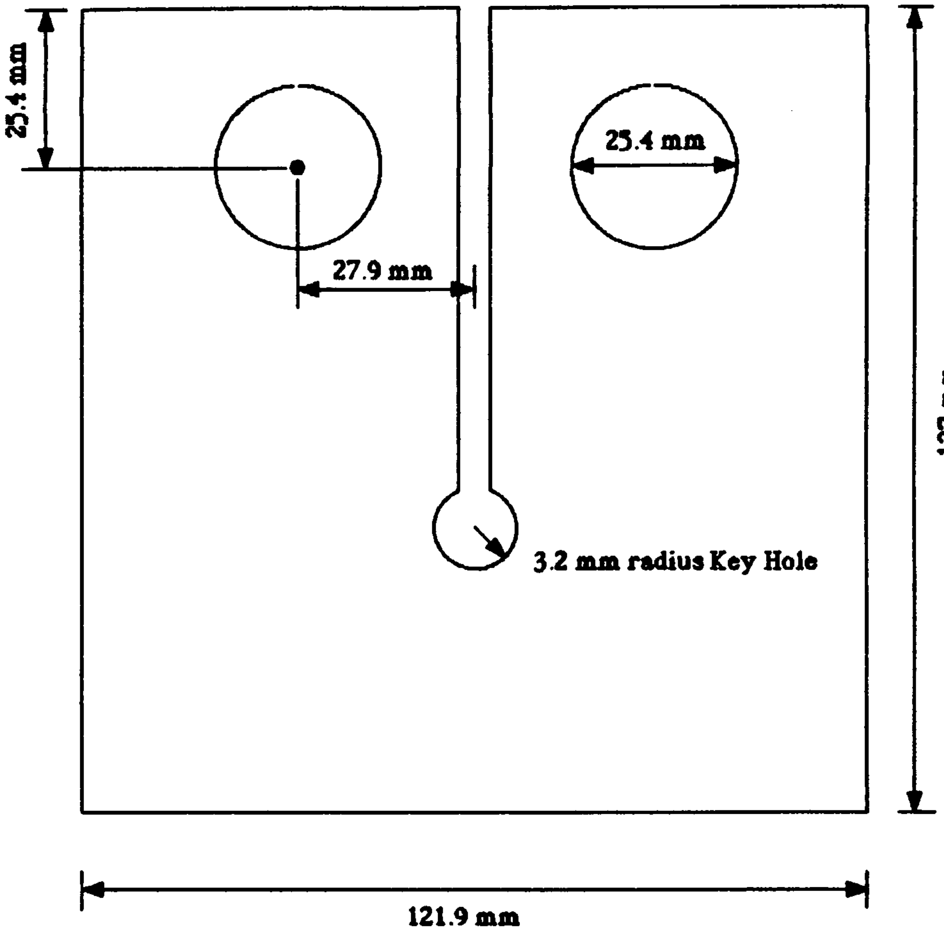

FIG. 11—*Schematic representation of keyhole compact tension specimen.*

[30,31]. Nine different higher strength steels have been included here with yield strength ranging from 375 to 990 MPa. As for the previous case (Fig. 8) all data conform to a single band. However, application of cathodic polarization restored an endurance limit, which in the lower strength regime varied in proportion to tensile strength. This is illustrated by Fig. 14 [29].

Fatigue Crack Propagation

A fundamental problem associated with near-threshold fatigue experiments performed according to standardized practice [25] in the frequency range of present interest (0.05 to 0.5 Hz.) is that a period of up to one year may be required to generate the *dajdN-K* curve. Undoubtedly, this point is at least partly responsible for the general lack of data in this regime. With eight specimens being fatigued concurrently (Fig. 12) this time period appears to be more favorable; however, operation of the system under load control requires load

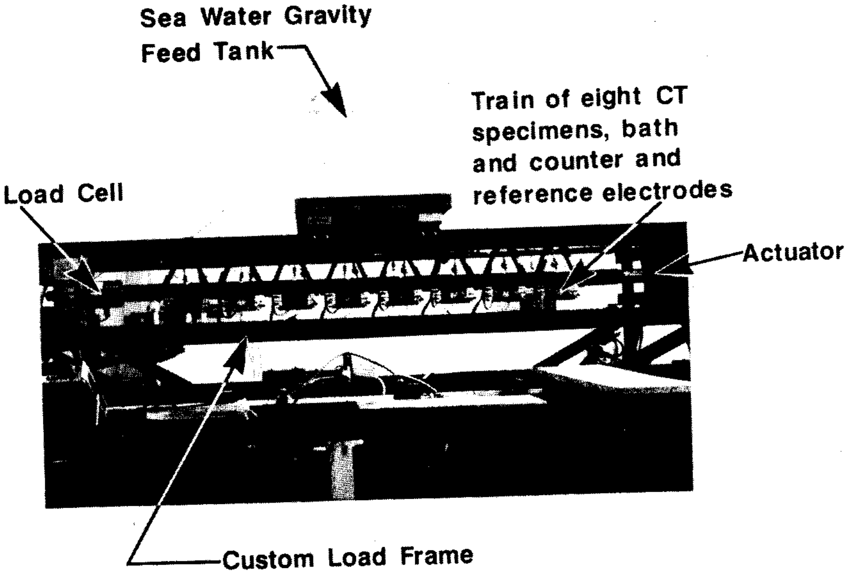

FIG. 12—*Test frame for multiple CT specimen fatigue experiments.*

shedding according to the single specimen for which crack length is greatest with little or no information being gained from the remaining ones.

It is proposed that this difficulty can be overcome by employing a modified, constant taper CT specimen. The original version of this was proposed by Mostovoy et al. [31] as a constant stress-intensity specimen, and it has been employed on a limited subsequent basis [32]. Figure 15 is a schematic representation of this along with a plot of stress intensity versus crack length. Thus, the progressive width increase of the specimen offsets the effect of crack extension to yield a range of crack length over which stress intensity is approximately constant.

To circumvent the problem presented previously for the standard CT specimen it is proposed that a greater taper than in Fig. 15 be employed. This is illustrated schematically in Fig. 16 along with the fact that K should decrease progressively as the crack grows. Thus, in multiple specimen testing the specimen with the most advanced crack should exhibit the lowest crack growth rate, thereby facilitating a balanced, stable situation. While this specimen type has been reported to experience migration of the crack from the intended, mid-plane orientation, this can probably be controlled by side grooves. This tendency is thought to be reduced, however, with increased specimen taper [31]. Design of the specimen taper should be accomplished in perspective of K-gradient criteria [25] so that closure effects are minimized.

Discussion

Development of fatigue data, as described previously, constitutes an approach to establishment of material property information that is critical to better assuring the integrity of marine structures undergoing small amplitude stress excursions at low frequencies. Ultimately, such data must be incorporated into an overall design criteria methodology which, in addition, includes other features. Foremost among these are: (1) realistic prediction of

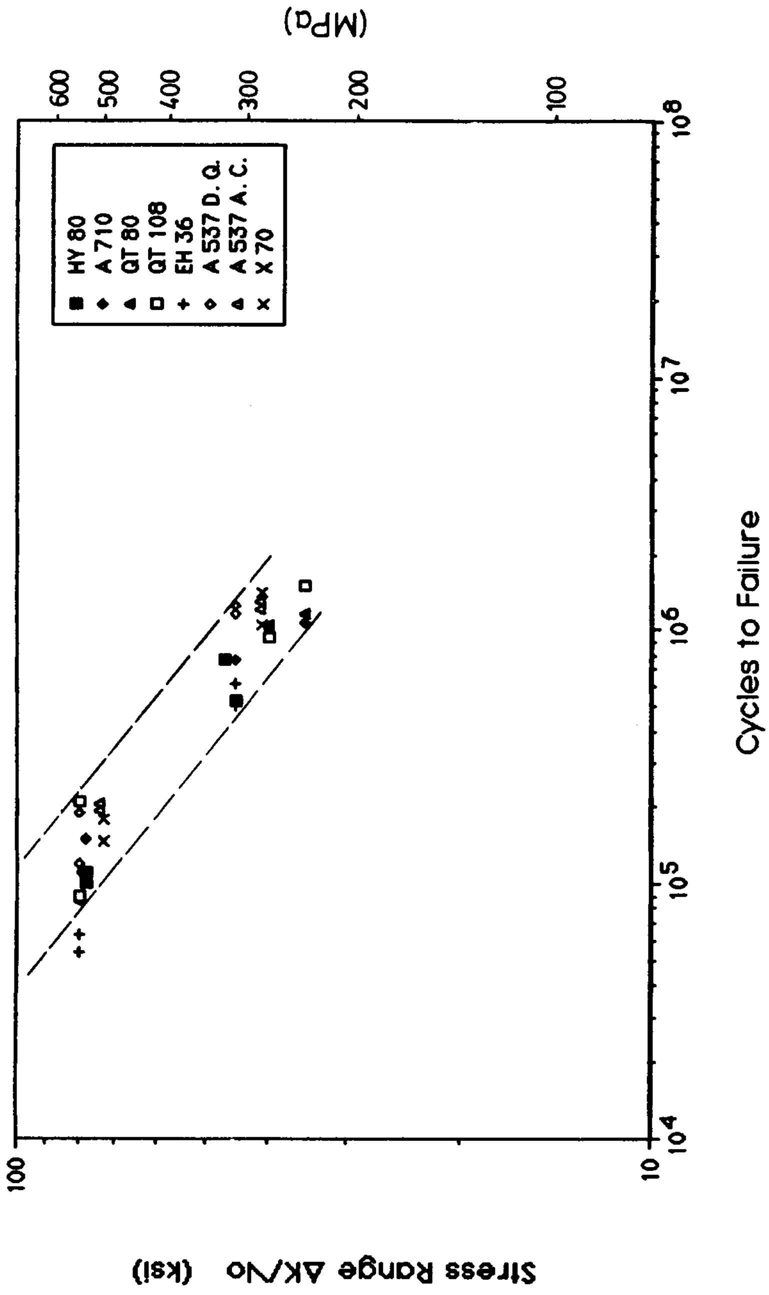

FIG. 13—*Data for freely corroding compact tension specimens fatigued in seawater at 1.0 Hz.*

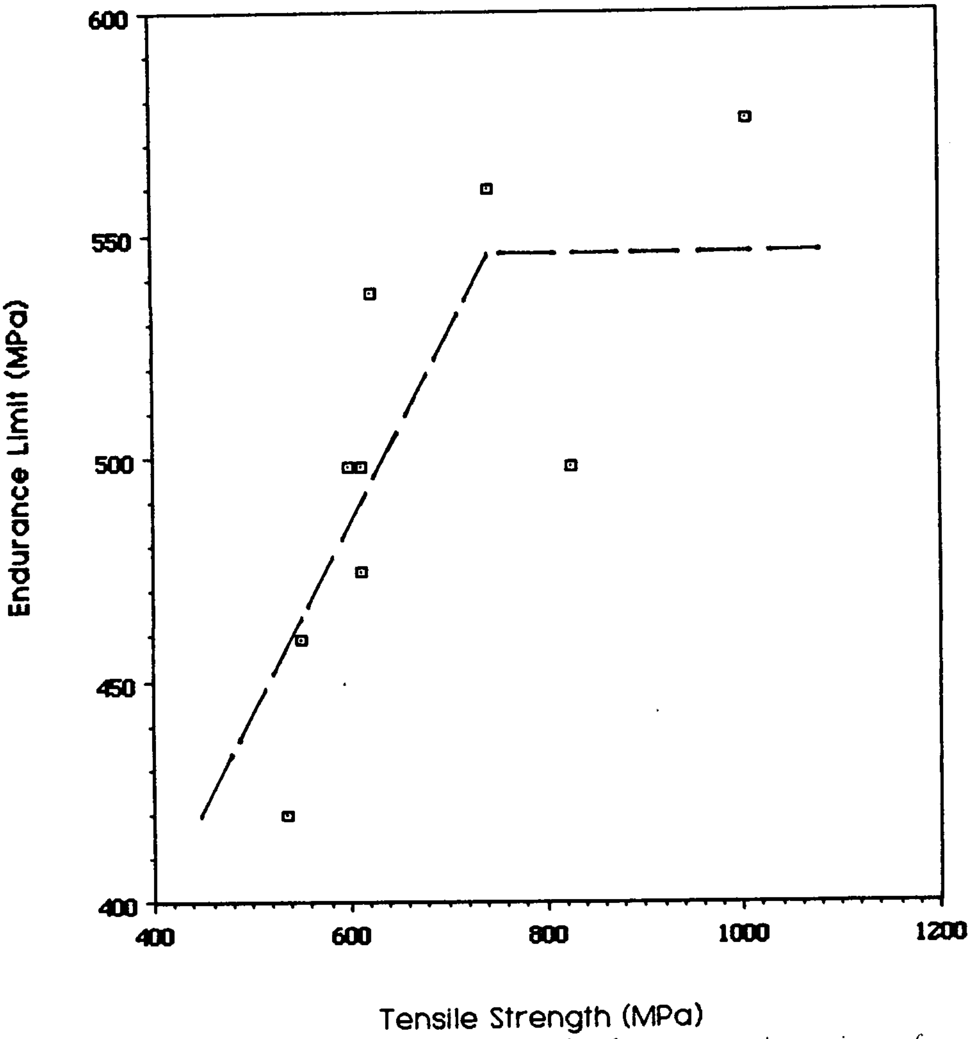

FIG. 14—*Endurance limit versus tensile strength data for compact tension specimens of higher strength steels fatigued in seawater at 1.0 Hz and −1.10 V (SCE).*

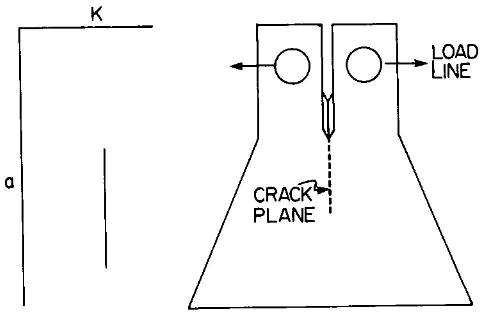

FIG. 15—*Schematic representation of tapered, constant stress-intensity CT specimen.*

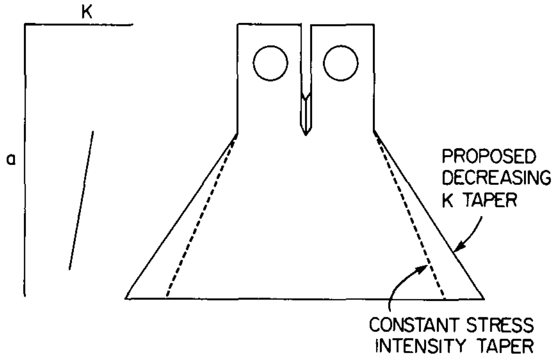

FIG. 16—*Schematic representation of tapered, decreasing stress-intensity CT specimen.*

service stress history, (2) accurate representation of nominal stresses at critical locations such as welded connections ("hot-spot" stresses), and (3) characterization of local weld geometry and assurance that this is comparable to that of actual structures. Once these are accomplished, then a realistic design procedure may be developed and implemented. A critical component is that the fatigue data and, hence, the design curve which is established from these, be applicable to the service application in question. Further, features which complicate application of fatigue data, such as load interactions, startup and transition effects, are represented by or included as factors of safety rather than being established by either deterministic or probabilistic analyses. Certainly a next step in the marine steels fatigue data development process should include addressment of these specific factors, since only in this manner can the design process be made more efficient and effective.

Acknowledgments

The author is indebted to the American Petroleum Institute (API) for financial support which has made possible the fatigue test system development reported here. Helpful comments and encouragement from the API Resource Group 7 on Welding, Testing and Materials is also appreciated. The efforts of Mr. Jack Hankison in fabrication and maintenance of the test systems are also acknowledged.

References

[1] Hicks, J. G., "Material and Structural Problems in Offshore Installations," *Proceedings*, Conference on Welding in Offshore Constructions, 1974, p. 1.
[2] Wintermack, H., "Materials and Welding in Offshore Constructions," 1975 Portevin Lecture, International Institute of Welding.
[3] Marshall, P. W., "Problems in Long-Life Fatigue Assessment for Fixed Offshore Structures," preprint 2638, American Society of Chemical Engineers' National Water Resources and Ocean Engineering Conference, San Diego, April 1976.
[4] Hartt, W. H., *Proceedings*, Second International Conference on Environmental Degradation of Engineering Materials, M. R. Louthan, R. P. McNitt and R. D. Sisson, Eds., Virginia Technical Printing Department, Blacksburg, VA., 1981, p. 97.
[5] Heller, S. R., Fioriti, H., and Vasta, J., *Journal Navigation Engineers*, Feb., 1965, p. 29.
[6] Wirsching, P. W., *International Journal of Fatigue*, Vol. 2, 1980, p. 77.
[7] Hertzberg, R. W., *Deformation and Fracture Mechanics of Engineering Materials*, Wiley, New York. Second Ed.. 1983. p. 461.

[8] Barsom, J. M. and Rolfe, S. T., *Fracture and Fatigue Control in Structures,* Prentice-Hall, Englewood Cliffs. NJ. Second Ed.. 1987. PP. 22-25.
[9] Nelson, D. V. and Socie, D. F., "Crack Initiation and Propagation Approaches to Fatigue Analysis," *Design of Fatigue and Fracture Resistant Structures, ASTM STP* 761, American Society for Testing and Materials, Philadelphia, 1982, p. 110.
[10] Hartt, W. H. and Lin, N. K., "Fatigue of Welded Steel in Sea Water as Applicable to Offshore Structures," USj Austria Joint Seminar on Stochastic Structural Mechanics, 4-5 May 1987, Boca Raton, FL.
[11] Baxter, C. F. G. and Booth, G. S., *Welding Institute Research Bulletin,* Sept. 1979, pp. 257-261.
[12] Haagensen, P. J., Dragen, A., Slind, T., and OIjasaeter, 0., *Proceedings,* Third International European Coal and Fuel Community Offshore Conference on Steel in Marine Structures, Elsevier, Amsterdam, 1987, pp. 689-698.
[13] Proceedings of Select Seminar, European Offshore Steel Research, Vol. I and II, U. K. Department of Energy, 1978.
[14] Endo, K. and Komai, K. in *Corrosion Fatigue: Chemistry, Mechanics and Microstructure,* O. Devereux, A. J. McEvily, and R. W. Staehle, Eds., National Association of Corrosion Engineers, 2, 1972, pp. 437-450.
[15] Taylor, M. E., and Barsom, J. M., *Fracture-Thirteenth Coriference, ASTM STP* 743, R. Roberts, Ed., American Society for Testing and Materials, Philadelphia, 1981, pp. 599-622.
[16] Endo, K. and Miyas, Y., *Bulletin,* Japanese Society of Mechanical Engineers, Vol. I, 1958, pp. 374-380.
[17] Petit, D. E., Hoeppner, D. W., and Hyler, W. S., *Effects of Environments and Complex Load History on Fatigue Life, ASTM STP462,* American Society for Testing and Materials, 1970, pp. 241-257.
[18] Wintermack, H., "Materials and Welding in Offshore Constructions," ı*Y/5 Portevin Lecture,* International Institute of Welding.
[19] Sablok, A. K., and Hartt, W. H., "Fatigue of High Strength Steels in Sea Water," *Proceedings,* Seventh International Offshore Mechanics and Arctic Engineering Conference, Vol. III, 1988, pp. 477-486.
[20] Jaske, C. E., Payer, J. H., and Balint, V. S., *Corrosion Fatigue of Metals in Marine Environments,* MCIC-81-42, Battelle Columbus Laboratory, July 1981, p. 60.
[21] Section 10: Structural Welding Code, ANSljAWS D1.1-86, American Welding Society, Miami, 1986, pp. 164-169.
[22] Lin, N. K., and Hartt, W. H., "Simulation and Prediction of Spectrum Fatigue for Offshore Structures," *Proceedings,* Specialty Conference on Computer Methods in Offshore Engineering, Canadian Society for Civil Engineers, 1984, pp. 189-211.
[23] Hartt, W. H., and Lin, N. K., "A Proposed Stress History for Fatigue Testing Applicable to Offshore Structures," *Journal of Fatigue,* Vol. 8, 1986, pp. 91-93.
[24] Hartt, W. H., Lin, N. K., and Chu, Z. H., "Fatigue Life of Welded Structural Steel Under Realistic Loading in Sea Water," *Proceedings,* Offshore Mechanics and Ocean Engineering Conference, Tokyo, American Society of Mechanical Engineers, 1986, pp. 256-261.
[25] E647-86a, "Standard Test Method for Measurement of Fatigue Crack Growth Rate," 1986 *Annual Book of ASTM Standards,* American Society for Testing and Materials, Philadelphia.
[26] Barsom, J. M. and McNicol, R. C., *Soil Specimen Preparationfor Laboratory Testing, ASTM STP* 599, American Society for Testing and Materials, Philadelphia, 1974, pp. 183-204.
[27] May, R. A., Stuber, A., and Rolfe, S. T., *WRC Bulletin No.* 243, Welding Research Council, 1978, pp. 1-26.
[28] Yoder, G. R., Cooley, L. A., and Crooker, T. W., "A Comparison of Microstructural Effects on Fatigue-Crack Initiation and Propagation in Ti-6AI-4V," Paper No. AIAA82-0660-CP, 23rd Structures, Structural Dynamics and Materials Conference, AIAAjASMEjASCEjAHS, 10-12 May, 1982, New Orleans.
[29] Rajpathak, S. S. and Hartt, W. H., "Keyhole Compact Tension Specimen Fatigue of Selected High Strength Steels in Sea Water," *Environmentally Assisted Cracking: Science and Engineering, ASTM STP 1049,* American Society for Testing and Materials, Philadelphia, 1990, pp. 425-446.
[30] Rajpathak, S. S. and Hartt, W. H., "Fatigue Crack Initiation of Selected High Strength Steels in Sea Water," *Proceedings,* Seventh International Offshore Mechanics and Arctic Engineering Conference, 1988, pp. 323-332.
[31] Mostovoy, S., Crosley, P. B., and Ripling, E. J., *Journal of Materials,* Vol. 2, 1967, pp. 661-681.
[32] Dunegan, H. L. and Tetelman, A. S., *Engineering Fracture Mechanics,* Vol. 2,1971, pp. 387-402.

George A. Andersen[1] and William Leong[1]

Corrosion Testing in New York Reservoirs and Investigations of In-Service Corrosion

---

REFERENCE: Andersen, G. A. and Leong, W., "Corrosion Testing in New York Reservoirs and Investigations of In-Service Corrosion," *Corrosion in Natural Waters, ASTM STP 1086.* C. H. Baloun, Ed., American Society for Testing and Materials, Philadelphia, 1990, pp. 70-79.

ABSTRACT: Immersion tests of various duration were performed on copper-based alloys, nickel-based alloys, cast irons, and stainless steels. Specimens were exposed at two upstate New York reservoirs as well as in a laboratory environment. The type of corrosion as well as the amount of corrosion varied with heat treatment condition and composition of the sample. All stainless steel samples showed minimal corrosion of any kind except a martensitic grade which exhibited crevice attack with attendant pitting. In-service corrosion of water mains has been also examined. Metallurgical failure analysis of cast iron water mains has revealed waterside corrosion to be only a minor contribution to the cause of failure in a majority of the breaks.

KEY WORDS: reservoir exposure tests, cast iron, potable water, Ni-Resist, chlorides, water mains, tuberculation, steadite, graphitization, failure analysis

In the early 1960s the Board of Water Supply (New York City) initiated a program of in-plant type corrosion tests of metals and alloys in several upstate New York reservoirs [1,2]. The Department of Environmental Protection (DEP) of The City of New York absorbed the Board in 1978 and had the task of continuing the corrosion testing program.

The Bureau of Water Supply-Quality Assurance Division of DEP has been interested in the study of corrosion behavior of various metals for a number of reasons which include:

(a) Realizing that corrosion of metals by potable waters is universal and that the most useful corrosion results are those obtained by tests in actual service waters;
(b) determination of the adequacy of a particular metal for use in water works which supply close to 1.5 billion gallons of water per day; it was of interest to test not only alloys of classes of materials commonly used in waterworks (for example, cast iron) but also to investigate many other metals that are used in rather small quantities in specific parts of water works equipment.
(c) construction of water works distribution systems which will enable the longest possible use without interruption because of need of repair or replacement.

This paper is a brief review of the results obtained from the following corrosion test performed within the last nine years.

1. Immersion tests of aluminum bronzes and stainless steels for 20 months duration conducted at Kensico Reservoir, Valhalla, New York.

---

[1] Metallurgical engineers, City of New York Department of Environmental Protection, New York, NY 10004.

II. Long-term (8.5 years) exposure tests performed at the Rondout Reservoir, Grahamsville, New York, on various alloys including copper-based alloys, nickel-based alloys, gray cast iron, ductile iron, and Ni-Resist irons.
III. Laboratory tests on several grades of wrought stainless steel immersed in potable water of varying chloride concentrations.
IV. Investigations of in-service corrosion of gray cast iron water mains by New York City potable water.

Immersion Tests of Alloy Samples in New York Reservoirs (I and II)

Immersion tests at both reservoirs consisted of exposing disk-shaped specimens with a machined finish attached to corrosion testing spools of the type described in ASTM Guide for Conducting Corrosion Coupon Tests in Plant Equipment (G 4-84). Stainless steel specimens were square shaped and had 120 grit finish on one side and sandblasted finish on the other. The test environment was semi-stagnant freshwater with temperatures ranging from 5 to 15°C, depending on the season. Table 1 shows the average analyses of the test waters.

Results and Discussion

Table 2 shows the types and composition of aluminum bronzes exposed at Kensico Reservoir. The corrosion rate of four specimens of each alloy, as determined by the standard methods described in ASTM Recommended Practice for Preparing, Clearing, and Evaluating Corrosion Test Specimens (G 1-88), are also shown.

Of the two wrought grades of aluminum bronze tested, the nickel-bearing grade, C630, showed a lower corrosion rate although it had some tuberculation with discoloration underneath. Type C613 experienced dealuminification in a crevice formed by the spool washer.

Alloy C952 was tested in the as-cast as well as in the annealed condition. In the annealed condition the corrosion rate is 0.940 p.m/year with only uniform attack. In the as-cast condition the corrosion rate is nearly 10 times greater with extensive dealuminification and tuberculation. Alloy C954 had one of the highest corrosion rates of the grades tested. The two cast nickel-aluminum bronzes C955 and C958 appear to be as susceptible to dealuminification as the nonnickel grades C953 and C954 although the attack on the nickel grades is more localized.

Results of exposure tests of wrought austenitic stainless steels in various metallurgical Conditions is shown in Table 3. These samples were prepared by the Welding Research Council

TABLE 1—*Average analyses of test water, mg/L.*

	Rondout	Kensico
Total solids	45.0	84.0
Chloride	3.4	7.6
Hardness	19.0	21.0
Alkalinity	16.0	18.0
Iron	trace	0.04
Manganese	trace	0.02
Carbon dioxide	2.2	4.0
Dissolved oxygen	11.5	11.6
pH	6.9	6.8
Specimen conductance	52 μmhos/cm	54 μmhos/cm
Phosphates, total	0.016	0.05

TABLE 2—*Aluminum bronzes exposed 20 months at Kensico Reservoir.*[a]

Alloy Type	Cu	Al	Fe	Ni	Mn	Others	Avg. Corrosion Rate,[b] μm/year
C613	90.71	6.72	2.21	0.02	...	0.34	2.670
C630	81.46	9.90	2.73	4.72	0.75	0.44	0.740
C952 as cast	87.99	8.82	3.16	0.02	...	0.01	7.775
C952 annealed	87.99	8.82	3.16	0.02	...	0.01	0.940
C953 annealed	88.8	9.65	1.20	0.14	0.10	0.13	1.525
C954 annealed	85.83	10.32	3.66	0.10	0.02	0.07	5.590
C955 quenched, drawn	80.86	10.23	4.17	4.14	0.54	0.03	0.710
C958 annealed	80.49	9.00	3.89	4.49	1.95	0.18	1.145

[a] Compositions in weight percent.
[b] In μm/year; multiply by 0.0373 to obtain mils per year.

[3]. The general corrosion rate for all types in all conditions is not more than 0.090 J.1m/year. No pitting was observed on any sample although one did show crevice attack. Generally the annealed condition of each type had the greatest corrosion resistance. There are inconsistencies in corrosion resistance between samples that were as-welded and those that were given a sensitizing treatment (677°C for 1 h, air cooled) for the same types investigated (for example Type 316L). Nevertheless, the corrosion rates involved are vanishingly small.

Tables 4 and 5 show, respectively, the corrosion rate and composition of ferrous alloys and nonferrous alloys exposed at Rondout Reservoir for 8.5 years.

TABLE 3—*Austenitic stainless steels exposed 20 months at Kensico Reservoir.*

Type	Condition	Avg. Corrosion Rate,[a] μm/year
302	annealed	0.0076
302	as-welded, E308	0.0153
304	1250°F, 1 h[b]	0.0483
304	as-welded, E308	0.0381
304L	annealed	0.0076
304L	1250°F, 1 h	0.0153
304L	as-welded, E308L	0.0153
316	annealed	0.1524[c]
316	1250°F, 1 h	0.0508
316	as-welded, E316	0.0890
316L	annealed	0.0508
316L	1250°F, 1 h	0.0711
316L	as-welded, E316L	0.0102
347	annealed	0.0508
347	1250°F, 1 h	0.0508
347	as-welded, E347	0.0711
321	annealed	0.0254
321	1250°F, 1 h	0.0254
321	as-welded, E347	0.0153

[a] In μm/year; multiply by 0.0393 to obtain mils per year.
[b] 1° F = −17.8°C.
[c] Crevice attack.

TABLE 4—*Non-ferrous metals exposed at Rondout Reservoir.*[a]

Material	Cu	Zn	Mn	Ni	Fe	Al	Sn	Pb	Si	Other	Avg. Corrosion Rate,[b] μm/year
Turbine metal	54.12	36.74	3.95	3.52	1.19	0.5	0.054				7.62
C865	68.15	39.08			1.17	0.31	0.40	0.14			7.37
C280	61.0	38.9			0.01		0.02	0.025			24.40
C905	88.0	10.0					2.0				10.42
Monel 400	30.25		1.19	67.12	1.17				0.12		0.25
C658	95.81		0.97		0.06				3.17		18.20
Nionel	1.88			40.13	29.65					21.82 Cr 3.67 Mo	0.01
C923	88.0	3.0					9.0				13.20

[a] Compositions in weight percent.

[b] In μm/year; multiply by 0.0393 to obtain mils per year.

Nickel-based Nionel underwent very little attack with an almost immeasurable uniform corrosion rate. Monel 400 also had a low uniform corrosion rate although there was crevice attack. Reedy found Monel 400 to be virtually corrosion resistant in Southern California potable water [4].

Cast tin bronze (C905), cast manganese bronze (C865), and turbine metal are next best in order of decreasing corrosion rate. Most of the weight and loss in the manganese bronze specimens were due to dezincification.

Muntz metal (C260) and silicon bronze (C658) exhibited somewhat higher corrosion rates than the other copper-based alloys.

TABLE 5—*Ferrous metals exposed at Rondout Reservoir.*[a]

Material	C	Si	Mn	Mg	Ni	Cr	Cu	Avg. Corrosion Rate,[b] μm/year
Gray cast iron	3.30	2.00	0.88					64.52
Ductile iron	3.79	2.30	0.30	0.035				69.60
Ni-Resist Type II	2.96	2.29	1.01		18.27	2.04		17.27
Ni-Resist Type II B	3.02	2.13	0.83		18.00	3.70		25.91
Ni-Resist Type II D	2.77	2.33	1.10	0.14	20.43	2.14		24.64
Ni-Resist Type D II B	2.86	2.77	1.21	0.11	20.80	3.77		24.91
Ni-Resist Type D III	2.44	2.20	0.60	0.11	29.63	3.10		24.38
Ni-Resist Type D IV	2.35	5.48	0.50	0.13	30.85	4.85		13.72
Ni-Resist Type hardenable		1.48	0.58		8.60	1.95	3.88	25.15
Gray cast iron[c]								66.30

[a] Composition in weight percent.

[b] In μm/year; multiply by 0.0393 to obtain mils per year.

[c] With monel spacers.

All of the ductile Ni-Resist grades had about equal corrosion resistance. The corrosion rate of these is about 25.0 /Lm/year. Ni-Resist ductile Type D IV, however, had a corrosion rate about one half of the ~ate of the other Ni-Resists. It is interesting to note that the silicon content of Type D IV is approximately double that of the other types. Ordinary ductile iron and gray cast iron showed about 2)1ȷtimes the corrosion rate of the Ni-Resist types, with ductile iron being just slightly worse than gray cast iron. The best of the ductile Ni-Resist types, Type D IV, had a corrosion rate close to that ofC923, leaded tin bronze.

Long-Term Laboratory Immersion Testing of Stainless Steel in Potable Water (III)

Briefly, the work reported herein involves the comparative behavior of four wrought grades of stainless steel; namely, Type 410 martensitic, Type 304 and 316L austenitic, and Type 630 H900 martensitic precipitation hardening in distilled New York City tap water containing four concentrations of chlorides. Maximum chloride concentration of New York City water is about 33 mg/L. Tests were conducted in accordance with ASTM Recommended Practice for Laboratory Immersion Corrosion Testing of Metals, G 31-72 (1985).

The samples of each alloy were in the form of 25 by 100 by 3.2 mm coupons with 180 grit finish and passivated in a 20% nitric acid solution. Plastic shims were fixed to the coupons by means of a nylon screw and nut in order to simulate a condition where crevice corrosion, if any, might occur. All samples were held in individual jars containing 900 mL of stagnant distilled water solutions at room temperature with chloride concentrations of 10\ 10^3, 10^2, and 10 mg/L; the test solution was changed monthly. After 8.5 years exposure, specimens were evaluated in accordance with ASTM Specification G 1. Three samples of each alloy were tested at each chloride concentration.

No specimens, except the Type 410 stainless steel, showed any crevice corrosion, pitting, or rusting. Actual data for the pitting which occurred under the shim are as follows for the Type 410 steel specimens:

Chloride Concentration, mg/L	Pit Depth, μm
10^4	1905
10^3	1625, 1370, 1220, 685
10^2	75
10	none

Type 410 martensitic stainless steel resists pitting and crevice corrosion by chlorides considerably less than the other grades of stainless steel. General corrosion rates of Type 304, Type 316L, and Type 630 H900 are all under 0.125 /Lm/year.

Investigation of Internal Corrosion in Water Mains (IV)

Several previous studies have suggested that the primary cause of water main breaks is loss of strength by corrosion [5,6]. It has been contended that the majority of breaks originate at locations along the pipe wall weakened by general corrosion and pitting of steel mains and by graphitization in the case of cast iron mains. In-house failure analysis capability of the Bureau of Water Supply Quality Assurance Division has allowed detailed analysis of each major water main break case. Major breaks are those which involve other utilities, property damage, or both.

Investigation of 30 major breaks of cast iron water main pipe ranging in age from 23 to 120 years old, Fig. 1, has revealed that corrosion is usually only a minor and contributing

FIG. 1—*Typical excavation at a major water main break. Main is 100 years old.*

factor to the break. Only in four cases did graphitization penetration exceed 20% of the pipe wall thickness from the waterside. Several breaks of subaqueous mains have showed excessive external corrosion by seawater. Also, there have been a few breaks of buried pipe entirely due to corrosion by aggressive backfill and stray current discharge.

When internal corrosion by potable water is encountered, it is almost always associated with tuberculation. Graphitization of the cast iron occurs beneath tubercules in such a way that the effect cannot be distinctly classified as surface, plug, or complete graphitization. Instead, the type of damage observed is usually a combination of surface and plug graphitization as shown in Fig. 2.

Table 6 shows corrosion rate data obtained through metallographic examination of samples from the main breaks that were investigated. In each case, the sample was removed from the origin of failure. Only internal corrosion by water is considered. The occurrence of external corrosion in New York City is widely varying and only in a few locations is there a frequent problem with external corrosion. This can be illustrated by considering the corrosion characteristics of four 914.40-mm (36-in.) diameter water mains, each over 80 years old. The rates of internal corrosion for those mains are 7.5, 15, 23, and 25 ILm/year; the highest rate is approximately three times the lowest rate. Rates of external corrosion, on the other hand, are 3.9, <2.5, 10, and 33 ILm/year, respectively. This represents a maximum rate that is more than 13 times greater than the lowest rate for the four water mains concerned.

This more extreme variation could be attributed to the variety of soil conditions that influence external corrosion rate. However, these rates tend to indicate galvanic action only, and therefore were not considered to effect internal corrosion.

Results and Discussion

The average penetration of graphitization at the failure origin for all cases is approximately 30 ILm/year, Table 6. Breaking the data down to corrosion penetration rate according to the

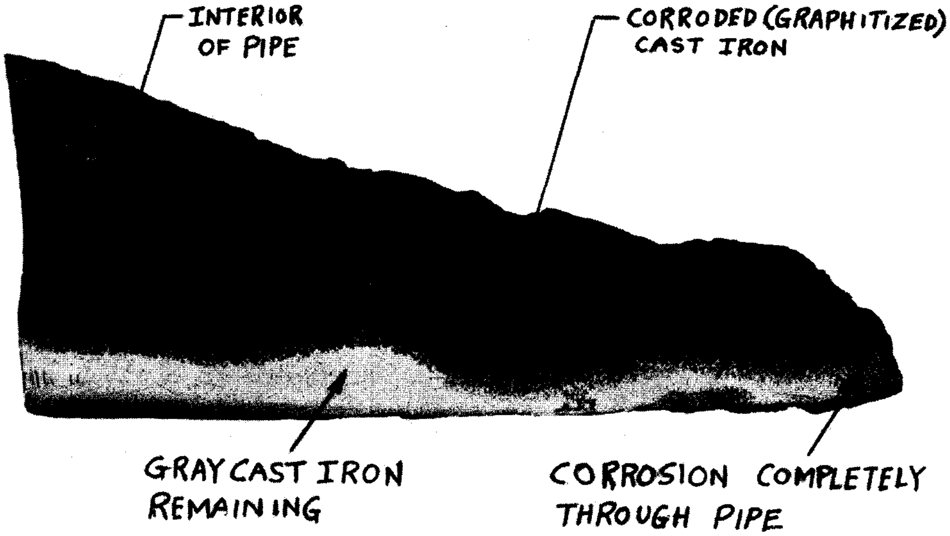

FIG. 2—*Graphitization along waterside of a gray cast iron main (×2).*

TABLE 6—*Internal corrosion data for gray cast iron water mains.*

Age of Water Main, years			
<60	60 to 80	81 to 99	100 and over
	Rate of Internal Corrosion[a]		
20.3	25.4	25.4	25.4
50.8	38.1	25.4	17.8
	50.8	15.2	33.0
	15.2	20.3	20.3
	88.9	15.2	0 (lined)
	101.6	25.4	5.0
17.8	17.8	38.1	17.7
	55.9	7.6	
	35.6	22.9	
	Average[b]		
29.6	47.7	21.7	17.0

[a] Expressed as equivalent depth of attack, μm/year.

[b] μm/year.

age of the main, it can be seen that mains in service 60 to 80 years have sustained the greatest rate of internal corrosion (48 J.Lm/year).The corrosion rate diminishes to about 21.6 J.Lm/year for mains in service 81 to 99 years, while for mains over 100 years old the rate decreases to approximately 17 J.Lm/year.For comparison, the corrosion rate of gray cast iron exposed for 8.5 years at Rondout Reservoir (Table 5) is 64.5 J.Lm/year.Thus, for thick-walled gray cast iron water mains, graphitization does not appear detrimental even after 100 years of service. In this sense, graphitization may be considered a form of corrosion control.

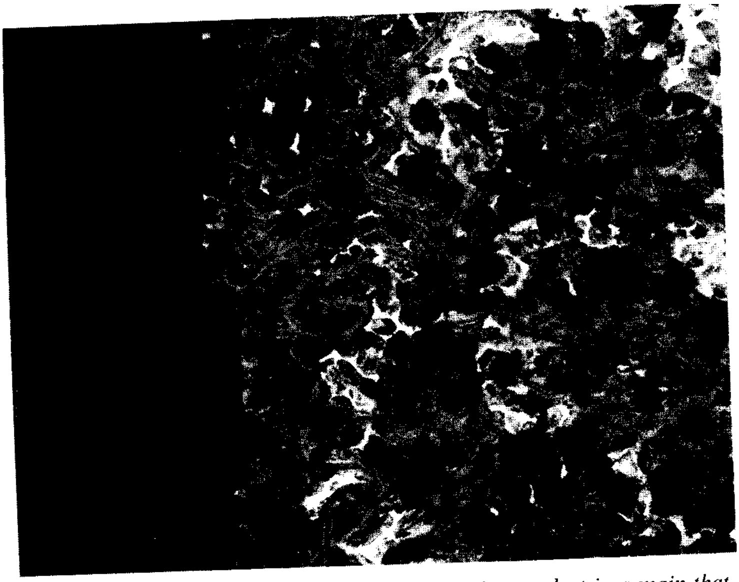

FIG. 3—*Abundance of steadite within the mass corrosion product in a main that graphitized at a rate of 4 mil/year (×50).*

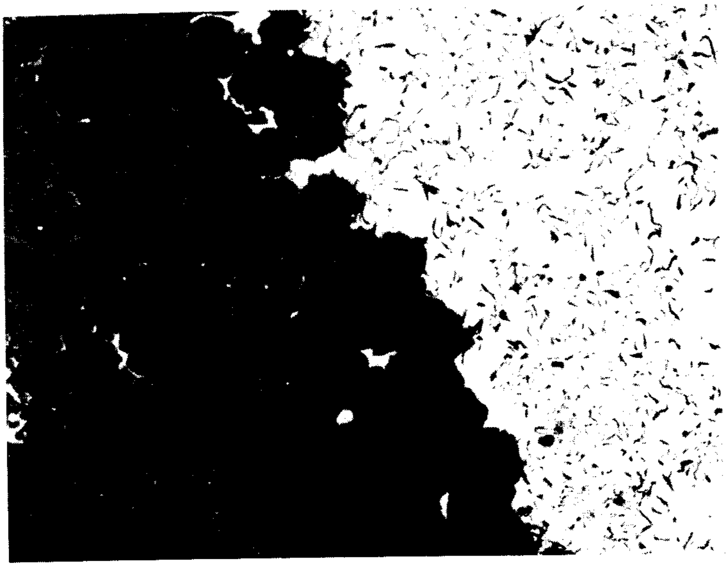

FIG. 4—*Minimal amount of steadite in a main that graphitized at a rate of 0.8 mil/year (×50).*

An interesting observation is that mains with greater percentage of internal corrosion also contained a greater proportion of steadite microconstituent than did mains that corroded internally at a low rate, say, 25 /Lm/year. This is illustrated by Figs. 3 and 4. Steadite, a eutectic of iron and iron phosphide, was also more predominant in the older mains because of the higher amounts of phosphorus allowed by pre-twentieth century pipe-making metallurgy. A correlation of these findings awaits further investigations.

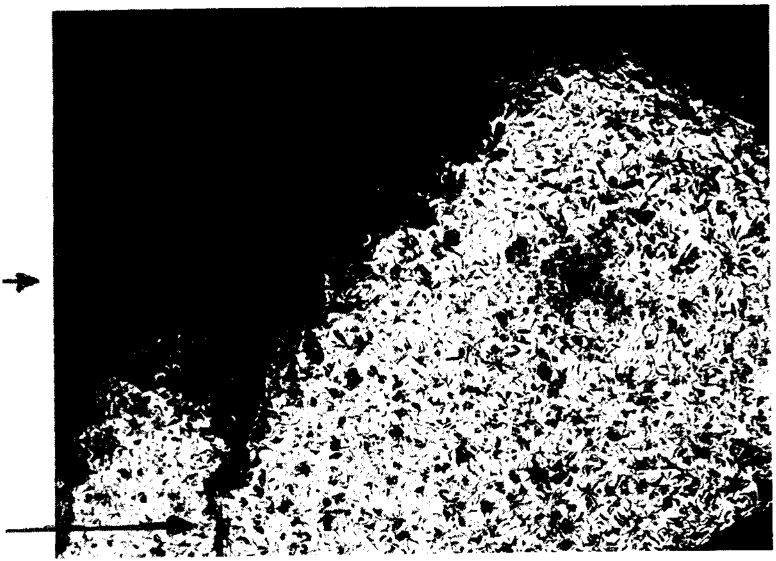

FIG. 5—*A secondary crack in a cast iron pipe that is graphitized all around (×10).*

Internal graphitization can also be useful in analyzing main breaks that were caused by external stress overloads. Figure 5 shows an example where an internal secondary crack is completely surrounded with graphitization products. This gives clue that the crack originated prior to, during, or shortly after installation.

Conclusions

Long-term immersion testing has provided results that are useful in selection of alloys for use in City Water Tunnel 3, currently under various design and construction stages, as well as for the maintenance of the existing Tunnels I and 2.

Laboratory results obtained from long-term tests of stainless steels in potable waters containing chlorides in concentrations many times greater than in New York City drinking water has not caused pitting or crevice corrosion except in a martensitic grade.

Metallurgical failure analysis of cast iron water mains has been conducted during the last five years. Graphitization of gray cast iron water mains in up to 120 years exposure to New York City potable water also has been characterized.

Acknowledgments

The authors wish to thank S. Goldspiel, P.E., for his work in the reservoir and laboratory testing. Thanks also go to W. McMurray, P.E., and E. Scheader, P.E., for their continued encouragement in this work.

References

[1] Geld, I. and McCaul, C. *Materials Protection and Performance,* Vol. II, No.2, 1972, p. 41.
[2] McCaul, C. and Geld, I. *Materials Performance,* Vol. 17, No.5, 1978, p. 27.
[3] Tice, E. A., *Welding Research Council Bulletin No.* 138, 1969.
[4] Reedy, D. R., *Materials Performance,* Vol. 12, No.4, 1973, p. 43.
[5] Fitzgerald, J. H. *Journal, American Water Works Association,* Vol. 60, No.8, 1968, p. 882.
[6] Jakobs, J. A. and Hewes, F. W. *Materials Performance,* Vol. 26, No.5, 1987, p. 42.

Prakash M. Temkar,[1] *Richard J. Scholze, Jr.,*[1] *Stephen W. Maloney,*[1]
and Chester H. Neff[2]

Evaluating Corrosion Control in Water Distribution Systems at U.S. Army Bases

REFERENCE: Temkar, P. M., Scholze, R. J., Jr., Maloney, S. W., and Neff, C. H., "Evaluating Corrosion Control in Water Distribution Systems at U.S. Army Bases," *Corrosion in Natural Waters, ASTM STP 1086,* C. H. Baloun, Ed., American Society for Testing and Materials, Philadelphia, 1990, pp. 80-100.

ABSTRACT: The U.S. Army Construction Engineering Research Laboratory (USA-CERL) has employed an apparatus known as the Pipe Loop System (CERL-PLS) to evaluate corrosion and corrosion control programs in distribution water systems. The apparatus uses multiple corrosion specimens of distribution system materials in direct contact with water under conditions simulating typical operation. At two U.S. Army water treatment plants, the CERL-PLS was used to monitor corrosion of mild steel and galvanized steel piping materials in the distribution system and determine the effect of a corrosion inhibitor on the long-term corrosion rates. At another Army installation, the effects of various water treatment options were studied for reducing lead dissolution from plumbing system materials. The data presented demonstrate the successful application of a pipe loop system for optimization of water treatment for corrosion control and hence to meet drinking water quality standards.

KEY WORDS: corrosion, water distribution system, pipe loop system, water quality, internal corrosion, water treatment, corrosion inhibitors

Water distribution systems represent a major investment for U.S. Army bases, and evaluation of their physical condition, and changes in that condition, are hindered by the inability to examine them without excavation. Water quality and distribution system materials vary throughout the world, thus general rules regarding the effect of a specific water on a specific material require addressing a large matrix of parameters. Many of these parameters are difficult and expensive to measure, thus a simple method of determining the overall effect of the water quality on a distribution system is highly desirable.

Internal corrosion has been estimated to cost the water works industry between $700 million and $1 billion dollars per year. Although the effects of corrosion cannot be completely eliminated from water distribution systems, substantial savings are possible by implementing various corrosion control programs [1]. Aside from economic concerns, regulatory issues must be considered. Corrosion products that enter the water distribution system may violate public health regulations, requiring that specific water quality criteria must be met at the consumer's tap. The U.S. Environmental Protection Agency (USEPA) recognizes that corrosion problems are unique to each water supply system. The USEP A has established regulations to identify potentially corrosive waters and to determine what materials are present in distribution systems [2].

---

[1] Environmental engineers, U.S. Army Construction Engineering Research Laboratory, Champaign, IL 61820-1305.

[2] Principal scientist, Illinois State Water Survey, Champaign, IL 61820.

The U.S. Army Construction Engineering Research Laboratory (USA-CERL) has developed and employed an apparatus known as the USA-CERL Pipe Loop System (CERL-PLS) to objectively evaluate corrosion and corrosion control techniques in water distribution systems on U.S. Army bases. The apparatus is designed to be flexible and is also capable of simulating the environmental conditions occurring in building potable water systems. The details and results of corrosion studies at two U.S. Army water treatment plants using the CERL-PLS are presented in this report.

Corrosion Monitoring Equipment and Methods

Standard pipe test loops were constructed of 19.05 mm (% in.), Schedule 40 polyvinyl chloride (PVC) and chlorinated polyvinyl chloride (CPVC) pipe and fittings as shown in Fig. I. PVC and CPVC materials are readily available and have suitable characteristics for potable water. These materials eliminate all metallic components, except for the corrosion specimens, and electrically isolate the corrosion specimens from one another in the test assembly. The pipe test loop is oriented vertically to minimize the amount of suspended matter deposited on the exposed surfaces of the corrosion specimens. A flow controller (FC), a flow rate meter (FR), and regulating valves (VI) are provided to maintain flow through the loop at desired rates. If fluctuating water pressure occurs, a pressure regulating valve (PRV) can be used on the inlet piping of the test loop. A totalizing water meter (M) is also included in the design to verify water usage information during monitoring intervals. A static mixer in the

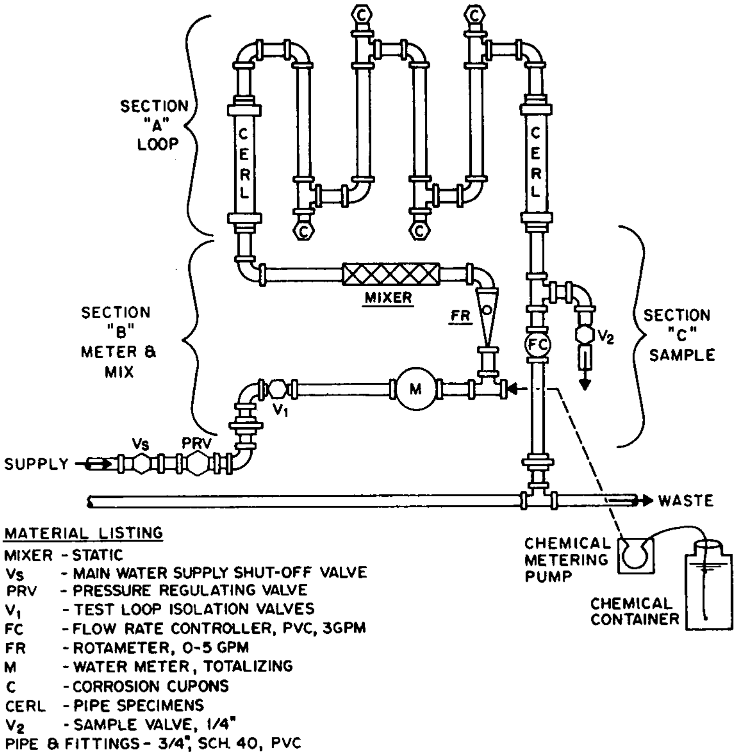

FIG. 1—*Schematic of USA-CERL pipe loop system.*

loop system is optional for mixing the water and chemical(s), injected by a chemical metering pump in order to study the effectiveness of a selected corrosion inhibitor. The continuous flow of both water and inhibitor insures that constant inhibitor concentrations are in contact with the corrosion specimens at all times. Sampling valves (Y2) were installed in the loop to collect water samples periodically for chemical analyses and to verify inhibitor concentrations.

The USA-CERL pipe specimen holder (Fig. 2) is different from the assembly used in the ASTM Standard Test for Corrosivity of Water in the Absence of Heat Transfer (Weight Loss Method) (O 2688-83 Method C). The CERL design eliminates the sleeve used in the ASTM design, reduces fabrication time, and with its uniform dimensions, allows holders to be interchanged. Unobstructed water flow is maintained through the pipe specimens to simulate deposition or corrosion processes occurring on the walls of piping in a distribution system.

Corrosion specimens were machined from standard pipe or tubing materials. The cleaning and preparation of pipe specimens were according to the ASTM test method. The exterior of the pipe specimens were coated with a high-build epoxy-polyamide paint limiting the exposed surface area during installation to 66 cm^2 of the interior wall. Two pipe corrosion specimens were installed in each specimen holder. The corrosion rates of the pipe specimens were determined on removal by weight loss measurements according to the aforementioned ASTM test method.

Four standard metal coupons can be installed in the test loop, all oriented in the same direction in relation to the flow of water through the loop. The coupons were mounted on a PYC pipe plug by means of a nylon or Teflon stem protruding into the middle of the pipe, exposing approximately 21.3 cm^2 of surface area to the bulk water. The coupons and mounting hardware were purchased from a commercial vendor and the ASTM test method was followed for determining corrosion rates by weight loss measurements.

All of the components of the test loop are assembled with pipe hanger supports on a plywood sheet 0.91 by 1.22 m (3 by 4 ft). The completed assembly requires minimal wall space when installed and is easily transported as a complete unit (Fig. 3).

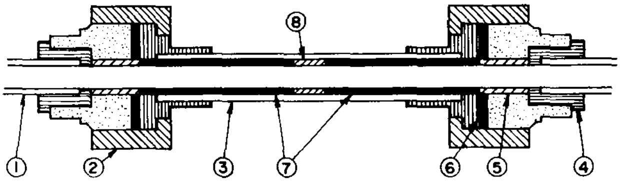

① 3/4" PVC SERVICE LINE
② 1" UNION, PVC, SOCKET TYPE
③ 1 x 10" PIPE NIPPLE, PVC, SCH. 40
④ 1 x 3/4" REDUCING BUSHING, PVC, SOCKET
⑤ 3/4" PVC SPACER, SCH. 40, O.D. REDUCED 0.015"
⑥ UNION GASKET
⑦ CORROSION SPECIMENS, 3/4", O.D. REDUCED 0.030", MACHINED FROM SCH. 40 GALVANIZED STEEL OR STEEL PIPE
⑧ 3/4 x = 2" SPECIMEN SEPARATOR, PVC, SCH. 40, O.D. REDUCED 0.015"

FIG. 2—*Cross section of pipe specimen holder.*

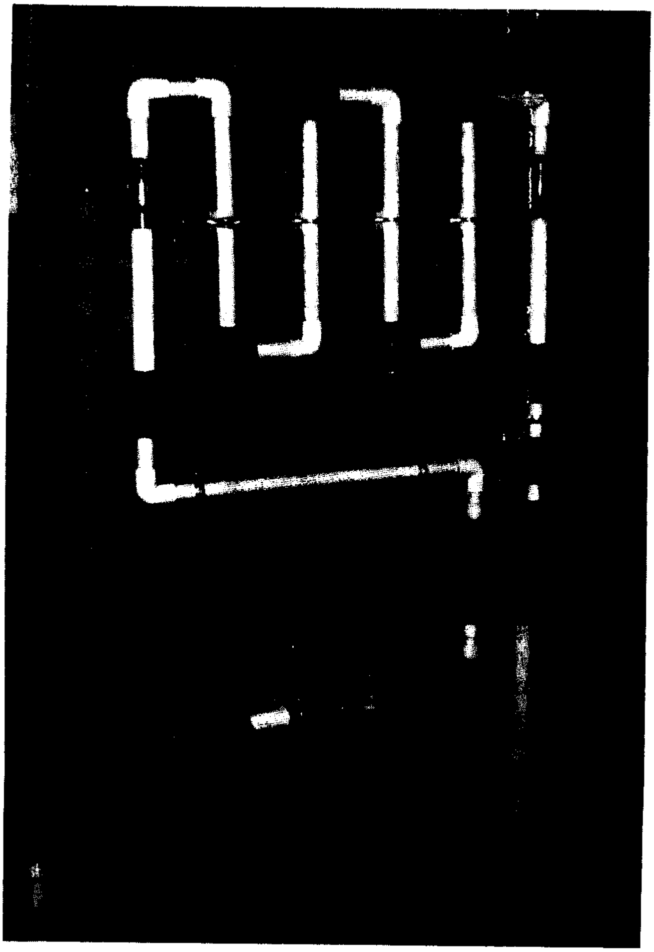

FIG. 3—*Assembled CERL-PLS.*

Corrosion Monitoring at Fort Bragg

The CERL-PLS was installed under field conditions at the Fort Bragg, North Carolina, water treatment plant and distribution system. Fort Bragg's drinking water source is a reservoir which collects water from the on-post watershed. The water treatment process consists of powdered activated carbon, alum coagulation, settling, sand-anthracite dual-media filtration, fluoridation, and chlorination. Treated water pH is adjusted by adding lime. A polyphosphate based corrosion inhibitor chemical is added (I mg/L) at the end of the treatment process for corrosion control. Table I presents typical finished water quality data at Fort Bragg, North Carolina.

A corrosion survey of domestic-water-side conditions found that the water was corrosive to steel and galvanized steel because it has an unusually low alkalinity (5 mg/L) and is nearly saturated with dissolved oxygen. The distribution system water had no tendency to deposit protective calcium carbonate scale based on the Langelier Saturation Index (LSI = 0 - 2.3).

TABLE 1—*Distribution water quality at Fort Bragg, North Carolina.*

Parameter	Units	Concentration
pH	pH units	7.4
CO_2, dissolved	mg/L	<5.0
O_2, dissolved	mg/L	8.0
Total alkalinity	mg/L $CaCO_3$	5.0
Total dissolved solids	mg/L	77.0
Total hardness	mg/L $CaCO_3$	36.0
Calcium	mg/L Ca	12.0
Magnesium	mg/L Mg	0.8
Zinc	mg/L Zn	0.07
Iron	mg/L Fe	0.09
Copper	mg/L Cu	<0.01
Manganese	mg/L Mn	0.03
Sodium	mg/L Na	2.2
Silica	mg/L SiO_2	8.0
Chloride	mg/L Cl	14.0
Sulfate	mg/L SO_4	13.0

The water plant personnel reported no current "red water" problems in the distribution system. Such problems were frequent in the past, before a corrosion inhibitor was used.

The objectives for installing the CERL-PLS at Fort Bragg were to determine: (I) corrosion rates of mild steel and galvanized steel, (2) effectiveness of the corrosion inhibitor in terms of corrosion rate reduction and "red water" control, and (3) adaptability of the pipe loop system under actual field conditions.

Figure 4 presents a schematic of the CERL-PLS locations in the Fort Bragg Water Plant and distribution system. A pipe loop (PLS-I) was located inside the water plant and received

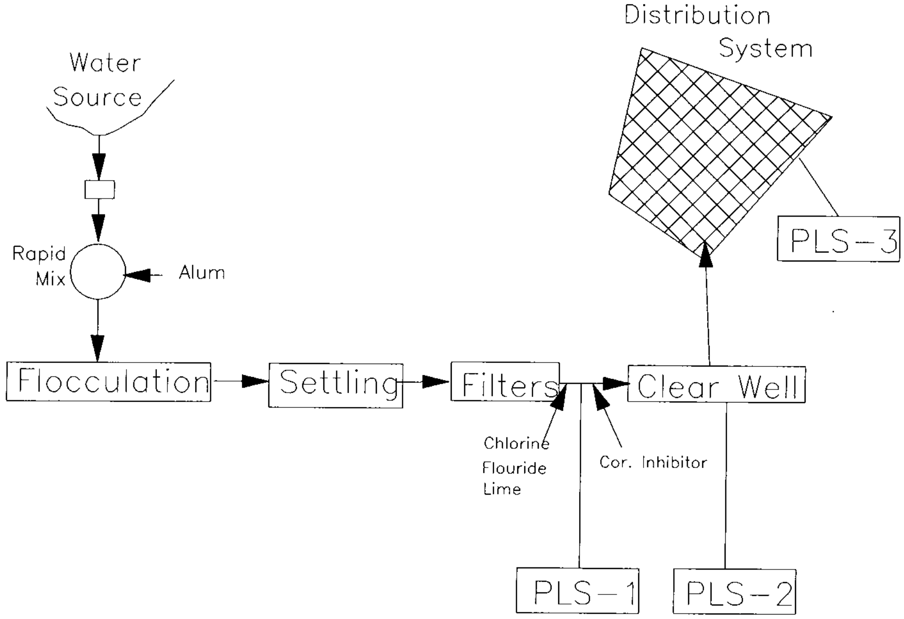

FIG. 4—*CERL pipe loop system locations.*

water just before the addition of corrosion inhibitor. A second pipe loop (PLS-2) was also installed inside the water plant but received finished water from the clear well which had been treated with a polyphosphate corrosion inhibitor. The third pipe loop (PLS-3) was installed in the distribution system at a booster pumping station. The water flowing through PLS-3 represented water quality in the distribution system.

The pipe loops were operated independently under the same conditions. All three pipe loop systems were provided with coupons and pipe specimens made of mild steel, galvanized steel or zinc. Water flowed continuously through each loop at an average rate of 2.5 gal/min. The eftluent water was discarded into a drain and hence the water flowed only once through the CERL-PLS. The coupons and pipe specimens were removed after a specified time interval to determine the corrosion rate. The coupons and pipe specimens were replaced with clean specimens and the experiments continued.

Short-Term Results at Fort Bragg

The first set of specimens were removed for observation and analysis after 3 months of operation. There was virtually no maintenance required in operating the equipment except for an occasional flow meter check, during the experimental period. The water quality parameters were continuously analyzed by the water plant laboratory to assure that the water quality did not change significantly during the study.

A significant difference was observed in the visual appearance of the specimens removed from PLS-2 and PLS-3 exposed to water containing the polyphosphate-based inhibitor. The condition of the interior of mild steel pipe after a three month exposure to water containing corrosion inhibitor is compared to a clean specimen by the photographs in Fig. 5. As

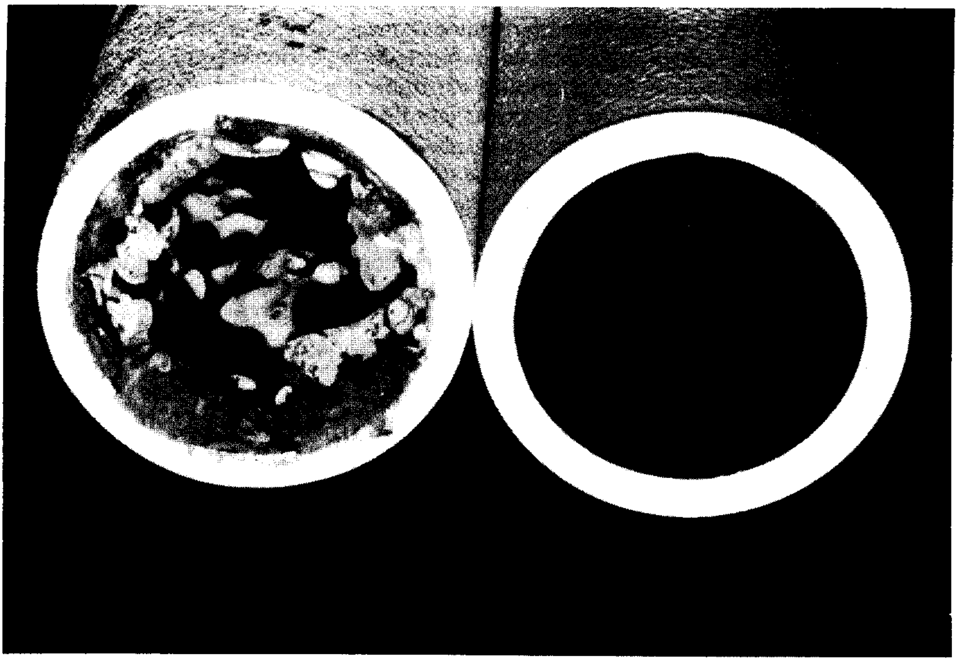

FIG. 5—*Comparison of new pipe specimen* (right side) *and pipe specimen removed from PLS-2 after exposure* (left side).

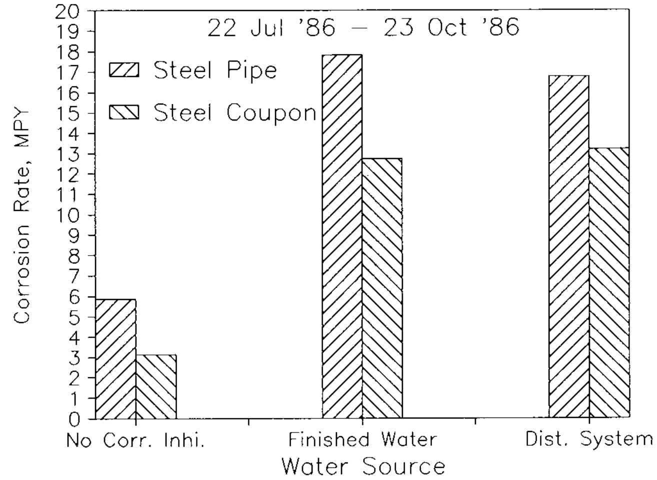

FIG. 6—*Corrosion rates of mild steel specimens at Fort Bragg, North Carolina.*

observed from the photograph, the pipe specimen exposed to water containing the inhibitor was coated with a thick layer of deposits (PLS-2). Whereas, no such coating was apparent on the mild steel pipe insert exposed to the same water without corrosion inhibitor (PLS-l). Similar effects were observed for both coupon and pipe specimens of mild steel and galvanized steel.

The observed corrosion rates for specimens from Fort Bragg installation are compared in Figs. 6 and 7 showing the effects of water without corrosion inhibitor, at the plant effluent, and water from the distribution system. Not surprisingly, corrosion rates of galvanized (zinc) specimens were lower when compared to the corrosion rate for mild steel specimens. However, as seen in the figures, the corrosion rates of mild steel and galvanized (zinc) steel were significantly higher in the water which was treated with corrosion inhibitor. These data contradict the general consensus that the presence of a polyphosphate-based corrosion inhibitor reduces the corrosion rate of steel piping in water distribution systems. The data also show that there are significant differences in corrosion rates obtained using coupons and the values obtained using pipe specimens.

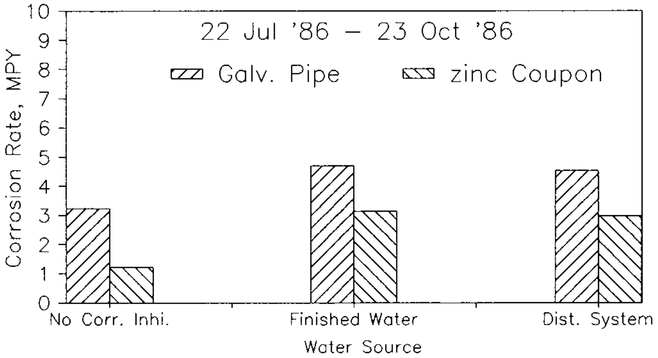

FIG. 7—*Corrosion rates of galvanized steel specimens at Fort Bragg, North Carolina.*

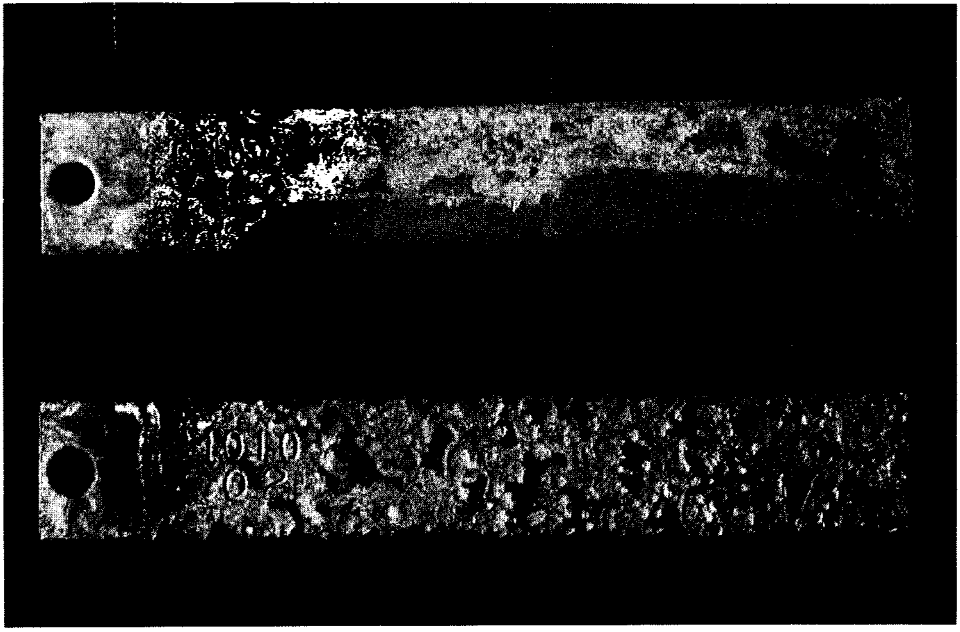

FIG. 8—*Comparison of cleaned mild steel coupon after exposure to water without inhibitor* (top) *and containing corrosion inhibitor* (bottom).

Figures 8 and 9 show photographs of the mild steel pipe specimens and coupons after the deposits were completely removed. The specimens exposed to water containing the polyphosphate corrosion inhibitor are severely pitted. The deposition (tuberculation) on the surface of the specimens and the surface deposits increased the pitting corrosion. Uniform corrosion with minor deposition was observed on the surface of the specimens exposed to water without the corrosion inhibitor. The weight loss due to the severe pitting was apparently greater than the weight loss due to uniform corrosion during the 90-day test. The effect of longer exposure periods is delineated in the next section.

Although there was an increase in corrosion rate in the presence of corrosion inhibitor, the corrosion inhibitor treatment evidently was effective in preventing "red water" problems (discoloration caused by corrosion products). A visual observation of flow meters in the pipe loop system (PLS-l) which received water without corrosion inhibitor treatment showed significant dark-brown staining, a sign of "red water" problem. Whereas, the flowmeters for PLS-2 and PLS-3 were not stained by the water treated with the corrosion inhibitor.

Long-Term Results at Fort Bragg

The CERL-PLS installation at Fort Bragg monitored corrosion rates of mild steel and galvanized steel continuously for over three years. Periodically the specimens were removed and visually inspected. The observations on physical conditions were found to be similar to the observations found during the first three months of operation.

Specimens were removed at selected intervals to determine the effect of various exposure periods on the corrosion rates. The effect of corrosion inhibitor on corros.ion rates for mild steel and galvanized steel in the Fort Bragg water system is presented in Figs. 10 and 11. The data presented are averages of corrosion rates determined from multiple specimens. The results of 90-day exposure were consistent with earlier observations of increased corrosion

FIG. 9—*Comparison of cleaned mild steel pipe specimens after exposure to water without corrosion inhibitor* (top) *and containing corrosion inhibitor* (bottom).

rate of steel in presence of corrosion inhibitor for both mild steel and galvanized steel. However, longer exposure periods clearly demonstrated that the corrosion rate of steel decreased with time in the presence ofthe corrosion inhibitor, whereas the corrosion rate in the absence of corrosion inhibitor increased with time. In the presence of corrosion inhibitor, a coating formed on the surface of the pipe which gradually reduced the corrosion rate, as the coating uniformly covered the pipe surface and developed sufficient thickness.

In the absence of corrosion inhibitor, the surface of the specimen corroded uniformly as the corrosion by-products were removed by the water flow. Therefore, no coating was able to form on the surface and corrosion progressed linearly with time. Although the weight loss due to uniform corrosion was perhaps slower in the absence of corrosion inhibitor, it was nevertheless cumulative. Thus higher corrosion rates were observed in the absence of corrosion inhibitor on specimens exposed for longer periods. These observations clearly demonstrate the need for a long-term comprehensive corrosion monitoring program in public water supplies.

Water Treatment Optimization for Lead Control

The USEPA has recently issued a proposed rule [3] for limiting lead and copper in drinking water. In the proposed rule, water suppliers unable to meet the lead and copper limitations, are required to optimize their water treatment process to reduce lead and copper dissolution from plumbing system materials. Further, the USEPA recommends use of techniques such as a pipe loop system to simulate conditions in household plumbing and to evaluate various treatment options to reduce lead and copper dissolution.

The CERL-PLS was used to simulate lead dissolution in the distribution system and to optimize water quality to reduce lead dissolution at a U.S. Army base. The installation is

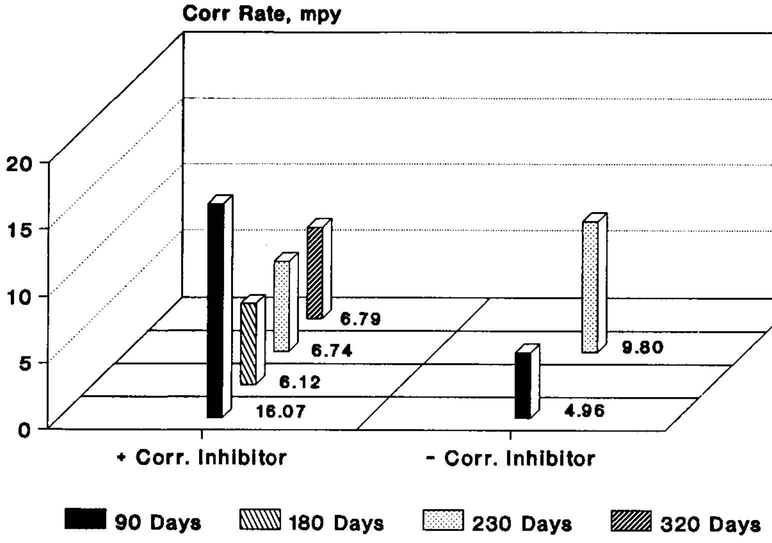

Mild Steel / Pipes

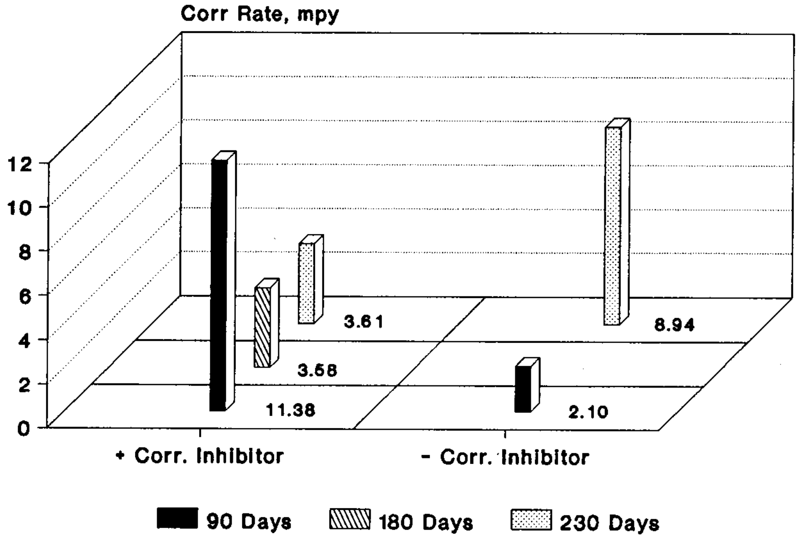

Mild Steel / Coupons

FIG. 10—*Effect of corrosion inhibitor on long term corrosion rates of mild steel at Fort Bragg, North Carolina.*

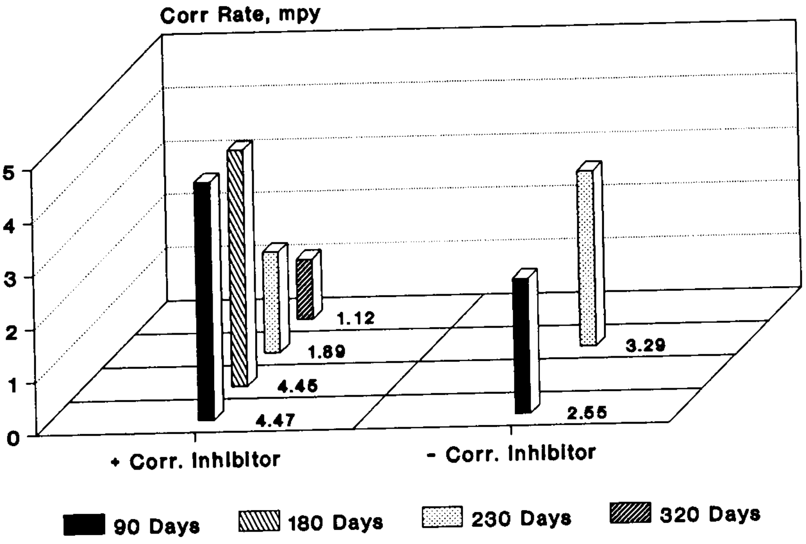

Galv Steel / Pipes

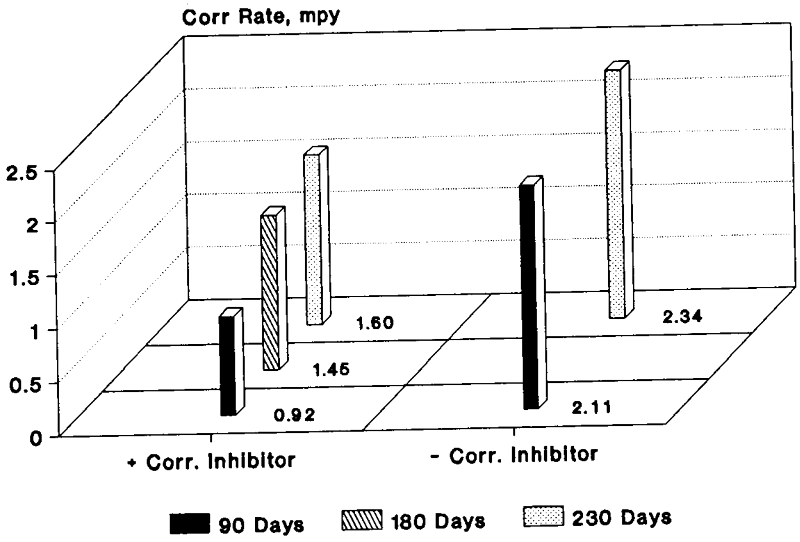

Zinc / Coupons

FIG. 11—*Effect of corrosion inhibitor on long-term corrosion rates of galvanized steel at Fort Bragg, North Carolina.*

located in the northeast part of the United States. The water treatment plant is a conventional rapid sand filtration facility and has been in service at least since World War II. In addition to serving the Army installation, the water treatment plant also occasionally delivers drinking water to a neighboring community when needed. The water plant produces an average of 2 Mgal/day. The raw water source is obtained from a stream with an alkalinity generally in the range of20 to 50 mg calcium carbonate/L and a pH of about 7.0. The treatment process include pre-chlorination, alum coagulation with pre-liming as needed, followed by sedimentation, rapid sand filtration, post-lime addition for pH adjustment, sodium silicate addition for corrosion control, fluoridation, and post-chlorination.

High lead concentrations in drinking water at consumers taps were discovered during a water quality survey initiated due to complaints of discolored water at some parts of the distribution system. The survey, conducted by the Water Quality Division of the Army Environmental Hygiene Agency (AEHA) [4] in March 1988, was comprehensive and tested for heavy metals, including lead, copper, zinc, and cadmium, in the first flush water samples at consumer's tap. Except for lead, all other water quality parameters met USEPA standards. Table 2 presents the pH and lead concentrations in the overnight stagnant and completely flushed water samples. As seen from Table 2 the average stagnant and flushed water pH was 7.9. The average lead concentration in stagnant water samples was 0.053 mgfL. Over 18% of the samples exceeded the present maximum contaminant level of 0.050 mg lead/L. About 45% of the samples contained over 0.010 mg lead/L which is the proposed maximum concentration allowed at the consumer's tap. The water samples taken at the water plant were below 0.005 mg lead, well within the proposed lead levels for water entering the distribution system. After a complete flushing of the household systems, none of the samples exceeded the proposed lead concentration of 0.0 10 mg/L at the consumer's tap.

As a result of this survey, several actions were taken to alleviate the high lead levels found in the overnight standing water. The installation commander issued a notification to all grounds personnel to flush water lines in buildings each morning. All family housing units were requested to flush kitchen taps each morning before using the water for drinking and cooking purposes. At the water plant, the lime dosage was adjusted to increase the distribution system water pH to 8.6.

In June 1988, another water quality survey was conducted to determine the status of lead dissolution in plumbing systems. The results of this survey are presented in Table 3. The major change noted in this survey is that the average distribution system water pH was 8.5. Only 5% of the water samples were reported to have a pH less than 8.0. The average lead concentration of the stagnant water sample was 0.030 mg/L which is within the current lead maximum contaminant level (MCL). However, 21% of the samples exceeded the 0.050 mg lead/L level. The proportion of water samples exceeding 0.005 and 0.010 mg lead/L were 79 and 67%, respectfully. After complete flushing, the average lead concentration was 0.00 I mg/L, well within the proposed rules.

Although the distribution system water pH increase reduced the average lead concentration, the percentage of samples exceeding the proposed MCL for lead increased by more than 20%. The March 88 water quality survey lead average was strongly influenced by an extremely high value (1.200 mg lead/L) observed in one sample. This value may be considered an outlier, but it is not unusual for lead concentrations in drinking water supplies to show this variability. When the median lead concentrations are compared for the two surveys, the distribution system water pH increase resulted in the median lead value increasing from 0.010 to 0.024 mg lead/L. In this case, the median lead concentration was more indicative of the pH effect than was the average lead concentration.

These results particularly demonstrate the advantage of using a pipe loop study rather than experimenting with an entire distribution system where consumers were subjected to

TABLE 2-*March* 1988 *water quality survey.*

Sample No.	pH		Lead, mgJL	
	Initial	Flushed	Initial	Flushed
1				
2			0.002	<0.001
3	7.4	7.5	0.014	0.001
4	8.5	8.6	0.021	<0.001
5	8.5	8.4	0.008	<0.001
6	8.0	7.4	0.086	0.002
7	7.7	7.4	0.065	<0.001
8	8.1	7.4	1.200	0.003
9	8.4	7.4	0.011	<0.001
10	8.2	7.4	0.006	<0.001
11	6.7	7.5	0.029	<0.001
12	7.2	7.4	0.019	<0.001
13	7.4	7.6	0.002	<0.001
14	8.1	8.3	0.087	<0.001
15	7.8	8.3	0.024	0.003
16	8.5	8.5	0.005	<0.001
17	9.0	8.9	0.004	<0.001
18	7.9	8.1	0.006	<0.001
19	8.0	8.1	0.004	<0.001
20	8.1	8.2	0.002	<0.001
21	8.2	8.2	0.009	<0.001
22	8.1	8.2	0.09	0.003
23	8.1	8.2	0.018	<0.001
24	8.1	8.0	<0.001	<0.001
25	7.8	7.6	0.003	<0.001
26	8.3	8.4	<0.001	<0.001
27	7.8	8.1	0.040	0.003
28				
29				
30	7.0	7.1	0.001	<0.001
31	7.3	7.4	0.004	0.002
32	7.1	7.2	<0.001	<0.001
33	7.3	6.9	0.081	0.002
34	8.3	8.2	0.020	<0.001
35	8.4	7.8	0.040	<0.001
36	7.7	7.8	0.003	<0.001
37	7.6	7.6	<0.001	<0.001
38	8.0	8.1	<0.001	<0.001
39				
40	6.5	6.6	0.077	0.005
41	8.2	8.2	0.037	<0.001
42	9.2	9.2	0.005	<0.001

increased lead contamination by a pH increase. A pipe loop study can evaluate and identify various treatment programs which may have either a negative or positive impact on lead dissolution without disrupting water quality in the distribution system.

Application of the Pipe Loop System for Optimization of Water Treatment

In August 1988 experiments were conducted at the U.S. Army water treatment plant to determine optimum water treatment to further reduce lead dissolution. Two pipe loop sys-

TABLE 3-*June* 1988 *water quality survey.*

Sample No.	pH Initial	pH Flushed	Lead mg/L Initial	Lead mg/L Flushed
1	8.5	8.5	0.001	0.005
2				
3	8.6	8.6	0.032	0.001
4	8.5	8.6	<0.001	<0.001
5	8.5	8.6		
6	8.8	8.8	0.072	<0.001
7	8.8	8.8	0.018	<0.001
8	8.3	8.8	0.146	<0.001
9	8.8	8.8	0.004	0.007
10	8.4	8.6	0.007	0.001
11	8.8	8.9	0.004	<0.001
12	8.6	8.8	0.024	<0.001
13	8.5	8.6		
14	8.4	8.5	0.095	0.002
15	8.0	8.5	0.025	0.002
16	8.4	8.4		
17				
18	8.3	8.5		
19				
20	8.3	8.4		
21	8.5	8.6		
22	8.5	8.5	0.062	0.002
23	8.6	8.6	0.016	0.002
26	8.7	8.7		
27	8.9	8.9	0.016	0.001
28	8.1	8.5		<0.001
29	8.5	8.4	0.049	<0.001
30	8.3	8.7		
31	8.3	8.7		
32	8.5	8.6		
33	8.6	8.5	0.024	0.001
34	8.7	8.7	0.024	0.001
35	8.2	8.7	0.061	0.005
36	8.6	8.7		
37	8.6	8.7		
38	8.9	8.9		
39	7.8	8.1	0.005	<0.001
40	7.6	8.1	0.028	0.004
41	8.6	8.7	0.007	<0.001
42	9.3	9.1		
43	8.8	8.8	0.008	<0.001
44	8.7	8.7	<0.001	0.002
45	8.2	8.7	0.033	0.001

terns were installed at the water plant in series as shown in Fig. 12. Loop A was fitted with a copper loop with 50:50 lead:tin soldered joints. This copper loop was about 1.82 m (6 ft.) long and contained 22 joints, and was fabricated by a licensed plumber following standard plumbing practices. In addition to the soldered joints in the copper loop, two galvanized pipe sections were inserted in the CERL-PLS, one on each side of the copper loop. The design of Loop A was intended to emulate guidelines delineated in USEPA's proposed rule on lead and copper.

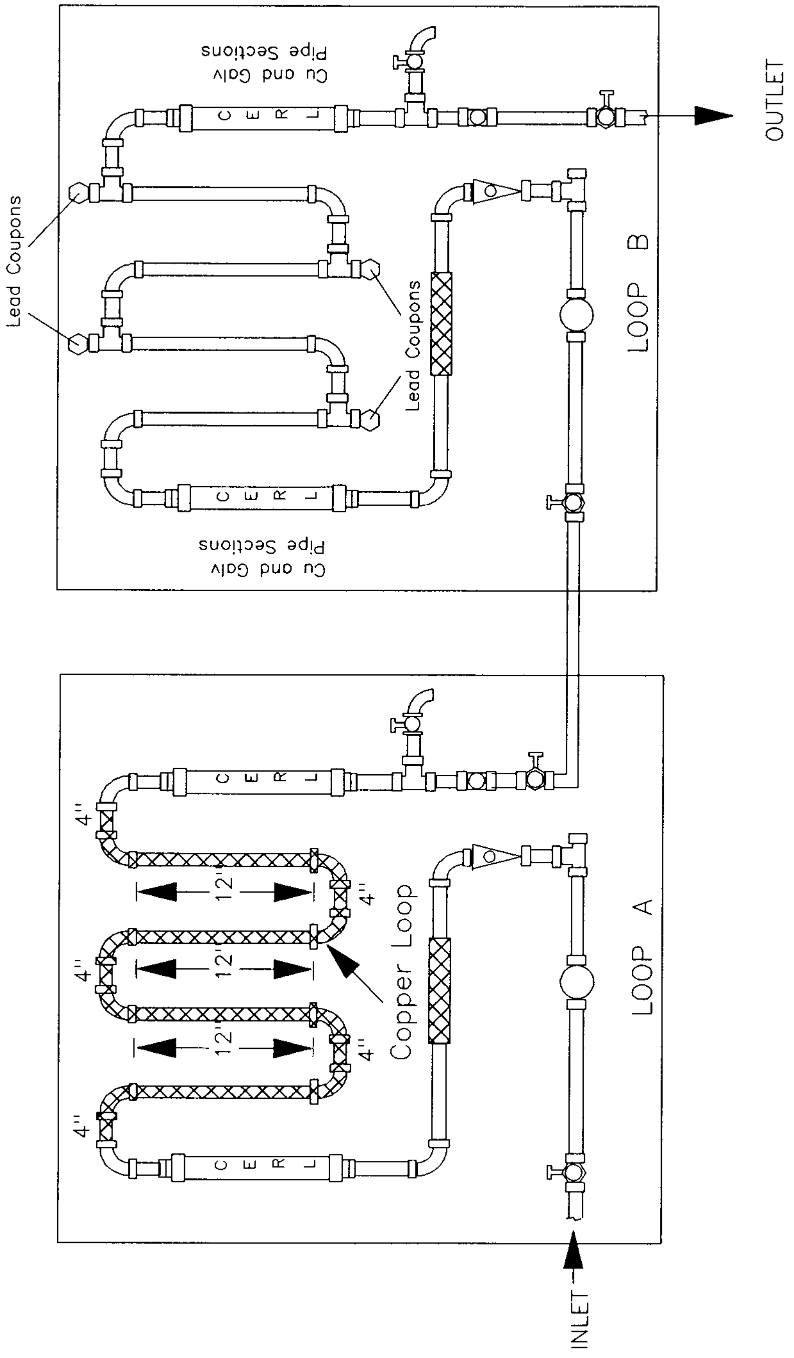

FIG. 12—*Schematic of experimental setup for lead dissolution study.*

The second CERL-PLS (Loop B) was provided with four lead coupons. Before insertion, the coupons were thoroughly polished with emery cloth to remove any coatings on the surface. In addition to the four lead coupons, duplicate pipe specimens of copper and galvanized iron, were installed to determine the dissolution of copper, zinc and cadmium. Loop B design offered an alternate approach to optimizing water treatment. As discussed later, this approach provided better experimental control.

A total of four experiments were conducted. The water samples were collected during each experiment following an established protocol. Loop A remained the same through the four experiments, whereas in Loop B the four coupons were replaced with clean, polished coupons at the beginning of each experiment. The sampling protocol was designed to simulate water usage patterns in a typical household and also to determine the effect of stagnation time on lead dissolution. Selection of 1, 5 and 15-h stagnation times facilitated graphical representation of data and extrapolation of lead dissolution for any other stagnation periods of possible interest. Experiments were started each morning at 8 a.m. by flushing the loop system for 1 h at a flow rate of 2 gal/min. Just before 9 a.m. a water sample was collected from both the loops while the water was flowing through the system. This sample, No.1, represented the water entering the distribution system. At 9 a.m. the water flow was stopped by closing the ball valves at both ends of Loops A and B. After a stagnation period of 1 h (9 to 10 a.m.), water samples were collected from Loops A and B. This was accomplished by first slowly opening the entrance valve for Loop A, collecting sample from sample port, then opening the exit valve for Loop A and entrance valve for Loop B, and finally collecting water sample from sample port for Loop B. This sample, No.2, represented water after I-h stagnation in the system. After the sample collection, the water was flushed through the system for another hour (10 to 11 a.m.) at 2 gal/min. Again, the water was shut off and allowed to stagnate for 5 h (11 a.m. to 4 p.m.). The 5-h stagnant sample, No.3, was collected using the same procedure described previously. The system was flushed for another hour (4 to 5 p.m.) at 2 gal/min and then was shut off. A final sample, No.4, was collected at 8 a.m. the following morning representing the 15-h stagnant water sample.

A total of 750 mL were collected for each sample and split into two portions of 500 and 250 mL. The 250 mL portion was acidified to pH <2.0 using 1:I nitric acid and was used for heavy metal analysis. The 500 mL portion was refrigerated and was analyzed for alkalinity (total and carbonate) and total dissolved solids. The samples were analyzed at the Army Environmental Hygiene Agency, Aberdeen Proving Ground, Maryland, laboratories following standard procedures. The detection limits for lead, copper, zinc, and cadmium concentrations were 0.001,0.025,0.015, and 0.001 mg/L, respectively.

Lead Dissolution Studies and Results

Four experiments were conducted at the Army base to evaluate the effect of certain chemical additives on the dissolution of lead in the distribution water system. Experiment No. I served as a control study representing the dissolution effect of the distribution water quality without chemical additives. The average water quality for this experiment is shown in Table 4.

For experiments Nos. 2, 3, and 4, a large volume ofthe distribution water was treated with the selected chemical additive(s) in polyethylene reservoirs. The resulting solutions were pumped from the reservoir through Loops A and B in accordance with the flushing and stagnation periods established by the sampling protocol.

Experiment No.2 was conducted to determine the dissolution effect caused by increasing the distribution system water alkalinity from 35 to 150 mg/L (as calcium carbonate). Sodium bicarbonate was applied to obtain the desired increase in alkalinity. Experiment No.3 was

TABLE 4—*Distribution water quality used in lead dissolution study.*

Parameter	Concentration
pH	8.8
Temperature	28 C
Total alkalinity ($CaCO_3$)	35 mg/L $CaCO_3$
Total hardness ($CaCO_3$)	82 mg/L $CaCO_3$
Iron (Fe)	<0.1 mg/L
Calcium (Ca)	20 mg/L
Lead (Pb)	<0.001 mg/L
Copper (Cu)	<0.025 mg/L
Zinc (Zn)	<0.015 mg/L
Cadmium (Cd)	<0.001 mg/L

conducted to determine the effect on lead dissolution due to the application of 10 mg/L of sodium silicate into the distribution water. The combined effects of increasing the alkalinity to 150 mg/L and applying 10 mg/L of sodium silicate was investigated in experiment No.4.

Results of Optimization Studies

The results from the metal dissolution experiments are presented in Tables 5 and 6. The average lead concentration of the water entering the distribution system was 0.005 mg/L, with a range of 0.001 to 0.010 mg/L. The lead concentration increased with increasing stagnation time in any given experiment. This trend is graphically presented in Figs. 13 and 14 for both lead-solder (Loop A) and pure lead (Loop B) piping materials. Significant differences in lead dissolution were observed for each treatment condition. The major difference in lead concentrations found in the Loop A and Loop B data is assumed to be related to the difference in both materials and the exposed surface area.

TABLE 5—*Loop A metal dissolution results.*

Experiment No.	Treatment	Stagnation Time, h	pH, units	Metal Concentration, mg/L Pb	Cu	Zn
1	none	0	8.8	0.0096	<0.025	<0.015
1		1	9.2	0.3010	<0.025	0.124
1		5	8.2	0.8850	0.077	0.342
1		15	8.8	1.1580	0.059	0.478
2	$NaHCO_3$	0	8.6	0.0044	<0.025	<0.015
2		1	8.5	0.0806	0.056	0.067
2		5	8.4	0.2160	0.167	0.267
2		15	8.4	0.3870	0.289	0.600
3	silicate	0	9.1	0.0011	<0.025	<0.015
3		1	8.6	0.0411	<0.025	0.094
3		5	8.5	0.1400	0.064	0.315
3		15	8.5	0.1620	0.061	0.944
4	$NaHCO_3$ + silicate	0	8.1	0.0071	<0.025	<0.015
4		1	8.2	0.0153	0.080	0.103
4		5	8.4	0.0402	0.186	0.340
4		15	8.3	0.0597	0.271	0.702

TABLE 6—*Loop B metal dissolution results.*

Experiment No.	Treatment	Stagnation Time, h	pH, units	Metal Concentration, mg/L		
				Pb	Cu	Zn
1	None	0	8.7	0.0068	<0.025	<0.015
1		1	9.2	0.0172	<0.025	0.080
1		5	8.4	0.0522	0.053	0.180
1		15	9.1	0.0829	0.041	0.673
2	$NaHCO_3$	0	8.6	0.0029	0.057	<0.015
2		1	8.5	0.0178	0.032	0.049
2		5	8.4	0.0358	0.080	0.185
2		15	8.5	0.0699	0.128	0.370
3	silicate	0	9.1	0.0046	<0.025	<0.015
3		1	9.0	0.0112	<0.025	0.071
3		5	8.6	0.0307	0.032	0.315
3		15	8.6	0.0471	0.028	0.787
4	$NaHCO_3$ + silicate	0	8.2	0.0072	<0.025	<0.015
4		1	8.3	0.0193	0.066	0.044
4		5	8.4	0.0429	0.038	0.164
4		15	8.3	0.0569	0.059	0.143

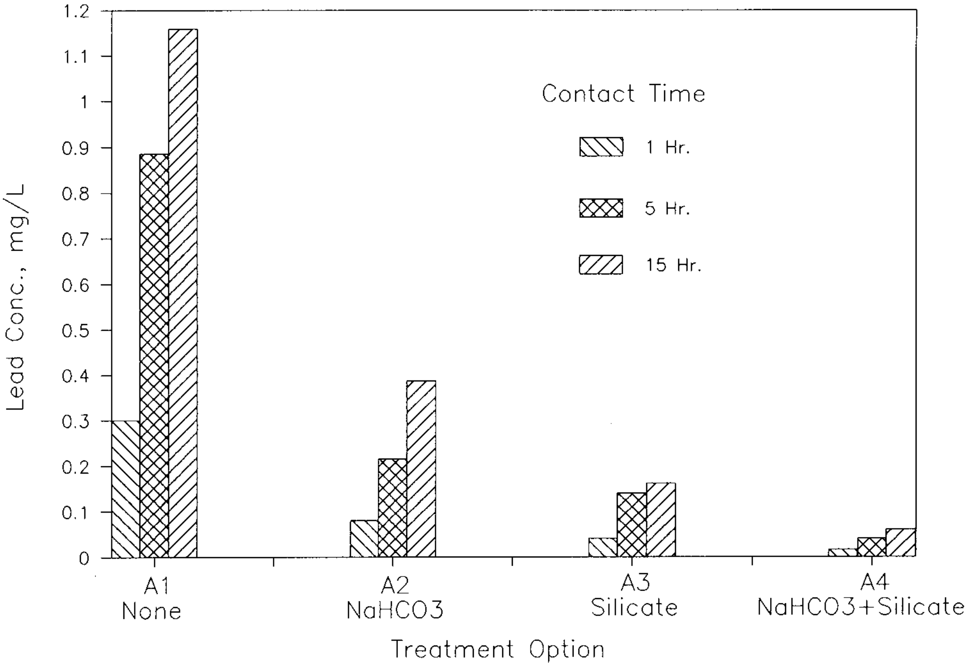

FIG. 13—*Lead leaching from copper loop with soldered joints, Loop A.*

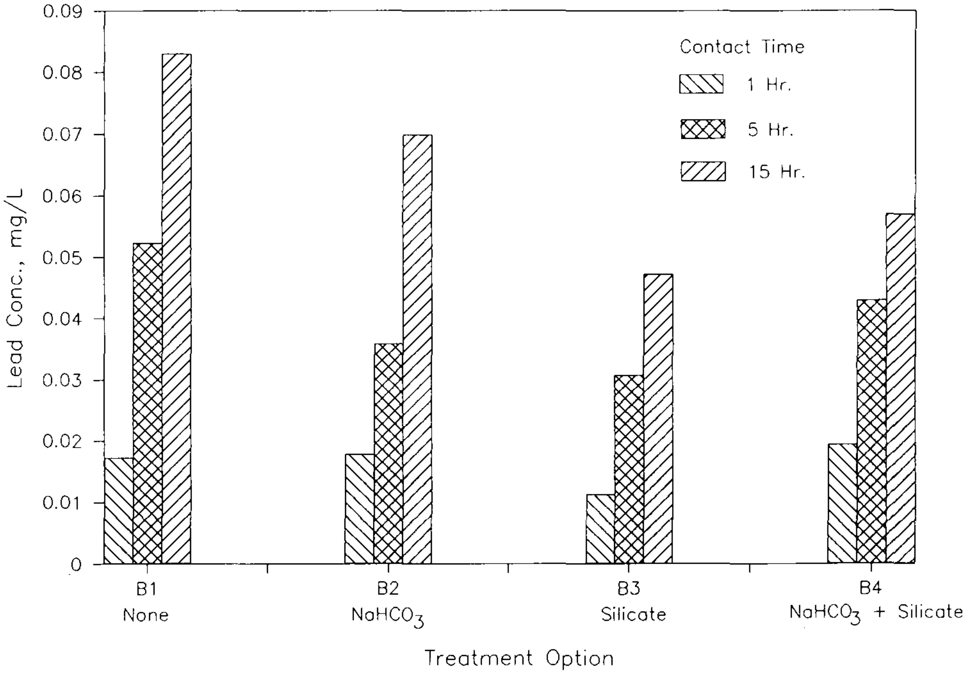

FIG. 14—*Lead leaching from lead coupons, Loop B.*

The results of Loop A experiments show that lead concentration decreased with each succeeding experiment. The lead dissolution from the soldered joints of the copper loop in these experiments depends on two major factors. The primary factor is the amount of soldered surface exposed to the water and therefore available for dissolution by water. Also, lead is likely dissolved by the acidic flux during the soldering process and is slowly redissolved with use. Since the copper loops in Loop A were not replaced at the beginning of each experiment, the lead dissolution may have been reduced in following experiments due to the formation of protective films or by the flux dissolution from the previous experiment. An additional factor was the effect of chemical additives of the water on the lead dissolution from the soldered joints. The results were not sufficient to quantitatively differentiate between these factors. In order to determine the effect of water treatment alone on the lead dissolution from soldered joints, a new identical copper loop must be used for each experiment. Also, longer experimental periods would be required to approximate water distribution system conditions in terms of lead dissolution attributable to water quality and treatment. It must be noted, however, that fabrication of copper loops with identical solder exposure surface could be impractical if not impossible.

The experimental conditions for Loop B were better controlled than for Loop A, in order to be able to determine the water treatment effect on lead dissolution. Four lead coupons with a total exposure area of approximately 87 cm^2 were installed in Loop B and were the only source of lead.

Coupons with clean and polished surfaces were used at the beginning of each experiment. Copper and galvanized steel specimens were also installed in Loop B to observe the dissolution of these metals.

The effects of the chemical additives on the lead dissolution for Loop B experiments are shown in Fig. 14. Among the options studied, the most effective treatment for reducing lead dissolution was the application of 10 mg/L of sodium silicate to the distribution system water without any additional adjustment of the alkalinity. The application of sodium silicate and sodium bicarbonate together to also increase the alkalinity to 150 mg/L (as calcium carbonate) produced a slightly higher lead dissolution than the silicate treatment did alone. The lease effective treatment in this study was the application of only sodium bicarbonate to increase the distribution system water alkalinity from 35 to 150 mg/L, although lead dissolution was somewhat reduced.

In addition to monitoring lead concentrations during the experiments, zinc, copper, and cadmium concentrations were also measured. The source of these heavy metals were the copper and galvanized steel pipe specimens that were installed in Loop A and Loop B. Although measurable quantities of zinc and copper were leached from the materials into the water during the experiments, the concentrations did not exceed the established MCLs for these metals (Tables 5 and 6). Cadmium was below or near the detection limit in all samples.

Although the results shown in Fig. 14 demonstrate the potential usefulness of a pipe loop system as a tool for optimizing water treatment, this type of corrosion study should be repeated many times over several months. The effect of an inhibitor over time can best be accomplished by the continuous application of chemical additives into the flowing water entering the pipe loop. This technique has been employed by CERL at other installations. However, the USEPA sampling protocol will be looking at the worst-case scenario for corrosion; that is, sampling for lead from new plumbing installations that are most likely to exceed the MCL. Therefore, water utilities may be more interested in the results of short-term studies to indicate treatment options which will provide immediate results in reducing lead dissolution. A standard procedure for optimizing water treatment corrosivity for public water supplies is yet to be established but both the short-term and long-term corrosion effects must be considered when one is developed.

Summary and Conclusions

Monitoring the lead and copper concentrations of water distribution systems will identify the systems which are not in compliance with the maximum contaminant level for these metals set by federal regulations. When this occurs, noncompliant systems will be required to either improve or install corrosion control treatment adequate to meet the regulations or demonstrate that they have optimized treatment. The regulations will allow pipe loops, laboratory, pilot scale studies, field studies, or all four to optimize corrosion control treatment programs.

USA-CERL has successfully employed a pipe loop system (CERL-PLS) for use at Army facilities to optimize water treatment and to study the corrosivity of the distribution water. Although many pipe loop systems have been proposed, none are commercially available or have received universal acceptance as the standard for use in public water supplies. The CERL unit is a modification of common pipe loop systems, but designed to reduce construction costs, increase availability, and to provide a standard corrosion monitoring method for Army facilities.

Corrosion studies at two U.S. Army bases using the pipe loop approach provided valuable information on water treatment plant operations. At one location, the use of a polyphosphate corrosion inhibitor was successful in preventing red water problems in the distribution system, but pipe loop studies discovered that the polyphosphate caused tuberculation of exposed steel surfaces and increased the initial corrosion rate of new steel pipe. At another location, various treatment options were investigated revealing that a 10 mg/L sodium silicate treatment program was superior in reducing lead dissolution to a treatment program using sodium bicarbonate to increase the alkalinity of the distribution water. No advantage was found by the pipe loop studies in combining these two treatment options.

The problems with using the entire distribution system (field study) in studies to optimize a treatment program was clearly shown at one Army facility. The application of lime to increase the distribution water pH from 7.9 to 8.3 resulted in a 22% increase in the percentage of water samples exceeding the MCL for lead. A properly designed pipe loop study could have provided this information without subjecting consumers to some of the undesirable effects from experimentation ..

The pipe loop system was used to simulate lead dissolution in stagnant water from lead soldered plumbing and lead service lines. Lead concentrations were shown to increase in the pipe loop system with stagnation time as observed in building plumbing systems and reported by many published studies. Generally, pipe loops can provide superior control of the stagnation period for sampling which is likely the primary cause for the variability found in lead concentrations from household plumbing.

Further research and an extensive corrosion data base need to be developed to assist water plant operators in optimizing corrosion control programs. A standard procedure for pipe loop studies should be developed to improve correlation of corrosion data with other factors within a single water distribution system or with corrosion data from other water supplies. The CERL-PLS has shown this capability and further research and development is being pursued at other U.S. Army facilities.

References

[1] Singley, J. E., DeBerry, D. W., Beaudet, B. A., Kidewell, J. R., Markey, P. H., and Malish, D. A., *Corrosion Prevention and Control in Water Treatment and Supply Systems,* Pollution Technology Review No. 122 Noyes Publications, Park Ridge, NJ, 1985.

[2] "National Interim Primary Drinking Water Regulation," *Code of Federal Regulations,* Title 40, Part 141, United States Environmental Protection Agency (USEPA), Washington, DC, 1981, pp. 309-354.

[3] "The Proposed Lead and Copper Rule," *Federal Register,* 53 FR 31516, United States Environmental Protection Agency (USEPA), Washington, DC, 18 Aug. 1988.

[4] Temkar, P. M., Phull, K. K., Valcik, J. A., and Runyon, T, R., "Treatment Process Evaluation for Reducing Lead Dissolution From Plumbing Systems Using CERL Pipe Loop System," submitted to Office of Drinking Water, U.S. Environmental Protection Agency, Washington, DC, 25 Oct. 1988.

[5] Neff, C. H., Schock, M. R., and Marden J. I., "Relationship Between Water Quality and Corrosion of Plumbing Materials in Buildings, Vol. I; Galvanized Steel and Copper Plumbing Systems, Vol. II, Appendices," Contract Report CR808566-02, U.S. Environmental Protection Agency, Washington, DC, 1987.

Neil G. Thompson[1] *and John A. Beavers*[1]

Effect of Ground-Water Composition on the Electrochemical Behavior of Carbon Steel: A Statistical Experimental Study

---

REFERENCE: Thompson, N. G. and Beavers, J. A., "Effect of Ground-Water Composition on the Electrochemical Behavior of Carbon Steel: A Statistical Experimental Study," *Corrosion in Natural Waters, ASTM STP 1086,* C. H. Baloun, Ed., American Society for Testing and Materials, Philadelphia, 1990, pp. 101-121.

ABSTRACT: Historically, the study of the effects of environmental variables on the corrosion behavior of metals has been performed by varying a single species at a time. At most, a two or three variable matrix of tests has been performed. In this study, a statistically designed matrix of tests was performed to examine the main-term effects and several two-factor interaction terms of 15 environmental variables present in ground-water solutions on the corrosion behavior of carbon steel. Cyclic potentiodynamic polarization experiments were performed to determine several characteristic polarization parameters. Regression analyses established which of the environmental variables had a statistically significant effect on each of the polarization parameters. The environmental variables were selected to simulate basalt rock ground-water solutions with the emphasis being the application of carbon steel as a high-level nuclear waste container (overpack). It was found that, to accurately describe the effects of ground-water variables, two-factor interaction terms were often as important, or more so, than the main-effect terms. A limitation of the technique is that, with the large concentration ranges used, the design concentrations could not be achieved due to ion interaction; this produced a correlation among factors in the regression model and inaccuracies in the predictions.

KEY WORDS: corrosion, potentiodynamic polarization, experimental design, regression analysis, main-effect, interactions, statistical test matrix, ground waters, pitting corrosion, high-level nuclear waste, carbon steel

This study was a subtask in an overall program with the objective to provide an improved understanding of the long-term performance of materials used for high-level waste packaging. The program was funded by the Office of Research, The Nuclear Regulatory Commission. More specifically, the purpose of the electrochemical task was to identify electrochemical processes or environmental conditions that may tend to promote premature degradation of the performance of the waste package materials. The primary focus of the study was to examine the behavior of carbon steel in basalt ground-water environments. One candidate high-level nuclear waste repository is located near Richland, Washington in a basalt rock formation. In addition to the potentiodynamic polarization studies, of which a portion are described in this paper, the corrosion studies also included pit propagation, high-temperature autoclave studies, and stress corrosion cracking studies [1].

The environments simulated in this study included three primary sources of environmental variables/species: (I) basalt rock ground water which is one proposed burial site for the

---

[1] President and senior scientist, respectively, Cortest Columbus, Inc., 2704 Sawbury Blvd., Columbus, OH 43235.

TABLE 1—*Concentrations of species in basalt ground water or in actual or simulated basalt repository environments.*

Variables	Concentration Ranges					
	Ref *3*	. . .[a]	Ref *4*	Ref *5*	Ref *6*	Ref *7*
1. pH	9.7 (5.7)	. . .	. . .	. . .	. . .	. . .
2. Cl^{-1}	98 to 297(500) ppm	. . .	. . .	. . .	. . .	. . .
3. F^{-1}	11 to 42(50) ppm	. . .	. . .	. . .	. . .	. . .
4. Fe^{+2}-Fe^{+3}	0 to 0.6(0.5)[Fe^{+2}] ppm	0.009 ppm	. . .	. . .	. . .	4%[Fe_2O_3][d]
5. Al^{+3}	0.02(20) ppm	0.007 ppm	. . .	. . .	. . .	18%[Al_2O_3][d]
6. CO_3^{-2}-HCO_3^{-1}	4 to 55/45 to 118(70/200) ppm	. . .	. . .	. . .	. . .	. . .
7. NO_3^{-1}-NO_2^{-1}	. . .	. . .	. . .	. . .	. . .	. . .
8. PO_4^{-3}	. . .	0.2[P] ppm	. . .	. . .	. . .	0.8%[P_2O_5][d]
9. BO_3^{-3}-$B_4O_7^{-2}$	0 to 1.5(5)[B^{+3}] ppm	1.3[B] ppm	. . .	. . .	. . .	. . .
10. SiO_3^{-2}	30 to 170(2000)[Si] ppm	· . . .	. . .	. . .	30[SiO_2] ppm	59%[SiO_2][d]
11. H_2O_2	. . .	. . .	. . .	0.34 ppm	. . .	. . .
12. ClO_4^{-1}	. . .	. . .	. . .	. . .	. . .	. . .
13. O_2	. . .	. . .	. . .	3.2 ppm	0.5%[c]	. . .
14. CO	. . .	. . .	. . .	. . .	. . .	. . .
15. H_2	. . .	. . .	. . .	0.02 ppm	76.6%[c]	. . .
Na^{+1}	161 to 350(500)	. . .	. . .	. . .	. . .	2.2%[d]
K^{+1}	3 to 25(100)	. . .	. . .	. . .	. . .	0.7%[K_2O][d]
Ca^{+2}	0.8 to 10(100)	. . .	. . .	. . .	. . .	1.7%[CaO][d]
Mg^{+2}	0 to 0.2(50)	. . .	. . .	. . .	. . .	2.1%[MgO][d]
SO^{-2}	4 to 197(200)	. . .	. . .	. . .	300 ppm	. . .
S^{-2}	0(100)	. . .	. .	. . .	. . .	. . .
N_2	. . .	. .	25 ppm[b]	. . .	29.3%[c]	. . .
CH_4	. . .	. . .	700 ppm[b]	. . .	0.3%[c]	. . .
CO_2	. . .	. . .	. .	. . .	2.3%[c]	. . .
E_H	-0.5 to $-0.53(+0.2$ to $-0.4)V_{SHE}$	. . .	. . .	. . .	. . .	. . .

[a] T. E. Jones personal communication to J. Means, Battelle Columbus Division, 1983.

[b] Measurements at 25°C.

[c] Composition of gas phase for simulated irradiated Grande Ronde basalt ground water.

[d] Composition of bentonite.

carbon steel containers, (2) bentonite clay to be used as a backfill around the containers, and (3) radiolysis products which will be produced by the interaction of gamma radiation with the environment at, or near, the container surface. A literature survey [2] identified many species that are present in the ground water, that may intrude into the repository, or be generated by radiolysis that may significantly affect the localized corrosion behavior of carbon steel. Table I presents a list of these species with the 15 species to be used in the present study identified. Also included in Table 1 are references that provide justification in selecting concentrations used in this study [3-7].

Synthetic environments which, historically, have been used to simulate field conditions in laboratory corrosion studies are usually relatively simple. More often than not, the effects of variables are studied by varying a single variable at a time, or at most providing for a two or three variable matrix. Such an approach does not account for the dependency of effects among multiple variables. Because of (I) the large number of variables examined in this study, (2) the desire to examine each variable in the presence of other variables, and (3) the desire to examine interaction effects among variables, a statistically designed experimental approach was performed. The statistical approach used was specifically designed to examine corrosion behavior in complex environments [8]. By using a statistically based experimental design, a mathematical expression (regression model) was developed that relates a dependent variable or response, such as corrosion rate, to a number of independent solution variables or factors, such as species concentration, temperature, and pH. In such an analysis, the mathematical expressions can include main-term effects (linear), two-factor interactions (cross products), and quadratic terms. Higher order terms such as three-factor interactions, can be also evaluated, but their physical significance is often difficult to explain, and the magnitude of the terms are expected to be much smaller than the main-effect terms or two-factor interaction terms. Many more details of the statistical approach and analysis used in this study can be found in the reference by Koch et al. [8].

Cyclic potentiodynamic polarization (CPP) experiments were used to establish the corrosion behavior of carbon steel in each of the statistically designed solutions. This permitted the significance of each variable to be determined on each of the individual polarization parameters selected from the CPP curves. Although it is realized that such data probably do not lend themselves to the long-term predictions required for high-level nuclear waste burial, the purposes of these tests were to determine trends and to identify environmental variables or combinations of variables which may lead to premature degradation of the carbon steel containers.

Experimental

Cyclic Potentiodynamic Polarization Tests

Cyclic potentiodynamic polarization (CPP) techniques were used to evaluate the influence of environmental variables on the polarization behavior of carbon steels in a variety of solutions. The CPP technique was selected for its relatively short measurement time and its ability to provide information on the tendency for a metal to undergo general corrosion, pitting corrosion, and possibly stress corrosion cracking. The equipment used for these experiments included a PAR Model 173 potentiostat in conjunction with an ECG Model 567 function generator, coupled to a computer data acquisition system. A three-compartment electrochemical cell containing a saturated calomel reference electrode (SCE) and a platinum counter electrode was used. The three-compartment electrochemical cell separates the working electrode from the counter electrode, thus preventing solutions in the different compartments from mixing during the CPP test. The working electrode specimens were cylindrical rods of 1020 carbon steel drilled and tapped at one end and then sealed using polytetrafluoroethylene (PTFE) gaskets. The specimens were 0.6 cm in diameter and 1.9 cm in length; the actual area of each specimen was measured prior to immersion in the electrochemical cell. The electrodes were polished with successively finer grades of silicon carbide paper, finishing with a 600 grit finish.

Prior to testing, the working electrode remained in the test solution overnight while the solution was sparged with the desired gas mixture. The polarization scans were then performed approximately 16 h after the working electrode was immersed in the cell. Partial cathodic and full anodic polarization curves were obtained by scanning at a rate of 0.6 V/h beginning the scan approximately 100 mV more negative than the free-corrosion potential. The current for the anodic curve was then scanned until it attained a density of approximately 3 X 10^{-3} A/cm^2; the scan was then reversed until repassivation occurred or the current changed polarity, becoming cathodic.

Screening Matrix of Experiments

The statistical experimental design was performed in two stages; Stage 1 was a screening matrix of experiments and Stage 2 was the main matrix of experiments. Table 2 gives the 15 variables examined in the screening matrix of experiments along with the high and low concentrations selected for each of the variables. As can be seen, a wide range of high and low concentrations was selected (100 to 10 OOOX).This large concentration range was selected to simulate concentration of species at the canister surface due to local boiling. The purpose of the screening matrix of experiments was to determine which of the 15 species discussed previously have a significant effect on general corrosion and pitting corrosion of carbon steel. The screening matrix was used to select the species that significantly affect corrosion, for examination in the main matrix.

To estimate the individual main-effect terms of each of the 15 species, a statistical design was used to define the optimal compositions of the test solutions. The statistical design was a partial factorial design of resolution IV. This design permits the main-effect terms of the fifteen variables to be estimated free and clear of other main-effect terms and of any two-factor interactions. The design required 32 tests to be performed to estimate the main-effect terms of the 15 variables, each at two levels. This test matrix is given in Ref 8 and will not be reproduced here. In addition, four experiments were also performed using the midpoint of each species concentration to provide an estimate of error for the polarization experiments.

At the completion of the screening matrix of experiments, a regression analysis was performed on the different corrosion parameters with the aid of a multiple regression routine on the MINITAB[2] statistical computer program. The regression analysis calculated the "F" ratio and the regression coefficient for each of the 15 species. The F statistic is a ratio of two variances, that is, the sum of squares explained by each factor when entered in the equation, divided by the residual mean square (error). In general, when the calculated F ratio for a factor is large, it means that a large amount of experimental variation is explained by this term compared to the error variation. If a calculated F ratio exceeds the appropriate tabulated F value, then it can be assumed that the solution variable has a statistically significant effect on a particular polarization parameter. A 90% probability that a species is significant

---

[2] Minitab Project, Statistics Dept., 215 Pond Laboratory, The Pennsylvania State University, University Park, PA, 16802, 1981.

TABLE 2—*High and low concentrations of species selected for evaluation in the electrochemical experiments.*

Variables	High Concentration	Low Concentration
1. pH	9.3	6.0
2. Cl^{-1}	100 000 g/m^3	100 g/m^3
3. F^{-1}	10 000 g/m^3	10 g/m^3
4. Fe^{+2}-Fe^{+3}	100 g/m^{3a}	0.05 g/m^{3a}
5. Al^{+3}	1 000 g/m^3	0.1 g/m^3
6. CO_3^{-2}-HCO_3^{-1}	1 M^a	0.001 M^a
7. NO_3^{-1}-NO_2^{-1}	1 000 g/m^3 [N][a]	0.1 g/m^3 [N][a]
8. PO_4^{-3}	1 000 g/m^3 [P]	0.1 g/m^3 [P]
9. BO_3^{-3}-$B_4O_7^{-2}$	1 000 g/m^3 [B][a]	1 g/m^3 [B][a]
10. SiO_3^{-2}	1 000 g/m^3 [Si]	10 g/m^3 [Si]
11. H_2O_2	100 g/m^3	0
12. ClO_4^{-1}	100 g/m^3	0
13. O_2	2% (vapor)	0
14. CO	1% (vapor)	0
15. H_2	80% (vapor)	1%

[a] Each of the oxidation states listed.

is usually acceptable for most experimental work and implies that one accepts a 10% chance of being wrong in assuming the factor has a significant effect.

The regression coefficients are multiplicative terms for the factors in a regression equation and were determined by a linear least square fit of the data. The regression coefficients determined in this study were calculated based on the high and low concentrations (+ 1 and - 1) of the various chemical species. For the screening matrix, these factors were based on the design concentration range of the species indicated in Table 2. Because precipitation occurred in several solutions, the actual concentrations achieved in the test solutions were not the designed values. Therefore, the regression coefficients provide relative magnitudes of the measured effects and were not meant to give a quantitative measure of the effects for the screening tests. Actual concentrations of the soluble species and measured pH values were used in the main matrix analysis to permit more quantitative relationships to be developed.

Main Matrix of Experiments

The primary purpose of the main matrix of experiments was to examine which two-factor interaction terms significantly affect the corrosion behavior of carbon steel. Also, an improved estimate of the main-effect term of each of the species selected for the main matrix of experiments was determined with the aid of the larger database available and because measured concentrations of species were used instead of the designed values. The use of measured concentrations of species and pH values is an important aspect of the data analysis since it is clear that certain designed concentrations are mutually exclusive. For example, high pH-high iron concentrations are not possible. These dependencies among variables produced high correlations in the data between certain factors (main-effect terms or two-factor interactions or both) which ideally should be independent (see Results section). Also, the analysis does not distinguish between the multiple oxidation states of certain variables (COr HC03, Fe+^{2}-Fe+3, etc.). It is clear that the ratio of one oxidation state to another will vary depending on the remaining environmental variables, but in this study the effect of the species was determined, regardless of oxidation state.

The design of the main matrix of experiments was accomplished with a computer-aided design program called COED (Computer Optimized Experimental Design). The COED program is an interactive computer program that allows scientists involved in experimental investigations to plan their experiments to obtain maximum information at minimum cost. COED picks an optimal subset of experiments to be run from the total number of possible experiments. The selection process is based on determinant optimality theory; that is, it determines the experiments that minimize the error of prediction at each possible experimental design point. COED can be used to generate an entire experimental design or to build upon an existing experimental effort.

In this case, the COED program was used to select 30 additional experiments, which, when combined with the preliminary matrix experiments, allowed for the estimation of the eleven main-effect terms (eleven variables in the main matrix) and 21 two-factor interaction terms. Table 3 gives the design matrix for the 30 additional test solutions selected by COED for the main matrix of experiments. The pluses and minuses refer to the high- and low-concentration values given in Table 2, except in the case of pH. In the main matrix of experiments, the nominal high and low values for pH were 11.5 and 6.0,[3] respectively, compared to 9.3 and 6.0 in the screening matrix.

In an initial analysis of the main matrix data, the design concentrations given in Table 2 were used. Therefore, as in the screening matrix, the accuracy of the analysis was reduced because the design concentrations were not always achieved. To improve the analysis, the solutions were analyzed, and the actual elemental concentrations were then used in the final analysis presented in the Results section.

During the polarization experiments, solution samples were collected. As part of the collection procedure, a filtering process removed any precipitate present in the test solution. Therefore, the samples consisted of only the dissolved species present when the tests were performed. Prior to analysis, any precipitates that formed during storage of the samples were redissolved so that the analysis provided elemental concentrations representative of those present in solution at the time of testing.

Analyses for fluoride, iron, and silicon were performed on all solutions. Spot analyses were performed for chloride, nitrogen, and boron depending on whether precipitates were observed during testing and whether the high or low concentration was used for a particular solution. Because peroxide is a nonstable species, the design concentration was used, although it was realized that that concentration was not likely achieved during testing. The pH of the test solution, as measured immediately after testing, was used in this analysis. The carbonate-bicarbonate concentration was determined through equilibrium calculations based on the hardness of the solution and pH. Design concentrations were used for oxygen and carbon monoxide. Table 4 gives the range of measured values for the solution variables. Note that total B, N, Fe, and CO_3-HCO_3 are used in the analyses, and it is realized that the ratio of the different oxidations states of these species may vary.

Results

Screening Matrix of Experiments

In the screening matrix of experiments, 36 CPP experiments were performed; 32 experiments, each with different high and low combinations of the 15 variables being examined,

---

[3] Design values.

TABLE 3-*Experimental design developed utilizing COED for main matrix of experiments."*

Experiment	Ph	CI	F	Fe	CO_rHC0_3	$N0_3$-$N0_2$	$B0_3$-B_40_7	$Si0_3$	H_20_2	O_2	CO
37	+	+		+	+	+	−		−		+
38	+	−	+	−	+	+		+	+		
39	+	+	−	+	+	−	−	+	+	+	−
40	+	+	−	+	+		−	+	+	+	−
41	+	−		+		+	+	+	+	+	+
42	−			−	+	+	−	+	−		+
43		+			+	+	+	−	+		+
44	+	−	+	−	−	+	+	+		−	+
45	−	+		+	−	−	+	+	+	+	+
46	+	−	−		+	+	+		+		−
47	+	−	−	+	−	+		−	−	+	
48	+	+	+		−	+		−	+	−	+
49	+		+	−	+	−	+	+	−	+	−
50	+		+	−	−		−		+	+	+
51	+	−		+	+	+	+	−	−	+	+
52	+	−		+		−		+	+		−
53	+	+	−	+	−	−	+	+		+	+
54	+	+		−	−	−	−		−	−	−
55	+	+	+	−	+	−	+		+	+	−
56		−	−	+	−	−	+	−	+		−
57	−		+	+	−	+	+	+	+	−	
58	+		−	+	+			+		−	+
59	−	−	+	+	+	+	−	−	+	+	+
60	+	+		−	+	+	+	+	−		−
61	−		−	+	−	−	+	−	−	+	+
62	+	+	+	+	+	−	+		−	−	−
63	+	+	+	−	+	−	+	+	+		+
64	+	+	+	+	−	+	+	−	+	+	
65	+	+	−	+	+	+	−	+	−	+	+
66	+	−	−	+	+	−	−	−	+	+	+

[a] (+) and (-) refer to the high and low concentrations, respectively, as indicated in Table 2 (except for pH). Solutions I through 36 comprise the screening matrix.

TABLE 4-*Measured range values of solution variables in main matrix of experiments.* [a]

Variables	Range
pH	5.3 to 13
CI	100 to 114000 *g/m*^{3}
F	10 to 8 200 glm^3
Fe	0.1 to 23 *g/m*^{3}
$C0_3$-$HC0_3$	60 to 239 000 *g/m*^{3}
N	0.2 to 2 000 glm^3
B	I to 2 080 glm^3
Si	14 to I 360 *g/m*^{3}
H_20_2	0 to 100 *g/m*^{3}
O_2	0 to 2% (vapor)
CO	0 to I% (vapor)

[a] Actual measured values at end of test.

and four replicate experiments with midrange values for each of the variables. Figures 1 and 2 show CPP curves for the 1020 carbon steel in Solutions 11 and 14, respectively. Figure 1 is representative of a curve in which pitting occurred and a hysteresis loop is present upon reversing the scan. Figure 2 indicates a solution condition in which no pitting occurred on the carbon steel. For the purposes of the statistical analysis, the pitting potential was set equal to the protection potential, which is in reality a breakdown potential since no hysteresis or pitting occurred for the carbon steel specimen. As indicated by the two typical curves shown, passive conditions typically existed at the free-corrosion potential and an active peak typically was not observed.

Table 5 provides the polarization parameters of corrosion rate (icor), free-corrosion potential (E_{cor}), passive current density (ipas), pitting potential (E_{pit}), and protection potential (E_{pro},) for each of the 36 experiments performed in the screening test matrix. Recall that experiments 33 through 36 had the same solution makeup (the midpoint in the concentration range). The data for these tests provide an indication of the reproducibility of the potentiodynamic polarization curves. The data indicate that the CPP experiments provide reasonably reproducible data for the polarization parameters examined. As can be seen from Table 5, a wide range of polarization behavior was observed by varying the high and low concentrations of the 15 environmental variables. Solutions 28 and 30 indicated active behavior such that no values for ipas, Epih and Eprot could be selected. Solutions 4, 18, and 26 exhibited a pitting potential only slightly above the free-corrosion potential, with the current increasing rapidly from the free-corrosion potential such that no passive current density could be selected.

Results of the statistical analysis performed on the polarization data presented in Table 5 are given in Table 6. The F value indicates the significance of the species, and the coefficient indicates the relative magnitude of the effect. Coefficients are given only for those variables that have a significant effect based on a 75% or greater probability. For the majority of the discussions, a 90% or greater probability is required before an effect is considered significant. A positive coefficient indicates that an increase in concentration of the variable increases the value of the polarization parameter, and a negative coefficient indicates that an increase in concentration of the variable decreases the value of the polarization parameter.

Table 6 indicates that most species have an effect on at least one polarization parameter, with the exceptions of perchlorate ($CI0_{4}$ -) and hydrogen (H_{2}), based on a 90% or greater probability of significance. Many of the effects were expected such as oxygen and nitrate increasing *Econ* and chloride decreasing E_{pit}. Other effects, such as chloride decreasing *Econ* were not particularly expected, but can be explained since chloride may tend to make the steel more active. It is also noteworthy that several species had a significant effect on ipas. Pitting behavior also was affected significantly by some of the species. Chloride, as expected, tended to decrease E_{pit} and Eproh indicating more severe pitting conditions. Oxygen, borate, and pH all tended to increase E_{pit} and Eprot with increasing concentration.

The primary purpose of the screening matrix was to select variables that had a significant effect on the corrosion behavior of carbon steel for the main matrix of experiments. The screening matrix was necessary since the number of tests needed to examine all fifteen variables would be excessively large. Because of the large number of variables which indicated a 90% or greater probability of significance for at least one of the corrosion parameters, the number of variables included in the main matrix of experiments could not be significantly reduced.

Main Matrix of Experiments

Based on the results of the screening matrix, eleven variables were selected for examination in the main matrix of experiments. It was determined that the largest experimental matrix

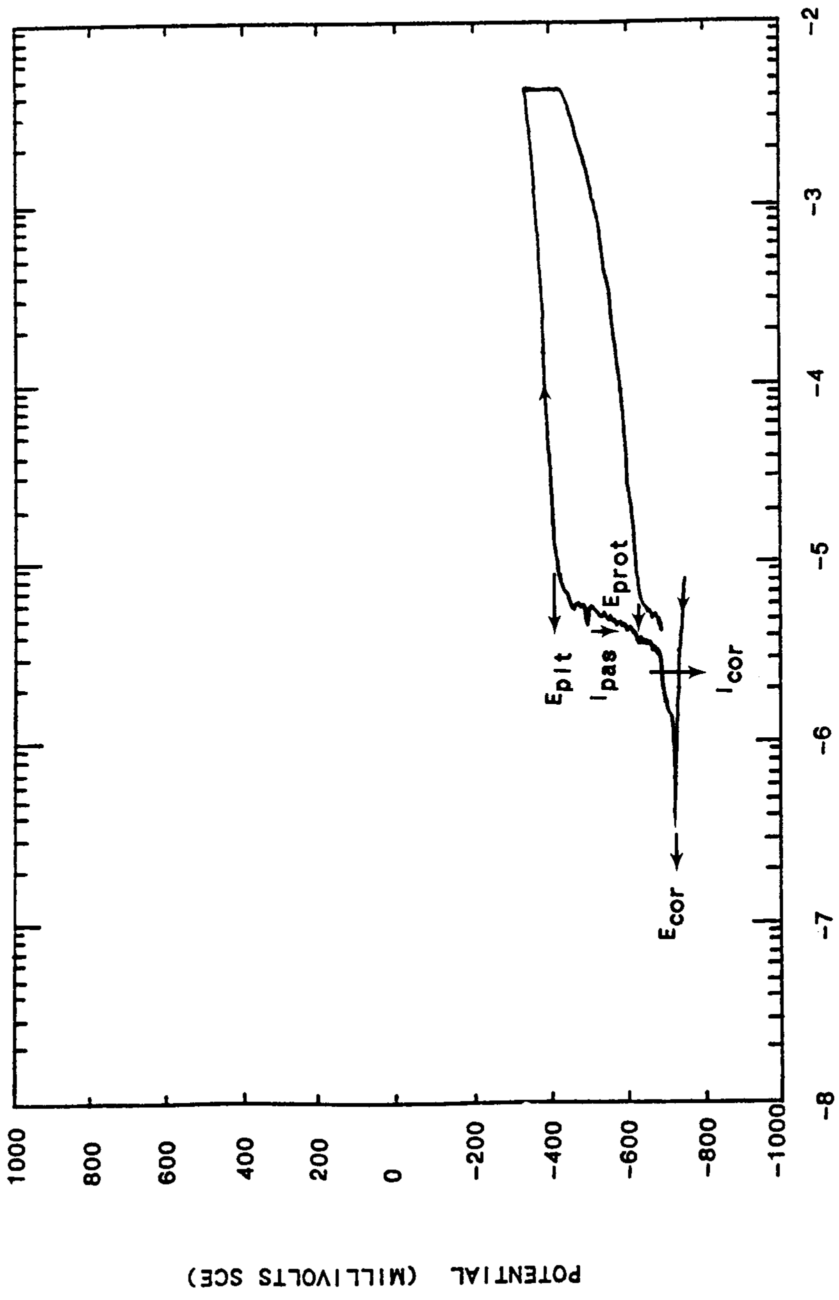

FIG. 1—*Cyclic potentiodynamic polarization curves for 1020 carbon steel in Solution 11.*

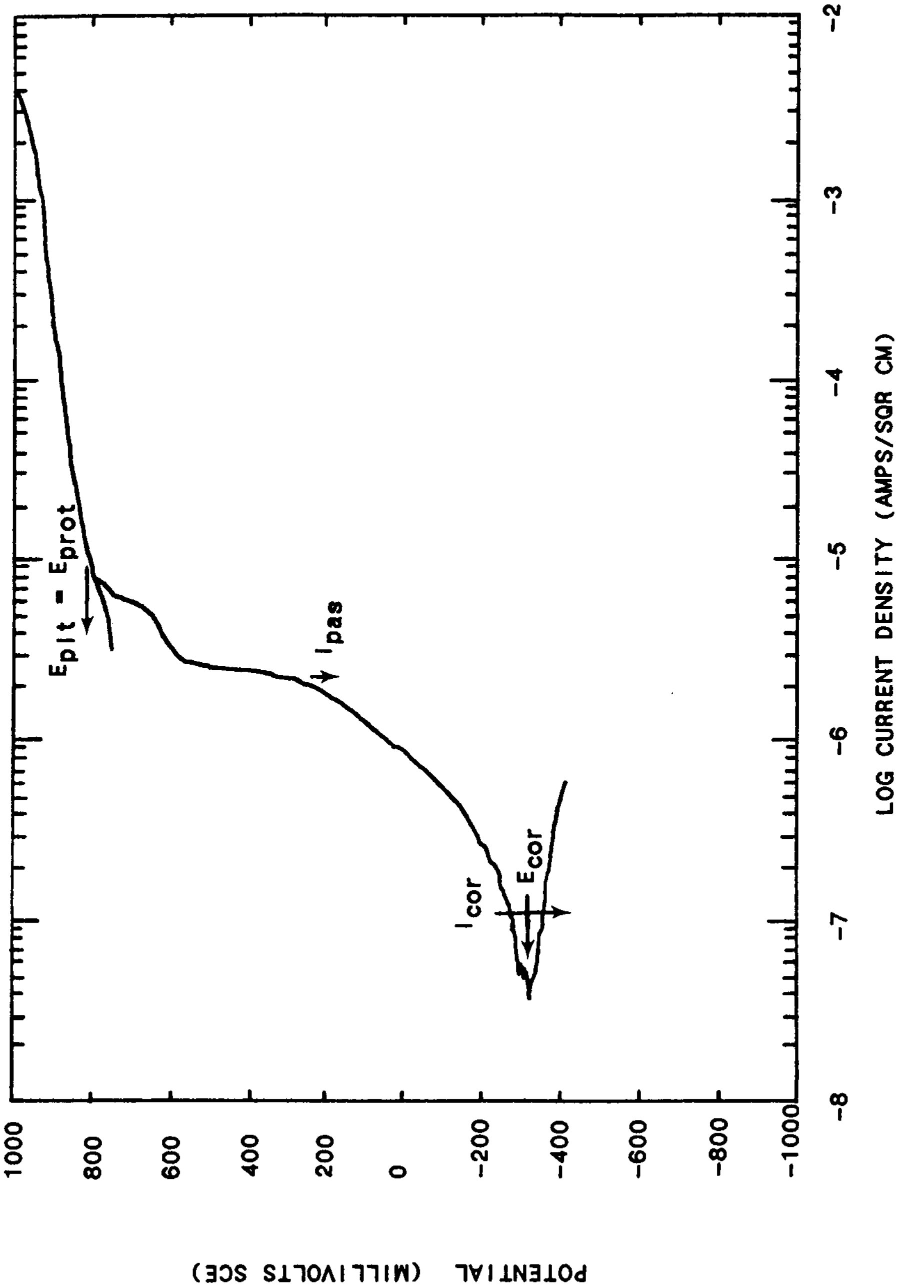

FIG. 2—*Cyclic potentiodynamic polarization curve for 1020 carbon steel in Solution 14.*

TABLE 5—*Experimentally measured polarization parameters for the 36 CPP experiments included in the screening tests.*

Solution	i_{cor}, A/cm^2	E_{cor}, V(SCE)	i_{pas}, A/cm^2	E_{pit}, V(SCE)	E_{prot}, V(SCE)
1	7.78×10^{-6}	−0.422	2.21×10^{-5}	−0.254	−0.527
2	2.0×10^{-7}	−0.200	3.01×10^{-6}	−0.776[a]	−0.776[a]
3	1.0×10^{-6}	−0.574	4.61×10^{-6}	−0.461	−0.593
4	7.32×10^{-7}	−0.767	...[b]	−0.576	−0.718
5	1.0×10^{-4}	−0.325	7.84×10^{-4}	1.0[a]	1.0[a]
6	1.57×10^{-4}	−0.859	8.97×10^{-5}	0.808	0.808[a]
7	7.44×10^{-5}	−0.515	9.33×10^{-4}	−0.200	−0.544
8	4.21×10^{-5}	−0.891	2.29×10^{-5}	−0.042	−0.625
9	1.38×10^{-5}	−0.781	1.30×10^{-5}	−0.562	−0.657
10	1.1×10^{-6}	−0.200	2.63×10^{-6}	0.557	−0.261
11	2.97×10^{-6}	−0.735	5.25×10^{-6}	−0.422	−0.640
12	5.44×10^{-6}	−0.623	2.73×10^{-5}	−0.471	−0.547
13	5.74×10^{-5}	−0.461	7.78×10^{-5}	−0.330	−0.471
14	1.0×10^{-7}	−0.310	2.42×10^{-6}	0.808[a]	0.808[a]
15	8.51×10^{-5}	−0.725	4.05×10^{-5}	−0.557	−0.640
16	9.19×10^{-7}	−0.515	2.73×10^{-6}	0.540	−0.452
17	6.05×10^{-6}	−0.657	1.11×10^{-5}	−0.483	−0.718
18	8.97×10^{-6}	−0.625	...[b]	−0.466	−0.576
19	5.83×10^{-6}	−0.435	2.33×10^{-6}	0.825	0.776
20	8.58×10^{-5}	−0.498	1.32×10^{-4}	−0.247	−0.608
21	2.03×10^{-6}	−0.940	1.51×10^{-5}	0.588	−0.342
22	5.08×10^{-5}	−0.576	1.96×10^{-4}	−0.420	−0.515
23	3.25×10^{-5}	−0.876	6.53×10^{-5}	0.745[a]	0.745[a]
24	2.12×10^{-6}	−0.310	8.58×10^{-6}	0.800	−0.088
25	6.0×10^{-6}	−0.657	4.44×10^{-5}	−0.400	−0.576
26	1.09×10^{-6}	−0.640	...[b]	−0.483	−0.718
27	1.6×10^{-7}	−0.562	7.38×10^{-7}	0.083	−0.530
28	7.26×10^{-4}	−0.688	...[b]	...[b]	...[b]
29	8.58×10^{-6}	−0.562	1.07×10^{-4}	0.800	−0.042
30	3.04×10^{-4}	−0.703	...[b]	...[b]	...[b]
31	6.43×10^{-4}	−0.845	1.52×10^{-4}	0.684[a]	0.684[a]
32	5.49×10^{-6}	−0.781	6.25×10^{-6}	−0.544	−0.657
33	2.5×10^{-6}	−0.544	6.25×10^{-6}	−0.293	−0.576
34	1.1×10^{-6}	−0.466	3.73×10^{-6}	−0.310	−0.576
35	1.37×10^{-6}	−0.530	4.27×10^{-6}	−0.232	−0.576
36	1.48×10^{-6}	−0.530	4.61×10^{-6}	−0.310	−0.576

[a] $E_{pit} = E_{prot} \doteq E_B$ (breakdown): no pitting.
[b] Not measured from polarization behavior.

which could be performed under the present program, due primarily to economic considerations, included the examination of eleven main-effect terms and 21 two-factor interaction terms. Table 7 gives the main-effect terms and the two-factor interaction terms which were included in the main matrix of experiments. These variables and interaction terms were selected based on the results of the screening matrix of experiments and past experience.

As previously mentioned, the computer-aided design program, COED, permitted the selection of 30 additional experiments which, when combined with the screening matrix of experiments, allowed for the estimation of the 21 two-factor interaction terms and permitted an improved estimate ofthe main-effect terms of the eleven variables. The designed high and

TABLE 6—*Results of statistical analysis indicating the effect of each chemical species on the polarization parameters measured by cyclic potentiodynamic polarization.*

	E_{cor}		Log i_{cor}		Log i_{pas}		E_{pit}		E_{prot}	
	F	Coef	F	Coef	F	Coef	F	Coef	F	Coef
pH	0.5		6.4	-0.34^a	174	-0.18^a	27	$+0.31^a$	13	$+0.22^a$
Cl	7.6	-0.06^a	0.2		34	$+0.06^a$	26	-0.25^a	30	-0.32^a
F	0.5		1.0		39	-0.08^a	0.0		0.3	
Fe	0.9		0.9		86	$+0.41^a$	0.0		0.3	
Al	1.1		0.8		36	$+0.03^a$	1.7		0.1	
CO_3/HCO_3	8.4	-0.07^a	0.3		3.6	-0.16^b	2.9	$+0.06^b$	0.9	
NO_3/NO_2	15.0	$+0.09^a$	1.1		19	$+0.64^a$	4.0	$+0.13^b$	0.1	
PO_4	1.1		0.4		28	$+0.10^a$	0.3		2.6	-0.10^b
BO_3/B_4O_7	1.9	$+0.03^b$	0.1		29	$+0.78^a$	6.0	$+0.14^a$	5.1	$+0.13^a$
SiO_3	1.1		7.2	-0.36^a	138	-0.85^a	0.0		0.1	
H_2O_2	0.3		4.2	$+0.27^a$	16	$+0.25^a$	0.0		0.2	
ClO_4	0.2		0.1		1.2		0.2		1.3	
O_2	3.9	$+0.05^a$	0.5		1.3		9.3	$+0.13^a$	8.2	$+0.15^a$
CO	0.1		0.1		22	-0.64^a	1.1		0.0	
H_2	0.0		1.7	$+0.17^b$	0.3		1.2		0.1	

[a] Greater than 90% probability that effect is significant.
[b] Greater than 75% but less than 90% probability that effect is significant.

low values for the eleven variables examined in the main test matrix were previously given in Table 3. As previously mentioned, in the final regression analysis, actual measured concentrations of several of these variables were used as opposed to the design variable concentration because of precipitation in the solution. A close examination of the measured values of the solution variables as compared to the design values indicates a significant discrepancy for several of the solutions. As would be expected, the carbonate-to-bicarbonate ratio was highly dependent on pH. Furthermore, the total carbonate/bicarbonate concentration varied significantly from the high and low values of the design matrix, with the low values being quite often higher than designed. Both silicon and iron varied significantly from their designed concentrations for both high and low concentrations. For silicon, this may be partly

TABLE 7—*Main effects and interactions selected from screening tests which were examined in main test matrix.*

Main Effects	Two-Factor Interactions	
pH	pH × Cl	Cl × H_2O_2
Cl	pH × CO_3	CO_3 × H_2O_2
F	pH × NO_3	CO_3 × O_2
Fe	pH × BO_3	NO_3 × BO_3
CO_3-HCO_3	pH × SiO_3	NO_3 × O_2
NO_3-NO_2	pH × H_2O_2	NO_3 × SiO_3
$BO_3-B_4O_7$	pH × O_2	BO_3 × SiO_3
SiO_3	pH × CO	BO_3 × H_2O_2
H_2O_2	Cl × CO_3	SiO_2 × O_2
O_2	Cl × NO_3	H_2O_2 × O_2
CO	Cl × BO_3	

TABLE 8—*Terms that had a high degree of correlation.*

Terms	Correlated Terms
pH and	CO_3
F and	SiO_3
CO_3 and	pH $\times$ CO_3
SiO_3 and	$SiO_3 \times O_2$
SiO_3 and	pH $\times$ SiO_3
SiO_3 and	$BO_3 \times SiO_3$
pH and	pH $\times$ SiO_3
BO_3 and	$BO_3 \times SiO_3$
O_2 and	$NO_3 \times O_2$
O_2 and	$H_2O_2 \times O_2$
pH $\times$ CO_3 and	pH $\times$ SiO_3
pH $\times$ Cl and	Cl $\times$ CO_3
pH $\times$ H_2O_2 and	$CO_3 \times H_2O_2$
pH $\times$ O_2 and	$CO_3 \times O_2$
$NO_3 \times SiO_3$ and	$BO_3 \times SiO_3$

due to (1) leaching from the walls of the glass cell, especially when fluoride was present, and (2) limited solubility. Iron deviated from the designed values due to limited solubility and corrosion product formation. The high concentration of fluoride was typically less than half the designed 10 000 gjm^3 value due to limited solubility.

Due primarily to the fact that the design concentrations were not always achieved, a high degree of correlation existed between certain main-effect terms and interaction terms. Therefore, all of the main-effect terms and two-factor interaction terms examined in this study

TABLE 9—*Results of statistical analyses for main-effect terms showing coefficients, intercept, significance level, and explained variability for each polarization parameter in final model.*

Main Effect	E_{cor}, V(SCE) RC (SL)[a]	Log i_{cor}, (A/cm^2) RC (SL)	Log i_{pas}, (A/cm^2) RC (SL)	E_{pit}, V(SCE) RC (SL)	E_{prot}, V(SCE) RC (SL)
pH	...	−1.456 (99%)	−1.436 (99%)	−0.659 (99%)	...
Cl	−0.072 (99%)	...	...	...	−0.418 (99%)
F	...	+0.402 (96%)	+0.272 (97%)	...	...
Fe	−0.112 (99%)	...	...	...	...
CO_3	...	...	...	+0.923 (99%)	+0.234 (99%)
NO_3	+0.060 (99%)	−0.637 (99%)	...	...	...
BO_3	...	...	...	...	...
SiO_3	...	...	...	...	...
H_2O_2	...	...	...	...	...
O_2	...	...	...	+0.065 (91%)	...
CO	...	...	...	...	...
Intercept	−0.644	−5.329	−4.844	+0.736	−0.094
R^2[b]	54%	62%	73%	78%	71%

[a] RC = regression coefficient; SL = significance level (% probability of significance).
RC > 0 indicates that the parameter increases with increasing concentration.
RC < 0 indicates that the parameter decreases with increasing concentration.
A large SL indicates that the term is significant.

[b] R^2: coefficient of determination for the final model. The R^2 term is the percentage of total variability explained by the model.

TABLE 10—*Results of statistical analyses for interaction terms showing coefficients and significance level for each polarization parameter in final model.*

Interaction Term	E_{cor}, V(SCE) RC (SL)[a]	Log i_{cor}, (A/cm^2) RC (SL)	Log i_{pas}, (A/cm^2) RC (SL)	E_{pit}, V(SCE) RC (SL)	E_{prot}, V(SCE) RC (SL)
pH × Cl	...	...	...	−0.279 (99%)	−0.315 (99%)
pH × CO_3	...	...	...	−0.852 (99%)	−0.227 (97%)
pH × NO_3	−0.059 (96%)	...	...	...	...
pH × BO_3	...	...	...	...	...
pH × SiO_3	...	...	−0.610 (91%)	...	...
pH × H_2O_2	...	...	...	...	...
pH × O_2	...	...	+0.232 (95%)	−0.165 (97%)	−0.173 (95%)
pH × CO	...	...	...	−0.157 (96%)	−0.147 (90%)
Cl × CO_3	...	...	−0.208 (98%)	+0.416 (99%)	...
Cl × NO_3	...	+0.219 (96%)	+0.221 (99%)	...	+0.092 (93%)
Cl × BO_3	...	...	...	−0.113 (98%)	−0.138 (98%)
Cl × H_2O_2	...	...	−0.249 (99%)	...	...
CO_3 × H_2O_2	−0.032 (91%)	...	...	...	...
CO_3 × O_2	...	...	...	...	...
NO_3 × BO_3	...	...	...	...	...
NO_3 × SiO_3	...	−0.647 (99%)	−0.148 (94%)	−0.104 (97%)	...
NO_3 × O_2	...	−0.201 (96%)	+0.216 (99%)	...	...
BO_3 × SiO_3	...	...	...	−0.119 (98%)	−0.186 (99%)
BO_3 × H_2O_2	...	...	...	...	...
SiO_3 × O_2	−0.043 (98%)	...	...	...	...
H_2O_2 × O_2	−0.37 (98%)	...	...	...	...

[a] RC = regression coefficient; SL = significance level (% probability of significance).
RC > 0 indicates that the parameter increases with increasing concentration.
RC < 0 indicates that the parameter decreases with increasing concentration.
A large SL indicates that the term is significant.

were not independent of one another as desired. Table 8 gives the terms that had a high degree of correlation. These correlations have to be taken into account in the final analyses.

The final regression model was based on a step-wise regression analysis. This technique begins with no variables in the model and adds variables one at a time. For each variable, an F statistic is calculated that reflects the variable's contribution to the model if it were to be included next. The variable contributing most to the model is added provided that the F statistic is significant at the 85% level of being significant. After a variable is added, however, a backward elimination is performed to delete any variable that does not contribute significantly to the model. This process continues until no variables can be added or deleted. Tables 9 and 10 present the coefficients and significance levels for the main-effect terms and two-factor interactions terms in the final model, respectively. The final model included all terms with a 90% or greater probability of being significant. Coefficients are presented for each term present in the model, with a positive value indicating that the parameter increases with increasing concentration and a negative value indicating that a parameter decreases with increasing concentration. As can be seen from Tables 9 and 10, several main-effect terms and interaction terms remain in the regression model at a 90% probability of significance. The R^2 term is important since it estimates the percentage of total variability that is explained by the model. The R^2 terms are lower than desired, which is likely due to variations inherent in the CPP experiments or due to the variation from designed concentrations during the experiments or both.

Discussion

Figures 3 through 7 show graphically the main-effect terms and interactions terms with their relative magnitudes for E_{cor}, log i_{cor}, log i_{pas}, E_{pit}, and E_{prot}, respectively. Because the analysis represents normalized concentrations from +1 to −1 for each variable, comparisons of relative magnitude of the effect can be made for the concentration ranges examined. Figures 3 through 7 present the data in such a way that determining the significance of a main-effect term and any interaction terms is relatively easy. For example, in Fig. 3 it is seen that iron has the largest main-effect on E_{cor}; E_{cor} decreases with increasing iron concentration. Nitrate, on the other hand, tends to increase E_{cor} with increasing concentration, and the

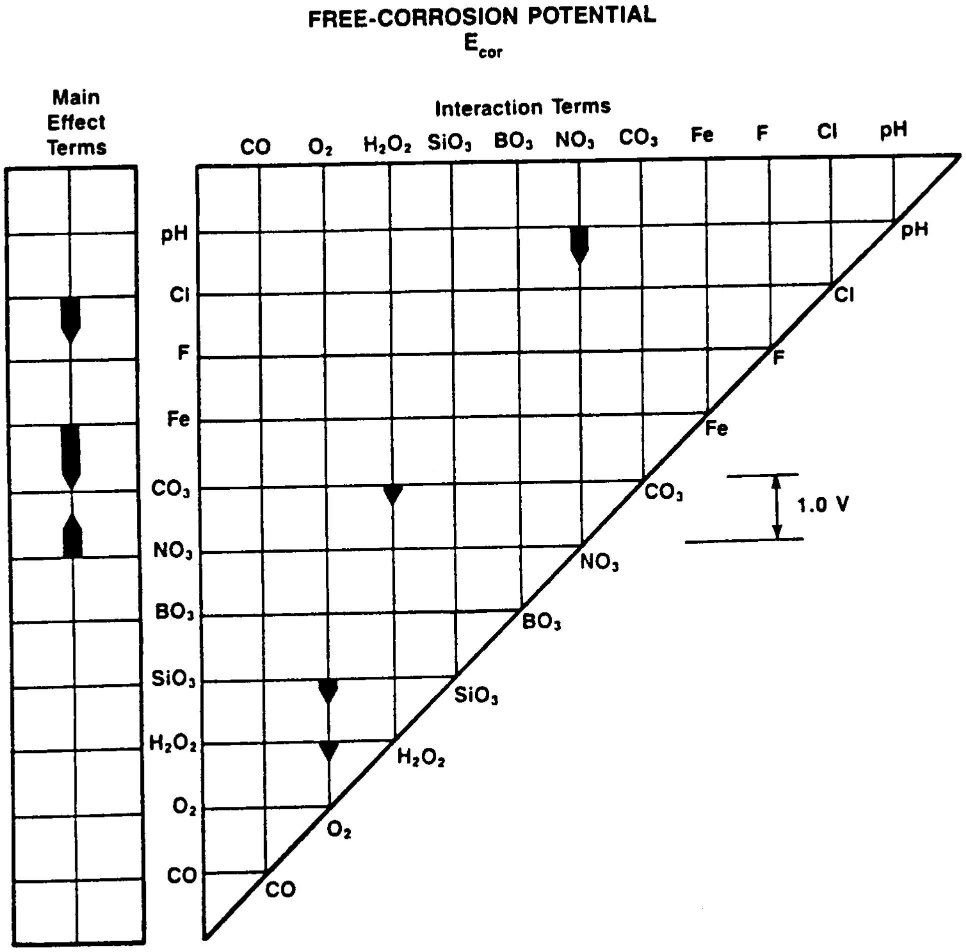

FIG. 3—*Schematic showing the relative magnitude and direction of significant main effects and two-factor interactions on* E_{cor}. *The direction of the arrow indicates the direction of effect of that single species* (left) *or that two-factor interaction* (right) *on* E_{cor}. *The length of the arrow indicates the magnitude. For example,* NO_3 *increased* E_{cor} *by about 0.67 V while the* $BO_3 \times SiO_3$ *interaction decreased* E_{cor} *by about 0.25 V.*

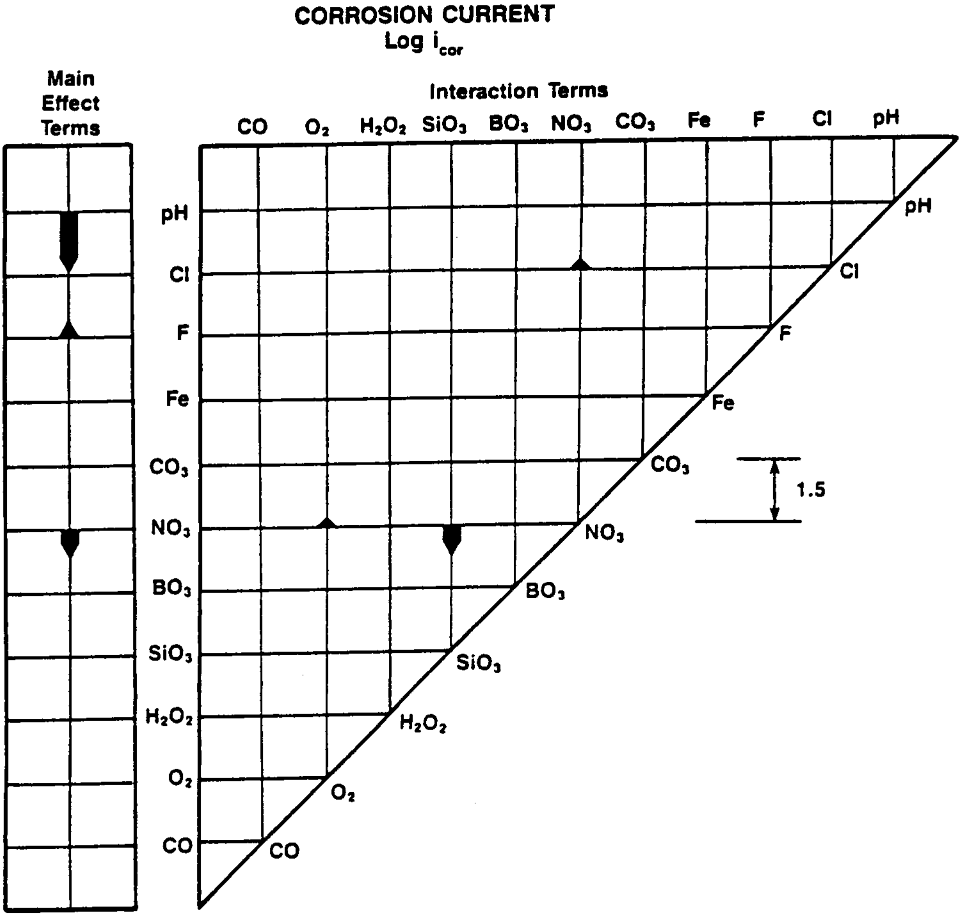

FIG. 4—*Schematic showing the relative magnitude and direction of significant main effects and two-factor interactions on* i_{cor}.

nitrate X *pH* two-factor interaction is significant. The effects of chloride and nitrate are easily explained; however, the relatively large decrease of E_{cor} due to iron is more difficult to explain. Iron was added as equal amounts of ferric and ferrous ions, and because E_{cor} decreases with increasing iron, it appears that the effect of ferrous ions is dominating. Figure 4 shows that the effect of pH is much more significant on the corrosion rate than any of the other main-effect terms or two-factor interaction terms. This is also true for the passive current density shown in Fig. 5.

The pitting tendency for a solution can be described by E_{pil} and E_{prot}. A variable that tends to decrease either of these parameters would typically be considered to promote pitting. To determine whether pitting would occur in any given environment, E_{cor} also would have to be considered. It should be noted, however, that, for E_{pih} several of the variables included in the regression model and shown in Fig. 7 are included in Table 8 as having a high degree of

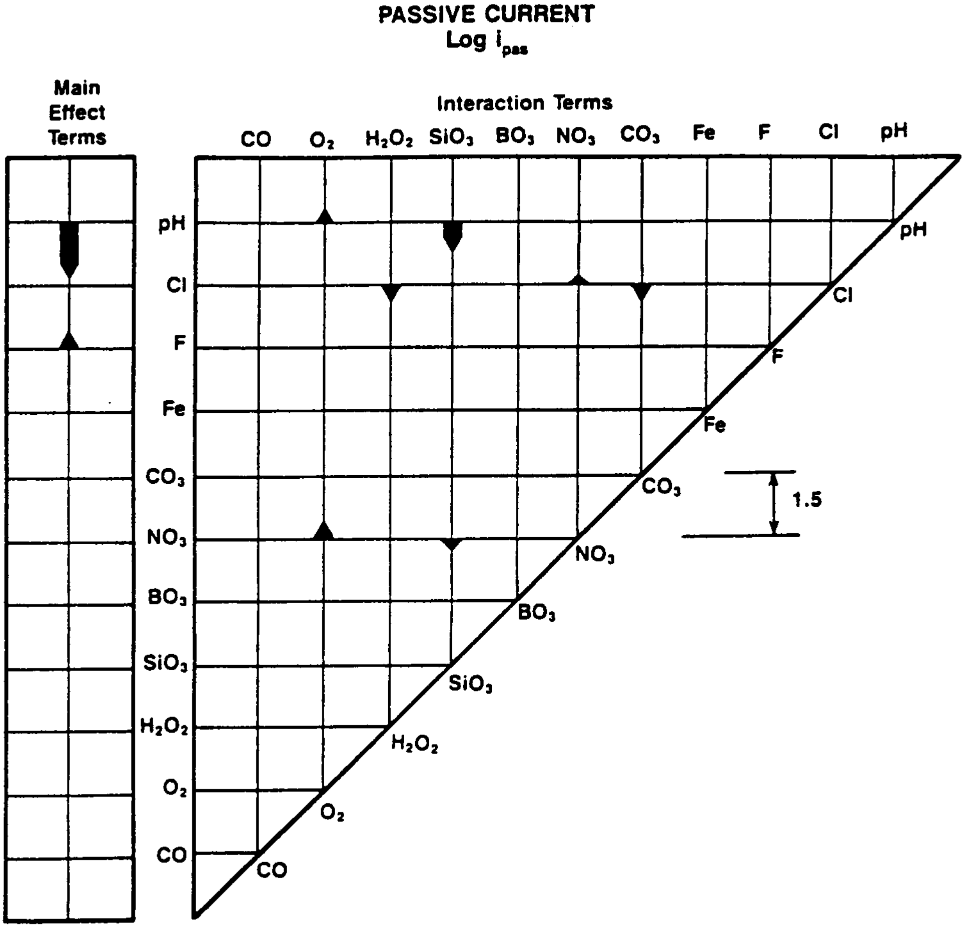

FIG. 5—*Schematic showing the relative magnitude and direction of significant main effects and two-factor interactions on* i_{pas}.

correlation because the designed concentrations were not achieved due to chemical interaction: (1) pH and carbonate, (2) carbonate and *pH* X *carbonate,* (3) *pH* X *chloride* and *chloride* X *carbonate,* and (4) *borate* X *silicate* and *nitrate* X *silicate.* The consequence of these correlations is a decreased ability of the regression model to predict the pitting behavior especially beyond the ranges for concentrations of the variables contained in the model.

To perform a statistical analysis of the main-effect terms and two-factor interaction terms, the data given in Tables 9 and 10 were normalized to a range of + 1 to - 1 for each variable using the following transformation

$$X_i^* = 2\left(\frac{X_i - L_i}{M_i - L_i}\right) - 1 \qquad (1)$$

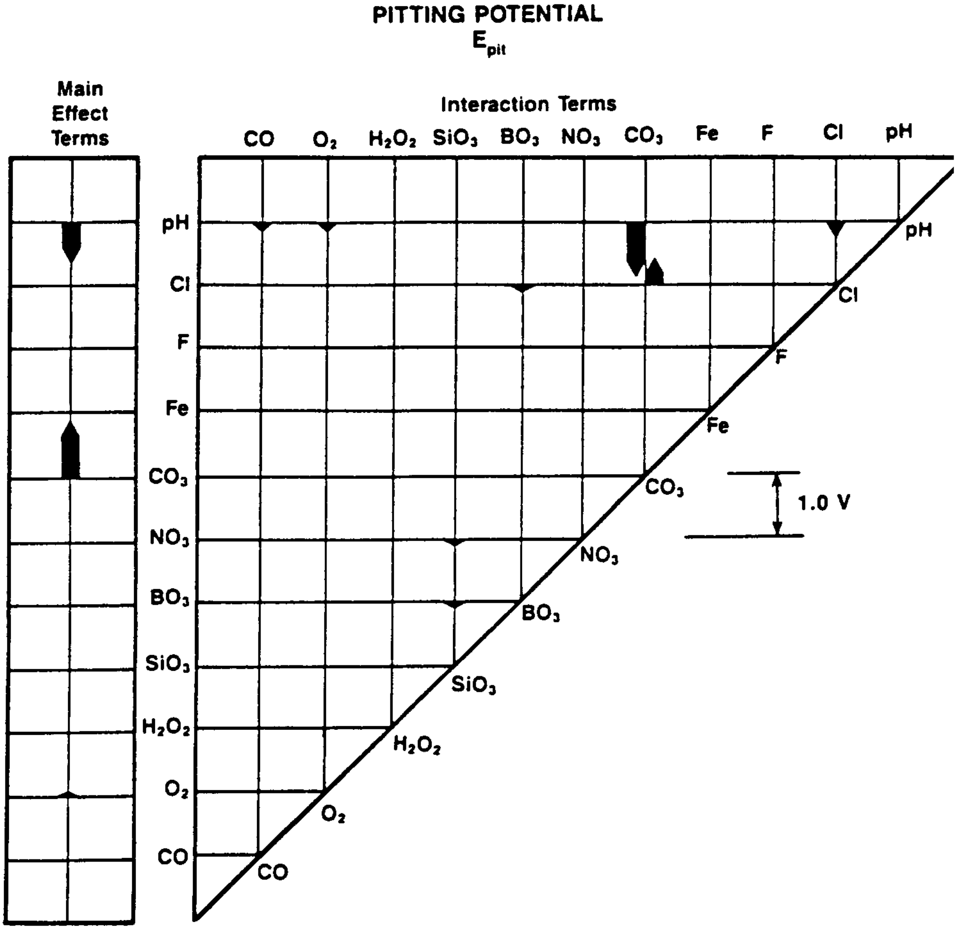

FIG. 6—*Schematic showing the relative magnitude and direction of significant main effects and two-factor interactions on* E_{pit}.

where

X^* = transformed concentration of variable i,
X_i = actual concentration,
L_i = minimum concentration, and
M_i = maximum concentration.

The equation for any particular parameter, Y, can be expressed as follows

$$Y = a_o + b_i X_i^* + c_{ij} X_i^* X_j^* \quad (2)$$

where

a_o = intercept,
b_i = coefficient for the main-effect terms, and
c_{ij} = coefficient for the two-factor interaction terms.

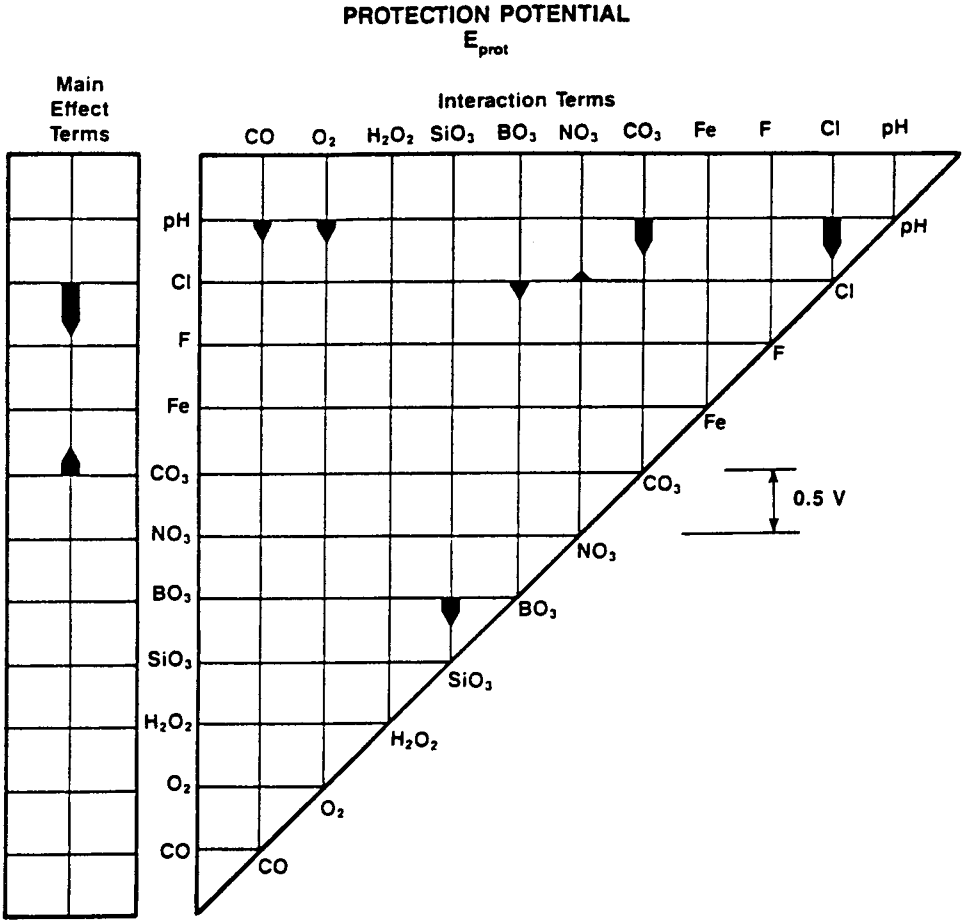

FIG. 7—*Schematic showing the relative magnitude and direction of significant main effects and two-factor interactions on* E_{prot}.

The transformation (Eq 1) is such that at the maximum concentration (when $X_i = m_i$), $X_i^* = +1$; when X_i equals the minimum concentration, $X_i^* = -1$; and when X_i equals the median concentration, $X_i^* = 0$. For this discussion, the median concentration will be referred to as an average concentration. Therefore, for an average solution (a solution with all variables set to their median concentrations), the parameter Y is equal to a_o, since X_i^* is equal to 0 for all variables. For solutions other than an average solution, the effect of the solution concentration on the corrosion parameter Y can be calculated using Eqs 1 and 2.

Table 11 shows the effect of the concentration range for each variable with all other variables held at their median values. For this condition, all of the terms in the model go to 0 except for the variable of interest. For example, with all variables held at their median values except for chloride, E_{cor} is given as follows

$$E_{cor} = -0.664 - 0.072X_{Cl}^* \quad (3)$$

TABLE 11—*Effect of concentration range for each variable (with all other variables held at their median values) on the corrosion parameters.*

Variable	Range	E_{cor}, V(SCE)	i_{cor}, A/cm^2	i_{pas}, A/cm^2	E_{pit}, V(SCE)	E_{prot}, V(SCE)
pH	5.3 to 13	...	1.3×10^{-4} to 1.6×10^{-7}	3.9×10^{-4} to 5.2×10^{-7}	+1.39 to +0.08	...
Cl	100 to 114 000 g/m^3	−0.59 to −0.74	...	...	...	+0.32 to −0.51
F	10 to 8 200 g/m^2	...	1.8×10^{-6} to 1.2×10^{-5}	7.7×10^{-6} to 2.7×10^{-5}	...	...
Fe	0.1 to 23 g/m^3	−0.55 to −0.78	...	...	...	...
CO_3	60 to 239 000 g/m^3	...	...	...	−0.19 to +1.66	−0.33 to +0.14
NO_3	0.2 to 2 000 g/m^3	−0.72 to −0.60	2.0×10^{-5} to 1.1×10^{-6}	...	...	...
BO_3	1 to 2 080 g/m^3	...	...	...	...	...
SiO_3	14 to 1 360 g/m^3	...	...	...	...	...
H_2O_2	0 to 100 g/m^3	...	...	...	...	...
O_2	0 to 2% (vapor)	...	...	...	+0.67 to +0.80	...
CO	0 to 1% (vapor)	...	...	...	...	...

where X_{Cl}* is given as follows

$$X_{Cl}^* = 2\left(\frac{X_{Cl} - 100}{114\,000 - 100}\right) - 1 \tag{4}$$

Therefore, Table 11 shows the magnitude of the effect of varying any particular variable in an otherwise "average" solution.

Conclusions

The objective of this study was to evaluate the influence of environmental variables on general corrosion and pitting corrosion behavior of carbon steel in basalt ground-water environments. These tests show that a statistically designed matrix of experiments can be used to examine the individual and interactive effects of multiple environmental variables which typically make up the complex environments found in ground-water solutions. The COED program is ideal for this type of approach since it optimizes the number of experiments required to achieve specific research goals.

These tests also pointed out many of the problems associated with performing a large matrix of experiments in which large concentration ranges of the environmental variables are desired. The primary problem is that certain combinations of solution variables are restricted, which alters the actual concentrations achieved. This can produce correlation among the terms which are designed to be independent, requiring more careful analysis of the data.

The results indicate that two-factor interactions are required to completely model the effects of environmental variables on corrosion of carbon steel in ground-water environments. All eleven primary variables were shown to be significant as either a main-effect term or in a two-factor interaction term. Solution pH had the largest effect on i_{cor} and ipas. Chloride, iron, and nitrate had the largest effect on E_{cor}' Solution pH, chloride, and carbonate had the largest effect on the pitting parameters.

References

[1] Beavers, J. A., Thompson, N. G., Markworth, A. J., Cialone, H. J., Majumdar, B. S., and McCoy, J. K., Topical Report "Long-Term Performance of Container Materials for High-Level Waste," NUREGjCR-4955, Nuclear Regulatory Commission, Washington, DC, 1987.

[2] Beavers, J. A., Thompson, N. G., and Parkins, R. N., Topical Report "Stress-Corrosion Cracking of Low-Strength Steels in Candidate High-Level Waste Repository Environments," NUREGjCR-3861, Nuclear Regulatory Commission, Washington, DC, 1987.

[3] "Draft Technical Position on Repository Environmental Parameters Relevant to Assessing the Performance of High-Level Waste Packages," NUREG-1076, Nuclear Regulatory Commission, Washington, DC, 1984.

[4] Gray, W. J., "Gamma Radiolysis Effects on Grande Ronde Basalt Groundwater," *Proceedings,* Materials Research Society-Scientific Basis for Nuclear Waste Management, Boston, MA, Nov. 1983.

[5] Simonson, S. A. and Kuhn, W. L., "Predicting Amounts of Radiolytically Produced Species in Brine Solution," *Proceedings,* Materials Research Society-Scientific Bases for Nuclear Waste Management, Boston, MA, Nov. 1983.

[6] Grause, E. P., Brewster, C., and Soo, P., "Determination of the Waste Package Environments for a Basalt Repository: Phase I-Gamma Irradiation Conditions in the Absence of Methane," Report No. BNL-NUREG-24297, Nuclear Regulatory Commission, Washington, DC, 1984.

[7] "NRC Nuclear Waste Geochemistry '83," *Proceedings,* The U.S. Nuclear Regulatory Commission, Reston, VA, Aug. 1983, p. 245.

[8] Koch, G. H., Spangler, J. M., and Thompson, N. G., "Corrosion Studies in Complex Environments," *The Use of Synthetic Environments for Corrosion Testing, ASTM STP 970,* P. E. Francis and T. S. Lee, Eds., American Society for Testing and Materials, Philadelphia, PA, 1988, pp. 3-17.

C. V. Lundberg[1]

Long-Term Weathering of Organic and Inorganic Coatings on Steel and on Aluminum

REFERENCE: Lundberg, C. Y., "Long-Term Weathering of Organic and Inorganic Coatings on Steel and on Aluminum," *Corrosion in Natural Waters, ASTM STP 1086,* C. H. Baloun, Ed., American Society for Testing and Materials, Philadelphia, 1990, pp. 122-155.

ABSTRACT: This study reports on the protection offered to steel and aluminum by selected formulations offluidized-bed-applied vinyl, epoxy, polyester, ethylene-acrylic acid copolymer, and nylon powder coatings; solvent-borne vinyl, epoxy and chlorinated rubber coatings; ceramic coatings; hot-dipped and flame-sprayed zinc and aluminum coatings; and flame-sprayed 67-33 zinc-aluminum coatings. Most of the coatings fully protected the metals when exposed for ten years to a polluting industrial atmosphere. Some of the solvent-borne organic and flame-sprayed metallic coatings protected the metals during eleven years on a North Carolina ocean beach. Some of the flame-sprayed metallic coatings protected the metals during twelve years of Florida saltwater and mud exposure. The aluminum substrate panels retained their structural integrity whether exposed with or without coatings.

KEY WORDS: organic coatings, inorganic coatings, fluidized-bed-applied coatings, ceramic coatings, flame-sprayed aluminum and zinc coatings, hot-dipped aluminum and zinc (galvanized) coatings, solvent-borne coatings, Resistance of coated steel and aluminum to an industrial atmosphere, to an ocean beach atmosphere, to seawater, to burial in salt sandy-mud

In order to get information on the lasting qualities of protective coatings, accelerated and natural aging of coatings are required. Accelerated tests consist of oven aging at normal or elevated humidity, with or without exposure to light of various types; and salt-spray exposure. Some tests involve imposition of an electrical potential to accelerate corrosive effects.

But regardless of all the work that has been done in developing accelerated tests, outdoor exposure tests are still universally used by coating suppliers and large coating users. Atmospheric exposures of coatings are made in various sections of the country on so-called "fences" for long-time periods. Usually, coated panels are examined periodically for color changes, loss of gloss, chalking, blistering, peeling, and corrosion of metal substrates. Coatings designed for marine use are laboratory evaluated in freshwater or saltwater and the promising ones are exposed in natural waters, fresh and salt.

This study concerns the long-term protection offered to steel and to aluminum substrates by selected formulations of fluidized-bed-applied organic coatings, solvent-borne organic coatings, an electrostatic-sprayed powder coating, ceramic coatings, and hot-dipped and flame-sprayed metallic coatings. The study was originated in 1968 when concern increased for the growing amount of underground telephone plant. The original program included soil burial of a variety of molded and extruded plastics at Bainbridge, Georgia (acid soil) and Roswell, New Mexico (alkaline soil), but this part of the program was terminated in 1972 because of the low corrosivity of the soils at these test sites [1].

[1] Retired, AT&T Bell Laboratories, Murray Hill, NJ 07974.

Procedure

Specimens

Organic coatings on metal panels are normally exposed as flat panels with no external strain applied. Adhesive joints when under stress and exposed to moist conditions can be adversely affected. Unsaturated rubbers can be severely crazed and cracked by atmospheric ozone when exposed in a stretched condition. Brouillette [2] revealed that the pressure of porcelain insulators against the edges of flat exposure panels induced strains in coatings that caused premature blistering of the coatings and rusting of the substrates. Because of the effects of externally applied stresses and strains on some organic materials, it was decided to expose)i2-in. (0.794-mm) thick coated metal panels in a strained condition to observe the coatings for adverse strain effects. The coated panels were assembled with molded-plastic spacers and end-bars so that the)i2-in. (0.794-mm) panels were slightly curved and sloped 7 deg from the horizontal at each specimen end when they were bolted to)i-in. (3.175-mm) thick panels identically coated. The)i-in. (3.175-mm) panels were sufficiently stiff to resist bending. The)i2-in. (0.794-mm) panels were deformed within their elastic limits. The bolts were tightened to the point where the gap between the)i2-in. (0.794-mm) panel center and the spacer was I50-mil (3.81O-mm) as determined with a Teflon feeler gage, resulting in an applied strain in the)i2-in. (0.794-mm) panels. The ceramic coatings on steel cracked under this strain and were bolted with an 85-mil (2.159-mm) deflection rather than the 150-mil (3.81O-mm) deflection used for the other panels. The ceramic coating on aluminum did not crack and was assembled with the I50-mil (3.81O-mm) deflection. All of the panels measured 3~ by 5 in. (88.9 by 127 mm). Chemical analyses of the aluminum and steel panels are shown in Table I. For atmospheric exposures stainless steel bolts and nuts were used to hold the assemblies together and were isolated from the test panels with polyethylene sleeving and phenolic washers. For water and mud exposures polyvinyl-chloride bolts and nuts were used. Figure I shows the panel assembly of stressed and unstressed panels.

Racking and Exposure

The specimen assemblies were mounkd on glass-reinforced-polyester racks holding up to 88 assemblies. Five replicates per coating were provided per exposure period at each location. The top channel of each water immersion rack was made of Monel, and Monel fasteners and eyebolts were used. Critical frame joints of the marine racks were reinforced with fasteners of Harper Alloy 13A.

Exposures were installed at three locations as follows:

I. Atmospheric exposures were established on the roof of the garage occupied by the Ohio Bell Telephone Co. on 6th Street in Steubenville, Ohio. This site had been used for other exposure studies because of the presence of steel mills and other industrial activity in the vicinity and the possible corrosive atmosphere. The specimen racks were supported on an elevated framework at an angle of 30 deg to the flat roof, facing west. The strained)i2-in. (0. I74-mm) panels were directly exposed to the sun and weather; the unstrained)i-in. (3.175-mm) panels were below the strained panels and partly shaded from direct exposure.

2. Atmospheric exposures were located in the 80-ft (25-m) lot (beach) at Kure Beach, North Carolina, owned by the LaQue Center for Corrosion Technology. The specimen racks were supported on a framework above the ground at an angle of 30 deg to the ground, facing southeast. As at Steubenville, the strained)i2-in. (0.794-mm) panels were directly exposed to the sun and weather; the unstrained)i-in (3.175-mm) panels were below the strained panels and partly protected from direct exposure. Atmospheric data for Kure Beach are shown in Table 2.

TABLE 1—*Chemical analyses of test panel substrates.*

Element	Metal	
	For Use with All Coatings Except Ceramics	
	6061 T6 Aluminum (analysis), %	
	⅛ in. (3.175 mm)	1/32 in. (0.794 mm)
Magnesium	0.99	0.89
Silicon	0.43	0.47
Copper	0.24	0.27
Chromium	0.19	0.17
	SAE 1010 Steel (analysis), %	
	⅛ in. (3.175 mm)	1/32 in. (0.794 mm)
Manganese	0.34	0.34
Chromium	0.03	0.02
Nickel	0.03	0.01
Silicon	0.03	0.03
Phosphorus	0.008	0.009
Carbon	0.058	0.101
Sulfur	0.016	0.016
	For Use with Ceramic Coatings	
	3003 H14 Aluminum (reported), %	
Manganese	1.0 to 1.5	
Silicon	0.6 max	
Iron	0.7 max	
Copper	0.7 max	
Zinc	0.1 max	
Other elements	0.05 max	
	Zero Carbon Steel (reported), %	
Carbon	0.003 to 0.006	
Manganese	0.5 max	
Phosphorus	0.1 max	
Silicon	0.1 max	
Sulfur	0.1 max	

3. Saltwater immersed exposures were made at Daytona, Florida, at the Battelle Florida Marine Research Facility. The specimen racks were suspended vertically and completely submerged in tidal saltwater. Figure 2 shows a rack being installed in seawater at Daytona, and Fig. 3 shows racks encrusted with marine life after long-term immersion in seawater and then following rough cleaning.

4. Mud burials were also made at the Daytona location. Racks were positioned in depressions made in the sandy bottom using a jet pump, and tide, current, and wave action soon covered the specimens with sandy mud. Data concerning seawater properties and burial conditions are shown in Table 3.

Coatings Evaluated

The coatings installed in 1970 consisted of the 33 sets of specimens listed in Table 4. Seven of the coatings were powder coatings applied by the fluidized-bed process. Vinyl, epoxy, poly-

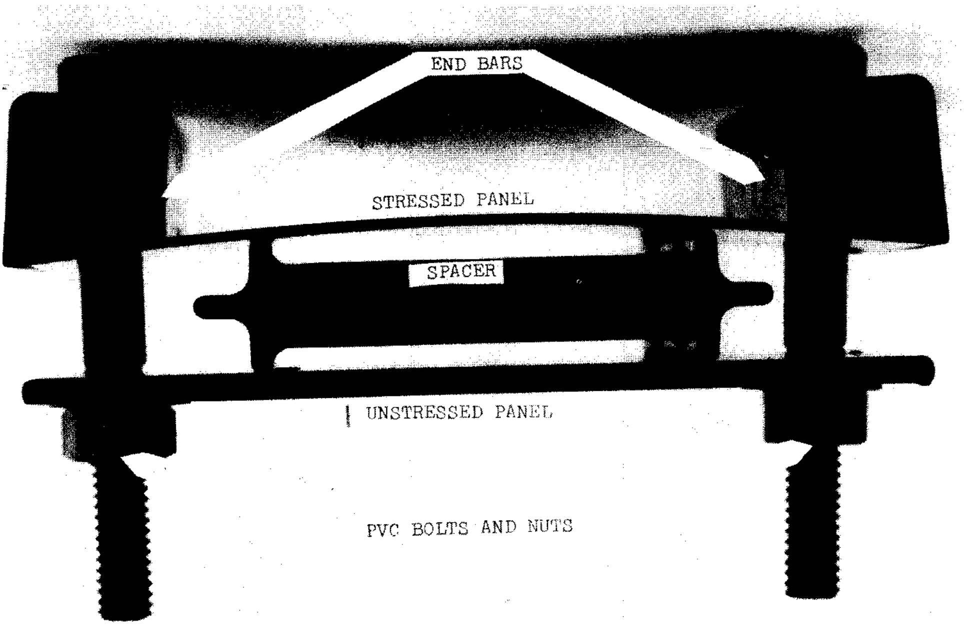

FIG. 1—*Panel assembly showing the strained and unstrained panels.*

ester, nylon, and ethylene-acrylic acid copolymer powder formulations were included. Ethylene-acrylic acid copolymer powder was also applied by electrostatic spray. All were evaluated over alkali-cleaned aluminum and over zinc-phosphated steel. Table 5 lists the original properties of the fluidized-bed powder coatings.

One ceramic composition was evaluated over alkali-cleaned aluminum and is listed in Table 4 as a one coat finish, complete edge coverage. Steel panels were coated with ceramic ground coat only, without and with special attention to edge coverage; ceramic ground coat plus finish coat, without and with special attention to edge coverage; and devitrified glass with complete edge coverage. All of the steel panels were chemically cleaned (pickled) prior to coating.

TABLE 2—*Atmospheric data for the 80-ft (25-m) lot, Kure Beach, North Carolina, circa 1970.*

Parameter	Low	High	Mean
Monthly wetness, days	11.2	29.5	26.6
Avg temp during wetness, °F[b]	42.4	76.7	60.4
Monthly SO_2, mg/dm^2/day	0.00	0.22	0.11
Monthly Cl^-, mg/m^2/day[a]	210	547	398

[a] Average 1970 to 1984.

[b] 42.4°F = 5.8°C,
76.7°F = 24.8°C,
60.4°F = 15.8°C.

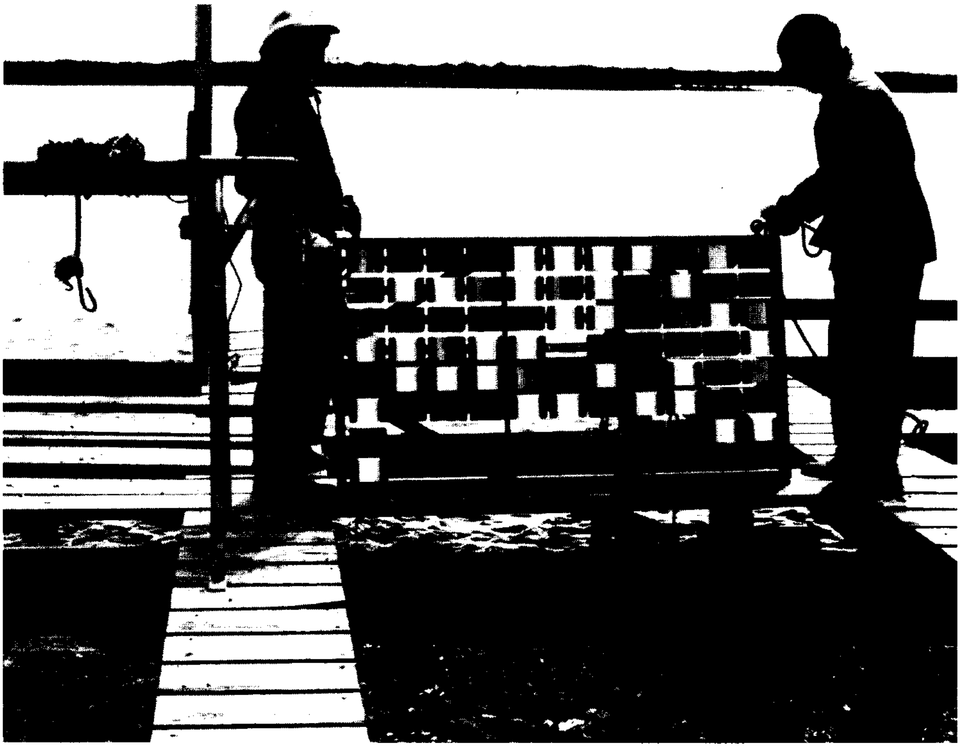

FIG. 2—*A rack of solvent-borne coatings being installed in seawater at Daytona in 1974.*

The remainder of the coatings were metallic, specifically, hot-dipped zinc and hot-dipped aluminum, flame-sprayed zinc, flame-sprayed aluminum, and flame-sprayed zinc-aluminum (67Zn-33Al), without and with vinyl or saran overspray sealers. See Appendix I for information on these sealers. All of the metal coatings were evaluated only over steel.

In 1974 seven organic liquid coatings were sprayed on steel and aluminum panels and added to the program and exposed at the various test sites. These coatings are herein referred to as "solvent coatings" or "solvent-borne coatings" or both. Hot-dipped aluminum on steel panels were also exposed at Kure Beach in 1974 where they had been omitted in 1970. Table 6 lists these coatings. Formulations and application procedures for the solvent coatings are shown in Appendix II.

Condensed Overall Results

The prime purpose of the program was to see if any of the coatings studied would provide protection to the aluminum and steel substrates during exposure to salt air, salt water, salt mud, and an industrial atmosphere high in particulates, dust fall, and sulfur dioxide (SO_2)' Therefore, the specimens were examined at various time intervals for coating blistering, peeling, cracking, unbonding, erosion, and for aluminum corrosion (oxide and pitting), and steel rusting and delamination.

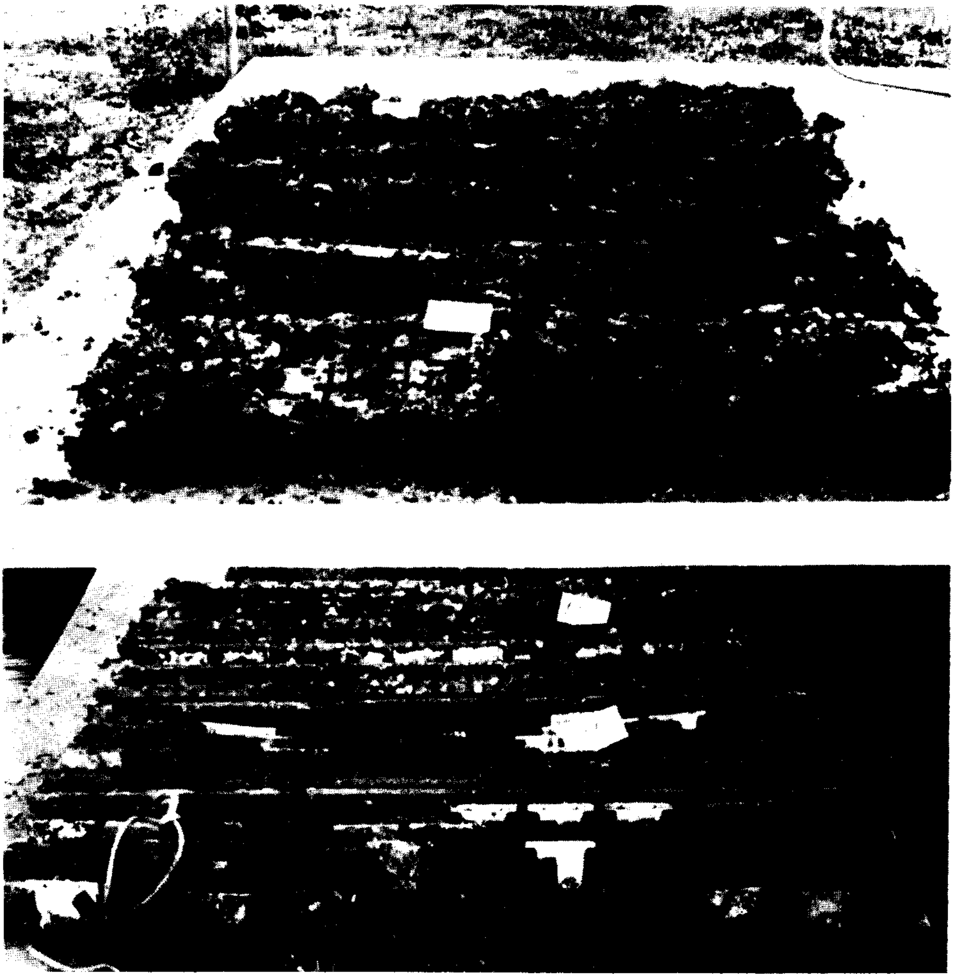

FIG. 3—*Specimen racks after recovery from Daytona seawater, showing marine life buildup,* above, *and following rough cleaning,* below.

TABLE 3—*Seawater properties and burial conditions at Daytona exposure site.*

Marine Water
Salinity 36 ppt
Water temperature 21.9°C, avg
Tidal change 4 ft (1.2 m)
Water depth low tide 8 ft (2.4 m)
Burial depth 2 to 6 in. (50.8 to 152.4 mm)
Bottom sandy mud

TABLE 4-*Coatings installed in 1970.*

Code	Coating	Coating Thickness, mil,mm	Substrate
101	vinyl VCA *1315*[a,b,c]	II (0.279)1	steel
102		12 (0.305)i	aluminum
103	epoxy LC *1506*[a,b,d]	II (0.279)i	steel
104		12 (0.305)1	aluminum
105	epoxy ECA *1283*[a,b]	12 (0.305)i	steel
106		12 (0.305)i	aluminum
109	polyester white *777N*[b,e]	II (0.279)i	steel
110		12 (0.305)i	aluminum
111	vinyl LC 1405 blacka,b,c	II (0.279)i	steel
112		II (0.279)i	aluminum
113	ethylene-acrylic acid copolymerW	...	steel
114		...	aluminum
115	nylon II NCA *na,b,g*	II (0.279)i	steel
116		9 (0.229)i	aluminum
201	ethylene-acrylic acid copolymerf,h,i	...	steel
202		...	aluminum
300	ceramic-one coat finish, complete edge coverage	4 (0.102)i *6 (0.152)k*	aluminum
301	ceramic-ground coat only, no special attention to edges	9 (0.229)i 8 *(0.203t*	steel
303	ceramic-ground coat plus finish coat, standard application	14 (0.356)i *15 (0.381)k*	steel
305	ceramic-ground coat only, complete edge coverage	9 (0.229)i *9 (0.229l*	steel
307	ceramic-devitrified glass coat only, complete edge coverage	15 (0.381)i *12 (0.305t*	steel
309	ceramic-ground coat plus finish coat, complete edge coverage	10 (0.254)i II *(0.279l*	steel
401	hot-dipped zinc	3 (0.076)i	steel
403	hot-dipped aluminum'	3 (0.076)i	steel
405	flame-sprayed aluminum	3 (0.076)i	steel
407	flame.sprayed zinc	3 (0.076)i	steel
409	flame-sprayed zinc plus aluminum-vinyl sealer	8 (0.203)1	steel
411	flame-sprayed zinc plus saran sealer	6 (0.152)1	steel
413	flame-sprayed aluminum plus aluminum-vinyl sealer	8 (0.203)i	steel
415	flame-sprayed aluminum plus saran sealer	5 (0.127)1	steel
417	flame-sprayed 67% zinc-33% aluminum	3 (0.076)1	steel
419	flame-sprayed 67% zinc-33% aluminum plus aluminum vinyl sealer	6 (0.152)i	steel
421	flame-sprayed 67% zinc-33% aluminum plus saran sealer	8 (0.203)1	steel

[a] Polymer Corp., Reading, PA. (now Morton Chemical Div., Morton Thiokol, Inc.).

[b] Coating applied by the fluidized-bed process.

[c] Primed with VCP Primer, Polymer Corp.

[d] Primed with EC Primer, Polymer Corp.

[e] Goodyear Tire and Rubber Co.

fDow Chemical Co. Ethylene-Acrylic Acid Copolymer SD449BK (Colored Black).

[g] Primed with NC Primer, Polymer Corp.

[h] Coating applied by electrostatic spray.

[i] Not installed at Steubenville or Kure Beach; installed in Daytona water and mud.

[j] Coating thickness, measured on %,-in. (0.794-mm) panel.

[k] Coating thickness, measured on)i-in. (3.175-mm) panel.

'Not installed at Kure Beach until 1974; installed at Steubenville and in Daytona water and mud in 1970.

TABLE 5—*Original properties of fluidized-bed powder coatings.*

Code	Coating	Substrate	Coating Thickness,[a] mil	Hardness, ASTM D1474 Pfund, diameter, mm	Elongation, ASTM D522, Conical Mandrel, %
101	vinyl VCA 1315	steel	11 ± 1[b]	10.5 ± 0.2	>30
102	vinyl VCA 1315	aluminum	12 ± 2[c]	10.2 ± 0.3	>30
103	epoxy LC 1506	steel	11 ± 1	3.96 ± 0.08	14 ± 4
104	epoxy LC 1506	aluminum	12 ± 1	3.60 ± 0.12	>30
105	epoxy ECA 1283	steel	12 ± 1	3.48 ± 0.13	breaks off
106	epoxy ECA 1283	aluminum	12 ± 1	3.17 ± 0.21	0
109	polyester 777N	steel	11 ± 1	3.83 ± 0.10	0
110	polyester 777N	aluminum	12 ± 1	3.98 ± 0.16	0->30
111	vinyl LC 1405	steel	11 ± 1	13.7 ± 0.6	>30
112	vinyl LC 1405	aluminum	11 ± 1	too soft	>30
115	nylon NCA 77	steel	11 ± 1	4.72 ± 0.31	11 ± 2
116	nylon NCA 77	aluminum	9 ± 1[d]	4.64 ± 0.22	>30

[a] Half the difference between the overall thickness, as measured with a micrometer, and the average substrate thickness (steel –0.032 in.; aluminum –0.031 in.).

[b] 0.279 ± 0.025 mm.

[c] 0.305 ± 0.051 mm.

[d] 0.229 ± 0.025 mm.

Fluidized-Bed Powder Coatings at Steubenville

After thirteen years all of the powder coatings were intact and no rusting of the steel or oxidation of the aluminum was evident. The upper surfaces of all the coatings on the li2-in. (0.794-mm) panels were dull and rough (eroded); the bottom surfaces were smooth, and wiping restored the gloss. The epoxies were chalked within one year.

Ceramic Coatings at Steubenville

After thirteen years the ceramic coatings on steel panels were intact and no rusting of the steel was evident-with one exception, in which the ground coat only with no special attention given edges (301)[2] was used, and resulted in edge rusting on one out of four %-in.(3.175-mm) panels. The upper surfaces of the li2-in. (0.794-mm) ceramic-coated aluminum panels were faded from their original deep blue and severely eroded, but the aluminum was not exposed.

Metallic Coatings at Steubenville

After thirteen years metallic coatings on steel panels were intact, and no rusting of the steel was evident with two exceptions. Hot-dipped zinc on steel (401) resulted in heavy rusting of the Ys2-in(0.794-mm) panels; the %-in. (3.175-mm) panels were not rusted. Flame-sprayed

---

[2] Number in parentheses is code designation in tables.

TABLE 6—*Coatings installed in 1974.*

Code	Coating[a]	Coating Thickness, mil[b]	Substrate
001	none	0	steel
002	none	0	aluminum
003	epoxy-polyamine	5[d]	steel
004		5	aluminum
005	coal tar-epoxy	17[e]	steel
006		17	aluminum
007	zinc-rich organic primer plus epoxy-polyamine	5	steel
008		5	aluminum
009	zinc-rich inorganic-silicate primer plus epoxy-polyamine	5	steel
010		5	aluminum
011	epoxy-polyamide	5	steel
012		5	aluminum
017	vinyl	5	steel
018		5	aluminum
023	chlorinated rubber	. . .	steel
024		3 to 4[f]	aluminum
403	hot-dipped aluminum[c]	2.7[g]	steel

[a] All except 403 are organic solvent-borne coatings. See Appendix II for formulations.
[b] Coating thickness as stipulated in Appendix II. Exceptions: 024 and 403 measured.
[c] Installed at Kure Beach in 1974; installed at other locations in 1970.
[d] 0.127 mm.
[e] 0.432 mm.
[f] 0.076 to 0.102 mm.
[g] 0.069 mm.

zinc on steel (407) resulted in rust spotting of the upper surfaces of the ~2-in. (0.794-mm) panels; the Xl-in.(3.175-mm) panels were not rusted.

Solvent Coatings at Steubenville

After ten years the solvent coatings exposed in 1974 were intact, and no rusting of the steel or oxidation of the aluminum was evident. All coatings chalked except the vinyl and chlorinated rubber. Heavy rust was present on the uncoated steel panels; the uncoated aluminum panel appearance was good.

Kure Beach

It is important to note that beach-exposed specimens were subject to sand erosion as well as moist salt air. During the years from 1970 through 1984 a number of severe storms passed through or near the exposure site. The most recent one, Hurricane Diana, passed over this area on 12 and 13 Sept. 1984 at 110 miles per hour, with gusts to 135. Examination of panels subsequent to the hurricane showed severe sand erosion on the upper surfaces facing southeast and relatively little erosion on the under leeward surfaces. Figure 4 shows the appearance change due to sand erosion of a chlorinated rubber coating on a steel panel after eleven years exposure at Kure Beach, where the original light gray color has changed to a darker gray in areas where sand erosion occurred.

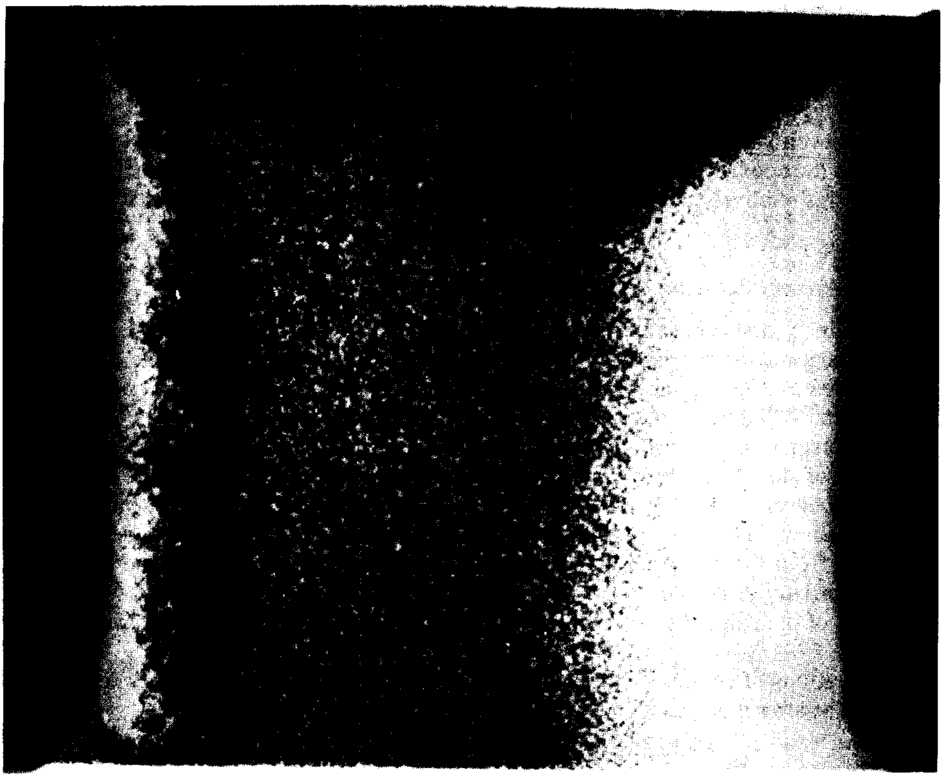

FIG. *4-Appearance change due to sand erosion of a chlorinated rubber coating on a steel panel after* 11 *years' exposure at Kure Beach. The original light gray color has changed to a darker gray in areas where sand erosion has occurred.*

Fluidized-Bed Powder Coatings at Kure Beach

After one year the fluidized-bed powder coatings showed surface appearance changes attributed to chalking, color fading, loss of gloss, sand erosion, and salt effects, none of which caused coating failure so as to expose metal, with one exception-the %-in. (3.175-mm) panels coated with vinyl LC 1405 (111) showed several rust spots.

The next observations on fluidized-bed specimens at Kure Beach were made after nine years exposure and revealed that except for the ethylene-acrylic acid copolymer (113), all of the coatings on steel panels had failed so that the steel panels were severely rusted and delaminated. The ethylene-acrylic acid copolymer-coated panels appeared good all over except at the tab on one side where steel delamination had occurred. The tabs were metal projections about ~-in. (12.7-mm) square on one edge of each panel and were used for suspending these panels during the coating operation. If not adequately "touched-up," these tabs are the location for moisture ingress and corrosion. On the aluminum panels the coatings remained intact after nine years except for epoxy ECA 1283 (106) which exhibited peeling, epoxy LC 1506 (104) which blistered, and ethylene-acrylic acid copolymer (114) which blistered only at the tab. The aluminum, in all cases where visible, retained a good appearance.

After eleven years the \i2-in. (0.794-mm) steel panels coated with ethylene-acrylic acid copolymer (113) were blistered, but the steel was not rusted. The coatings on the %-in.(3.175-mm) steel panels had separated at the tab edge with resultant steel delamination in the tab area. All other steel panels were badly rusted and delaminated as they were after nine years.

After eleven years observations on coated aluminum panels showed that vinyl LC 1405 (112) and the epoxies LC 1506 (104) and ECA 1283 (106) had peeled, but the aluminum in all cases was relatively unaffected and still mechanically strong (Table 7).

Ceramic Coatings at Kure Beach

After nine years' exposure at Kure Beach all of the ceramic-coated steel panels exhibited edge rusting. Paying special attention during preparation to obtain complete edge coverage still resulted in edge rusting. With a ground coat only, the %2-in.(0.794-mm) panels had rust spots [\\\6 in. (4.762 mm) diameter]. The use of a finish coat over the ground coat eliminated the spot rusting on the thin panels. After modest surface wiping with a rag there was only a slight loss of gloss from the original. The only aluminum panels exposed were coated with a single coat of ceramic and treated to obtain complete edge coverage (300). The upper surfaces on the %2-in.(0.794-mm) ceramic-coated aluminum panels were severely eroded and discolored gray from their original blue, but the aluminum was not exposed. The bottom thick panels, partially protected by the upper thin panels from the sun and sand, were still blue over 50% of their upper surfaces; the remaining 50% of their upper surfaces was discolored gray.

Observations of ceramic-coated panels after eleven years at Kure Beach were essentially the same as after nine years.

Metallic Coatings at Kure Beach

After one year exposure at Kure Beach all of the metallic coatings on steel panels prevented rusting of the substrate steel with the exception of the flame-sprayed 67Zn-33Al panels (417) which had minor rusting in one of ten drilled mounting holes in the thin panels, and the hot-dipped zinc on steel panels (401) which had rust spotting on both the thin and the thick panels. The saran sealer and the aluminum-vinyl sealers had small interior bubbles on some of the panels.

After nine years' exposure no rusting occurred on any of the coated steel panels except for the hot-dipped and flame-sprayed zinc on steel panels (401, 407) where both the thin and thick panels had rust spots.

After eleven years' exposure the hot-dipped zinc (401) and the flame-sprayed zinc (407) steel panels again showed rust spotting of thin and thick panels. Some edge rust spots developed on the flame-sprayed zinc coated with the saran sealer (411). The flame sprayed 67Zn-33Al (417) exhibited pinpoint rust spots on thin and thick panels. The use of either the aluminum-vinyl sealer or the saran sealer over the 67Zn-33Al coating (419,421) prevented rust spotting. A I%-in.(38-mm) diameter rust spot developed on one out of five %-in.(3.175-mm) steel panels flame-sprayed with aluminum (405).

Free of rust after eleven years of sun, salt, and sand were the hot-dipped aluminum (403), the flame-sprayed zinc with the aluminum-vinyl sealer (409), the flame-sprayed aluminum with the aluminum-vinyl sealer (413), and with the saran sealer (415), and the 67Zn-33Al flame-sprayed coating with either one of the sealers (419, 421). Table 8 contains the Kure Beach metallic coatings data.

TABLE 7—*Powder coatings exposed at Kure Beach.*

Code[a]	Coating	Panel Thickness, in.	11 Years' Exposure Panel Appearance: Steel Panels	11 Years' Exposure Panel Appearance: Al Panels
101 102	vinyl VCA 1315	1/32[j] and 1/8[k]	blistered, rusted, delaminated[d]	coating[c] intact
103 104	epoxy LC 1506	1/32	rusted, delaminated[f]	coating[h] peeled, Al good
		1/8	rusted, delaminated[d]	coating[c] separated at edges, Al good
105 106	epoxy ECA 1283	1/32	rusted, delaminated[d]	coating[i] peeled, Al good
		1/8	rusted, delaminated[d]	coating[c] separated at edges, Al good
109 110	polyester 777N	1/32 and 1/8	blistered, rusted, delaminated[d]	coating[c] intact
111 112	vinyl LC 1405	1/32	not available[d]	coating[c] 50% peeled on top, bottom surface smooth and glossy, Al good
		1/8	not available[b,d]	coating[c] intact
113 114	ethylene-acrylic acid copolymer	1/32	coating blistered, no rust[e]	coating[c] intact
		1/8	coating separated and steel rusted and delaminated at tab[e]	coating[g] intact
115 116	nylon 11 NCA 77	1/32 and 1/8	rusted, delaminated[d]	coating[c] intact

[a] Odd numbers on steel, even numbers on aluminum.
[b] After one year 1/8-in. (3.175-mm) panels had rust spots; all other coated steel panels were rust-free.
[c] Coating intact after nine years.
[d] Rusted, delaminated after nine years.
[e] Rusted, delaminated at tab after nine years.
[f] Rusted after nine years.
[g] Blistered at tab after nine years.
[h] Blistered after nine years.
[i] Peeled after nine years.
[j] 0.794 mm.
[k] 3.175 mm.

Solvent Coatings at Kure Beach

After five and seven years the uncoated steel panels were rusted out, and the uncoated aluminum panels had minor corrosion or sand erosion or both but were structurally sound. All of the coatings on steel panels were intact and none of the coated panels were rusted with the exception of the panels coated with zinc-rich organic primer topcoated with epoxy-polyamine (007), in which case the coatings had blistered and broken so that the steel was rusted and delaminated. Figure 5 is a photograph showing one of these rusted panels after seven years at Kure Beach compared to a steel panel coated with zinc-rich inorganic-silicate primer topcoated with epoxy polyamine, which is rust-free. Aluminum panels with these two coating systems were not recovered at Kure Beach.

TABLE 8—*Metallic coatings on steel exposed at Kure Beach.*

Code	Coating	Panel Thickness, in.	1 Year Exposure Panel Appearance	9 Years' Exposure Panel Appearance	11 Years' Exposure Panel Appearance
401	hot-dipped Zn	1/32[b] and 1/8[c]	rust spots	numerous rust spots	numerous rust spots
403	hot-dipped Al	1/32 and 1/8	not available[a]	not available now but no rust after 5 years exposure	no rust
405	flame-sprayed Al	1/32 and 1/8	no rust	no rust	no rust
			no rust	no rust	one 1½-in. (38-mm) dia rust spot on 1 out of 5 panels
407	flame-sprayed Zn	1/32 and 1/8	no rust	scattered rust spots	scattered rust spots
409	flame-sprayed Zn plus Al-vinyl sealer	1/32 and 1/8	no rust	sealer blistered, white corrosion, no rust	coating surface very rough, white corrosion, no rust
411	flame-sprayed Zn plus saran sealer	1/32	top surfaces dull, no rust	no rust	coating surface rough, some rust spots at one edge
		1/8	small bubbles in sealer, no rust	no rust	some coating blisters, no white corrosion, some rust spots at one edge
413	flame-sprayed Al plus Al-vinyl sealer	1/32 and 1/8	no rust	no rust	no rust
415	flame-sprayed Al plus saran sealer	1/32 and 1/8	no rust	no rust	some blisters in sealer, no rust
417	flame-sprayed 67Zn-33Al	1/32	rust in 1 of 10 drilled holes	no rust	pinpoint rust spots
		1/8	no rust	no rust	pinpoint rust spots
419	flame-sprayed 67Zn-33Al plus Al-vinyl sealer	1/32 and 1/8	small bubbles in sealer, no rust	no rust	no rust
421	flame-sprayed 67Zn-33Al plus saran sealer	1/32 and 1/8	no rust	no rust	no rust

[a] Hot-dipped Al (403) not exposed in Kure Beach until 1974.
[b] 0.794 mm.
[c] 3.175 mm.

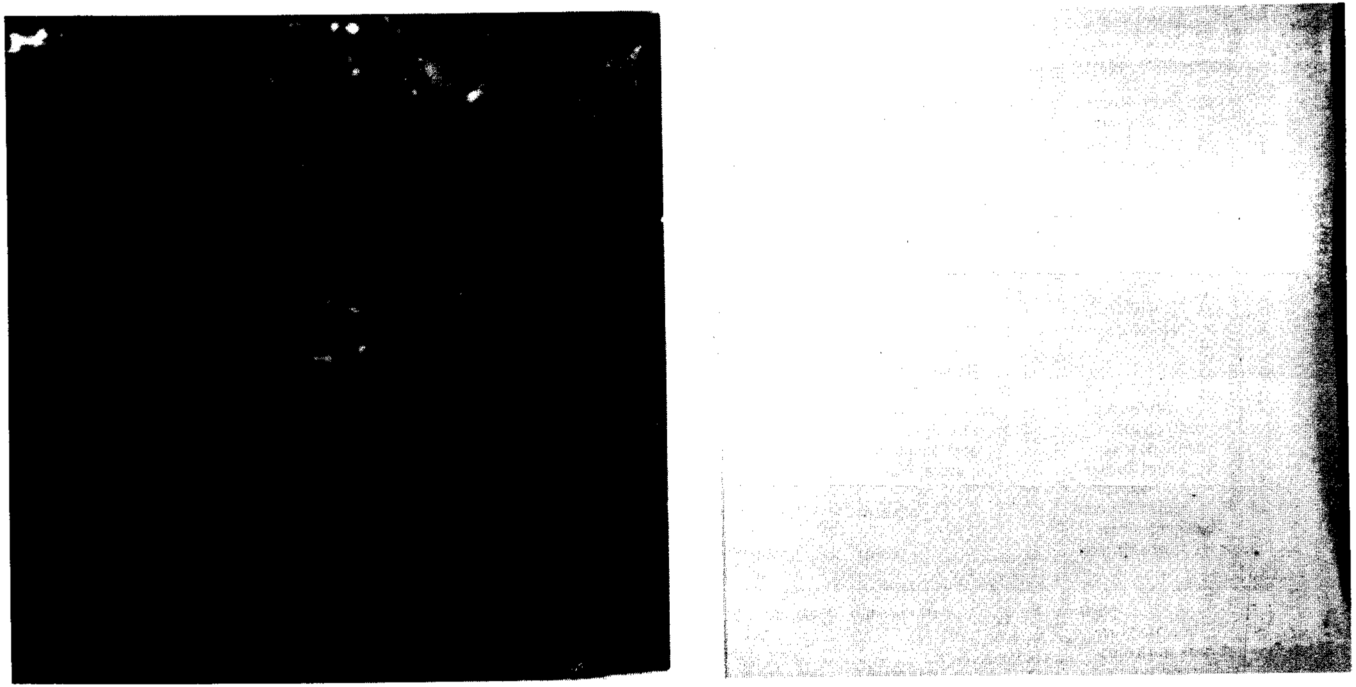

FIG. 5—*Steel panels coated with a zinc-rich organic primer on the left and a zinc-rich inorganic-silicate primer on the right, both topcoated with epoxy-polyamine, after 7 years' exposure at Kure Beach.*

TABLE 9—*Solvent coatings exposed at Kure Beach.*

Code[a]	Coating	Panel Thickness, in.	5 and 7 Years' Exposure[b] Panel Appearance		11 Years' Exposure Panel Appearance	
			Steel Panels	Al Panels	Steel Panels	Al Panels
001 002	none	1/32[c]	rusted out	minor corrosion and/or sand erosion	rusted out	upper surface minor corrosion and/or sand erosion
		1/8[d]	rusted out	minor corrosion and/or sand erosion	rusted out	good
003 004	epoxy-polyamine	1/32	coating intact, chalked, no rust	coating intact, chalked	rusted	coating upper surface badly chalked
		1/8	coating intact, chalked, no rust	coating intact, chalked	rusted	coating intact, chalked
005 006	coat tar-epoxy	1/32 and 1/8	coating intact, chalked, no rust	coating intact, chalked	coating intact, chalked, gloss partially restored by wiping, no rust	coating intact, chalked, gloss partially restored by wiping
007 008	Zn-rich organic primer plus epoxy-polyamine	1/32 and 1/8	coating blistered and broken, steel rusted and delaminatd	not available	coating blistered, steel rusted and delaminated	not available
009 010	Zn-rich inorganic-silicate primer plus epoxy-polyamine	1/32 and 1/8	coating intact, chalked, no rust	not available	coating chalked and/or sand-eroded on top, steel rusted and delaminated at edges	not available
011 012	epoxy-polyamide	1/32	coating intact, chalked, no rust	coating intact, chalked	coating chalked and/or sand-eroded, no rust	coating upper surface chalked and/or sand-eroded
		1/8	coating intact, chalked, no rust	coating intact, chalked	coating intact, chalked, no rust	coating intact, chalked
017 018	vinyl	1/32 and 1/8	coating intact, no rust	coating intact	coating intact, no rust	coating intact
023 024	chlorinated rubber	1/32	coating intact, no rust	coating intact	coating sand eroded, no rust	coating sand-eroded
		1/8	coating intact, no rust	coating intact	coating intact, no rust	coating intact

[a] Odd numbers on steel, even numbers on aluminum.

[b] Same appearance after five and after seven years' exposure.

[c] 0.794 mm.

[d] 3.175 mm.

After eleven years' exposure at Kure Beach the effects of sand erosion were plainly evident on many of the coatings. The survivors included the coal tar-epoxy (005, 006), the epoxy-polyamide (011, 012), the vinyl (017, 018), and the chlorinated rubber coatings (023, 024). These coatings were intact so that no rusting of the steel panels or corrosion of the aluminum panels had occurred. The gloss of the coal tar-epoxy was partially restored by rag wiping (Table 9). Figure 6 is a photograph of an uncoated aluminum panel after eleven years exposure at Kure Beach. It had developed a very fine surface texture as a result of minor corrosion or sand erosion or both.

Daytona Seawater

Most seawater specimens rapidly build up firmly attached sea life which prevents or delays coating deterioration at the attachment. Water ingress and coating deterioration usually begin at the panel edges and then spread along the panel faces. Figure 7 shows the buildup of marine life during two years of Daytona seawater immersion.

Fluidized-Bed Powder Coatings in Daytona Seawater

After six years in seawater all fluidized-bed powder-coated steel panels exhibited edge rusting. Vinyl VCA 1315 (101), epoxy LC 1506 (103), epoxy ECA 1283 (105), and nylon NCA

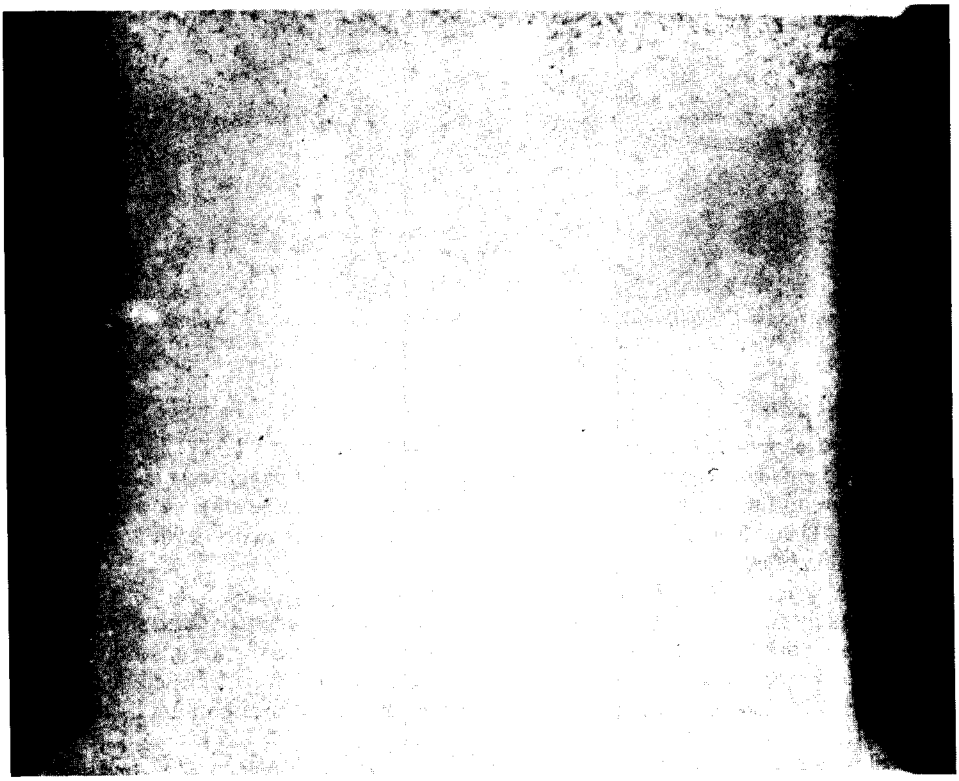

FIG. 6—*Uncoated 6061 T6 aluminum after 11 years' exposure at Kure Beach. The surface has a very fine texture as a result of minor corrosion or sand erosion or both.*

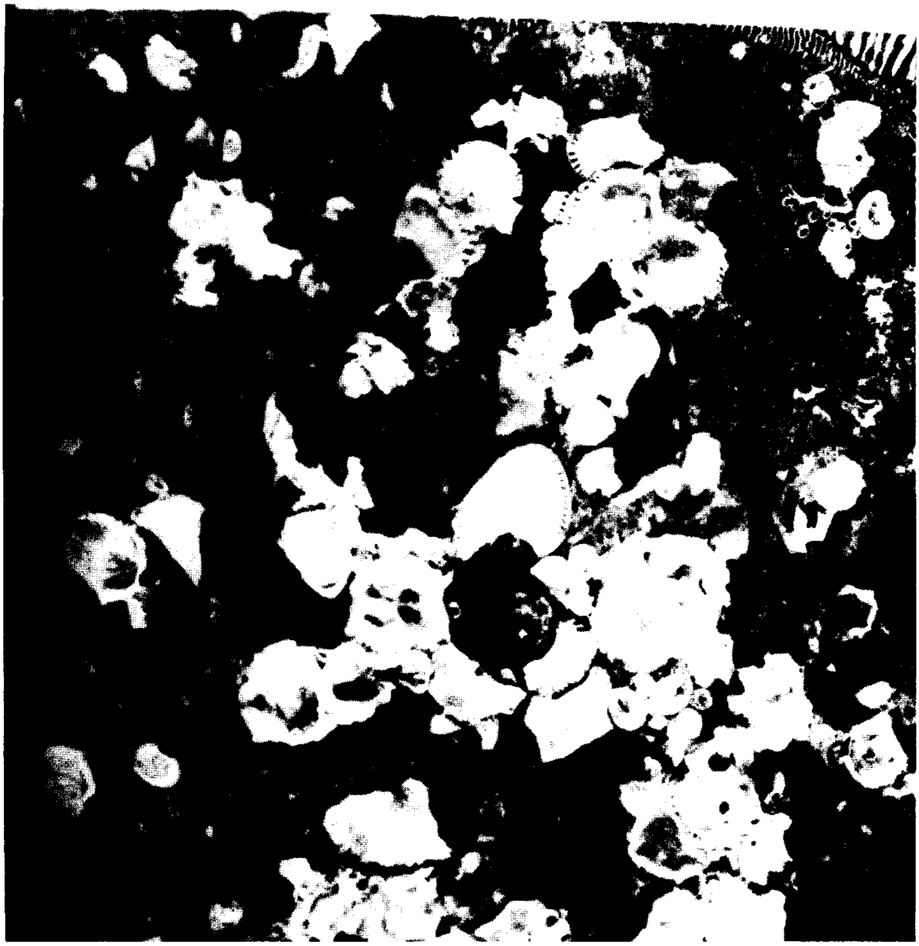

FIG. 7—*Marine life buildup on a coated panel during two years of Daytona seawater immersion.*

77 (115) coated panels had minimum edge rusting while polyester 777N (109), vinyl LC 1405 (111), and ethylene-acrylic acid copolymer (113, 201[3]) coated panels were badly rusted. All of the aluminum panels were mechanically sound even though the ethylene-acrylic acid copolymer (114) had blistered, and the nylon NCA 77 (116) and ethylene-acrylic acid copolymer (202[3]) had peeled.

After twelve years none of the fluidized-bed coatings were recovered. Some of the steel panels most likely rusted out, and the specimen assemblies disintegrated. Others may have been lost because of rack failure. Marine growth constantly increased the weight of the racks, and they had to be rebuilt at one time. Also, the coated aluminum panel assemblies were not recovered and must have been lost, also due to rack failure, as the aluminum used main-

---

[3] 201 and 202 were applied by the electrostatic spray process.

tains sufficient mechanical integrity in saltwater in twelve years so that the specimen assemblies would not have disintegrated.

Ceramic Coatings in Daytona Seawater

After six years' immersion in Daytona seawater all ceramic-coated steel panels showed edge rusting. White corrosion and pit corrosion were evident on the 3003 H 14 aluminum panels.

After twelve years all coated steel panels showed edge rusting which had spread inwards on the panel faces during the 6 to 12 year interval. The panel centers were free of rust.

Metallic Coatings in Daytona Seawater

After six years in Daytona seawater flame-sprayed zinc with the saran sealer (411), flame-sprayed aluminum without and with either the aluminum-vinyl or saran sealers (405, 413, 415), and flame-sprayed 67Zn-33Al without and with either sealer (417,419,421) remained intact and protected the steel panels from rusting (Table 10). Figure 8 is a photograph comparing the rusted hot-dipped aluminized steel to the nonrusted flame-sprayed aluminum on steel after six years immersion in Daytona seawater.

After twelve years flame-sprayed aluminum with saran sealer (415), and flame-sprayed

TABLE 10—*Metallic coatings on steel exposed at Daytona in seawater.*

Code	Coating	Panel Thickness, in.	6 Years' Exposure Panel Appearance	12 Years' Exposure Panel Appearance
401	hot-dipped Zn	1/32[a]	rusted out	not available
		1/8[b]	badly rusted	not available
403	hot-dipped Al	1/32	badly rusted	not available
		1/8	very minor rusting	not available
405	flame-sprayed Al	1/32 and 1/8	no rust	rust spots
407	flame-sprayed Zn	1/32	badly rusted	not available
		1/8	spot and edge rusting	not available
409	flame-sprayed Zn plus Al vinyl sealer	1/32	badly rusted	not available
		1/8	spot and edge rusting	not available
411	flame-sprayed Zn plus saran sealer	1/32 and 1/8	no rust	spot and edge rusting
413	flame-sprayed Al plus Al vinyl sealer	1/32 and 1/8	no rust	a few rust spots on 2 out of 10 panels
415	flame-sprayed Al plus saran sealer	1/32 and 1/8	no rust	no rust
417	flame-sprayed 67Zn-33Al	1/32 and 1/8	no rust	no rust
419	flame-sprayed 67Zn-33Al plus Al vinyl sealer	1/32 and 1/8	no rust	no rust
421	flame-sprayed 67Zn-33Al plus saran sealer	1/32 and 1/8	no rust	no rust

NOTE: Most water-immersed specimens covered with marine growth.

[a] 0.794 mm.

[b] 3.175 mm.

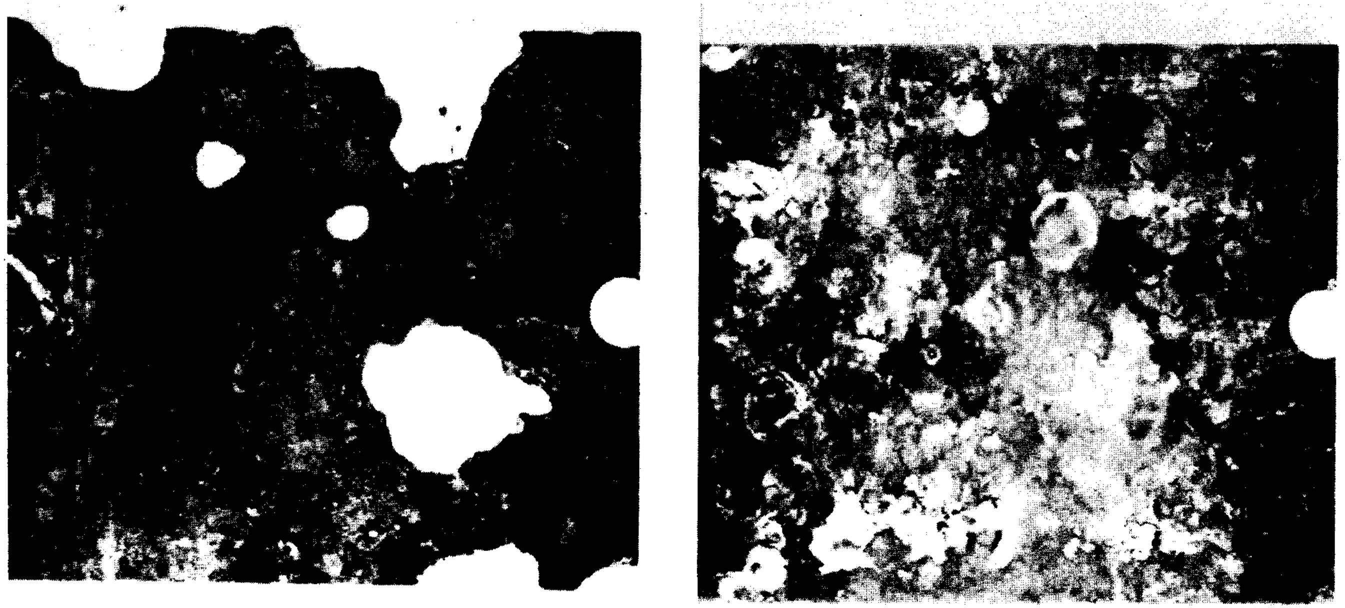

FIG. 8—*Hot-dipped aluminum on steel,* on the left, *compared to flame-sprayed aluminum on steel,* on the right, *after 6 years' exposure in Daytona seawater. The hot-dipped panel is badly rusted; the flame-sprayed panel is rust free.*

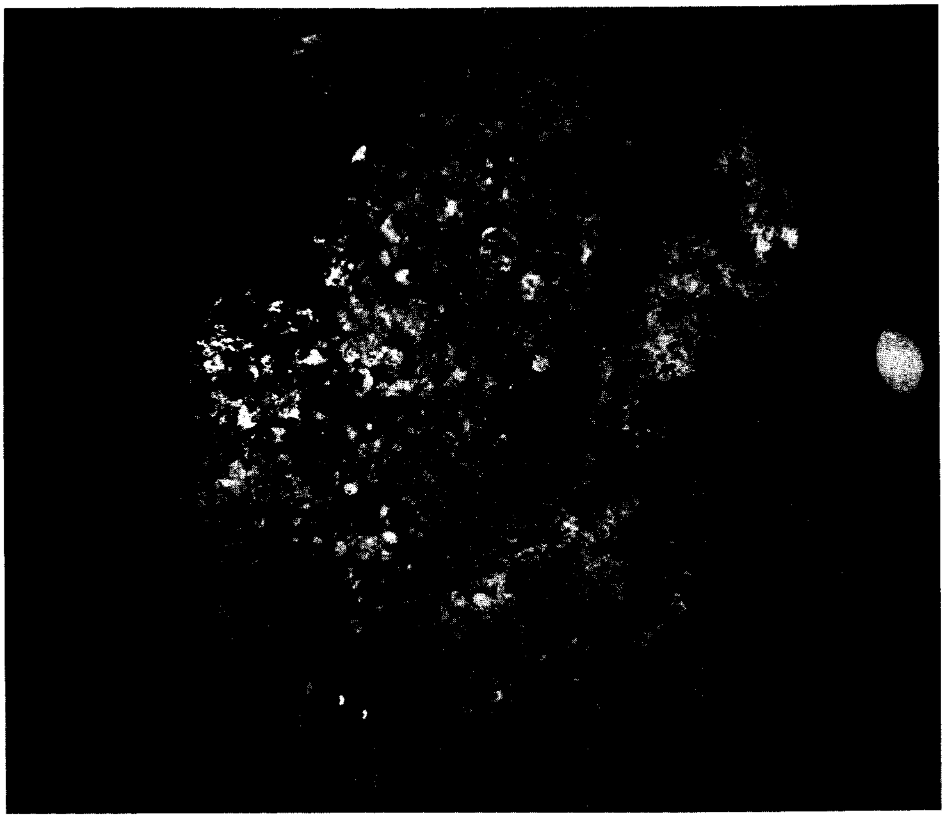

FIG. 9—*This flame-sprayed 67Zn-33Al on steel panel is covered with marine life but rust free after 12 years in Daytona seawater.*

67Zn-33Al without and with either sealer (417,419,421) on steel panels remained intact and prevented rusting (see Table 10). Figure 9 is a photograph of flame-sprayed 67Zn-33AI on a steel panel after twleve years in Daytona seawater. It is covered with marine life but free of rust.

Solvent Coatings in Daytona Seawater

In two years the uncoated steel panels were severely rusted and delaminated. All of the solvent coatings on steel performed poorly in Daytona seawater in only two years. All coated steel panels blistered and peeled in varying degrees. The steel panels coated with zinc-rich inorganic-silicate primer topcoated with epoxy-polyamine (009) and the steel panels coated with epoxy-polyamide (0 II) exhibited spot and edge rusting; the others were more extensively rusted.

After two years, the coatings on the aluminum panels remained intact, and there were no indications that the aluminum had been adversely affected. Even the uncoated aluminum panels retained a good appearance.

After eight years in Daytona seawater all of the %2-in.(0.794-mm) steel panels were rusted out; the %-in. (3.175-mm) steel panels coated with coal tar-epoxy (005) were rusted only at the edges. The %-in. (3.175-mm) steel panels coated with zinc-rich inorganic-silicate primer topcoated with epoxy-polyamine (009) and the %-in. (3.175-mm) steel panels coated with epoxy-polyamide (Oil) showed edge and spot rusting. The other coated %-in. (3.175-mm) steel panels were rusted out.

After eight years in Daytona seawater the coatings on the li2-in. (0.794-mm) and %-in. (3.175-mm) aluminum panels remained intact, and there were no indications that the aluminum had been adversely affected. As after two years, even the uncoated aluminum retained a good appearance. The aluminum panels with the zinc-rich primers topcoated with epoxy-polyamine (008, 0 I0), were not available for two or eight year observations.

Daytona Mud

Many specimens buried in the mud and sand at Daytona must at times during their exposure have been uncovered and exposed directly to saltwater, as marine life which built up on some of them appeared similar to that which built up on similar specimens suspended in saltwater. Thus, the specimens may have been subjected to variable exposure conditions depending on what percentage of the time they may have been buried in mud or exposed to water. Some of the specimens were not recovered and may have washed away.

Fluidized-Bed Powder Coatings in Daytona Mud

After twelve years epoxy ECA 1283 (105) coating on both li2-in. (0.794-mm) and %-in. (3.175-mm) steel panels was still intact, and no rust was visible. Steel panels with three other coatings showed minor edge rusting, namely, vinyl VCA 1315 (101), nylon NCA 77 (l15), and ethylene-acrylic acid copolymer (201) applied by electrostatic spray.

After twelve years the aluminum panels retained good appearance even where the coating was blistered or broken at the panel edges.

Not recovered were the polyester (109, 110), the epoxy LC-1506 (103), the vinyl LC-1405 (III, 112), the epoxy ECA 1283 (106), the nylon NCA 77 (116), and the ethylene-acrylic acid copolymer applied by electrostatic spray (202) coated steel and aluminum panels.

Ceramic Coatings in Daytona Mud

After twelve years of Daytona mud exposure only three of the six originally placed ceramic coating systems were recovered, and two of these exhibited severe edge rusting, namely, the system with the ground coat only and complete edge coverage (305), and the system with the ground coat plus finish coat, standard application (303). The third one, devitrified glass with complete edge coverage (307), exhibited less edge rusting than the other two and retained much of its original gloss so that marine life was sparse on the flat surfaces.

Metallic Coatings in Daytona Mud

After twelve years in Daytona mud only five of the original eleven coating types were recovered. Those lost were hot-dipped zinc (401), hot-dipped aluminum (403), flame-sprayed aluminum (405), flame-sprayed zinc (407), and flame-sprayed 67Zn-33Al (421). Of those recovered only the flame-sprayed 67Zn-33Al with the aluminum-vinyl sealer (419) remained free of rust. The flame-sprayed zinc plus the saran sealer (411) developed slight edge rusting on one out of ten panels.

Solvent Coatings in Daytona Mud

In two years the)i,-in. (0.794-mm) uncoated steel panels were completely rusted out; the \i-in. (3.175-mm) uncoated panels were rusted and delaminated. The uncoated aluminum panels appeared unaffected. The)i,-in. (0.794-mm) steel panels coated with epoxy-polyamine (003) exhibited heavy rusting but the coatings on the \i-in. (3.175-mm) steel panels were intact and the steel was not rusted. The coal tar-epoxy (005) on the)i,-in. (0.794-mm) and \i-in. (3.175-mm) steel panels remained intact and prevented the steel from rusting. Steel panels coated with zinc-rich inorganic-silicate primer topcoated with epoxy-polyamine (009) developed blistering and minor edge rusting on thin and thick panels, and several rust spots on the thick panels. The vinyl (017) peeled and rust developed on two out of ten panels. All other coated steel panels blistered and peeled, and rusted in the peeled areas.

In two years the coatings on the aluminum panels were intact and the substrate aluminum panels were apparently unaffected.

After eight years burial in Daytona mud, the best appearing steel panels were those coated with the zinc-rich inorganic-silicate primer topcoated with epoxy-polyamine (009), where edge rusting had occurred but where the panel interior surfaces showed no rusting.

Two out of four)i,-in. (0.794-mm) uncoated aluminum panels exhibited edge corrosion or sand erosion or both after eight years of mud exposure (Fig. 10, upper right edge of right panel). The companion \i-in. (3.l75-mm) aluminum panels developed no obvious edge changes. These, along with the uncoated aluminum panels at Kure Beach, were the only 6061 T6 aluminum panels of the hundreds in all the various exposures where an effect was readily apparent. It is possible that the edge effect was due to mechanical wear caused by shifting sand and mud. On the left of Fig. 10 is an uncoated aluminum panel after eight years of saltwater exposure. None of the ten uncoated panels exposed developed obvious edge or face corrosion. In all cases where coated aluminum panels were recovered the coatings were intact and the aluminum was apparently unaffected.

Discussion

As described in the specimens section of this report, a)i,-in. (0.794-mm) panel was bent in an arrangement with a \i-in. (3.1 75-mm) panel and a plastic spacer and plastic end-bars, and this assembly was bolted together (see Fig. I). The)i,-in. (0.794-mm) panel and the coating on it were strained by this arrangement. The thicker \i-in. (3.175-mm) panel was stiff enough to resist bending, and thus, the unstrained coating on the \i-in. (3. 175-mm) panel could be compared to the strained coating on the)i,-in. (0.794-mm) panel. As one can understand by reading the foregoing and observing Fig. I, specimen preparation became complex. During atmospheric exposure at Steubenville and at Kure Beach, the specimen assemblies were exposed with the)i,-in. (0.794-mm) panel on top directly exposed to the sun, while the \i-in. (3.175-mm) panel was below and partly shielded from the sun by the)i,-in. (0.794-mm) panel. It was observed that sun did get to the lower panel along the two unobstructed edges, but it did not shine directly on the center of the lower panel except, perhaps, when the sun was close to the horizon when its effectiveness was at its lowest. Thus, additional flat, unstrained panels should have been directly exposed to the sun for a better comparison of unstrained to strained panels. With the exposure arrangement used, no differences were observed between the coatings on the)i,-in. (0.794-mm) strained panels and the coatings on the unstrained \i-in. (3.175-mm) panels that can be ascribed to strain. It might be that the strain was insufficient to show an effect. The applied strain was kept below that which would permanently bend the)i,-in. (0.794-mm) steel and aluminum panels. Also, the original stress

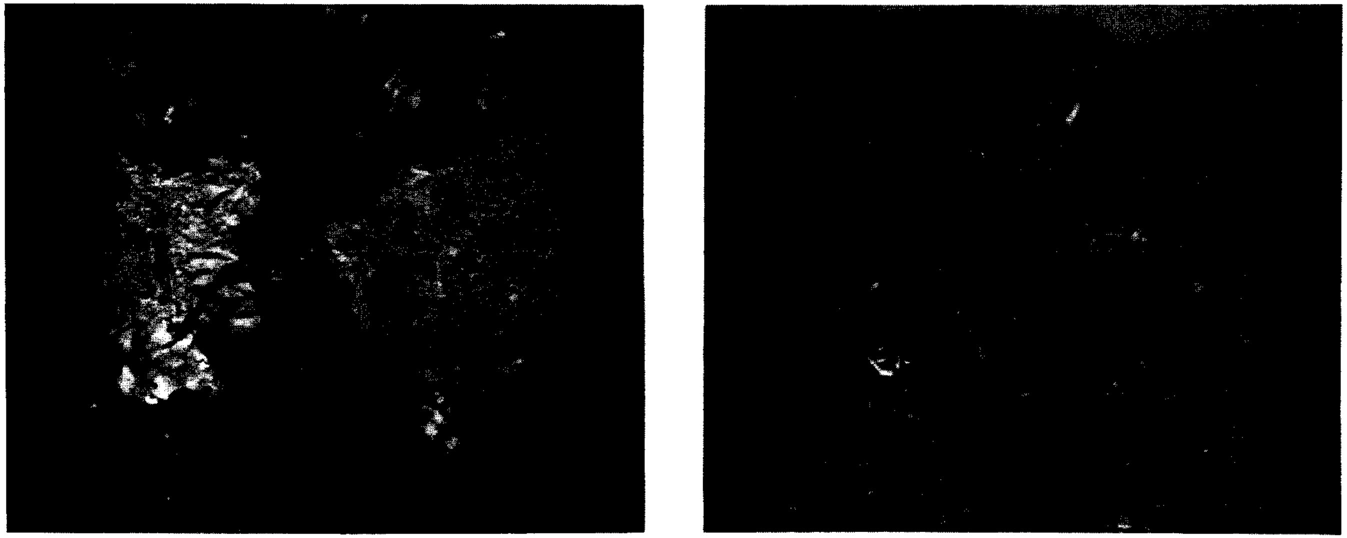

FIG. 10—*The uncoated aluminum panel on the right exhibits edge corrosion or sand erosion or both on its upper right edge after 8 years of Daytona mud exposure. The uncoated aluminum panel on the left after eight years of Daytona saltwater exposure developed no obvious edge or face corrosion. The surfaces are coated with marine life.*

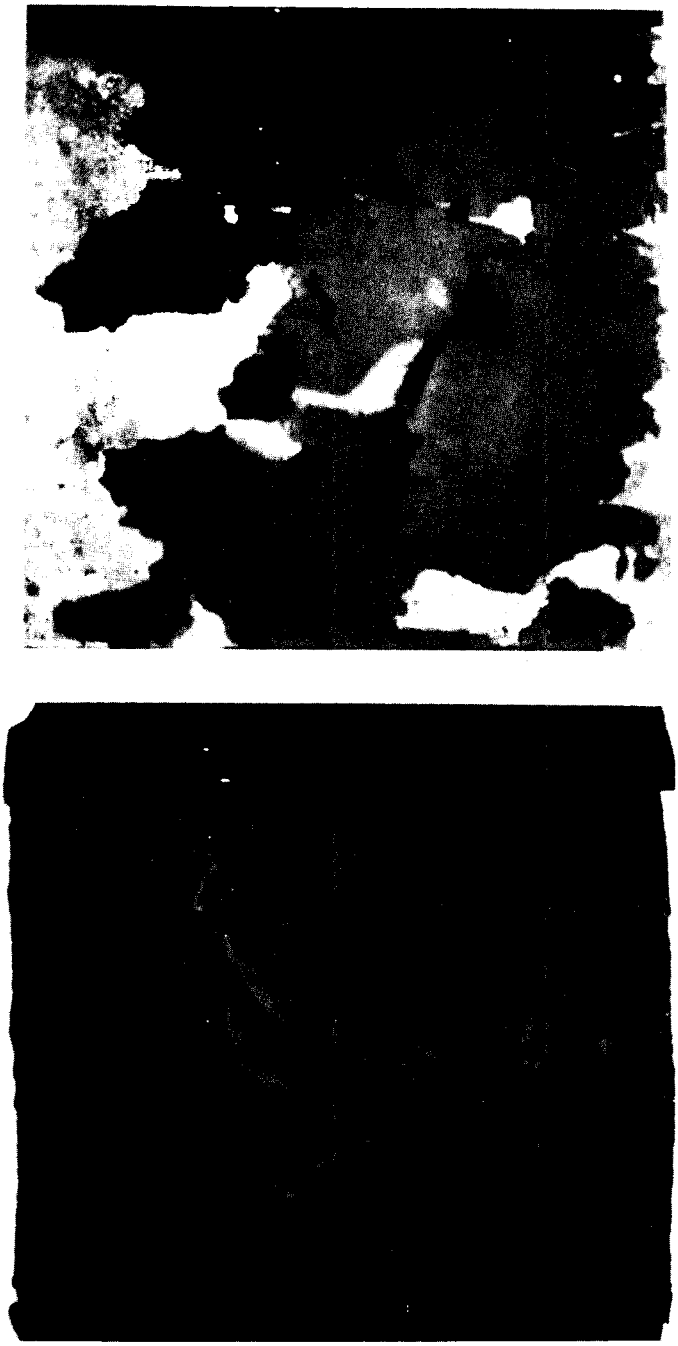

FIG. 11—*Fluidized-bed epoxy ECA 1283 on steel* (on the left), *and on aluminum* (on the right), *after 11 years' exposure at Kure Beach.*

in the organic coatings may have been relieved by flow within the coatings as a function of time.

Rusting of most steel panels begins at the outer edges or around the holes which are placed in the panels for processing or mounting purposes. At these edges the coatings are thinner. Most panels are suspended from a hook during the coating operation, and the suspension point is often a corrosion starting point. The fluidized bed organic coatings were treated with touchup coatings at the suspension points to improve their corrosion resistance. The solvent-coated panels were not treated with touchup coatings at the suspension points but were coated with primer plus two finish coats in a procedure which required resuspending each panel for each coat, so that a continuous coating was obtained at the suspension hole edge.

All ceramic-coated steel panels developed edge rusting at Kure Beach whether particular attention was paid during processing to obtain good edge coverage or not. Also, application of a finish coat did not prevent edge rusting at Kure Beach, but it did prevent rust spotting on the panel faces. All ceramic-coated specimens in Daytona seawater appeared about the same; whether a finish coat had been applied or not, they developed edge rust but not rust spotting on the panel faces. Perhaps, marine life buildup offered some protection to the flat panel surfaces, although buildup was less on some of the ceramic-coated panels because of their original glossy surfaces. The ceramic coating on aluminum lacked stability and eroded in the atmospheric exposures in Steubenville and Kure Beach, and in Daytona seawater. The mud specimens were not recovered. After six years in Daytona seawater the ceramic coating was eroded down to the aluminum, and the 3003 Hl4 aluminum substrate had developed some pit corrosion and a white corrosion product. The blue color of this ceramic was not stable and tended to fade to gray-brown.

Figure 11 shows fluidized-bed epoxy ECA 1283 on steel and on aluminum panels after eleven years at Kure Beach. By examining the aluminum panel we can surmise the failure mode on the steel. The epoxy coating has zero elongation as determined by the conical mandrel test when tested on steel and on aluminum (see Table 6). Thus, it is brittle, and it cracked and flaked away from the aluminum as it probably did from the steel. The adhesion to the aluminum was actually good, however, because the original color photograph shows a thin layer of red epoxy over the visible aluminum surface. The flaking from the aluminum resulted from cohesive failure within the epoxy. Epoxy cracking and flaking from the steel resulted in direct rusting of the flaked-off areas, and underfilm corrosion of areas where the coating remained temporarily in place, as on the right edge of the left steel panel in the photograph.

Normally, one associates increased coating thickness with increased atmospheric resistance. But, most of the fluidized-bed coatings, which were 11 to 12 mil (0.279 to 0.305 mm) thick, failed to protect steel panels from rusting during eleven years at Kure Beach, yet three of the solvent coatings, which were not more than 5 mil (0.127 mm) thick, protected steel panels from rusting during eleven years' exposure. Coating thickness was one difference, but the formulations differed even though two polymer types were the same, epoxy and vinyl. Also, the degree of wetting and the resulting adhesion to steel of the solvent coatings may have been superior to these properties of the fluidized-bed powder coatings. Figure 12 is a photograph showing the superiority of the solvent-borne vinyl over fluidized-bed YCA 1315 vinyl in rust resistance after eleven years' exposure at Kure Beach.

The coal tar-epoxy solvent coating was 17 mil (0.432 mm) thick (1 mil (0.025 mm) of primer and two 8 mil (0.203 mm) topcoats) and it fully protected the steel panels at Kure Beach, but did not offer complete rust protection in Daytona seawater and mud.

The use of aluminum-vinyl sealer and saran sealer over flame-sprayed zinc, aluminum and 67Zn-33Al coatings often improved the rust resistance of the substrate panels at both

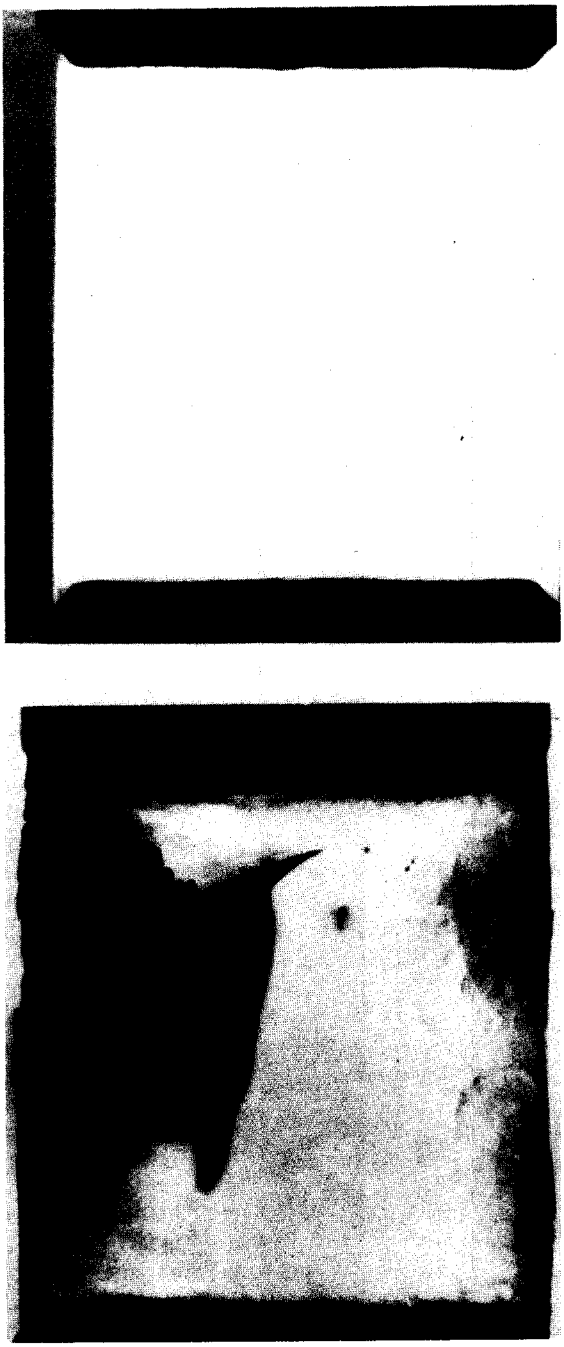

FIG. 12—*During 11 years' exposure at Kure Beach, underfilm corrosion of the steel panel has developed beneath the fluidized-bed VCA 1315 vinyl* (on the left), *while the solvent-borne vinyl* (on the right) *has fully protected the steel panel from rusting.*

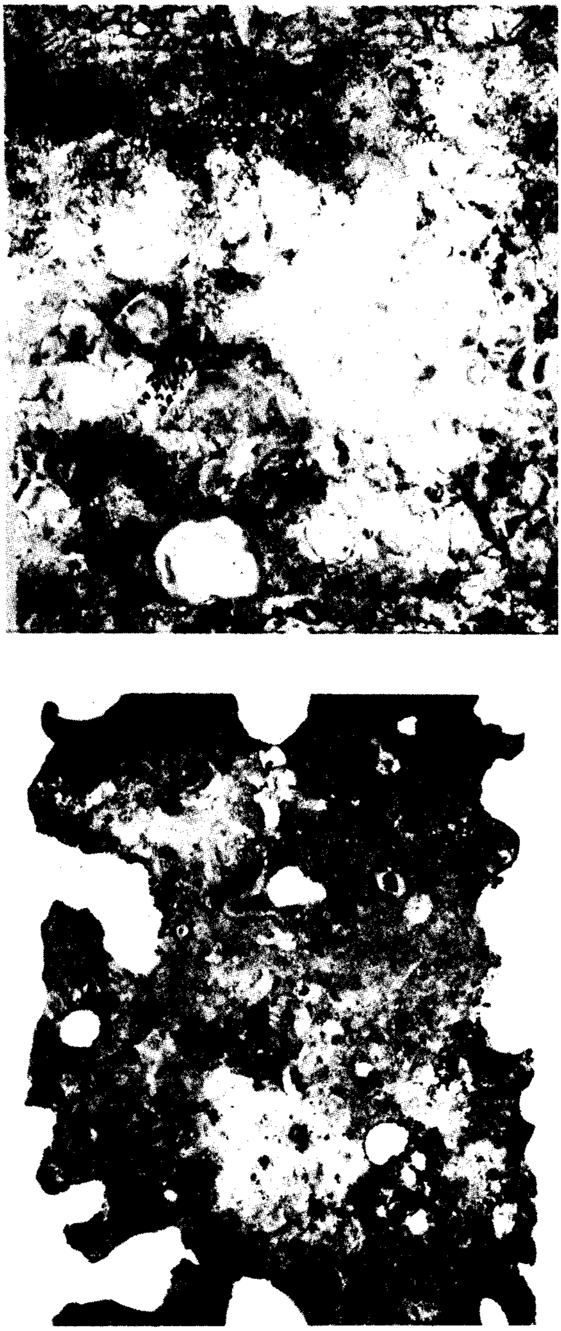

FIG. 13—*Both steel panels were flame-sprayed with zinc; the panel on the right was oversprayed with saran sealer and is rust free and covered with marine life, whereas the unsealed panel on the left is severely rusted.*

Kure Beach and Daytona. The flame-sprayed coatings had a rough texture which was not fully leveled by application of the sealers. In some cases small bubbles were observed within the sealers. Figure 13 is a photograph of two coated steel panels after six years immersion in Daytona seawater. Both panels were flame-sprayed with zinc; the panel on the right was oversprayed with saran sealer. The steel panel without the sealer is severely rusted; the panel with the sealer is rust free and covered with marine life. The rusted panel has some marine life on it, but most of the marine life probably lost its adhesion to the zinc-coated steel as a result of the formation of weak underfilm corrosion products.

Summary

1. No differences were observed between the strained coatings on the %2-in.(0.794-mm) panels and the unstrained coatings on the %-in. (3.175-mm) panels that can be ascribed to strain.
2. The 6061 T6 aluminum substrate panels retained their structural integrity whether exposed with or without coatings. Some spot or pit corrosion, or sand abrasion, occurred on uncoated aluminum panels at Kure Beach and in Daytona mud.
3. All coatings protected steel panels at Steubenville from rusting for ten or more years except hot-dipped zinc and flame-sprayed zinc.
4. The fluidized-bed powder coatings, although II to 12 mil (0.279 to 0.305 mm) thick, failed to protect steel panels from rusting during nine years at Kure Beach and six years in Daytona seawater.
5. The ceramic-coated steel panels developed edge rust at Kure Beach and Daytona regardless of whether special attention was paid during processing to obtain good edge coverage or not. The use of a ceramic finish coat over a ground coat prevented rust spotting of the panel faces.
6. Four solvent coatings protected steel panels from rusting during eleven years at Kure Beach, but none of the solvent coatings offered rust protection for two years in Daytona seawater.
7. Hot-dipped aluminum and flame-sprayed aluminum steel panels were generally superior in rust resistance to the corresponding zinc-coated steel panels.
8. Flame-sprayed 67Zn-33AI coated steel panels were more rust resistant than steel panels coated with flame-sprayed zinc or flame-sprayed aluminum.
9. Use of vinyl or saran sealers over the zinc and aluminum flame-sprayed coatings on steel panels generally increased the rust resistance of the specimens.
10. Whether the ethylene-acrylic acid copolymer was applied by the fluidized-bed method or by the electrostatic spray method made little difference in rust resistance of steel panels in Daytona saltwater and mud.

Acknowledgments

The author wishes to thank John J. Blee of the AT&T Bell Laboratories Materials Engineering and Chemistry Department for his part in program planning; preparation, exposing and retrieval of specimens; analyses of data; and review of this paper. Also involved over the years, were R. A. Connolly and R. Sabia of the Outside Plant Department; R. G. Baker, R. J. Caroselli and K. A. Holtzman of the Chemical Research Laboratory; and P. R. White and J. C. Williams of the Materials Research Laboratory.

References

[1] Connolly, R. A., *The Bell System Technical Journal.* Vol. 51, No. I, Jan. 1972, pp. 1-163.

[2] Brouillette, C. V. and Curry, A. F., "Performance of Ten Generic Coatings During 15 Years of Exposure," Technical Report R 786, Naval Civil Engineering Laboratory, April 1973. Report distributed by National Technical Information Service, U.S. Dept. of Commerce, Sills Bldg., 5785 Port Royal Rd., Springfield, VA 22151.

Flame-Sprayed Aluminum and Zinc Bibliography

[1] Fischer, K. P., Thomson, W. H., and Finnegan, J. E., "Electro-Chemical Performance of Flame-Sprayed Aluminum Coatings on Steel in Seawater," *Material Performance.* Vol. 26, No.9, Sept. 1987, pp. 35-41.

[2] Gartland, P.O., "Cathodic Protection of Aluminum-Coated Steel in Seawater," *Material Performance,* Vol. 26, No.6, June 1987, pp. 29-36.

[3] Kain, R. M., and Baker, E. A., "Marine Atmospheric Corrosion Museum Report on the Performance of Thermal Spray Coatings on Steel," *Testing of Metallic and Inorganic Coatings. ASTM STP* 947, American Society for Testing and Materials, Philadelphia, 1987, pp. 211-234.

[4] Lieberman, E. S., Clayton, C. R., and Herman, H., "Thermally-Sprayed Active Metal Coatings for Corrosion Protection in Marine Environments," Report No. SUSB 84-1, State University of New York at Stony Brook, Jan. 1984. Report distributed by National Technical Information Service, Springfield, VA 22151.

[5] Longo, F. N. and Durmann, G. J., "Corrosion Prevention with Thermal-Sprayed Zinc and Aluminum Coatings," *Formability Topics-Metallic Materials, ASTM STP* 646. American Society for Testing and Materials, Philadelphia, 1978, pp. 97-114.

[6] Mead, G. G., "Investigation of the Corrosion Susceptibility of Flame-Sprayed and Electric Arc-Sprayed Anodic Metal Coatings of Aluminum, Zinc and an Aluminum-Zinc Alloy," Thesis, Naval Postgraduate School, Monteray, CA, March 1983. Report distributed by National Technical Information Service, Springfield, VA.

[7] Shaw, B. A., Leimkuhler, A. M., and Moran, P. J., "Correlation Performance of Aluminum and Zinc-Aluminum Thermal Spray Coatings in Marine Environments," *Testing of Metallic and Inorganic Coatings. ASTM STP* 947. American Society for Testing and Materials, Philadelphia. 1987, pp. 246-264.

[8] Shaw, B. A., and Moran, P. J., "Characterization of the Corrosion Behavior of Zinc-Aluminum Thermal Spray Coatings," *Material Performance,* Vol. 24, No. II, Nov. 1985, pp. 22-31.

APPENDIX I

Organic Sealers.

Saran Sealer

MIL-L-18389 (Formula No. 113/54 Saran) supplied by Randolph Products Co., Carlstadt, New Jersey.

Applied in two coats, the first orange and the second white.

Aluminum- Vinyl Sealer

Wash primer applied and topcoated with aluminum-vinyl sealer.

Wash primer (Metcoseal PR) resin component	*Percent by Weight*
insoluble zinc chromate	8.2
polyvinyl butyral resin	9.5
butyl and isopropyl alcohol	82.3

Acid component	
phosphoric acid	16.0
ethyl or isopropyl alcohol and water	84.0

Mix 4 parts resin component with I part acid component

Aluminum-vinyl sealer (Metcoseal AV)	*Percent by Weight*
nonleafing aluminum flake	10
vinyl copolymers and plasticizer	20
toluene and ketones	70

APPENDIX II

Solvent-Borne Coating Formulations and Application Procedures.

Vinyl paint	*Percent by Weight*
Vinyl resin VMCH, Union Carbide	11.59
Vinyl resin VYHH, Union Carbide	4.70
Tricresyl phosphate, ASTM D363	1.90
Arochlor 1254, Monsanto	1.10
Ti-Pure R-960, DuPont	11.21
#635 Alumina, Whittaker, Clark & Daniels	5.01
2-nitropropane, Commercial Solvents	16.20
Toluene, ASTM D362	32.20
Methyl ethyl ketone, ASTM D3729	16.09

Vinyl primer	*Percent by Weight*
Vinyl resin VAGH, Union Carbide	16.73
Tricresyl phosphate, ASTM D363	1.44
X-2127, Hercules	9.27
Nytal 300, R. T. Vanderbilt	5.79
Lampblack No. 12, Columbian Carbon	0.23
Aluminum Stearate V, Nopco Chemical	0.12
Methyl isobutyl ketone, ASTM D1153	39.85
Toluene, ASTM D362	26.57

Epoxy-amine primer		*Percent by Weight*
Part A		
Epon 1002, Shell Chemical	75.00	34.13
Methyl isobutyl ketone, ASTM D1153	16.65	
Xylene, ASTM D364	8.35	
SR-82, General Electric Silicone Products		0.27
1681, Reichard-Coulston		7.49
Oncor-M50, National Lead		20.40
ASP 101, Englehard Minerals & Chemicals		4.06
399 magnesium silicate, Whittaker, Clark & Daniels		5.47
Bentone 27, National Lead	78.00	0.81
Solox, U.S.I. Chemicals	22.00	

Solvent-Borne Coating Formulations and Application Procedures.

Epoxy-amine primer		*Percent by Weight*
Methyl isobutyl ketone, ASTM D1153		7.44
Xylene, ASTM D364		19.93
Part B		
Epon 1002, Shell Chemical	75.00	22.46
Methyl isobutyl ketone, ASTM D1153	16.65	
Xylene, ASTM D364	8.35	
ZZL-0806, Union Carbide		6.34
Xylene, ASTM D364		12.55
Butyl alcohol, ASTM D304		19.71
Methyl cellosolve, Union Carbide		19.23
Solox, U.S.I. Chemicals		19.71
Mixing ratio = 4 of A to 1 of B by volume		

Epoxy-amine paint	*Percent by Weight*
Part A	
Araldite 471-X75, Ciba	43.79
Beetle resin 216-8, American Cyanamid	1.38
Ti-pure R-960, DuPont	27.06
Methyl isobutyl ketone, ASTM D1153	15.21
Xylene, ASTM D364	12.56
Part B	
Araldite 835, Ciba	100.00
Mixing ratio = 5 of A to 1 of B by volume	

Epoxy-polyamide paint	*Percent by Weight*
Part A	
37-618, Reichhold Chemicals	27.39
Lampblack No. 12, Columbia Carbon	3.69
Nytal 400, R. T. Vanderbilt	21.92
Celite 289, Johns-Manville	10.96
Aluminum stearate V, Nopco	0.36
Xylene, ASTM D364	21.56
Butyl alcohol, ASTM D304	8.64
Isopropyl alcohol, ASTM D770	5.48
Part B	
38-507, Reichhold Chemicals	57.21
Xylene, ASTM D364	3.30
Methyl isobutyl ketone, ASTM D 1153	39.49
Mixing ratio = 1 of A to 1 of B by volume	

Epoxy-polyamide zinc-rich primer	*Percent by Weight*
Part A	
Epon 1001, Shell Chemical	9.98
Glycerine, ASTM D1257	0.36
Cab-o-Sil M-5, Cabot	0.96
Syloid ZN-1, W. R. Grace	0.96
Zinc dust #22, New Jersey Zinc	70.08
Xylene, ASTM D364	11.67
Cellosolve, Union Carbide	5.99

Solvent-Borne Coating Formulations and Application Procedures.

Epoxy-polyamide zinc-rich primer	*Percent by Weight*
Part B	
Versamid 125, General Mills	26.81
Cab-o-Sil M-5, Cabot	5.11
Xylene, ASTM D364	61.42
Cellosolve, Union Carbide	6.66
Mixing ratio = 4 of A to 1 of B by volume	

Coal tar-epoxy paint	*Percent by Weight*
Part A	
Coat tar pitch C-200, Allied Chemical	34.62
Epotuf 37-612, Reichhold Chemicals	11.39
DMP-30, Rohm & Haas	1.29
Bentone 27, National Lead	1.46
Nytal 300, R. T. Vanderbilt	30.72
Xylene, ASTM D364	19.51
Solox, U.S.I. Chemicals	1.01
Part B	
Epotuf 37-140, Reichhold Chemicals	100.00
Mixing ratio = 3½ of A to 1 of B by volume	

Lithium-silicate zinc-rich primer	*Percent by Weight*
Part A	
Polysilicate 48, DuPont	99.00
Potassium dichromate, 5%	1.00
Part B	
Zinc dust #44, New Jersey Zinc	100.00
Mixing ratio = 6.6 lb (2.9937 kg) A to 19.26 lb (8.7362 kg) B	

Chlorinated rubber primer	*Percent by Weight*
Parlon S20, Hercules	14.6
Chlorafin 40, Hercules	5.65
Arochlor 5460, Monsanto	3.65
ERL-2774, Union Carbide	0.44
Epichlorhydrin, Dow	0.07
X-2127, Hercules	6.42
Mica, 325 Mesh, The English Mica Co.	6.86
Asbestine 3X, International Talc	6.42
Ti-Pure R-960, DuPont	2.55
Zinc oxide AZO-22, American Zinc Sales	3.28
Xylene, ASTM D364	50.06

Chlorinated rubber midcoat	*Percent by Weight*
Parlon S20, Hercules	15.84
Chlorafin 40, Hercules	6.09
Arochlor 5460, Monsanto	3.94
ERL-2774, Union Carbide	0.48
Epichlorhydrin, Dow	0.08
Mica, 325 Mesh, The English Mica Co.	5.04
Bentone 38	0.55
Asbestine 3X	12.29

Solvent-Borne Coating Formulations and Application Procedures.

Ti-Pure R-960	3.15
Lampblack No. 12, Cities Service	0.31
Toluene, ASTM 0362	52.23

Chlorinated rubber topcoat	*Percent by Weight*
Parlon S 10, Hercules	15.52
Chlorafin 40, Hercules	4.78
Arochlor 5460, Monsanto	3.74
Monoplex DOS, Rohm & Haas	1.53
ERL-2774, Union Carbide	0.47
Epichlorhydrin, Dow	0.08
Ti-Pure R-970, DuPont	17.93
Lampblack No. 12, Cities Service	0.18
Xylene, ASTM 0364	55.77

Vinyl application procedure
I. Degrease metal panels.
2. Apply 0.3 ± 0.1 mil Off" MIL-P-15328B wash primer. Air dry 2 to 4 h.
3. Apply 1.1 ± 0.1 mil DFf[b] vinyl primer. Air dry 16 to 24 h.
4. Apply 2.1 ± 0.1 mil DFf[c] vinyl paint. Air dry 16 to 24 h.
5. Repeat step 4 for a second coat. Air dry 72 h.

Epoxy-aminejepoxy-amine primer application procedure
I. Degrease metal panels.
2. Apply 1.1 ± 0.1 mil DFf[b] epoxy-amine primer. Air dry 24 h.
3. Apply 2.1 ± 0.1 mil DFf[c] epoxy-amine paint. Air dry 24 h.
4. Repeat step 3 for a second coat. Air dry 72 h.

Epoxy-aminejlithium-silicate zinc-rich primer application procedure
I. Grit blast (#60 aluminum oxide) metal panels.
2. Apply 1.1 ± 0.1 mil DFf[b] lithium-silicate zinc-rich primer. Air dry 8 h, min.
3. Apply 2.1 ± 0.1 mil DFf[c] epoxy-amine paint. Air dry 24 h.
4. Repeat step 3 for a second coat. Air dry 72 h.

Epoxy-polyamidejepoxy-amine primer application procedure
I. Degrease metal panels
2. Apply 1.1 ± 0.1 mil DFf[b] epoxy-amine primer. Air dry 24 h.
3. Apply 2.0 ± 0.1 mil DFf[d] epoxy polyamide paint. Air dry 24 h.
4. Repeat step 3 for a second coat. Air dry 72 h.

Coal tar-epoxyjepoxy-amine primer application procedure
I. Degrease metal panels.
2. Apply 1.1 ± 0.1 mil DFf[b] epoxy-amine primer. Air dry 24 h.
3. Apply 8.0 ± 0.5 mil Off' coat tar-epoxy paint. Air dry 24 h.
4. Repeat step 3 for a second coat. Air dry 72 h.

Epoxy-aminejepoxy-polyamide zinc-rich primer application procedure
I. Degrease metal panels.
2. Apply 1.1 ± 0.1 mil DFf[b] epoxy-polyamide zinc-rich primer. Air dry 24 h.
3. Apply 2.1 ± 0.1 mil DFf[c] epoxy-amine paint. Air dry 24 h.
4. Repeat step 3 for a second coat. Air dry 72 h.

Solvent-Borne Coating Formulations and Application Procedures.

Chlorinated rubber application procedure

1. Degrease metal panels.
2. Apply 1.5 ± 0.1 mil *DFTJ* chlorinated rubber primer. Air dry 24 h.
3. Apply 3.0 ± 0.1 mil *DFTg* chlorinated rubber mid-coat. Air dry 24 h.
4. Apply 1.1 ± 0.1 mil *DFT*[b] chlorinated rubber topcoat. Air dry 72 h.

---

[a] 0.0076 ± 0.0025 mm *DFT* (dry film thickness).
[b] 0.0279 ± 0.0025 mm *DFT* (dry film thickness).
[c] 0.0533 ± 0.0025 mm *DFT* (dry film thickness).
[d] 0.0508 ± 0.0025 mm *DFT* (dry film thickness).
[e] 0.2032 ± 0.0127 mm *DFT* (dry film thickness).
JO.0381 ± 0.0025 mm *DFT* (dry film thickness).
[g] 0.0762 ± 0.0025 mm *DFT* (dry film thickness).